MICROSTRUCTURE-PROPERTY DEVELOPMENT AND DEFECT CHARACTERIZATION OF AL-X FRICTION WELDS FOR AUTOMOTIVE APPLICATIONS

By

NAN ZHOU

A thesis submitted to The University of Birmingham for the degree of

DOCTOR OF PHILOSOPHY

School of Metallurgy and Materials
College of Engineering and Physical Sciences
The University of Birmingham
March 2020

ACKNOWLDEMENTS

I would like to acknowledge my work unit in China, Guangdong Institute of Materials and Processing (GIMP), for supplying the study opportunity in the University of Birmingham. I would also like to give my thanks towards Guangzhou Municipal Science and Technology Bureau, which sponsored the project “Research and industrialization of friction welding in key parts of automobile and high-end electric appliances” I am working on for the PhD project, and the cooperation company of this project, Guangzhou Kinbon Non-ferrous Alloy Metals Co., Ltd, for the financial support, as well as the University of Birmingham Guangzhou Centre which helped a lot in the project management and the PhD application.

I would like to acknowledge my supervisor Prof. Moataz M Attallah for the technological guidance and academic advice in all the aspects during my PhD course. Besides, the help and support especially in my experimental work from Dr. Chunlei Qiu and Dr. Ji Zou are highly appreciated. I would also like to thank Prof. Wenjun Qi in GIMP, China, for his advice on the experiment scheme of my PhD course. Also, I would like to thank my leaders in GDAS and GIMP especially Prof. Min Liu and Prof. Kaihong Zheng, colleagues in GIMP especially Mr. Dongfu Song, Dr. Xiaohui Li and Dr. Chunlei Gan, and fellows in the AMP lab especially Dr. Sheng Li and Dr. Xiqian Wang for their support and help.

I would like to thank the Department of Metallurgy and Materials for offering the excellent laboratory facilities and environment, as well as the technicians and staff for the technical support. Besides, I would like to thank Northwest Polythechnical University and Shaanxi Key Laboratory of Friction Welding Technologies for accessing the LFW facility as well as the technical support.

Finally, I would like to express my love and gratitude to my wife, parents, son and all the family members for their understanding and support.

ABSTRACT

Friction Welding (FW) has broad application prospects in the fields of automotive industry. In the industrial production as well as big amounts of literatures, various defects can have a significantly influence on the quality of the FW joints. However, the formation mechanism of the defects in the welds as well as the effect regulation on the properties of the welds have not been systematically studied. Therefore, the present work has been focused on the relationship between the microstructure and mechanical properties in friction welding joints, which covered ordinary butt joints of friction stir welding (FSW), friction stir lap welding (FSLW) as well as linear friction welding (LFW), especially on the characterization of various defects in these friction welds and their influence regulations on the mechanical properties.

FSW butt welds for AA5083-H112 were prepared at various welding parameters. The microstructural and property development throughout the welds were evaluated, with a special focus on the kissing bond defect, which can have a substantial effect on the microstructure and properties of the FSW joints. It was found that the length of the kissing bond had a reasonably linear relation with heat input (HI), which depends mostly on the tool rotation speed as well as feed rate. Moreover, with the increasing length of the kissing bond, the tensile strength and elongation increased first and then decreased, however, the yield strength had no obvious trend. Besides, better fatigue results were shown for the weld with shorter kissing bond. It was also found that the kissing bond can affect the fracture type, which were strongly correlated with the tensile strength and fatigue life.

FSLW of a wrought aluminium alloy (AA6061-T6) to a casting aluminium (as-cast A356) sheets was prepared, with the investigation on the microstructure evolution, second-phase distribution and microscale defects. In the microstructure, kissing

bond and another kind of defect named hook were detected. It was found that the kissing bond did not significantly affect the shear behaviour of the joints. However, the hook defect, increased in height and range with the increasing tool rotation speed, was found to have a remarkable influence on the shear behaviour of the joints.

LFW of AA5083 welds and dissimilar AA5083-Cu C101 welds were prepared using different forging pressures, to assess the impact of the defects, as well as the forging pressure on the mechanical properties and microstructural development. In the LFW of AA5083, discontinuous lack of connection defects were detected on the welding interface, where crack source formed on the in the stretching process. With the increase of the forging force, which led to the increase in heat input, the size of the defect was significantly decreased, resulting in the increase of the mechanical properties. In dissimilar AA5083 Cu C101 LFW joints, the LFW process can lead to the formation of an intermetallic phase across the weld interface, which affected the mechanical properties based on the morphology and extent of the intermetallic phases. In general, high forging pressure resulted in the formation of a layered intermetallic phase (identified as Al_2CuMg), which was the most detrimental to the mechanical properties, compared with a scattered distribution of fragmented Cu-particles and intermetallics across the joint interface in lower to intermediate forging pressure.

TABLE OF CONTENTS

TABLE OF FIGURES

LIST OF TABLES

NOMENCLATURE

Item	***Description***
AS	**Advancing Side**
BM	**Base Material**
CFD	**Computational Fluid Dynamics**
DRX	**Dynamic Recrystallisation**
DSC	**Differential Scanning Calorimetry**
EDM	**Electrical Discharge Machining**
EDS	**Energy-Dispersive Spectroscopy**
EDX	**Energy Dispersive X-Ray Spectroscopy**
EL	**Elongation**
EPMA	**Electron Probe Micro-Analyser**
FEM	**Finite Element Method**
FIB	**Focused Ion Beam**
FSLW	**Friction Stir Lap Welding**
FSW	**Friction Stir Welding**
FW	**Friction Welding**
HAZ	**Heat Affected Zone**
HI	**Heat Input**
IQF	**Index of weld quality with reference to the fatigue properties**
JLR	**Joint Line Remnant**
LBW	**Laser Beam Welding**
LFW	**Linear Friction Welding**
LOP	**Lack of Penetration**
MIG welding	**Metal Inert-Gas welding**
NDT	**Non-Destructive Testing**
OM	**Optical Microscope**
PWHT	**Post Welding Heat Treatment**
RD	**Rolling Direction**
RS	**Retreating Side**
SEM	**Scanning Electron Microscope**
SSM	**Semi-Solid Metal**
SSSS	**Super-Saturated Solid Solution**
SZ	**Stirring Zone**
TEM	**Transmission Electron Microscope**
TMAZ	**Thermal-Mechanical Affected Zone**
UTS	**Ultimate Tensile Strength**
WD	**Welding Direction**
WZ	**Weld Zone (in linear friction welding)**
XRD	**X-Ray Diffraction**
YS	**Yield Strength**

1 Introduction

1.1 General Introduction

With the rapid development of automobile industry and the increasingly serious problems of energy shortage and environmental pollution in the world, the requirements for energy saving and environmental protection of automobiles are becoming highly strict. According to the analysis, the 100kg decrease of the automobile weight can lead to approximately 0.7L reduction of the fuel consumption per 100 kilometres[1]. On the premise of ensuring safety and comfort, reducing auto self-weight is of great significance to energy conservation. Therefore, lightweight materials, innovative structures and advanced manufacturing technology have become the main theme for automobile manufacturing.

Aluminium, as a light weight material, are characterized by a high strength/weight ratio so that they allow the production of light structures without using expensive composite materials. Besides, aluminium alloy has the advantages of good corrosion resistance, good plasticity, unparalleled superiority in terms of production cost, part quality, material utilization, manufacturing technology, mechanical properties, sustainable development, etc. Therefore, aluminium alloy has become the preferred lightweight material in automobile industry.

Fig. 1. 1 shows the trend of aluminium content per vehicle in North American from 1975. It can be seen that aluminium alloys have developed rapidly since entering the field of automobile industry, and the amount of aluminium alloy has been increasing year by year and will be raising even faster. At present, the United States, UK, Germany are the countries with a large number of aluminium alloys used in automobiles, such as Cadillac CT6, Ford F150, Jaguar XE/XF, AudiA8, A2, and other body aluminium alloys. Unlike traditional cars, new energy vehicles use new energy as power to drive cars, which are powered by the weight of power batteries. The restriction of power battery mileage and the restriction of automobile energy saving and emission reduction policy, in vehicle design and application of materials, the lightweight of the vehicle body becomes the first problem to be considered by car enterprises. In some parts aluminium has become the primary choice of new energy automobile manufacturers. For example, Tesla model S and X have used aluminium car body, which can reduce 320kg per vehicle and increase only 160 US$ in cost[2].

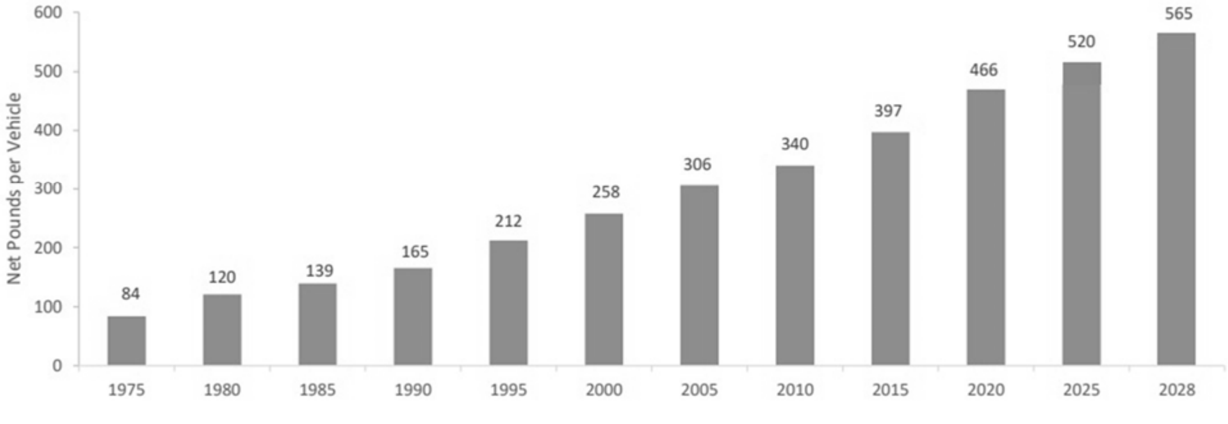

Fig. 1. 1 The aluminium content per vehicle in North American[2]

There is a continual requirement to make things perform better, be more predictably reliable, cost less, and use less energy. This often leads to requirements to make components for them that are complex shapes or that have properties that vary from one location to another. These requirements are often difficult or expensive to satisfy by conventional machining and mechanical processing, but joining allows us to make complex shapes, potentially of materials with different properties. The disadvantage is that, often, joints require mass to be added to a design to carry the locally increased forces surrounding the joint. Alternatively, the joint must be prepared and produced very carefully and may still have properties below those of the parent material. Extra mass or reduced properties (again requiring extra mass) increase the raw material costs and typically reduce the energy efficiency of the final product.

Friction welding (FW) offers an extremely promising way to make joints with minimal requirements for extra mass and with extremely good final product properties showing very low distortion. Friction welding is a solid-phase joining technology, which means no metal melting occurs during the welding, with the characteristic of high joint performance. Particularly for aluminium alloys appealing advantages are the solid-state joining nature of the process so that it can avoid the formation of Al_2O_3 which can quickly cover the weld at high temperature and the extreme hardness causes the failure of the joint. Consequently, all the aluminium alloys have good weldability for friction welding (see Fig. 1. 2). Besides, all the FW processes are very reliable and repeatable, which are necessary for industrialization of the technology. Among these kind of friction welding technologies, friction stir welding (FSW) and linear friction welding (LFW) are the most promising technologies with wide application prospects.

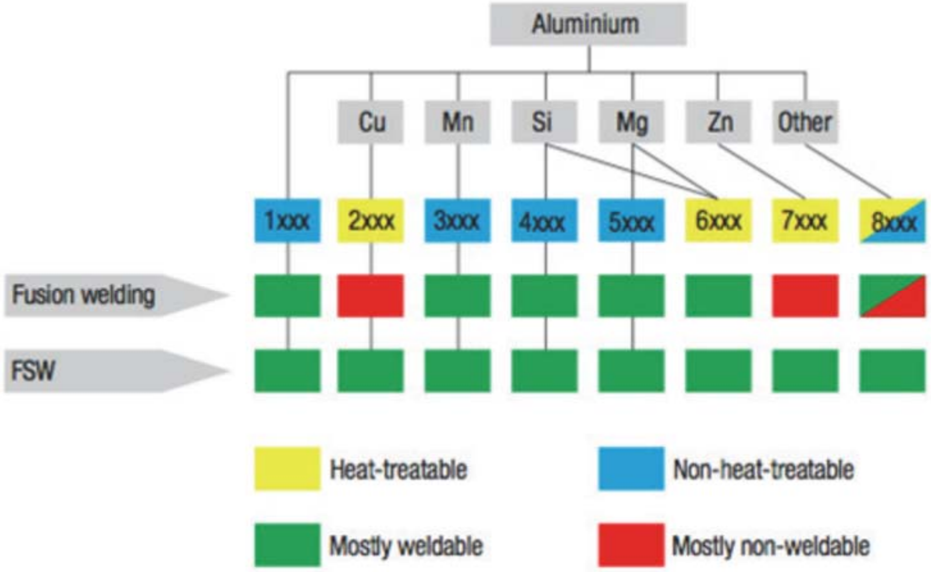

Fig. 1. 2 Weldability of aluminium alloys[3]

In automotive manufacturing, FW can be used to join the spoke and the rim of a wheel hub. The advanced technology of connecting two parts of a car wheel by FSW has been invented in Norway and successfully demonstrated by Hydro Aluminium[4]. Aluminium alloy wheels manufactured by FSW can greatly reduce the weight and improve the performance of the product. Moreover, it is suitable for large-scale industrial production. Therefore, an increasing number of wheel rims are also being produced by conventional friction welding. In Germany, a fully automated manufacturing cell has been built by Kuka to join the rim and the wheel disc of hollow-spoke alloy wheels by rotary friction welding in mass production. This is an economic way to produce lightweight wheels with only a 6 second welding time and achieve a weight reduction of 27% for the front wheel of a sport car[5]. LFW has rarely been used in civil field due to the equipment barriers. However, it is appropriate for the connection of dissimilar metal materials such as titanium alloy to nickel alloy, aluminium to copper, etc. Therefore, LFW also has a wide application prospect in civil areas including automobile and electric appliance[6, 7].

The application researches of friction welding technology in aerospace, marine, military and other fields have been promoted, some of which have been industrialized and achieved considerable economic benefits[8, 9]. The representative organizations working on friction welding are the Universities of Birmingham, Manchester, and TWI (UK), Tohoku University (Japan), Northwestern Polytechnical University and China FSW Centre (China), University of Ulsan (South Korea), among others. Currently, linear friction welds are already being used in high performance parts in aircraft engines. The friction stir welding family of applications (FSW, FSSW (friction stir spot welding), FSP (friction stir processing), etc.) are used in the manufacture of structures utilising aluminium alloy plates of every grade. However, in friction weldments, defects can influence the properties, for example, mechanical, fatigue, etc., with varying degrees. Research on FW is expected to encourage the further spread of this technology in the industrial field, notably by getting a clear understanding of the defects in the FW joints and the mechanisms of the defect formation. Simultaneously studying the effect of the various defects on the material properties in the representative kinds of FW including FSW butt and lap welding, as well as linear friction welding.

1.2. Project Aim, Objectives & Approach

The aim of this study is to establish a fundamental relationship among processes, microstructure and property development during FW, e.g. FSW and LFW, which have broad application prospect in automobile field. A special focus is on the defects in the FW joints, with the system investigation on the effect of the various defects on the mechanical properties of the welds. Materials related are similar AA5xxx series Al alloy, dissimilar alloys between a wrought Al alloy (AA6xxx) and a cast Al alloy (A3xx), as well as different materials between Al alloy and pure copper. A special focus is on the defects produced in the FW process. The specific objectives to achieve are:

- ✧ Experimental research on the influence of the welding parameters or welding heat input on the formation, morphology and distribution of the defects produced in the welding processes, as well as the crystallographic morphology and mechanical properties of the friction welds.
- ✧ Investigation of the microstructure of the FSW and LFW weldments, to identify the type of the defects which are produced in the welding procedure, as well as the defect which dominate the mechanical properties of the welds, and hence the influence mechanism on the failure of the weldments.
- ✧ Establishing the link among welding parameters, welding heat input, mechanical properties of the weldments and microstructural characteristics, especially micro-defects in the welds e.g. kissing bond or intermetallic particles, and the effect of these microstructural characteristics on the mechanical properties of the welds, for example hardness and tensile properties.

This thesis is divided into 7 chapters. The chapter 2 is literature review. In chapter 2, the general introduction of the Al alloy materials for welding involved in this dissertation is presented, including AA5083, AA6061 wrought aluminium alloys and A356 casting aluminium alloys, focusing on the microstructures, intermetallic phases, mechanical properties, and strengthening mechanism present in these alloys. Besides, the present research status on friction welding of Al-X similar/dissimilar welds is reviewed, summarising the influence of the process parameters on the microstructure and the mechanical properties, as well as the various types of the defects, concentrating how they affect the microstructure and mechanical properties of the friction welds. In addition, the physical metallurgy behaviour of the welding process for dissimilar materials Al and Cu is also reviewed. Detailed description of the experimental techniques used in this study is presented in chapter 3. The results and discussions are presented in chapters 4 to 6, detailed characterisation of the defects and their effects on the microstructure and mechanical properties in friction stir butt welding, friction stir lap welding, linear friction welding, respectively. Chapter 7 summarises the conclusions of this study as well as the possible future work. The appendix includes the published peer-reviewed papers related to this study.

1.3. References

[1] G.S. Daehn, Sustainable design and manufacture of lightweight vehicle structures, (2014) 433-461.

[2] https://www.ducker.com.

[3] D. Baffari, G. Buffa, D. Campanella, L. Fratini, F. Micari, Friction based Solid State Welding Techniques for Transportation Industry Applications, Procedia CIRP 18 (2014) 162-167.

[4] A. Amini, P. Asadi, P. Zolghadr, Friction stir welding applications in industry, (2014) 671-722.

[5] S. Kallee, D. Nicolas, Application of Friction Stir Welding to Lightweight Vehicles, International Body Engineering Conference & Exposition, Detroit, Michigan, 1998.

[6] I. Bhamji, M. Preuss, P.L. Threadgill, A.C. Addison, Solid state joining of metals by linear friction welding: a literature review, Materials Science and Technology 27(1) (2013) 2-12.

[7] I. Bhamji, A.C. Addison, P.L. Threadgill, M. Preuss, Appendix: Linear friction welding in aerospace engineering, (2012) 384-415.

[8] P.L. Threadgill, A.J. Leonard, H.R. Shercliff, P.J. Withers, Friction stir welding of aluminium alloys, International Materials Reviews 54(2) (2013) 49-93.

[9] A. Grimm, S. Schulze, A. Silva, G. Göbel, J. Standfuss, B. Brenner, E. Beyer, U. Füssel, Friction Stir welding of Light Metals for Industrial Applications, Materials Today: Proceedings 2 (2015) S169-S178.

2 Literature Review

The literature review begins with a general introduction of the base metals for friction welding involved in this research including AA5083, AA6061, A356 aluminium alloys as well as pure copper which is friction welded to AA5083, followed by a detailed review of the macro/micro structures and mechanical properties of the Al-X friction welding joints. At last, the various defects in friction welds and their effect on the mechanical properties are also reviewed in this chapter.

2.1 Physical metallurgy of the friction welding base metals

2.1.1 AA5083

AA5083 is a typical Al-Mg system alloy, which has medium strength, good weldability, and excellent corrosion resistance. It can also be processed into sheet, bar, profile, pipe, wire and other complex shapes. Therefore, AA5083 has been widely used in automotive industry, as manufactured into vehicle body panels, body interior plate, heat insulation, and other light-weight semi-products [1], showing a significant effect on reducing the weight of the vehicle body [2].

The chemical composition (in weight percent) of AA5083 according to ASTM B209M standard is: Mg (4.0~4.9%), Mn (0.4~1%), Cr (0.05~0.25%), Si (< 0.4%), Fe (< 0.4%), Cu (< 0.1%), Zn (< 0.25%), Ti (< 0.15%) and Al (balance). Fig. 2. 1 shows the equilibrium phase diagram of Al-Mg binary alloys. Mg is a major alloying element in Al-Mg alloy, with the maximum solubility in aluminium is up to 17.4%. The AA5083 is a kind of aluminium alloy that cannot be strengthened by heat treatment, due to the difficulty in precipitation phase nucleation, and the large size for precipitation phase, and thus the aging effect of the alloy is poor. Mg is preferentially deposited on the grain boundary mainly in the form of Mg_2Al_3 in the alloy, so that the alloy has the tendency to produce intergranular crack and stress corrosion [3]. Mg can obviously improve the strength of aluminium without excessively reducing its plasticity.

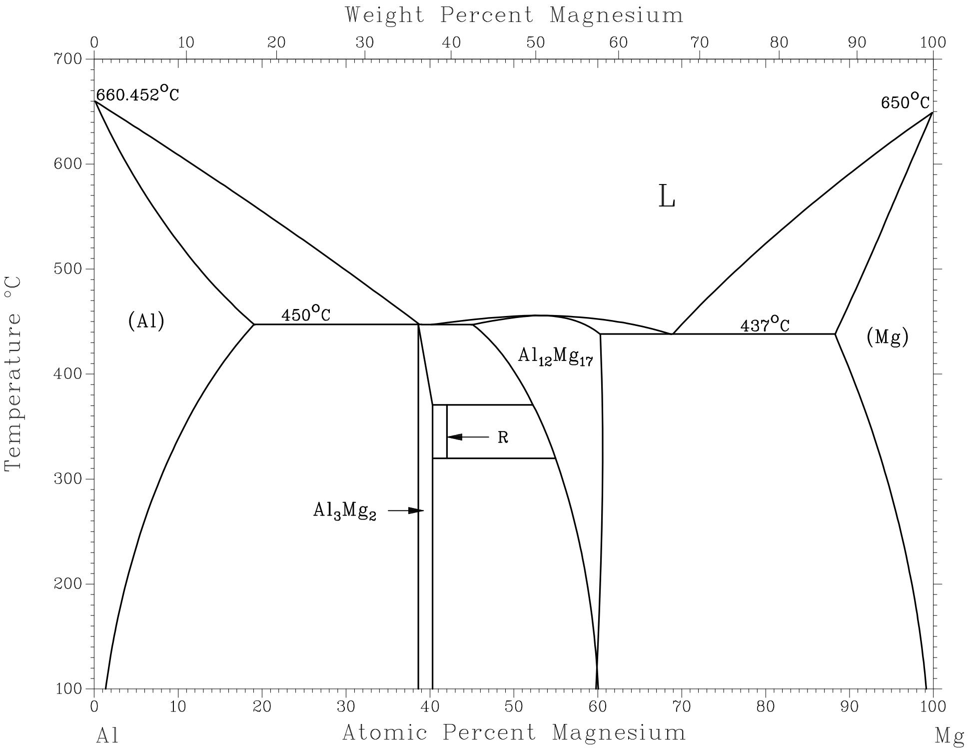

Fig. 2. 1 The binary Al-Mg equilibrium diagram.

The decomposition process of supersaturated solid solution (SSSS) in AA5083 alloy was identified by means of resistance testing, differential scanning calorimetry and transmission electron microscopy. The current recognized aging precipitation sequence is shown as follows:

SSSS → G.P. zone → β” phase → β’ phase → β phase [4]

G.P. zone was proposed by Guinier and Preston in studying the natural effect of single crystal of Al-Cu alloy. Now, G.P. zone has been used to refer to the pre-desolventing atomic segregation region in all alloys. In Al-Mg system alloys, the G.P. zone is a cluster of Mg atoms[5]. With the prolongation of the holding time, the G.P. zone grows into a thin sheet with a thickness of 1-2 atomic layers parallel to the direction of the matrix <100>, coherence with the matrix. G.P. zone generally occurs during the short aging at low temperature after quenching, with the dissolution temperature approximately 60-100°C[4].

With the prolongation of aging time, the G.P. zone can change to β” phase. The metastable phase β” is an $L1_2$ ordered phase with the composition of Al_3Mg[5]. With the increase of aging temperature, the G.P. zone and β” phase can be transformed into β’ phase. The β’ phase is the metastable phase of β, with the chemical formula Al_3Mg_2, the dense hexagonal crystal structure, and semi-coherent with the Al matrix[5]. The orientation relationship is[6]:

$$(0001)_{\beta'}//(001)_{\alpha} \qquad [01\bar{1}0]_{\beta'}//[110]_{\alpha}$$

When the aging temperature is 200°C, the metastable phase β’ is transformed into stable phase, and when the temperature is above 250°C, the β phase is dissolving. β phase has a cubic structure, with the chemical formula Al_3Mg_2, and incoherent with the matrix. The β phase has the following orientation relationship with the Al matrix[7]:

$(111)_{\beta}//(001)_{\alpha}$ $[110]_{\beta}//[010]_{\alpha}$

The TEM microstructures of β’ and β in Al-Mg alloy are respectively shown in Fig. 2. 2[8].

The dominant strengthening methods of AA5083 alloy are solution strengthening and deformation strengthening[9, 10]. Solution strengthening is the strengthening mechanism of the strength and hardness of the alloy when the alloy element is dissolved into the matrix metal to form a solid solution. The physical essence of the solid solution strengthening is the lattice distortion hinders the dislocation movement, that is the interaction between defects and dislocations caused by lattice irregularity and distortion is the main reason for strengthening. These defects can be divided into three categories, lattice distortion caused by the size difference between solute atoms and solvent atoms, the difference of the dislocation motion, and the pinning dislocations when solid solution atoms converge onto dislocation lines. In order to reduce the strain energy of the system, the solute atomic polymer, known as Cordell Atmosphere, was formed around the dislocation, to block the movement of dislocations and play a reinforcing role.

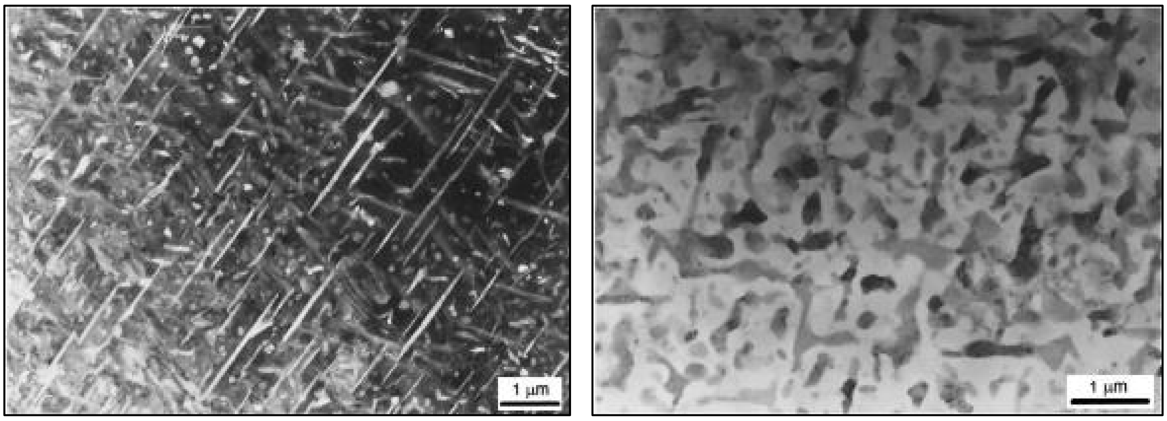

Fig. 2. 2 The TEM microstructures of β’ (left) and β (right) in an Al-Mg alloy[8].

The reason for the deformation strengthening is that the dislocations proliferate due to the strong plastic deformation, and the dislocation jogs in the process of movement so as to reduce the mobility. After the interaction, many dislocations are entangled together to form the dislocation tangles, so the movement would be more difficult, or the deformation would be more difficult. The greater deformation resistance of the material results in higher strength, but lower plasticity and toughness.

2.1.2 AA6061

AA6061 is a traditional Al-Mg-Si system alloy. After heat treatment, it has high strength and good comprehensive properties, such as corrosion resistance and process property, sufficient toughness, anodic oxidation and colouring, good welding property, no change in corrosion resistance in welding area[11-13]. It has good plasticity at high temperature and can be used to manufacture thin-walled and hollow extruded products with complicated structure, which can withstand large deformation degree such as tensile, die forging, deep drawing, etc. AA6061 is widely used as structural material in sports, construction, transportation and other fields, especially in automobile industry, instead of steel as mechanical parts material, such as body, chassis, engine, wheel, machine cover, motor shell, etc. Sheets and profiles of AA6061 have been widely used in transportation such as subway trains, railway trains and double-decker buses[14].

AA6061 is heat-treatable strengthened aluminium alloys, with the chemical composition (in weight percent) according to the standard ASTM B209M: Mg (0.8~1.2%), Si (0.4~0.8%), Cu (0.15~0.4%), Cr (0.04~0.35%), Fe (< 0.7%), Mn (< 0.15%), Zn (< 0.25%), Ti (< 0.15%) and Al (balance). Usually, some impurity elements such as Fe etc. are inevitably doped in the alloy[15].

The addition of these impurity elements will have a complex effect on the properties of the alloy. For the purpose of improving the performance of the alloy, some other alloy elements are often added to the alloy, such as adding a certain amount of Mn or Cr, which can reduce the side effect of Fe on the alloy[16]. Adding a small quantity of Cu or Zn to the alloy can improve the strength of the alloy without significantly reducing the corrosion resistance[17, 18]. Besides, the grain size of the alloy can be refined, and the strength of the material could be improved by adding Ti or Zr [19, 20].

Among these kinds of alloying elements, Mg and Si are main strengthening elements, forming Mg_2Si strengthening phase. The precipitation sequence in AA6061 alloy is as follows[21]:

SSSS → Si, Mg atom clusters → Mg clusters → Mg/Si co clusters → G.P. zone →

β” phase → β” & β’ phase → β phase (Mg_2Si)

The β” phase is the strengthening metastable phase which gives maximum strength to the alloy through its coherency with Al matrix. The TEM morphology of the β” phase in AA6061 is shown in Fig. 2. 3.[22]

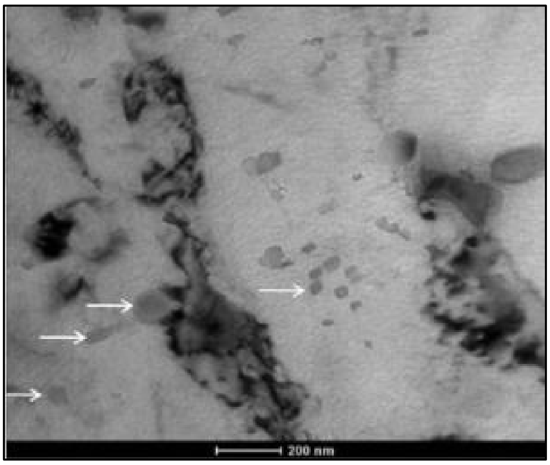

Fig. 2. 3 The precipitates of Mg_2Si in AA6061[22].

The maximum solution of Mg_2Si phase in aluminium alloy is greatly affected by the change of temperature. According to the Al-Mg_2Si phase diagram shown in Fig. 2. 4, the solid solubility can reach 1.85% at 595°C, but only 0.27% when the temperature drops to 300°C, which provides the possibility for heat treatment strengthening. Besides, when the weight ratio of Mg/Si in the alloy is greater than 1.73 which is the Mg/Si weight ratio of the strengthened Mg_2Si phase, the solubility of Mg_2Si phase in aluminium matrix decreases significantly due to the excess Mg element in the alloy, and the strengthening effect of Mg_2Si phase is also weakened[23]. In order to avoid the weakening of the strengthening effect, the atomic ratio of Mg/Si in the alloy is usually no more than 1.73. However, it was reported that the excess Si in the alloy cannot reduce the solubility of the Mg_2Si phase in the aluminium matrix but would decrease the intergranular corrosion resistance of the alloy[24, 25].

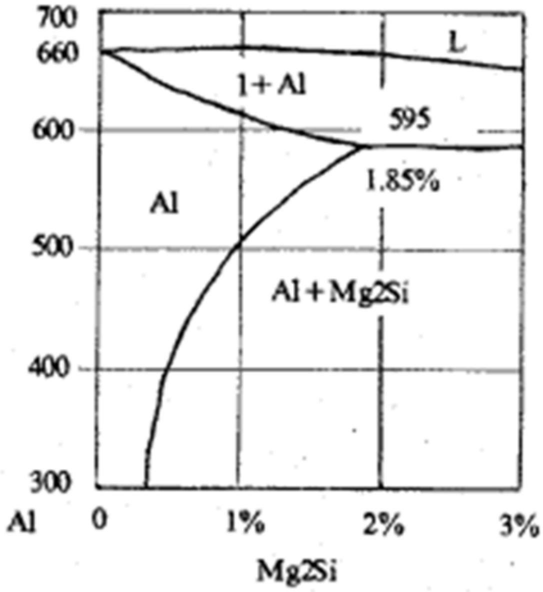

Fig. 2. 4 The phase diagram of Al-Mg_2Si (Al-rich corner)

The strength of AA6061 alloy can be improved by artificial aging as well as natural aging after solution treatment. Natural aging is characterized by low aging temperature and long aging time. In contrast to natural aging, artificial aging has higher aging temperature and shorter aging time. Compared with the artificial aging, the plasticity and corrosion resistance of AA6061 alloy by natural aging are better than that of artificial aging, but the strength is lower[26]. It should be noticed that AA6061 alloy has “Shelf-time Effect”. Therefore, the highest strength should be achieved by aging treatment immediately after solution treatment, or the strengthening effect would decrease if the alloy is treated by artificial aging after solution for a period of time at room temperature. In addition to precipitation hardening, the grain structure including grain size and grain morphology could also have a significant effect on the performance of the alloy[27].

2.1.3 A356

A356 series aluminium alloy, a typical Al-Si-Mg series ternary alloy, was developed by the United States in the 1970s. It has excellent comprehensive properties. It not only has good casting properties, such as good fluidity, small linear shrinkage, no hot cracking tendency, etc. It can also cast thin-walled castings with complicated shapes, and can achieve high strength, good plasticity and ideal synthesis of high impact toughness through heat treatment[28, 29]. Therefore, A356 series aluminium alloys have been widely used in automobile industry in the late 1980s. It has become the preferred material for casting aluminium wheels[30]. At present, the application of A356 series aluminium alloy in automobile industry is increasing with the development of light weight, energy saving and multi-variety development of automobile design. With the rapid development of automobile industry, new technology, new equipment will be used more widely in the automobile industry with the introduction of A356 series aluminium alloy.

Si and Mg are the main strengthening elements of A356 alloy. The microstructure of as-cast A356 alloy is shown in Fig. 2. 5 (a)[31]. Mg_2Si phase (see Fig. 2. 5 (b)) can be precipitated during aging procedure, which can obviously improve the strength and hardness of A356 alloy[32]. Natural aging has a limited influence on the precipitation of Mg_2Si, so the alloy can only be strengthened by artificial aging. A356 alloy has a relatively large content of Si, showing a coarse needle shape in the alloy, which can decrease the mechanical properties of the alloy significantly, and the cutting performance is also affected. Furthermore, once the needle-like structure is formed, it is difficult to improve by any kind of heat treatment[33]. However, if a proper amount of Na is added to the alloy solution before pouring, hypoeutectic structure consisting of primary Al and fine eutectic can be obtained, and the mechanical properties can be greatly improved[34]. Fe has a relatively low solubility in Al-Si alloy, so it is usually precipitated in the form of brittle Fe-rich intermetallic phase which is harmful to the mechanical properties of the alloy. The common precipitates are fishbone α Fe-rich phase and needle-shaped β Fe-rich phase (shown in Fig. 2. 5 (c, d)). The amount of needle-like brittle β phase grows up with the increase of Fe content, which can cut off the Al matrix, improve the stress concentration source, and seriously reduce the mechanical properties of the alloy[35].

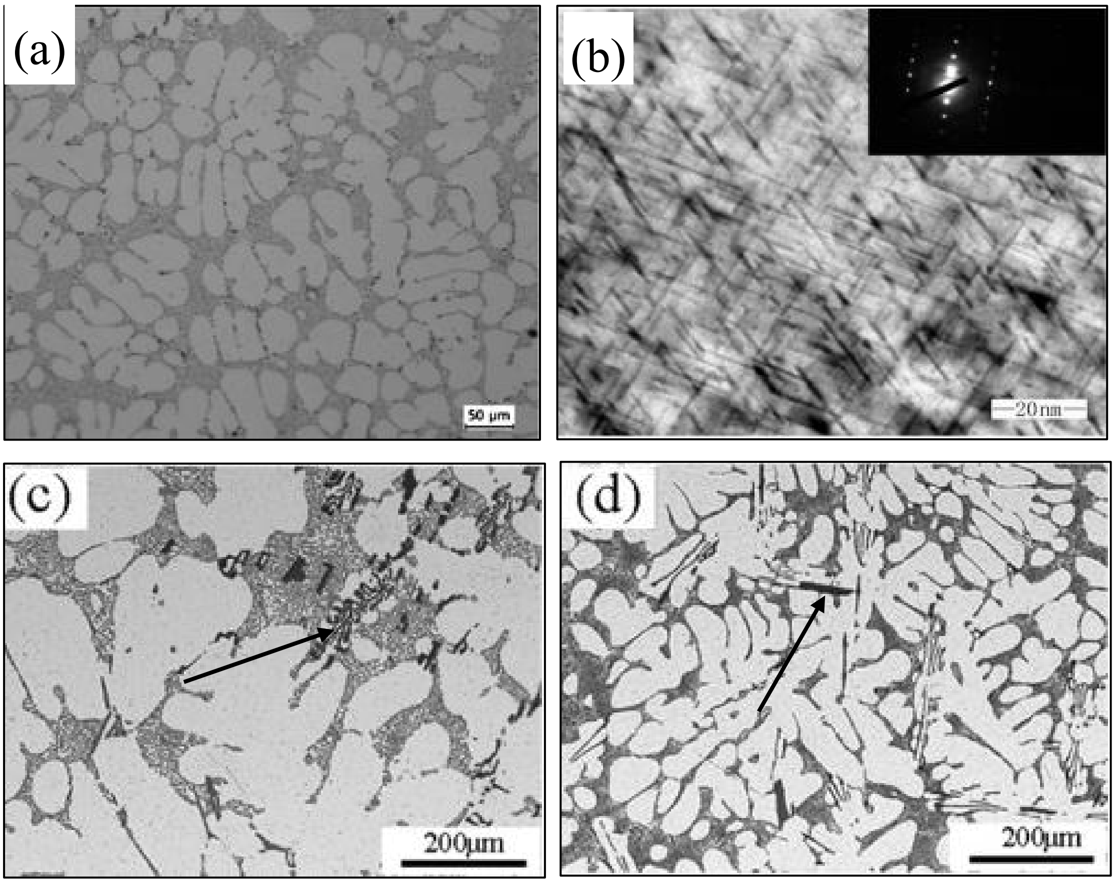

Fig. 2. 5 Typical microstructures of A356 alloy[31, 32, 35].
(a) Optical microscopy of as-cast A356, (b) TEM image showing Mg_2Si in A356-T6, (c) SEM image showing fishbone-like α Fe-rich phase, (d) SEM image showing needle-like β Fe-rich phase

Apart from Mg_2Si precipitation strengthening, adding modifiers into the A356 solution can change the morphology of silicon, refine the grain and improve the properties of the alloy. Na, Sr, Sb and some rare earth elements can play a role of modification in A356 alloy[34, 36-40]. Na can cover the silicon nucleus in the form of NaSi or dispersive colloid point in the Al solution, thus the growth of the crystal nucleus is inhibited. In addition, the addition of Na can increase the undercooling degree of the alloy, so that the coarse acicular silicon phase is modified into spherical and relatively fine silicon, and the (α+Si) eutectic structure changes to α+(α+Si) hypoeutectic structure. Therefore, the comprehensive properties of A356 alloy can be improved by modification. Sr as modifier of A356 have been widely used in Al casting enterprises, because the effective time of refining is long, and it has no pollution to the environment. However, the latency period of Sr modification is long, which can easily cause the hydrogen absorption and form shrinkage pores. Sb can refine the eutectic silicon which is transformed into spherical form by heterogeneous core Mg_3Sb_2, so that the effect of refinement and metamorphism is obvious. However, with the change of cooling rate of casting, the modification effect of Sb is also changed, having better effect for metal die casting than sand casting. Besides, the rare earth elements such as La and Ce are also good modifiers for A356 alloys, but the rare earth elements are easy to oxidize and form brittle compounds with relatively high solution point during the modification process, which results in segregation and damage of mechanical properties.

The mechanical properties of as-cast A356 alloy are low, which cannot meet the needs of application. The comprehensive properties of castings can be improved by heat treatment (shown in Fig. 2. 6)[41]. Heat treatment of has the following main purposes, which are, to improve the comprehensive mechanical properties of the alloy, to eliminate the internal stresses in the castings, and to eliminate the composition and microstructure segregation. A356 alloy castings can be strengthened by solution or solution with artificial aging.

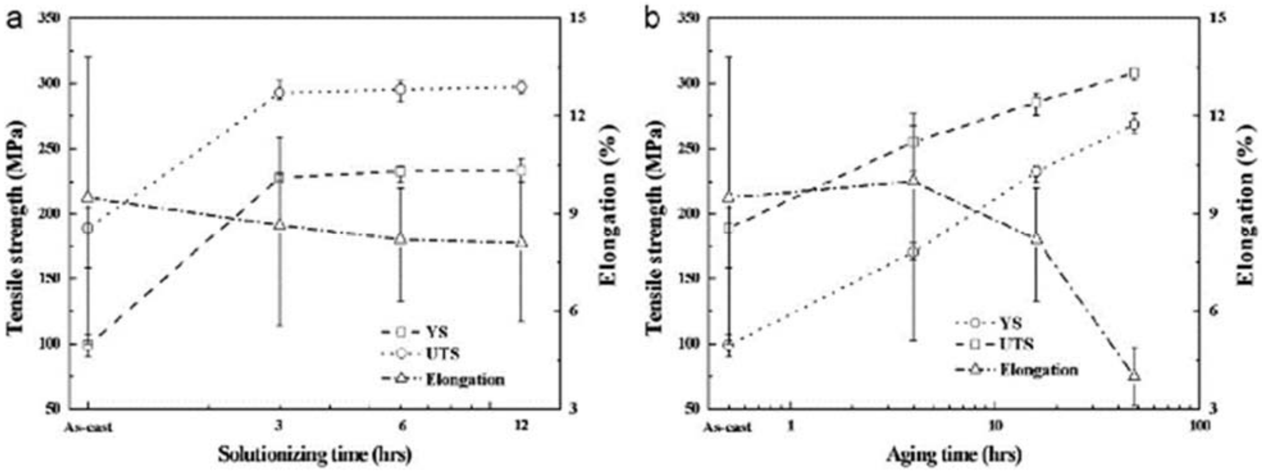

Fig. 2. 6 Variations in the tensile properties as a function of (a) solution and (b) aging time for A356[41].

2.1.4 Pure copper

Copper is a transition element, with the atomic number of 29. Pure copper is a soft metal, with excellent heat and electric conductivity. The elementary substance of copper is in purplish red colour. The melting temperature of copper is 1083°C and the density is 8.9 g.cm^{-3} (solid state), which is approximately three times heavier than aluminium. Pure copper is mainly used to make electrical equipment such as electrical generators, busbars, cables, switchgears, transformers was well as heat conduction equipment including heat exchangers, pipes, plate collectors for solar heating device, etc.

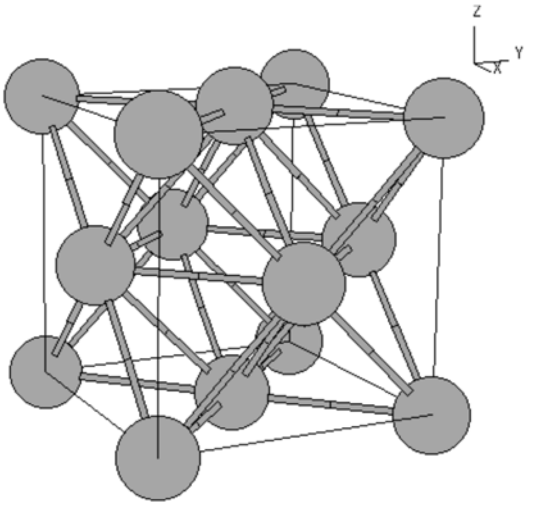

Fig. 2. 7 FCC lattice of copper

Copper has a face centred cubic lattice (FCC, Fig. 2. 7). The grain structure of the cast copper is composed of equiaxed grains of varying sizes. Besides, porosities can be observed in the microstructure because of the hydrogen evolution and shrinkage during the solidification process (Fig. 2. 8 (a)) [42]. However, no defects as gas pores can be detected in the wrought copper morphology, which consists of polyhedral grains with uniform size. In addition, annealing twins can also be observed in the microstructure of wrought copper (Fig. 2. 8 (b)) [42].

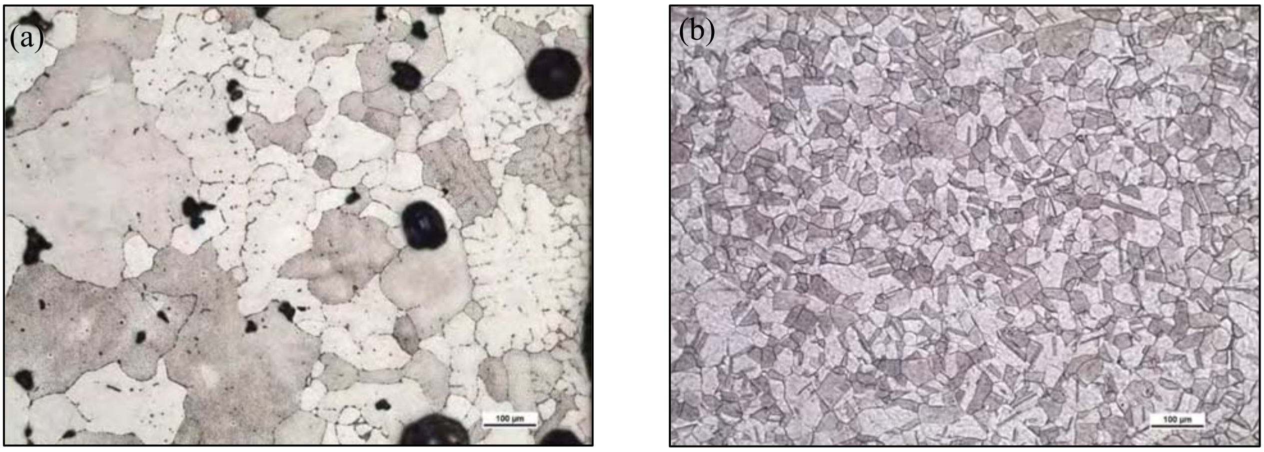

Fig. 2. 8 Microstructures of cast pure copper (a) and wrought pure copper (b)[42].

The mechanical properties of copper depend significantly on the temperature as well as the structure states. As can be seen in Fig. 2. 9, copper has good strength and elongation at room temperature. While, the strength properties decrease significantly with the increasing temperature. Besides, from ~200°C to ~500°C, the ductility of the copper drops and then increases form 500°C with the increasing temperature. Moreover, cold forming can influence the mechanical properties of copper significantly. With the increasing extent of cold forming, the tensile and yield strength increase but ductility decreases.

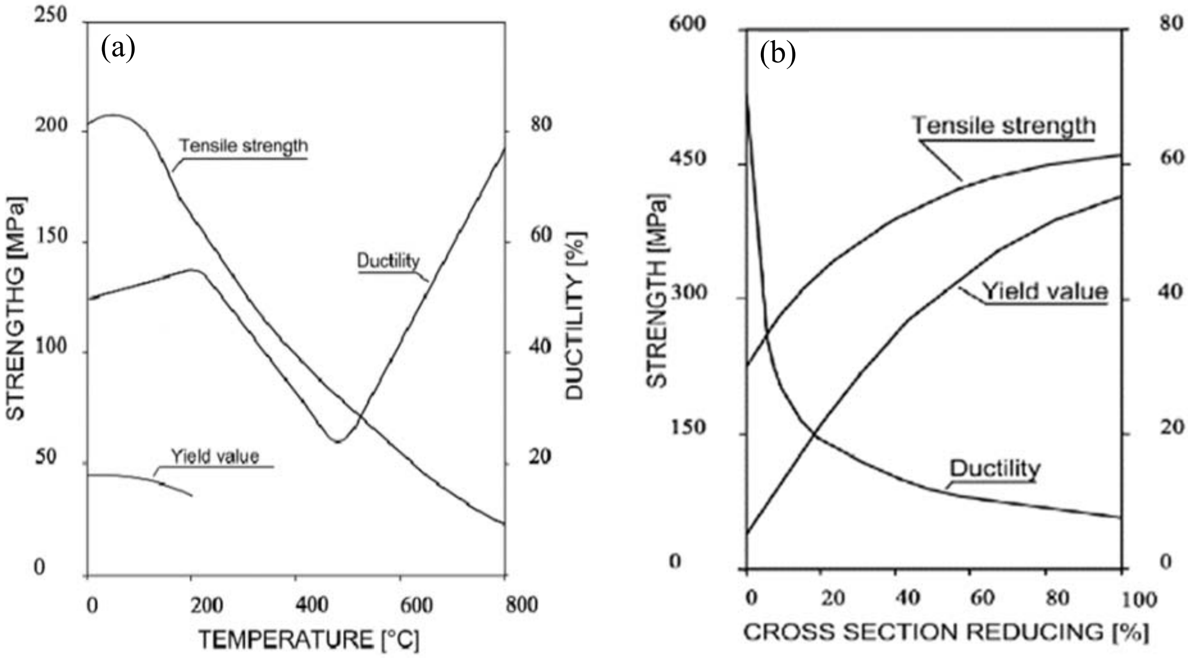

Fig. 2. 9 Mechanical properties of pure copper influenced by temperature (a) and cold forming (b)[42].

2.2 Macro/micro structure and mechanical properties of Al-X friction welds

2.2.1 Structure evolution

2.2.1.a FSW of similar Al alloy

An FSW butt joint can be divided into several zones, according to the extent of deformation and thermal input of the material within each zone. As shown in Fig. 2. 10[43], the microstructure of the base material shows elongated grains, while the centre of the weld, where the material experiences the maximum level of deformation and thermal input, is named as stirring zone (SZ), showing fine equiaxed recrystallised grains. In comparison, the thermal-mechanical affected zone (TMAZ) in the weld is characterised by severely deformed and distorted grains, which exists close to the SZ.

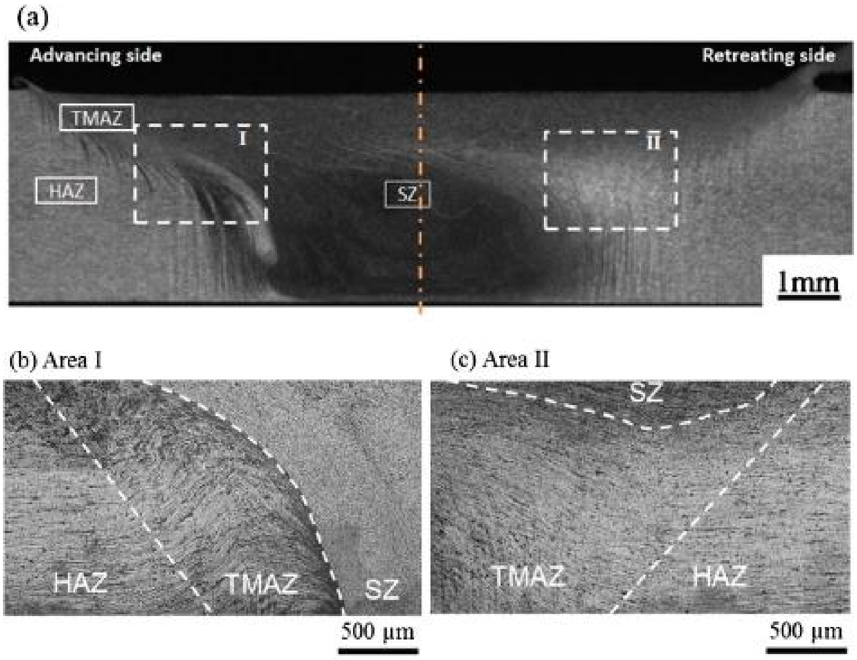

Fig. 2. 10 Transversal section of the weld seam of the Al-Mg-Sc FSW joint by optical microscopy (a) macrograph showing overview of the joint with respective weld zones, (b) the microstructure of the HAZ/ TMAZ of the advancing side and in (c) HAZ/ TMAZ of the retreating side [43].

Fig. 2. 10 displays a typical macro/microstructure profile of an Al alloy FSW cross section, showing the plane vertical to the tool feed direction. As can be seen, the outline of the weld nugget is clearly illustrated, as well as the deformation flow in the TMAZ. Besides, no significant defect is found in the microstructure. However, it is difficult to show the grain boundary using optical microscopy, due to the complex heat and deformation of the weld material during the FSW process, resulting in the nonuniformity in the weld microstructure (Fig. 2. 10 b and c). Based on the temperature trace during the FSW process [44], the material in heat affected zone (HAZ) can reach the temperature from 250°C to 350°C depending on the welding parameter, which determines the heat input (HI) during FSW. Therefore, the phase structure for most aluminium alloys would be influenced in this condition. Furthermore, in the TMAZ, the temperature of the material is measured to reach from 350°C to 450°C and server deformation is accompanied, resulting in torsional elongated and partially recrystallised grains in TMAZ. In the SZ, the temperature is expected to reach above 500°C, which exceeds the recrystallization temperature of Al, so that the entirely recrystallised grains with the size usually less than 10mm are produced. Therefore, it is not possible to measure the grain size of FSW joints by means of optical microscopy, due to the extremely fine grain size in the SZ as well as the low grain boundary contrast in TMAZ and HAZ.

In recent researches, EBSD has been widely used in characterising the grain structures of FSW joints. Etter et.al.[45] used the EBSD technique to investigate the microstructures of FSWed 5251-O plate from BM to SZ. It is shown in Fig. 2. 11 that, the BM grains are around 100μm long and 35μm high in the O sample. In HAZ, the initial grain microstructure of BM is still visible. In TMAZ of the 5251-O, grains are clearly rotated and elongated by plastic deformation. The SZ of the weld is composed of fine recrystallized and equiaxed grains, with the average grain size of 14μm.

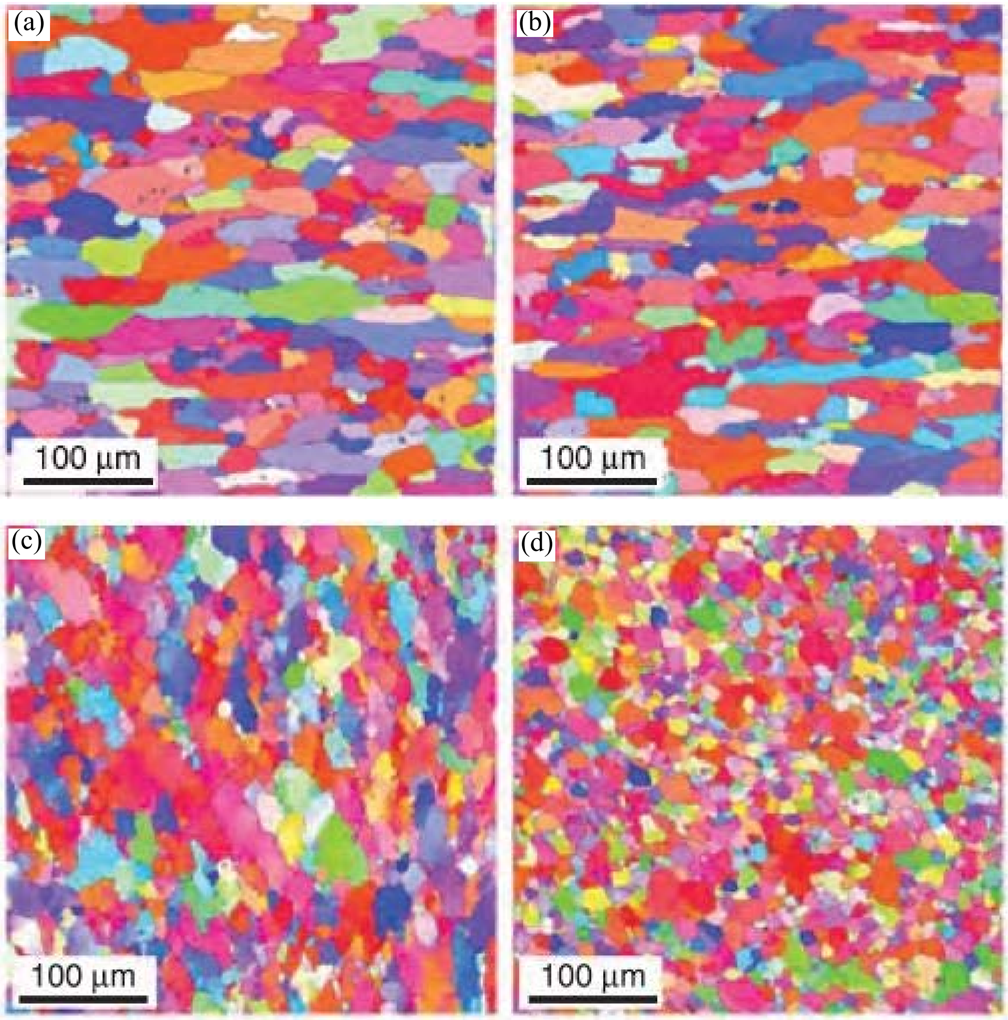

Fig. 2. 11 EBSD images of the FSW 5251-O joint at different regions. (a) BM, (b) HAZ, (c) TMAZ, (d) SZ [45].

2.2.1.b FSW of dissimilar Al alloys

The application of the FSW of aluminium alloys is growing rapidly, especially in the aerospace and automotive fields [46]. The recent researches have focused on the FSW technology for the connection of dissimilar Al alloys, especially a wrought Al alloy and a casting Al alloy, which has been recognized as impossible by traditional fusion welding. It has been found many applications of welding a wrought Al alloy to a casting Al alloy in fabricating airframe, automotive wheel and missile components etc. because the design of the components can be more flexible and efficient by fixing better-performance wrought materials at high loading points [47].

Lee et al. [48] conducted a detailed microstructural experiment of the FSW of A356/Al 6061 dissimilar alloys, and the results showed that the microstructure of the FSW dissimilar alloys is the mixed structures of both materials. The flow behaviour of the materials during FSW procedure was investigated. The results showed that the material of the SZ was mainly composed of the material located at the retreating side (RS) (as shown in Fig. 2. 12[48]). Moreover, as the strength of Al 6061 is much higher than A356, the strength of the welds was better when Al 6061 was located at RS.

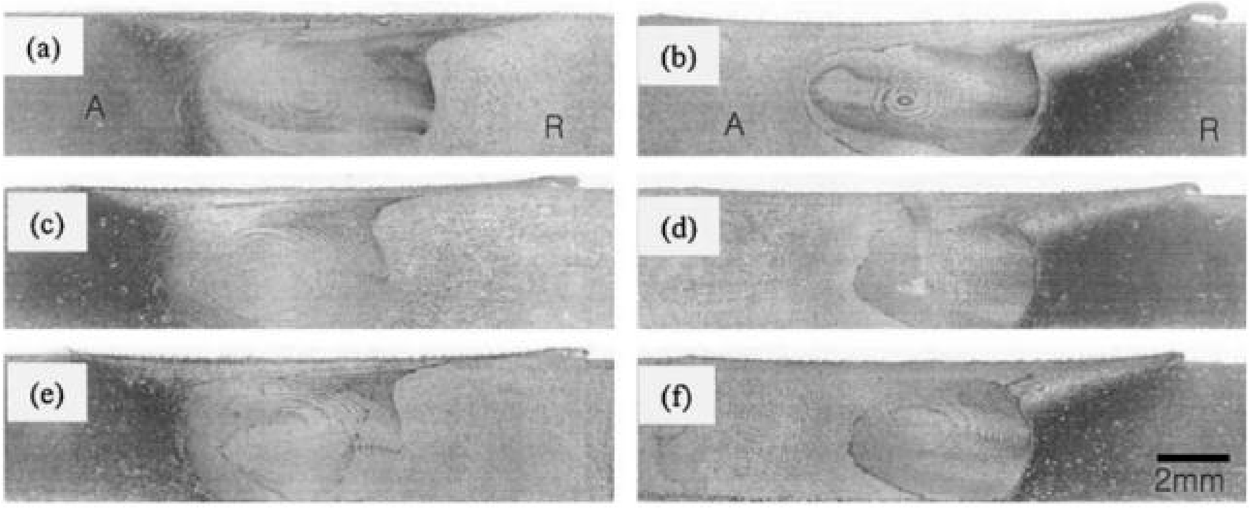

Fig. 2. 12 The macro cross-section views of friction stir weld zone. Left figures are A356 fixed at the retreating side and right figures are 6061 fixed at the retreating side. (R) represents retreating side and (A) represents advancing side[48].

Lap joint configuration is also being widely used in joining aluminium alloy structures in automotive and aerospace components [49]. Therefore, studies have been reported on friction stir lap welding (FSLW) of aluminium alloys [50-52]. Researches shows that it is more difficult in preparing an FSLW joint with well performance compared to the FSW butt joint. Lee et al. [53] prepared AA6061 and AA5052 FSLW welds and researched the microstructures and properties under different parameters. It was found that higher tool rotation angular velocity and/or lower tool traverse line speed which means higher heat input might result in lower material mixing and mechanical properties in welded zones (see Fig. 2. 13).

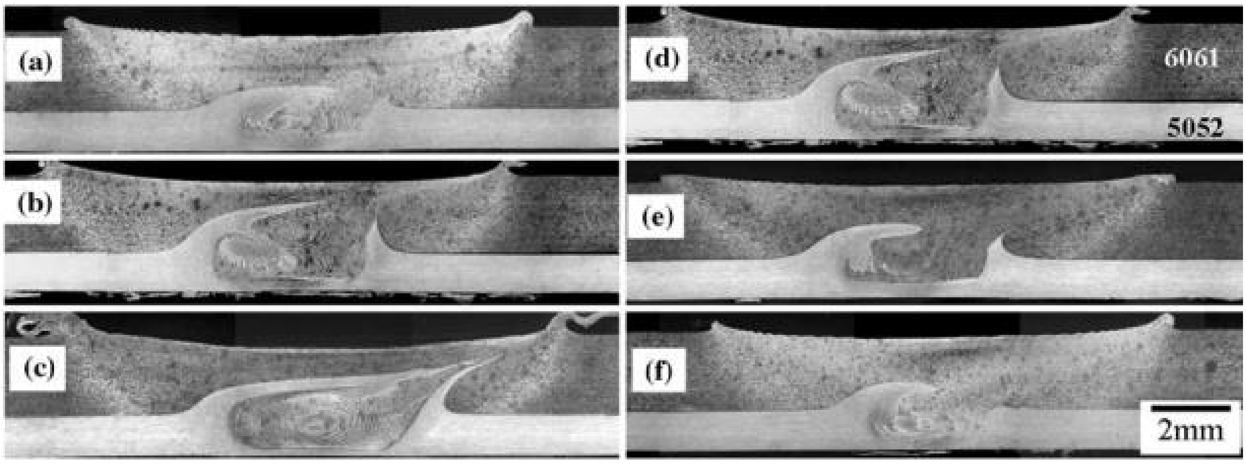

Fig. 2. 13 Optical images of lap-jointed AA6061 and AA5052 with various welding conditions: (a) 1250 rpm, (b) 2,500 rpm, and (c) 3600 rpm at fixed 267 mm/min, while (d) 127 mm/min, (e) 267 mm/min, and (f) 507 mm/min at fixed 1,600 rpm[53].

The lapping interface is an important feature of FSLW of aluminium alloys. Detailed analysis of the lap welds of AA6060 by Yazdanian et al. [54] have been conducted to identify the hooking-related features around the welding interface as well as their influence on the strength of the welds. The effect of rotation speed and welding speed on hook size was studied. It was suggested that the increase of stir zone size as rotation speed increases was the result of increase in temperature of stir zone. The hook size would increase rapidly when the stir zone size increased. It was also found that when the hook size was ＜30% of the plate thickness, the fracture property was not significantly influenced by the hook size, however, when it was ＞30%, the fracture property started to reduce rapidly, with the increasing hook size area.

2.2.1.c LFW weldments

Linear friction welding (LFW) is a rapidly growing solid-state joining process, which has been successfully applied in various components, notably for producing integrated bladed disks assemblies (blisks) in aeroengines[55, 56]. During LFW, the workpieces are firstly brought into contact, followed by oscillating one workpiece, while maintaining the other stationary. Frictional heating, combined with plastic deformation, results in a rapid temperature increase, creating a sideward extrusion of the softened material in the form of the typical “flash” and resulting in an axial shortening in the height of the workpieces, thus achieving consolidation within seconds. The weldments of linear friction welds are shown in Fig. 2. 13[57]. Flash can be seen at the interface, due to the extrusion of the plasticised material during LFW procedure. Besides, with the different materials being welded, the shape of the flash is usually various, because the flowabilities of the plasticised materials are not the same. Therefore, the length or the extent of the flash is different even for the welds of same materials if the welding parameters are changing.

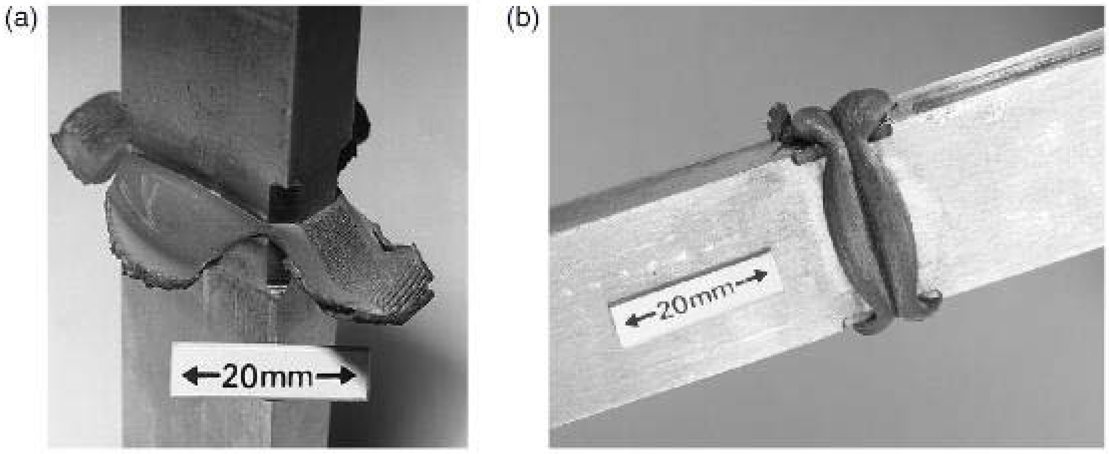

Fig. 2. 14 Linear friction welds of (a) titanium and (b) waspalloy[57].

For linear friction welds, there is no widely accepted nomenclature for microstructural regions, but based on a nomenclature according to the common welding and has been widely accepted for friction stir welding, four regions are defined as base material (BM), heat affected zone (HAZ), thermal-mechanical affected zone (TMAZ), and weld zone (WZ) (maybe slight difference in the statement in different literatures)[57]. BM is the material at some distance from the interface, and no difference is found in microstructure or properties of the BM. HAZ is the region where the microstructure and properties are influenced only by the friction heat, so that no plastic deformation occurs in HAZ. Changes are probably in grain size, hardness, and precipitate morphology, etc. TMAZ is the region where the material has been introduced heat as well as plastic deformation (see Fig. 2. 15 (d)). Moreover, phase transformations might also happen in most Al alloys in TMAZ. SZ has distinctive microstructure in the FSW of Al alloy, with the characterization of extremely fine equiaxed grains (see Fig. 2. 15 (c)), because of recrystallisation, and/or phase transformations [58].

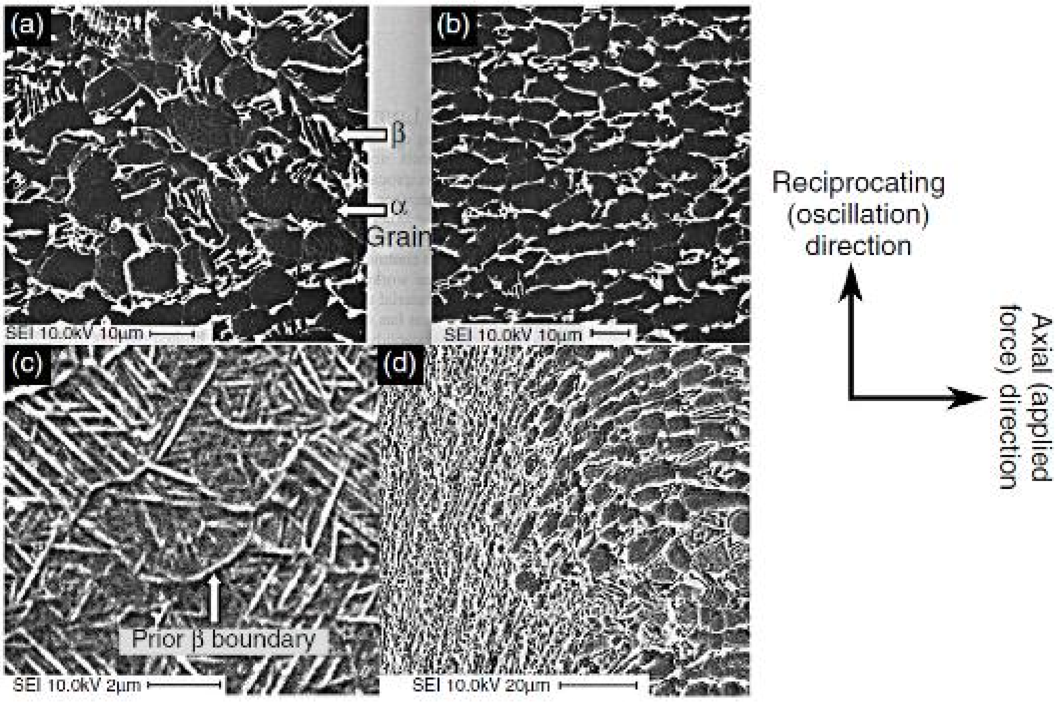

Fig. 2. 15 Microstructure of a Ti-64 linear friction weld. (a) and (b) BM; (c) WZ and (d) TMAZ[58].

2.2.2 Mechanical properties of Al-X friction welds

2.2.2.a Hardness distribution

Aluminium alloys can be divided into heat-treatable Al alloys and non-heat-treatable Al alloys, which have different distributions of hardness throughout the FSW welds [59]. During the FSW process, the heating temperature of the HAZ can usually cause the recovery of the material as well as coarsening of precipitates, resulting in hardness changes. The TMAZ has a significant change in grain size as well as a heat influence, which may show a slightly higher hardness than HAZ due to the work hardening. The SZ has recrystallised grains, where high hardness is detected in heat-treatable Al alloys due to the refinement of precipitates, or low hardness in non-heat-treatable Al alloys due to the recrystallization softening [60].

Therefore, in heat-treatable aluminium alloys, the hardness depends more on the size and distribution of the strengthening phases than on the grain size. Usually, with the increasing temperature or heat input, the hardness of the corresponding zone would decrease due to the dissolution or the size growth of the precipitates [59, 61].

In the FSW joints of heat-treatable 6xxx series Al alloy, the hardness is usually reduced in the SZ. While in the HAZ, the temperature reached would have an over-ageing effect on the material (The BM is usually in T6 peak aging state) as well as a decrease in dislocation density, resulting in the reduction of the local hardness. The TMAZ usually has the lowest hardness throughout the FSW of 6xxx series Al alloy, because of the significant annealing effect in the TMAZ. Furthermore, partial recrystallization happens close to the interface of TMAZ and SZ, which is severer in the advancing side (AS), than the retreating side (RS). Therefore, the minimum hardness is found in the TMAZ close to the RS [62, 63]. Fig. 2. 16 shows the hardness profile of FSW Al 6082-T6. It was found that the average hardness of the weld was approximately 33% lower than the parent material, and the lowest hardness was found in the TMAZ closed to the RS [63, 64].

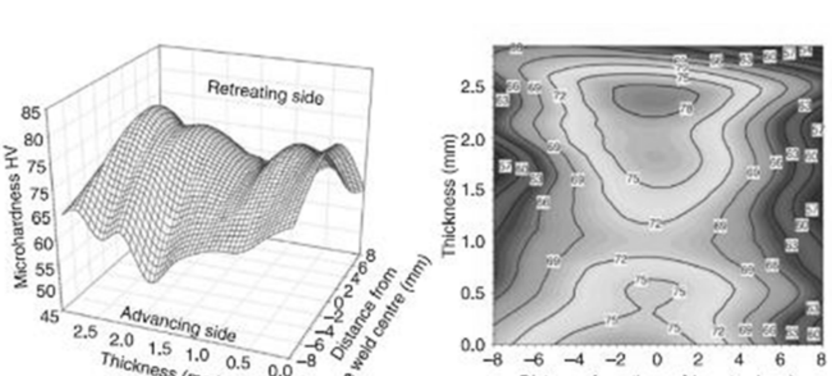

Fig. 2. 16 Hardness profile through the Al6082-T6 FSW joint thickness[64]

However, in the non-heat-treatable aluminium alloys, the hardness of the weld is not softened. Sato et. al. [65] found that in FSW Al1080-O, the hardness in the SZ was slightly higher compared with its parent material, because of the fine grain strengthening due to the presence of recrystallized grains even though the weld zone had a relatively low dislocation density. TMAZ was composed of sub-grain structure, so that the maximum hardness was found in this area. The hardness investigation of Al 5083-O FSW showed that no obvious difference was found throughout the weld, because the hardness of this alloy is determined by the dispersion strengthening [61].

For LFW weldments, the hardness usually depends on whether or not intermetallic is formed at the interface. For example, in the hardness profile for LFW welded 2124Al/25 vol.% SiC_p composite shown in Fig. 2. 17 [66], a decrease can be obviously detected in the welded zone by approximately 10% in respect to the base material, due to the concurrent effect of severe plastic deformation and recrystallization. Besides, the hardness comparation was conducted for the Al2024-Cu LFW welds with or without intermetallics at the interface [67]. The hardness profiles (refer to Fig. 2. 18) show that the width of the interface area is opproximately 300μm. Besides, hardness peaks corresponding to the intermetallics exist in this interface area; while no significant peak is shown in the interfacial zone where the welds are free from intermetallics.

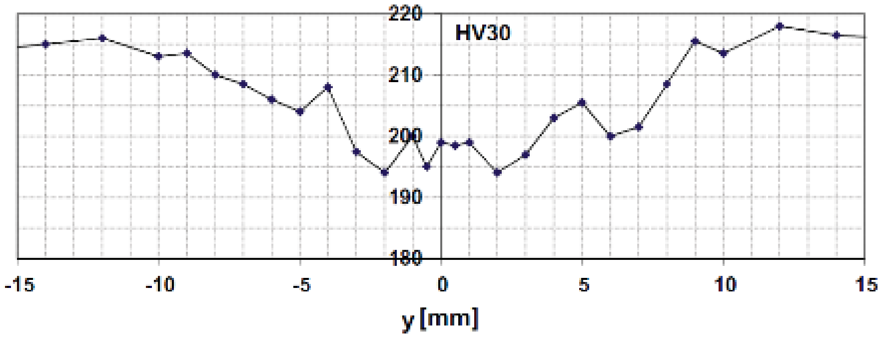

Fig. 2. 17 Hardness profile of 2124Al/SiC$_p$ LFW weld[66].

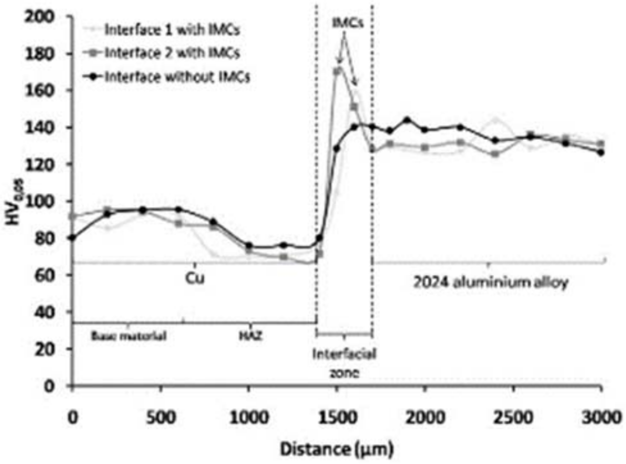

Fig. 2. 18 Microhardness profiles perpendicularly to the interface in the (YZ) transverse cross-section of the Al2024-Cu LFW joint [67].

2.2.2.b Tensile properties

The tensile strength and the ductility of FSW aluminium alloys are commonly lower than the parent metal [68-71]. Because the resistances to the deformation of the welds are inhomogeneous, due to the differences in grain size and precipitate size/distribution in different welding zones.

The FSW heat-treatable aluminium alloys usually have a welding efficiency (σ_W/σ_{BM} %) range from 65 to 96%. However, it is significantly higher than traditional fusion welds [59]. In the tensile tests, the fracture often occurs in the HAZ of the welds particularly for heat-treatable Al alloys, where a marked hardness gradient was observed [72, 73]. Tensile properties are significantly influenced by welding parameters. The research on FSW of Al 2024-T4 FSW found that the tensile strength was enhanced by controlling the ratio of the tool feed rate / tool rotation speed [59]. It was also found that with the decreasing thickness, the aluminium plates often got a higher welding efficiency [59]. Fig. 2. 19 compares the mechanical properties of Al 6082-T6 and Al 6061-T6 butt welding joints prepared by FSW and MIG welding [63]. The FSW joints showed the tensile strength efficiency of 70% and yield strength efficiency of 51%, which were much higher than the MIG welding.

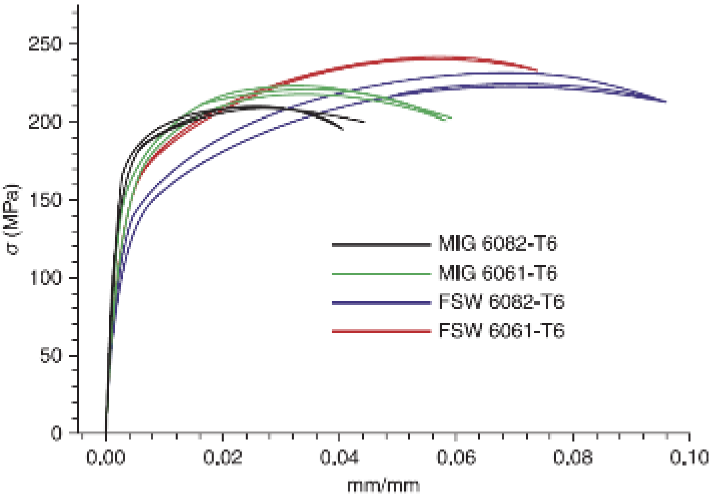

Fig. 2. 19 Tensile deformation curves of MIG and FSW welds of 6082-T6 and 6061-T6 [63].

Most researches have focused on FSW butt welding, however, other configurations including lap-welding, T-welding, etc. can be widely used in the industry. Cederqvist et.al.[74] studied the FSW lap joints for Al 2024-T3 and Al 7075-T6, with various welding parameters, resulting that the welding efficiencies of 86% could be achieved, close to FSW butt joints. FSW lap-welding of Al 2024-T3 was also prepared by Papadopoulos et. al. [75]. It was concluded that the mechanical properties could reach the level of BM if the process was well controlled.

It has been proposed that the FSW of dissimilar Al alloys especially castings and wrought alloys may have wide application prospects in fabricating airframe, automotive wheel and missile components etc. because the design of the components can be more flexible and efficient by fixing better-performance wrought materials at high loading points [76]. There are researches on mechanical properties of FSWed between a wrought Al alloy and a cast Al alloy in the literature. Lederich et al. found in an FSW of casting D357 and wrought Al 2024 that it has an extremely low tensile elongation for the weld [77]. Lim et al. explained this extremely low tensile properties referred to the FSW of dissimilar metals by researching the tensile behaviour of FSWed A356-T6/Al6061-T651 bi-alloy plate. The results showed that the tensile elongation of the FSWed bi-alloy plate was significantly lower than that of the base metal and the FSW of the same material of A356-T6 and Al 6061-T651. In the FSW of dissimilar alloy plates, the cluster of Si particles was detected locally around the fracture, which appeared to be as an initiation of fracture during the tensile process (see Fig. 2. 20) [77].

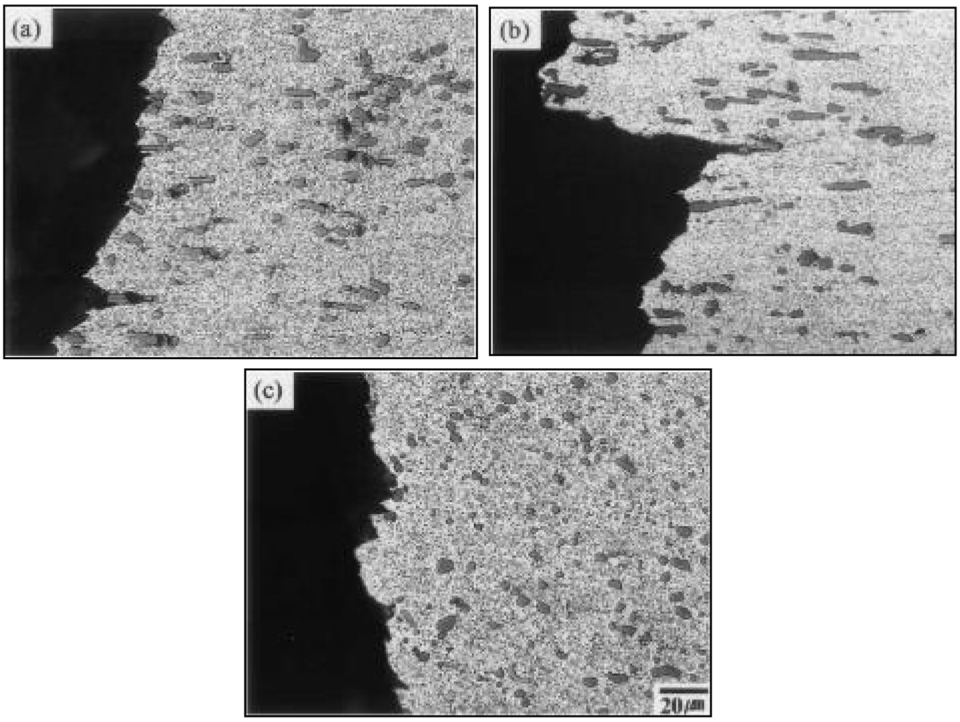

Fig. 2. 20 Microscopic cross-sectional views of the FSWed samples [77].
(a) 6061-A356 FSW, fracture in A356 side, (b) 6061-A356 FSW, fracture in zigzagged boundary, (c) A356-A356 FSW

Besides, the present study of A356-Al6061 FSW revealed that the fragmented eutectic Si particles in the weld zone of A356 side would have a significant influence on the Al6061 side, by means of the precipitation of acicular Si particles [77].

Ghosh et al. [78] conducted a detailed research on the influence of process parameters on the microstructure and properties of FSWed AA6061 and A356, under different tool rotation and traversing speed. It was found that tool rotation speed and feed rate have significant influences on the microstructure of welds. Welding at low rotation and traversing speed of the tool resulted in the refinement of the AA6061 grain size, reduction in residual stress, decrease of recovery–recrystallization effect, as well as the improvement of Si phase distribution, etc. Therefore, all these factors have synergistic effect in improving the mechanical properties of the dissimilar welds. Tehyo et al. [79, 80] prepared SSM356-6061 FSW joints and research the effect of the welding parameters on the properties of welds. The results showed that high tool rotation speed resulted in the increase of the ultimate tensile strength for SSM356. Besides, the elongation increased with the increasing tool rotation speed. The optimised welding parameters was found at the tool rotation speed of 2000 rpm and the tool feed rate of 80 mm/min.

Linear friction welds of similar Al-base alloys usually have acceptable mechanical properties compared with fusion welding than the base material. In 8009 [81] aluminium alloy (Al-Fe-V-Si) LFW joints, a slightly decrease of 14-16% was shown in strength at the welding interface compared with the base material. The over-aging or dissolution effect on the strengthening phases during the LFW process could be significant resulting in the reduction of the welding strength. Welds in AA5083–O (non-age-hardening and fully annealed) showed increased strength at the welding interface compared with the base material [57]. Besides, the LFW of aluminium matrix composites have also been reported [82-84], and results showed that the welds have good tensile properties. For example, in Al2124/SiC_p LFW joints [83], it was reported that the ultimate tensile strength was 82% compared to the base material, and the decrease was due to the heavily orientated plastic flow characteristic of the TMAZ.

However, it shows relatively poor strength of LFW joints for Al-X dissimilar materials, for example of Al-Mg LFW and Al-Cu LFW joints which have significant potential in automotive applications [85].

2.2.2.c Fatigue properties

The fatigue property of FSW joints is generally worse than that of the base materials in the same testing conditions. It was found in many studies that the fatigue property of 2024 [86], 6061 [87] and 7475 [88] FSW joints could get the similarity level than the base alloys, however, for most Al alloy materials, the fatigue property of FSW joints was significantly lower. Nonetheless, the fatigue property of the FSW Al alloys has far exceeded that of traditional fusion welds such as MIG welding etc. (see Fig. 2. 21 [89]).

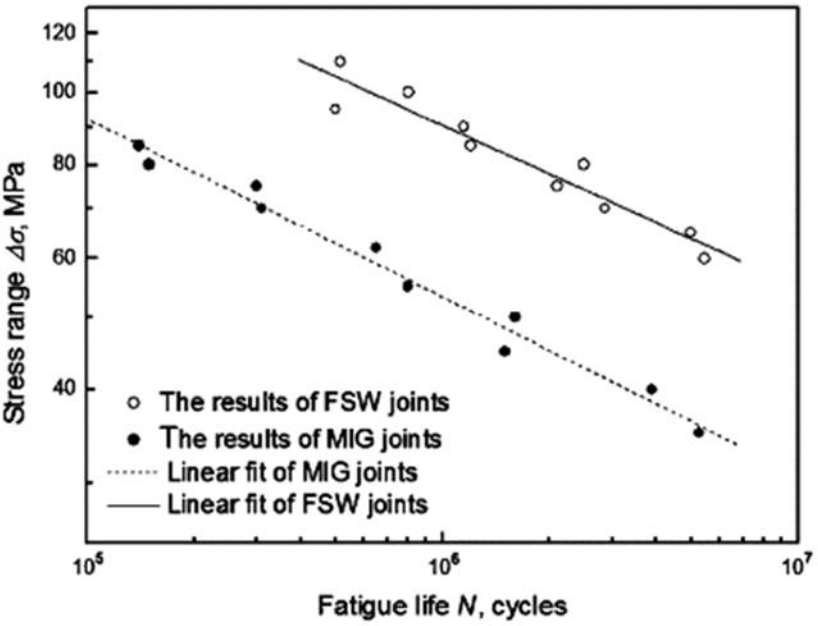

Fig. 2. 21 S–N curves of the joints of MIG and FSW of Al 5083 [89].

In general, three aspects trends to play a significant role in the fatigue property of the FSW joints, which are microstructure, defects and residual stress. It was well recognised that the refined recrystallised microstructure of FSW could result in the improvement of fatigue property than the coarse casting microstructure for fusion welds. Besides, the defects in FSW joints can significantly influence the fatigue property [90]. Fig. 2. 22 shows the typical fatigue fracture surface of the friction stir welding joint with a large planar defect [91]. James et al. [92] found that the onion ring defect, which usually locates in the SZ, could accelerate the propagation of the cracks in Al 5083. Dickerson and Przydatek [93] suggested that a less than 0.35 mm depth of the root flaws in FSW joints could not significantly influence the fatigue property compared with the welds with no flaw defects. It was also found that process parameters could not play an important role in determining the fatigue property of the FSW joints. Moreover, residual stress is the most significant factor on influencing the fatigue property because the fatigue crack propagation is strongly affected by the R value (maximum/minimum stress ratio) during the fatigue test, if the residual stress was considered, the change of R value could be detected, resulting in the acceleration of the fatigue propagation [94].

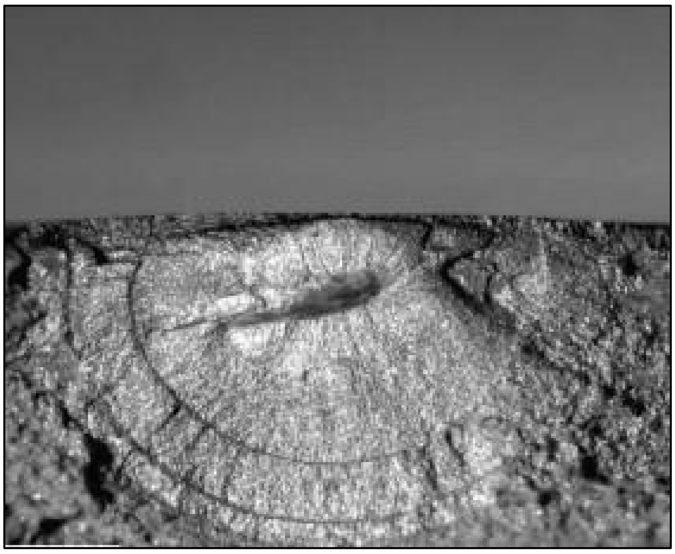

Fig. 2. 22 Large planar defect on the fracture surface of a weld made in 5083-H321 alloy[91].

A number of studies have been referred to the fatigue behaviour of FSW 5xxx series alloys. James et al. [92] found that fatigue lives could be influenced by tool travel speed, and high fatigue property could be obtained by decreasing the tool travel speed. Moreover, it was also found that the onion ring defects may act to reduce the fatigue life. Zhou et al.[95] found that the kissing bond would significantly affect the fatigue properties of the FSW Al5083 (see Fig. 2. 23). The crack initiation was found from the root tip of the kissing bond, and the crack path was exactly along the kissing bond defect. Apart from 5xxx alloy, the fatigue properties of FSW 6xxx series alloys were also widely investigated mostly for 6056 [96, 97], 6061[98] and 6082[99] alloys. It has been found that the dynamically recrystallised grains could restrict the fatigue crack propagation compared to the parent metal microstructure which are usually elongated grains.

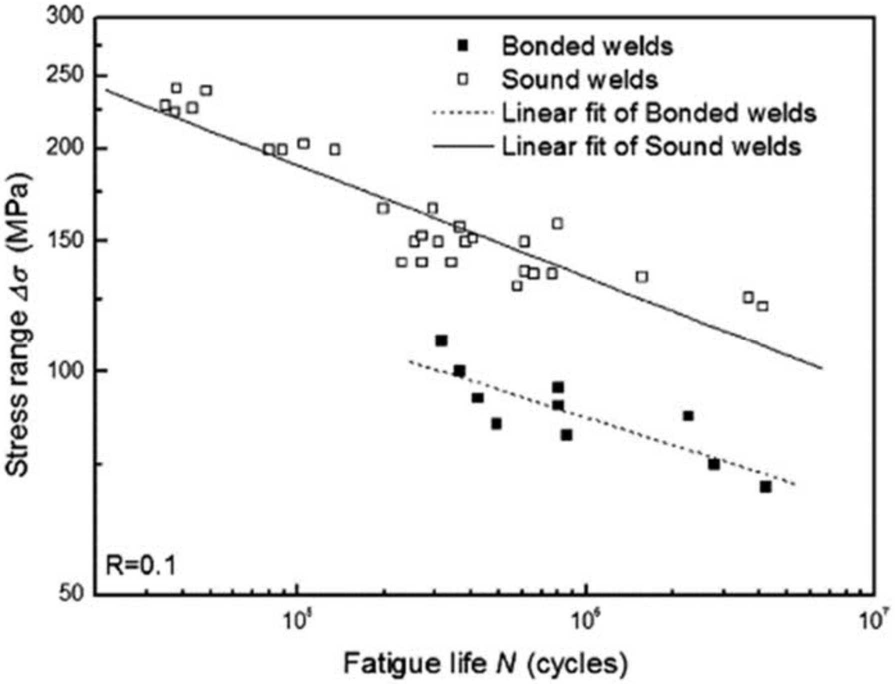

Fig. 2. 23 S-N curves of sound welds and the welds with kissing bond (Al5083)[95].

Compared to the friction stir butt welds, there is much less information accessible on FSLW. However, recent work by Huang et al. [100] found that optimised tool design could have a significant improvement on the FSLW joints because it can increase the volume of the material around the interface and can also decrease the hooking defect. Besides, Cantin et al. [101] also got the results for FSLW in Al 5083 by an optimise designed tool. It was found that using complex-structured tool could improve the properties of FSLW joints. Fersini et al. [102] has considered both straight line defect and hooking as cracks with the aim of the prediction for the fatigue life using FEM, finding that the fatigue lifetime is the time for crack propagation to a certain length.

2.3 Defects in the friction welds

As a solid-state joining method, friction welding does not suffer from the defects related to fusion welding such as porosity or slag. Because no melting occurs for the base material in the weld zone during the friction welding process.

Friction welding can be considered as a hot working process of the material. During the friction welding process, heat is required to promote the deformation of the material, but can also reform the microstructure through recovery, recrystallisation, grain growth and reorientation. As a result, the welding joint generally has different zones according to the extent of heat and deformation the material suffered, which means inhomogeneous in the weld zone, and therefore trends to form the defects [103]. Hence, if the friction welding process is in the condition of too hot or too cold, defects could occur during the process [104]. In terms of achieving the mass balance in the friction welding process, the control of material flow is necessary, generally in the way of control the heat input in the welding process, and fundamentally the welding parameters. For example, in FSW, low heat input may result in the insufficient material flow which leads to the defects of non-bonding, volumetric or void formation, while a too high heat input can lead to the defects of flash, the nugget collapse, as well as other microstructure changes as grain growth, etc. which can reduce the mechanical properties [104].

These defects which are significantly affected by welding parameters can usually be observed in macroscopic view. However, there is another type of defects which cannot be detected in macroscopic view. These joints, which are occasionally comparable with defect free joints, contain micro-scale defects as oxide layers within the weld nugget, as well as the intermetallics generated during friction welding process, etc. [50, 105-107]

The images of common defects in friction stir welds are shown in Fig. 2. 24. Many investigations have found that both macro-scale defects and micro-scale defects can affect the static and dynamic properties of the weld, in various degrees, compared to the base material, see Fig. 2. 25 and Fig. 2. 26[104].

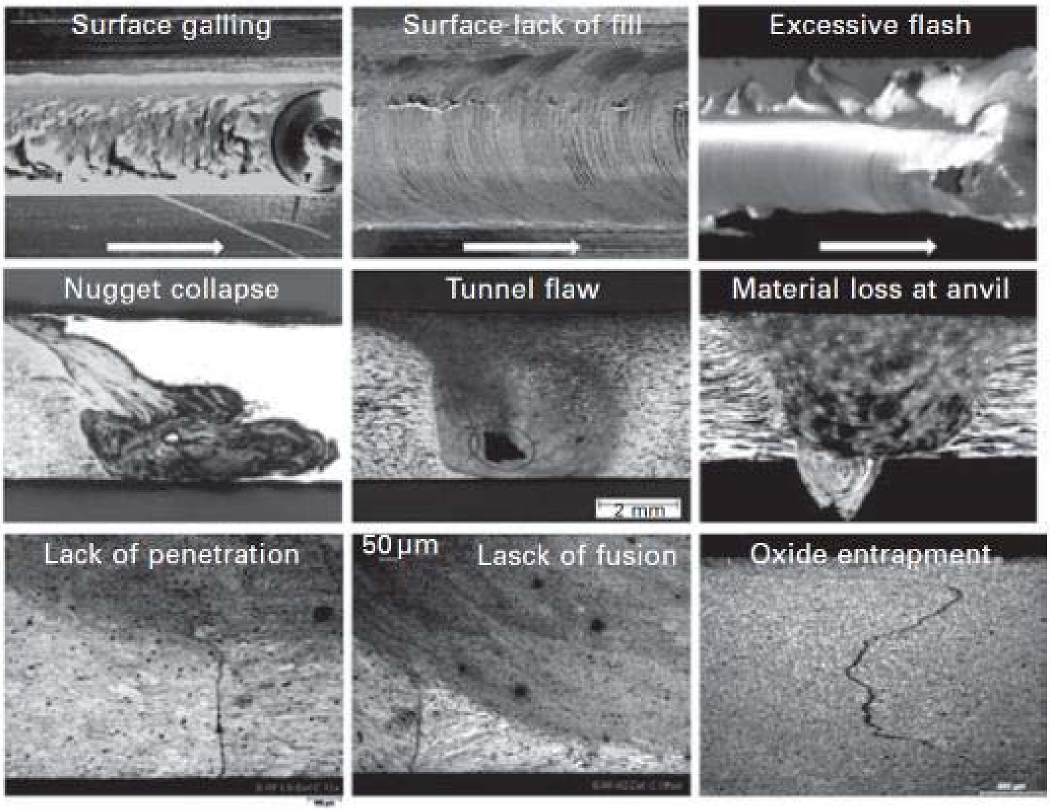

Fig. 2. 24 Defects in friction stir welds[104].

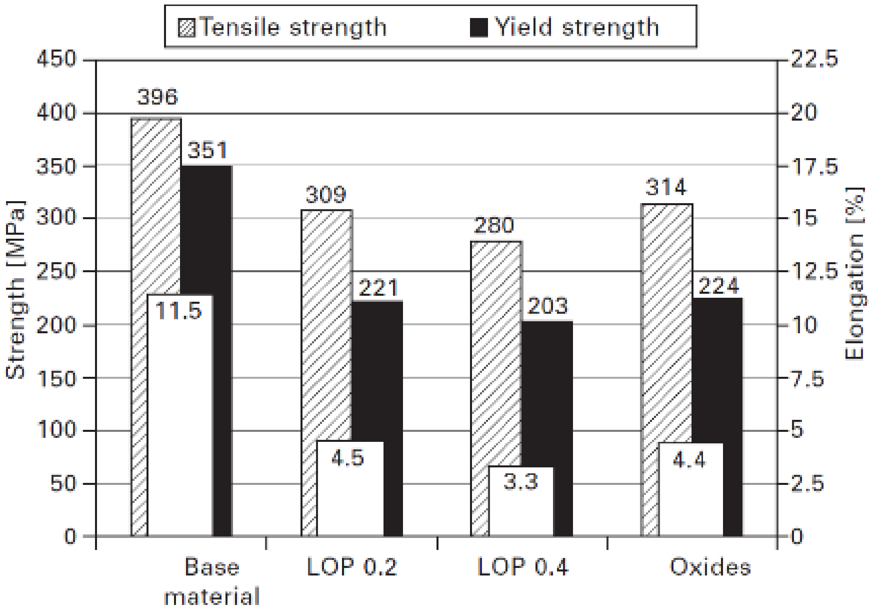

Fig. 2. 25 The tensile properties of friction stir welded aluminium alloy 6013-T6 for LOP (lack of penetration) and oxide defect compared against the parent alloy[104].

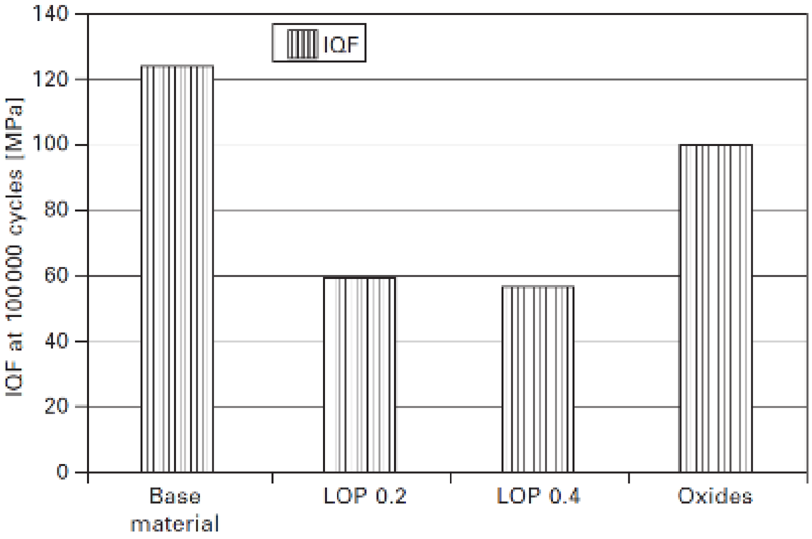

Fig. 2. 26 Index of weld quality with reference to the fatigue properties (IQF) of friction stir welded aluminium alloy 6013-T6 for LOP and oxide defect compared against the parent alloy[104].

2.3.1 Macro-scale defects

- **Tunnel defect**

A typical microstructure of void defect at the advancing side of a friction stir weld is shown in Fig. 2. 27a. Similar microstructure can also be detected near pin base position (Fig. 2. 27b) [108]. This kind of continuous tunnel defect can be controlled through the tool tilt or the optimization of the tool geometry. Fig. 2. 27c shows another form of void defect near the weld surface [109]. Generally, these defects above are not on the surface of the weld, so they cannot be observed visually or through surface inspection. However, X ray inspection NDT can easily detect these defects. Void defect or named tunnel defect for the whole length of the weld can be attributed to a number of reasons, including relatively lower weld pressure, over speed of tool feeding, insufficient tool rotation speed, or failed in controlling the gap between the two plates [110]. When the weld pressure is low, the weld would not get enough forging force from the tool shoulder in well connection. When welding at a too high feed speed, or a too slow tool rotation speed, the weld plates would not get enough stir effect, hence, the material cannot receive enough heat or temperature for plasticising, which lead to the incomplete connection [110, 111]. Colegrove and Shercliff [108] found that the tunnel defect shown in Fig. 2. 27b formed near the base of the pin was due to insufficient forging of the tool shoulder, and it can be solved through using the rounded tool without thread [112].

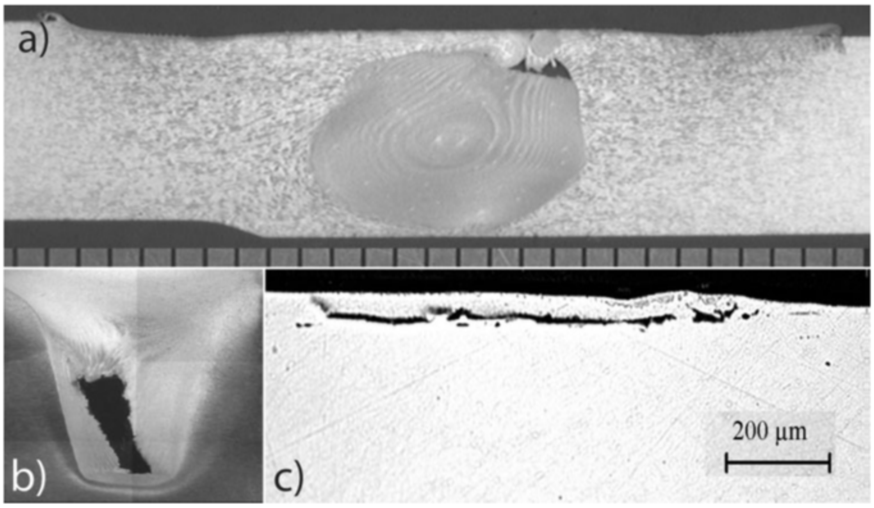

Fig. 2. 27 Characteristic void flaws in friction stir welds [109]:
(a) volumetric flaw; (b) tunnel defect; (c) surface defect

Mathematical modelling has been introduced to predict the presence of tunnel defects of the friction stir welding joints [108, 113]. Bendzsak et al. [113] illustrated the ‘chaotic’ motion at the interface of the two weld plates in FSW. The models predicted the material flow of this zone close to the advancing side, and found that the origin of tunnel defects was at the interface towards the advancing side [108]. The defects were due to the unsuitable welding parameters, including over speed of tool feed or too low speed of tool rotation. It was found that when the tool feed rate increased, or the tool rotation speed decreased furtherly, the tunnel detect would be enlarged and moved to the top surface, therefore a groove defect formed [114]. FSW could be considered as such a process which a void formed behind the welding tool and afterwards filled quickly by the plasticised material pushed by the following turning of the tool. When the welding parameter was not appropriated, the void could fail to be filled to form the tunnel [115]. Crawford et al. [116] found that the tunnel defect was easy to form under the condition of low tool rotation speed relative to the weld feed rate [116]. It was also found that under similar welding conditions, tunnel defect could not be detected when tapered or cylindrical pins with threads was used, because the thread was benefit to push the plasticised material.

- **Voids**

Voids is a common defect in friction welding. Large voids can occur when the choice of tool and weld parameters is unsuitable [117], while small voids occur due to the plastic flow of the material in the stir zone. It was proposed that a spot in the stir zone above and below where the material flow is in opposite directions, formed a vortex, which could result in the creation of voids in the stir zone, possibly affecting the quality of the weld. It was indicated that the vortex generation may provide one mechanism underlying voiding in the interior of the weld nugget, while a second mechanism arises from the complex plastic deformation processes involved in entrainment and mixing of dual streams of deformed material and the overall behaviour of the plasticised zone in the metal [118].

Voids could significantly affect the mechanical properties of the friction stir welds especially fatigue behaviour [119]. It was reported that voids are often associated with the initiation of fatigue cracks and Fig. 2. 28 indicates this association for 4-mm diameter specimen of 5083-H321 aluminium alloy tested in reversed bend at a peak stress of 136 MPa. The influence of the void cluster on the fatigue strength of that particular welded specimen is evident in Fig. 2. 29; fatigue life has been reduced to that found for defect-free specimens at an applied stress 30% higher (180 MPa).

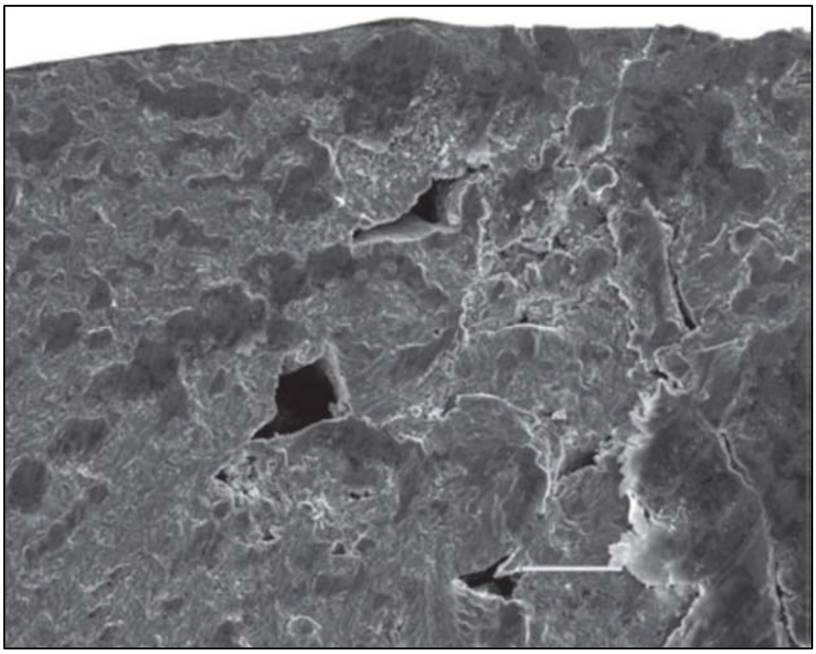

Fig. 2. 28 Association of voids with fatigue crack initiation site in reversed bend loading of 5083-H321 aluminium alloy at 136 MPa peak stress[104].

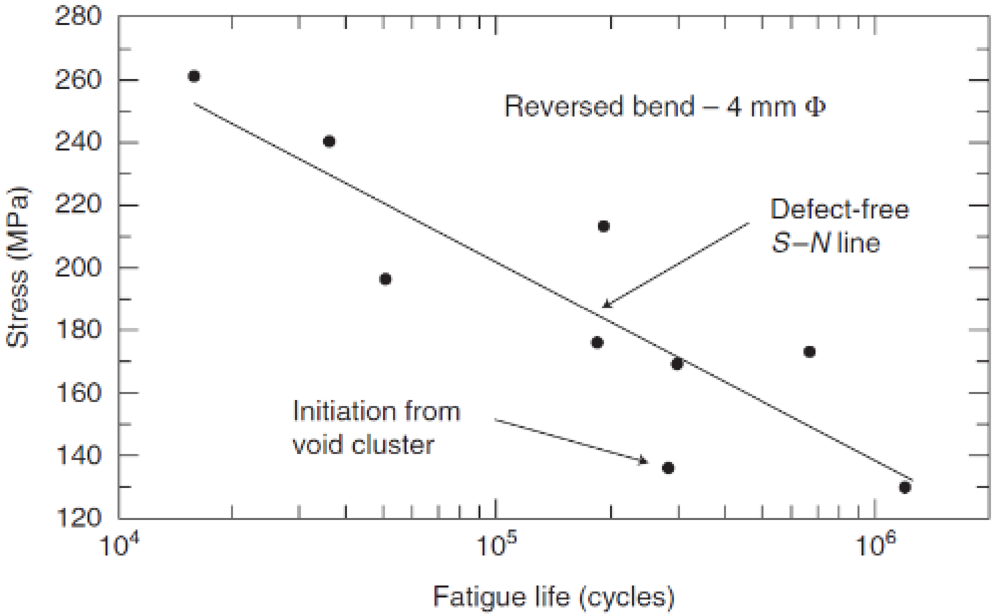

Fig. 2. 29 Influence of void cluster on fatigue strength of 4-mm diameter FS welded specimen of 5083-H321 aluminium alloy; fatigue life for the specimen tested at 136 MPa has been reduced to that found for defect-free specimens at an applied stress 30% higher (180 MPa)[104].

2.3.2 Micro-scale defects

A number of studies have considered the FSW defects that arise as a consequence of material flow mechanisms around the tool or of welding parameters including tool tilt or penetration into the joint (which has, of necessity, to be less than the full-plate depth). Commonly occurring defects are, for example, lack of penetration as well as root defect, that are also known as ‘kissing bond’, ‘lazy-S’ or zigzag defect [120-122]. However, other plasticity-related defects can occur in strain hardening alloys which appear to be contingent upon alloy and strain condition. These fall into the category of partial bonds but occur in the interior of the weld nugget, often as regular sequences related to the tool pitch and have been described as ‘onion skin’ or planar defects [123-125]. Besides, for the friction welding of dissimilar materials or alloys, intermetallics could generate during the welding process due to the friction heat. In most cases, these intermetallics could be considered as a defect because it can significantly affect the properties in most cases [126]. Compared to macro-scale defects, these micro-scale defects are unable to be detected through NDT and difficult to be eliminated by optimising the welding parameters.

- **Lack of penetration**

Tool penetration is commonly approximately 90–95% of the plate thickness, so, lack of penetration defects can occur if the plate has uneven thickness along the weld line or the plate is bowed. Tool penetration problems lead to extruded flash at the root of the weld near the pin if the tool depth is too high and to long root grooves towards the advancing side of the weld if the pin is too short. Extra problems can arise if the distance between plates is not strictly controlled [127-129]. Unpublished work by the present authors has indicated that a gap of around 5% of the plate thickness leads to a reduction in fatigue strength of some 10% at a fatigue life of 106 cycles. The induced defects are large voids and partial bonding which significantly reduce the fatigue crack initiation period. Chen et al. [130] also note that the generation of root defects is assisted by very small tool tilt angle (≤1.5°) and by higher angles (≥4.5°). They attribute this to influences of tool tilt angle on heat input and forging force and hence on the position of defects in the weld. At low tilt angles they postulate that there is insufficient downwards forging of the plasticised material leading to a root groove from lack of penetration. At larger tool tilt angles, weld flash can be generated on the retreating side with insufficient plasticised metal remaining to fill up the void left in the stir zone.

- **Joint line features**

Joint line feature is a kind of micro-scale structure characterization usually located through the weld cross-section, originating between the butt weld plates. These structure characterizations which are considered as defects have been reported by several researches commonly for most aluminium alloys [131, 132]. It was found that these defects are consist of Al oxides and maybe hydroxides which are generated due to the aluminium-based material contact with ambient atmosphere [133]. Therefore, during FSW process, the surface which includes oxides is segregated, at the same time, stirred into the weld. Because of the very thin layers as the oxides, the joint line feature is difficult to be detected by X-ray NDT but can be easily observed by optical microscopy. It often seems as a very thin zigzag curve [134]. Fig. 2. 30 shows the example of such features, which can be little more than a string of inadequately dispersed oxide particles, originating from the surfaces of the butt-welding plates.

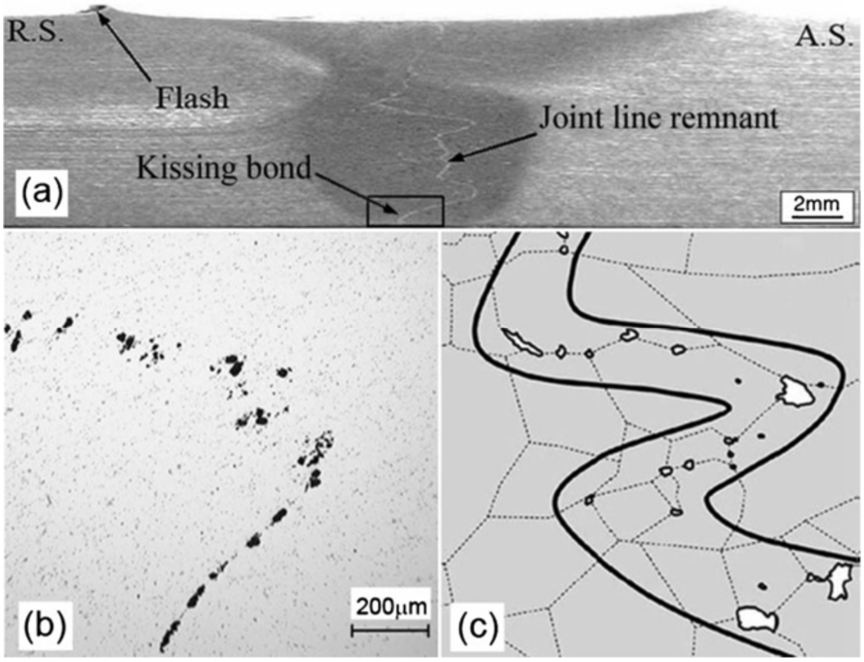

Fig. 2. 30 Joint line remnant in friction stir welds[135]
(a) oxide defect, (b) magnified view showing increased oxide inclusion level, (c) schematic of joint line remnant

Sato [127], Okamura [132] and Staniek [136] have investigated these defects of FSW Al alloy by means of electrical microscopy technology. Sato et al. [127] confirmed the joint line feature using TEM as Al_2O_3 particles. It was also found that the joint line feature was formed due to the presence of the natural aluminium oxide on the surfaces of the welding plates [132]. Moreover, the extent of the joint line feature could be influenced by the welding parameters, for example, increasing the welding speed can decrease oxide stirring into the weld [134]. Besides, the optimization of tool geometry could also help limiting these defects [132]. Consequently, if well controlled, the joint line feature could be innocuous to the weld quality [137]. In other studies, marking material experiments were used for tracing the surface material of the butt plates during the FSW procedure, suggesting that the final position of the initial surface shows a zigzag line [138, 139].

It is well recognized that the depth of penetration of the welding tool is significant for the material mixing throughout the full thickness of the welding plates. If the incorrect length of tool pin is used, for example, too short, the root place of the plates would not be well connected, remaining a root flaw, which is the origin of the joint line defect, or seriously, a complete lack of bonding [109] (Fig. 2. 31). In this situation, the welding quality improves close to the SZ. Consequently, a transition region forms as a weak bond, which is commonly known as a ‘kissing bond’, becoming widely accepted.

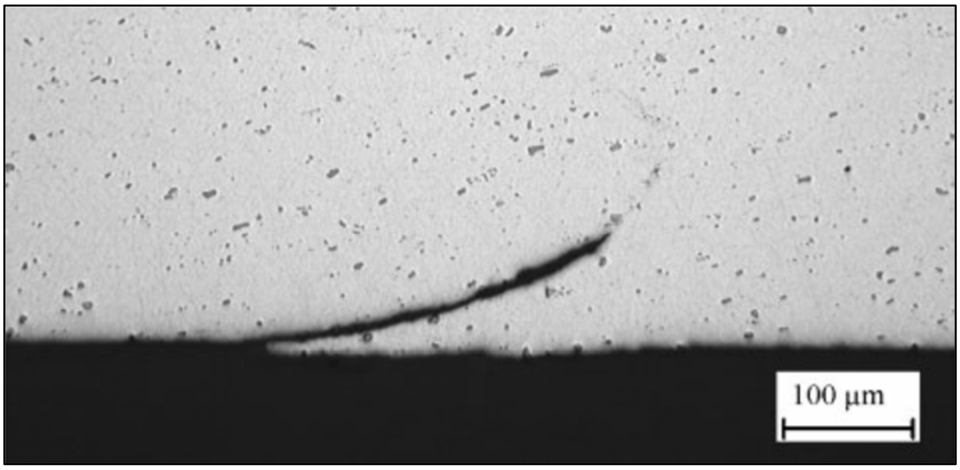

Fig. 2. 31 Characteristic root flaw in FSW 2014A caused by using a too short pin in 5083 alloy[109]

How the joint line defect or kissing bond affects the mechanical properties of the FSW joints have been widely investigated, but no unified conclusion has been reached due to the limitation of reliable methodology. Most researches have been found that the kissing bond is harmful to the mechanical properties of the welds. Zhou et al. [135] investigated the fatigue property of the FSW joints and found that, kissing bond can lead to 20–40 times shorter fatigue lives for Al 5083 welds and 30–80 times shorter lives for Al 2024 welds. The fatigue fracture surfaces results revealed that the welds fractured from the root tip. Fig. 2. 32 shows a tyipical microstrcture of a fracture from kissing bond root tip [109]. Le Jolu et al. [140] found the kissing bond defect in Al–Cu–Li alloy FSW joints, which significantly affect the fatigue property of the welds compared to the sound welds. While, Kadlec et al. [88] measured the size of kissing bond in FSW AA 7475 and found that kissing bond with large sizes had limited influence on the mechanical properties compared to the sound welds. Moreover, in FSW AA2024-T351 alloy, it was found that the kissing bond could not influence the mechanical properties as well as fracture behaviour compared to the sound welds [141].

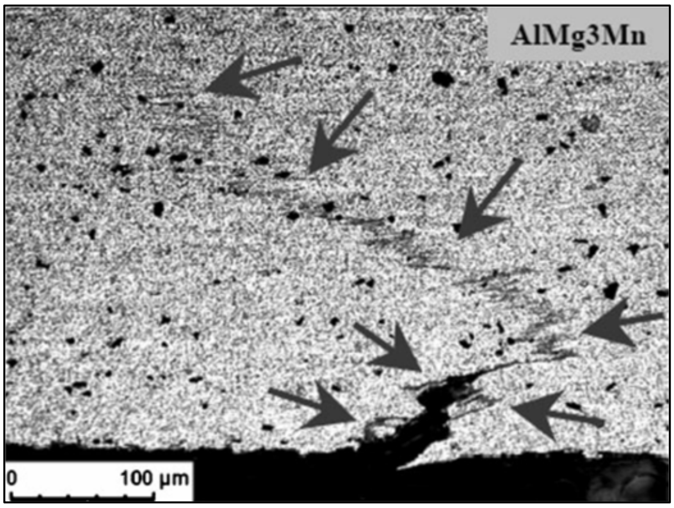

Fig. 2. 32 Cross-section of 5454 FSW specimen with crack after tensile test along kissing bond[109]

Systematically investigation [104] on the influence of natural surface extent on the FSW defects was carried out using the method, by which an oxidation pre-treatment was conducted to create the oxide layers with different thickness on the surface of the welding plates, and then, compared the results before and after FSW. It was found that, the welding plates having relatively thin surface layers could generate only a slight and faint root defect. Moreover, no evidence of nugget defect was detected for these welds. On the contrary, the welds with thick oxide layers showed very server root and nugget defects in the SZ. It was also found that the root defect was straight vertical to the weld surface, originating from the bottom in a distance of several 100 mm, before bending to the retreating side of the welds (Fig. 2. 33).

Therefore, it was suggested that oxidation occurs during the process of FSW. In the present study, however, it was shown that the joint line features inside the welds were originated from the oxide layers of the welding plates. Therefore, root and nugget defects could be limited in FSW, by means of the removal of the naturally grown oxide layers where the two welding plates get in connection before welding. Besides, the oxide layers can be dispersed and disrupted by using hot welding parameters during FSW process, especially high tool rotation speed.

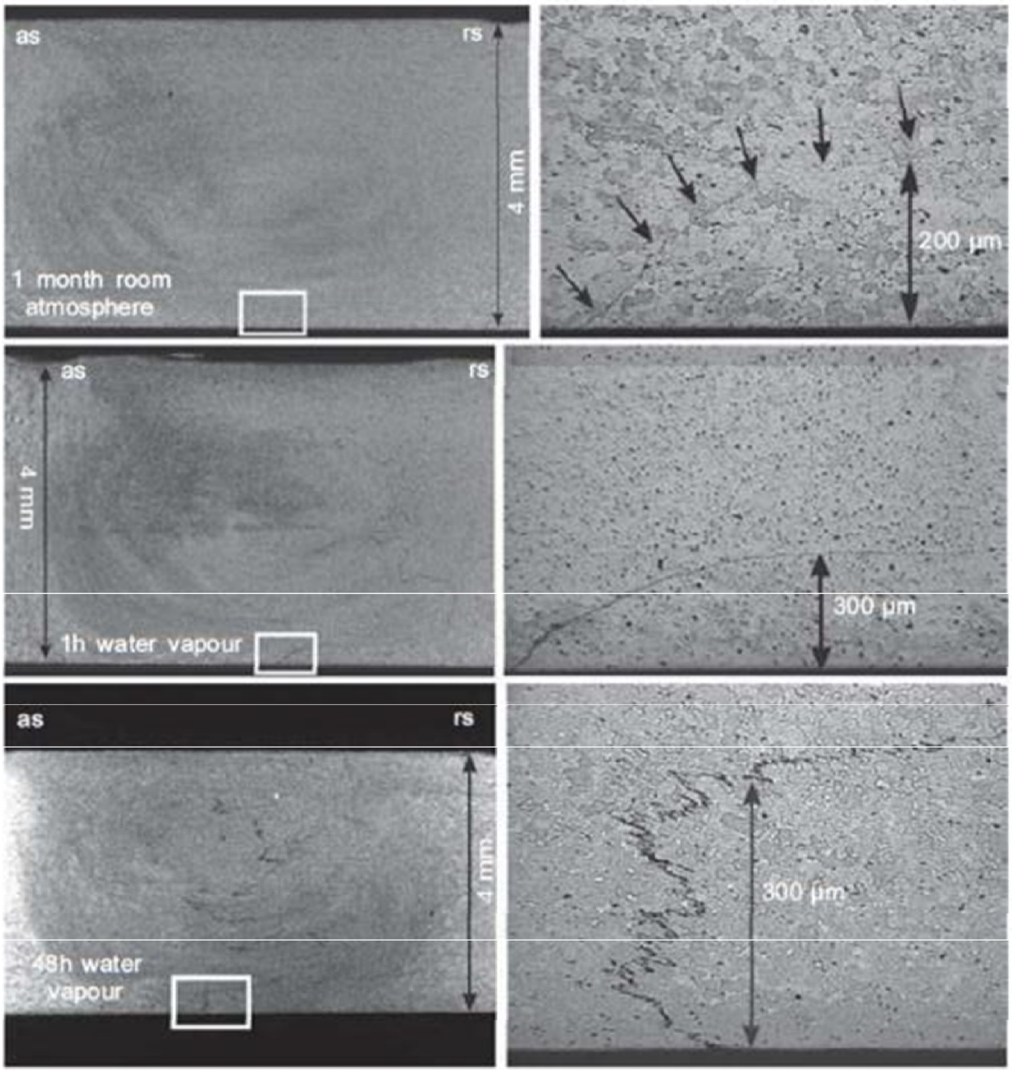

Fig. 2. 33 Optical micrographs of root- and nugget flaws formed by natural aluminium surface layers in 6013 T4-FSWs, cross sections [104].

- **Lap welding defects**

Some types of defects particularly as voids and joint line oxides which are usually encountered in butt welds can also happen in friction stir lap welds, for example, kissing bond, which often appears in a horizontal direction throughout the plate interface. Due to the connection configuration, root defects can rarely happen. It was found that the features at the edges of the bonded region of the lap welds have a significantly effect on the weld quality as well as mechanical properties. Babu et al. [142] reported that the features in friction stir lap welds could have a marked influence on the properties of the joints. The feature can generate form the top or bottom material determined by the welding parameters, leading to the reduction of the thickness of the plate. In many researches, the feature is named as 'hooking', which is usually detected at the edge of the bonded region towards the advancing side, easily by optical microscopy. Besides, the thickness reduction of the upper sheet can usually be found towards the retreating side, which can significantly weaken the bearing capacity of the welds (as shown in Fig. 2. 34). Apart from the welding parameters, Yang et al. [143] also found that the tool design had a significant effect on the morphology of the hooking defect, thus affecting the properties of the joints. In this research, CFD modelling was used to predict the change in the extent of hooking due to the tool profile modifications, which is of guiding significance to the tool design [144].

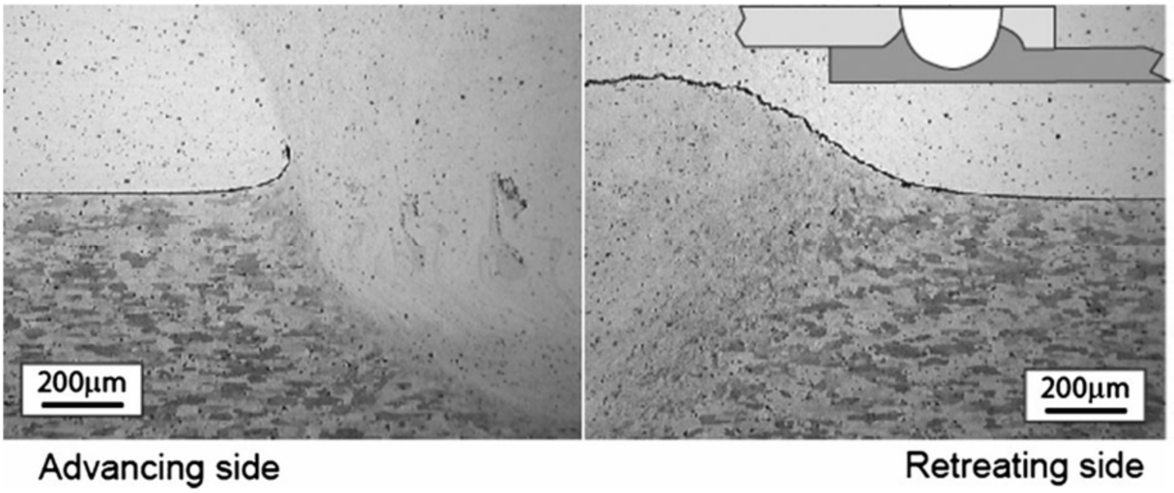

Fig. 2. 34 Lap weld defects showing hooking on advancing side and plate thinning on retreating side in lap welds between 7075 (upper) and 2024 (lower) alloys [109].

- **Intermetallics**

Al-Cu joints that are used in the power transmission applications due to the excellent electrical conductivities of Al and Cu. For Al and its alloys, the conductivity-to-density ratio is twice that of copper, making a strong industrial case for dissimilar Al-Cu joints for component weight reduction, in addition to the cost savings due to the lower cost of Al-alloys compared with Cu. Al-Cu joints are difficult to manufacture by fusion welding because of the significant difference in the chemical composition as well as physical properties for the base materials. Consequently, these types of dissimilar connection are usually welded through friction welding, in which base materials do not melt during the procedure.

However, the quality of the Al-Cu friction welds depends significantly on the weld microstructure formed, especially the presence of intermetallic phases, due to their detrimental influence on the mechanical properties. Because of the differences in thermal expansion coefficients and hardness between the intermetallic phases and the base metal matrices, cracks may form at the interface in the weld metal when stressed, significantly reducing its mechanical properties.

The intermetallics generated during Al-Cu friction welding process were identified in many research works. Elrefaey et al. [145] conducted the FSLW of 2 mm Al 1100 to 1mm pure copper. The resultants showed that intermetallic compounds in various morphologies were found in the SZ near the Al-Cu interface, including CuAl (η), CuAl2 (θ), and Cu9Al4 (γ). CuAl2 (θ) appeared black, CuAl (η) appeared gray, and Cu9Al4 (γ) appeared layered, which were identified by X-ray diffraction (XRD). The pictures of intermetallics and corresponding types are shown below (Fig. 2. 35). Abdollah-Zadeh et al. [146] also used FSLW for the connection of 4 mm Al 1060 and 3mm pure copper. Intermetallic compounds including CuAl (η), CuAl2 (θ) and Cu9Al4 (γ) were identified by energy-dispersive spectroscopy (EDS) in the SZ at the Al-Cu interface. Besides, Cu-rich fragments were observed in the SZ as well.

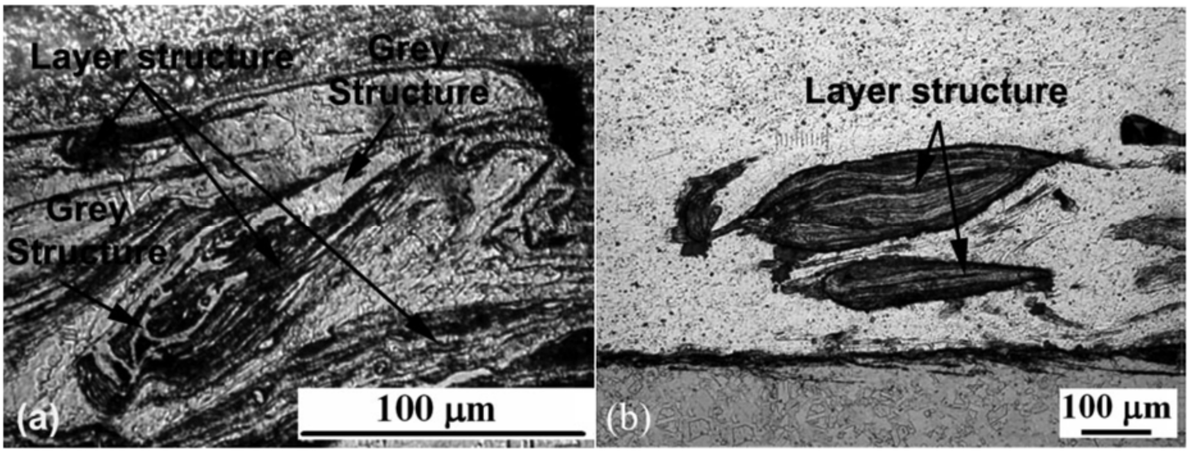

Fig. 2. 35 Microstructures formed in the area close to Al-Cu interface [145].
(a) Layer and grey structures, (b) Copper-rich fragment with layer structure

Wanjara et al. [147, 148] welded Al AA6063 and pure Cu by LFW. Two types of intermetallics were found at Al-Cu interface (Shown as Fig. 2. 36). The EDX results of Phase 1 and Phase 2 probably matched the composition of CuAl2 and Cu2Al, respectively. Different from FSW lap welding mentioned above, the CuAl2 (θ phase) and Cu2Al (probably Cu9Al4, γ phase) in LFW welds both showed layered structure. Besides, after heat treatment at 200℃-300℃, the layers became thicker, averaging 2 mm for CuAl2 and close to 10 mm for Cu2Al.

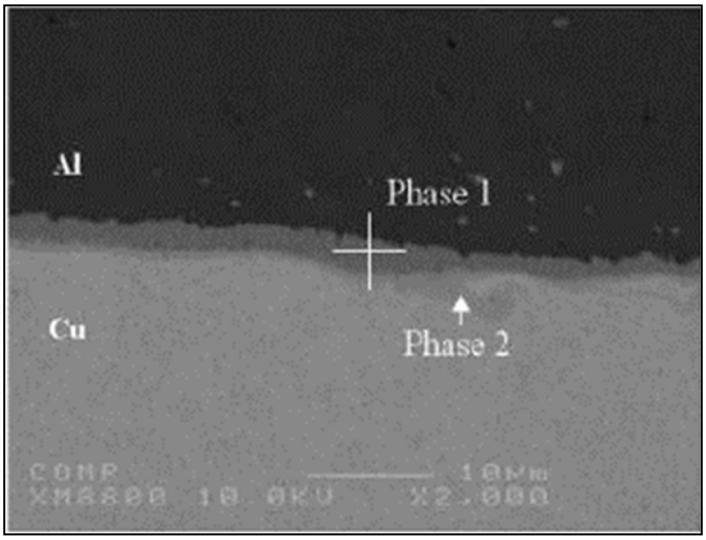

Fig. 2. 36 SEM image showing two types of phases [148].

Intermetallic phases are known to have a high hardness and electrical resistivity, which are likely to increase the brittleness of the joint and reduce the conductivity of the joint, respectively. According to the limited information concerning the influence of the intermetallics on the mechanical properties, generally, the intermetallics have a negative effect. Bhamji et al. [85] made LFW welds of aluminium (AA 1050) to copper (C101). No large layers of intermetallic was present at the weld interface but a lot of copper particles in Al base metal near the Al-Cu interface (shown in Fig. 2. 37). XRD results showed only CuAl2 (θ) phase exist in the welds among all the Al-Cu intermetallics. In this condition, the welds showed very good mechanical properties and electrical conductivity. Firouzdor et al. [149] welded Al 6061 to pure Cu using a modified structure which significantly improved the quality of the joints for Al-Cu lap FSW. Compared the conventional and modified structure, the modified can be improved twice in strength and 5~9 times in ductility. In terms of microstructure, the fracture surface of conventional welds contains intermetallic compounds including CuAl2 (θ) and Cu9Al4 (γ). While in the fracture surface of modified welds, dimples can be found with Cu particles in them. Therefore, intermetallic compounds were harmful to the properties of the Al-Cu welds.

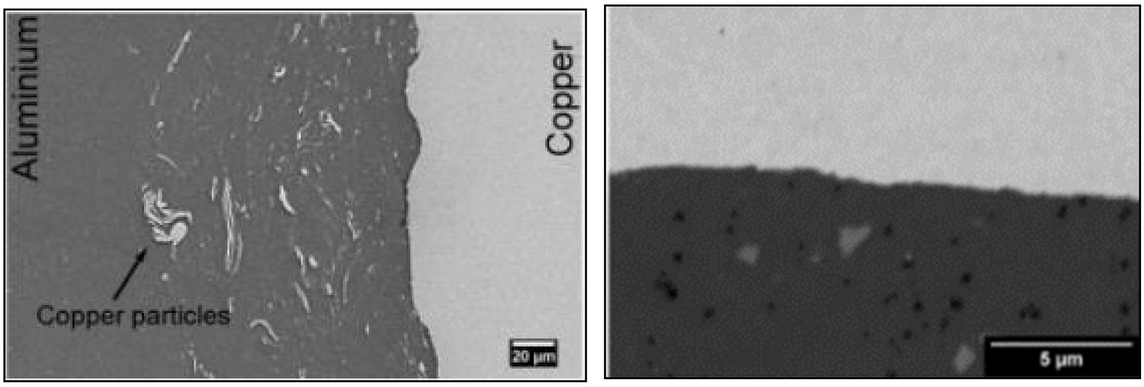

Fig. 2. 37 SEM pictures of Al-Cu LFW welds [85].

Besides, in Al-Mg friction welding joints, the formation of brittle intermetallic phases at the weld interface can significantly degrade the joint strength [150]. Bhamji et al. [151] found intermetallic phases $Al_{12}Mg_{17}$ and Al_3Mg_2 in Al6082-AZ31 linear friction weld, and these phases seemed to be the main reason for the welds having poorer mechanical properties than the base materials. Similar intermetallic phase was found in friction stir welding of 5083 Al alloy and AZ31B Mg alloy [152]. Layered intermetallics at the interface was detected with an identified composition of $Al_{12}Mg_{17}$ which resulted in virtually no ductility for the welds.

According to the analysis above, generation of Al-Cu or Al-Mg intermetallic compounds would lead to the failure of the bonding system and device, so effectively controlling the formation and growth of intermetallic compounds should be done for producing Al-Cu or Al-Mg solid-state welds with good performance. Fundamentally, controlling atomic diffusion, especially the diffusion of Cu or Mg atoms which can effectively prevent the formation of intermetallic compounds. Adding alloy elements are done to restrict the compounds by many institutions. Breedis et al. [153] used Cu-15%Ni alloy to restrain the generation of Al-Cu intermetallic compounds in a certain extent. Besides, the method of interface transition was also proposed to prevent the diffusion of atoms, and thus play an inhibitory effect. Elrefaey et al. [154] made Al-Cu FSW lap welding with a 50-μm Zn foil inserted between Al and Cu. It was found the strength was obviously improved due to the addition of the Zn which limited the generation of harmful Al-Cu intermetallics. It is obvious that the zinc content in the layer structure was decreased as it was away from the interface (see Fig. 2. 38).

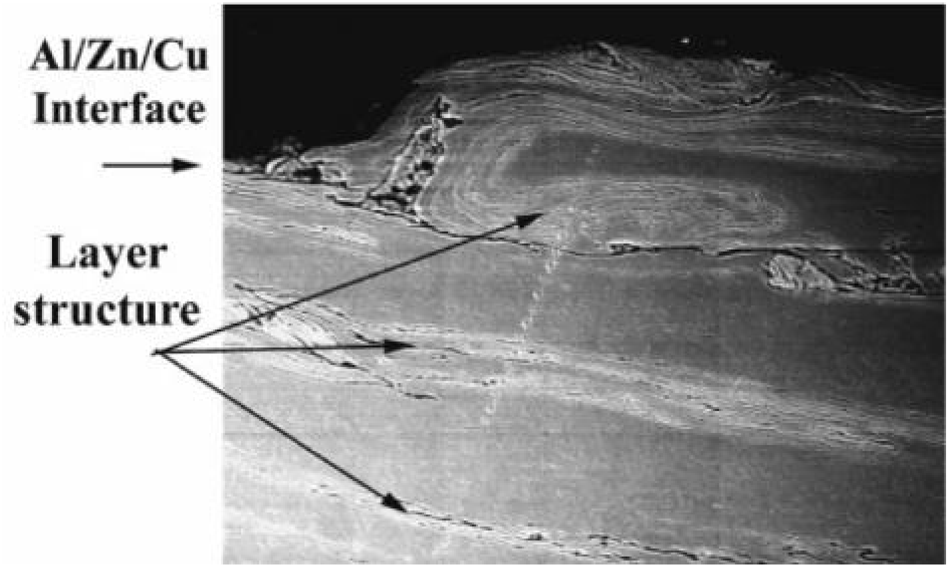

Fig. 2. 38 Microstructure at Al/Zn/Cu interface

2.4 Summary

This chapter summarises the microstructure, mechanical properties and various defects related to friction welding of Al-X joints. The following points summarise the current state of investigation, with the knowledge gap which needs further study.

- Aluminium alloys have a broad application prospect in the field of automobile due to the lightweight and relatively high mechanical properties. Among them, AA6061, AA5083 as the representative of the wrought aluminium alloy and A356 as the representative of the casting aluminium alloy are the most widely used alloys. It is of great importance for the investigation on the rapidly developed friction welding for these materials, in order to supply the basic data for industry. Besides, the friction welding of Al and Cu also has good prospect, because they were difficult to connect using traditional fusion welding.
- The FW which includes FSW, LFW, et al. is a solid-state connection technology. The microstructure of the FW joints can be clearly divided into several zones and each zone has its own characteristics. Generally, the weld zone has an equiaxed grain structure due to recrystallization, and the TMAZ has a deformed or torsional grain structure due to the synergistic effect of the friction force and the heat input. Because of the friction temperature rise, HAZ usually has coarser grains compared to the base material. Besides, the tensile strength and fatigue property of the FW joints are always worse compared to the base material but generally much better than the joints made by fusion welding. However, few reports can be found on the correspondence between the microstructure and mechanical properties in FW welds especially in LFW joints, obtained using different welding parameters.
- Defects in the FW joints can be classified as macro-scale defects and micro-scale defects. The

macro-scale defects which mainly include voids, tunnel, flash, surface galling, et al. are produced due to the improper flow of the welding materials. These defects can be detected by the naked eye or NDT, and in most cases can be eliminated by optimising the welding parameters. The micro-scale defects are unable to be detected by NDT, and difficult to avoid by adjusting welding parameters. Such defects as “kissing bond” or “lazy S” are produced in the FSW procedure due to the surface oxidation of the original welding material especially Al alloys. In addition, the intermetallics are generated around the welding interface, which usually happens in the FW of Al to Cu or Mg dissimilar materials. However, limited information can be found on the effect of the welding parameters on the morphology and distribution of the defects, as well as the effect of these defects on the mechanical properties of the welds and to what extent.

2.5 References

[1] R.A. Sielski, Research needs in aluminum structure, Ships and Offshore Structures 3(1) (2008) 57-65.

[2] Y. Birol, S. Kasman, Effect of welding parameters on microstructure and mechanical properties of friction stir welded EN AW 5083 H111 plates, Materials Science and Technology 29(11) (2013) 1354-1362.

[3] J. Seong, G. Frankel, N. Sridhar, Inhibition of Stress Corrosion Cracking of Sensitized AA5083, Corrosion (2015) 150825085022001.

[4] G. Yi, D.A. Cullen, K.C. Littrell, W. Golumbfskie, E. Sundberg, M.L. Free, Characterization of Al-Mg Alloy Aged at Low Temperatures, Metallurgical and Materials Transactions A 48(4) (2017) 2040-2050.

[5] T. Sato, Y. Kojima, T. Takahashi, Modulated structures and GP Zones in Al-Mg Alloys, Metallurgical Transactions A 13(8) (1982) 1373-1378.

[6] M. Bouchear, D. Hamana, T. Laoui, GP zones and precipitate morphology in aged Al-Mg alloys, Philosophical Magazine A 73(6) (1996) 1733-1740.

[7] R. Goswami, G. Spanos, P.S. Pao, R.L. Holtz, Precipitation behavior of the ß phase in Al-5083, Materials Science and Engineering: A 527(4-5) (2010) 1089-1095.

[8] M.J. Starink, A.M. Zahra, β′ and β precipitation in an Al–Mg alloy studied by DSC and TEM, Acta Materialia 46(10) (1998) 3381-3397.

[9] S. Vigneshwaran, K.S.V.B.R. Krishna, K.C. Sekhar, K. Sivaprasad, K. Venkateswarlu, R. Narayanasamy, A study on the work hardening and the effect of triaxiality on the fracture behaviour of some cryorolled aluminium alloys, Materials Science and Engineering: A 678 (2016) 165-177.

[10] P.T. Summers, A.P. Mouritz, S.W. Case, B.Y. Lattimer, Microstructure-based modeling of residual yield strength and strain hardening after fire exposure of aluminum alloy 5083-H116, Materials Science and Engineering: A 632 (2015) 14-28.

[11] C.M. Gómora, R.R. Ambriz, F.F. Curiel, D. Jaramillo, Heat distribution in welds of a 6061-T6 aluminum alloy obtained by modified indirect electric arc, Journal of Materials Processing Technology 243 (2017) 433-441.

[12] M. Weber, P.D. Eason, H. Özdeş, M. Tiryakioğlu, The effect of surface corrosion damage on the fatigue life of 6061-T6 aluminum alloy extrusions, Materials Science and Engineering: A 690 (2017) 427-432.

[13] S. Venukumar, B. Baby, S. Muthukumaran, S.V. Kailas, Microstructural and Mechanical Properties of Walking Friction Stir Spot Welded AA 6061-T6 Sheets, Procedia Materials Science 6 (2014) 656-665.

[14] G.B. Burger, A.K. Gupta, P.W. Jeffrey, D.J. Lloyd, Microstructural control of aluminum sheet used in automotive applications, Materials Characterization 35(1) (1995) 23-39.

[15] L.H. Pereira, G.H. Asato, L.B. Otani, A.M. Jorge Jr, C.S. Kiminami, C. Bolfarini, W.J. Botta, Changing the solidification sequence and the morphology of iron-containing intermetallic phases in AA6061 aluminum alloy processed by spray forming, Materials Characterization 145 (2018) 507-515.

[16] L. Lodgaard, N. Ryum, Precipitation of dispersoids containing Mn and/or Cr in Al–Mg–Si alloys, Materials Science and Engineering: A 283(1) (2000) 144-152.

[17] Y. Zheng, W. Xiao, S. Ge, W. Zhao, S. Hanada, C. Ma, Effects of Cu content and Cu/Mg ratio on the microstructure and mechanical properties of Al–Si–Cu–Mg alloys, Journal of Alloys and Compounds 649 (2015) 291-296.

[18] S. Zhu, Z. Li, L. Yan, X. Li, S. Huang, H. Yan, Y. Zhang, B. Xiong, Effects of Zn addition on the age hardening behavior and precipitation evolution of an Al-Mg-Si-Cu alloy, Materials Characterization 145 (2018) 258-267.

[19] W. Yuan, Z. Liang, Effect of Zr addition on properties of Al–Mg–Si aluminum alloy used for all aluminum alloy conductor, Materials & Design 32(8) (2011) 4195-4200.

[20] C. Li, X. Liu, G. Zhang, Heterogeneous nucleating role of TiB2 or AlP/TiB2 coupled compounds on primary Mg2Si in Al–Mg–Si alloys, Materials Science and Engineering: A 497(1) (2008) 432-437.

[21] G.A. Edwards, K. Stiller, G.L. Dunlop, M.J. Couper, The precipitation sequence in Al–Mg–Si alloys, Acta Materialia 46(11) (1998) 3893-3904.

[22] P. Nageswara rao, R. Jayaganthan, Effects of warm rolling and ageing after cryogenic rolling on mechanical properties and microstructure of Al 6061 alloy, Materials & Design 39 (2012) 226-233.

[23] K. Buchanan, K. Colas, J. Ribis, A. Lopez, J. Garnier, Analysis of the metastable precipitates in peak-hardness aged Al-Mg-Si(-Cu) alloys with differing Si contents, Acta Materialia 132 (2017) 209-221.

[24] F. Eckermann, T. Suter, P.J. Uggowitzer, A. Afseth, P. Schmutz, The influence of MgSi particle reactivity and dissolution processes on corrosion in Al–Mg–Si alloys, Electrochimica Acta 54(2) (2008) 844-855.

[25] S.M. Hirth, G.J. Marshall, S.A. Court, D.J. Lloyd, Effects of Si on the aging behaviour and formability of aluminium alloys based on AA6016, Materials Science and Engineering: A 319-321 (2001) 452-456.

[26] G.H. Tao, C.H. Liu, J.H. Chen, Y.X. Lai, P.P. Ma, L.M. Liu, The influence of Mg/Si ratio on the negative natural aging effect in Al–Mg–Si–Cu alloys, Materials Science and Engineering: A 642 (2015) 241-248.

[27] P.N. Rao, D. Singh, H.-G. Brokmeier, R. Jayaganthan, Effect of ageing on tensile behavior of ultrafine grained Al 6061 alloy, Materials Science and Engineering: A 641 (2015) 391-401.

[28] L.Y. Zhang, Y.H. Jiang, Z. Ma, S.F. Shan, Y.Z. Jia, C.Z. Fan, W.K. Wang, Effect of cooling rate on solidified microstructure and mechanical properties of aluminium-A356 alloy, Journal of Materials Processing Technology 207(1) (2008) 107-111.

[29] S.W. Youn, C.G. Kang, Characterization of age-hardening behavior of eutectic region in squeeze-cast A356-T5 alloy using nanoindenter and atomic force microscope, Materials Science and Engineering: A 425(1) (2006) 28-35.

[30] M. Tebaldini, C. Petrogalli, G. Donzella, G.M. La Vecchia, Estimation of Fatigue Limit of a A356-T6 Automotive Wheel in Presence of Defects, Procedia Structural Integrity 7 (2017) 521-529.

[31] C.D. Lee, Variability in the impact properties of A356 aluminum alloy on microporosity variation, Materials Science and Engineering: A 565 (2013) 187-195.

[32] G. Ma, R. Li, R. Li, Effect of Mg2Si particles on low-temperature fracture behavior of A356 alloy, Materials Science and Engineering: A 674 (2016) 666-671.

[33] T. Haskel, G.O. Verran, R. Barbieri, Rotating and bending fatigue behavior of A356 aluminum alloy: Effects of strontium addition and T6 heat treatment, International Journal of Fatigue 114 (2018) 1-10.

[34] S. Singh, D. patel, P. Ansari, D. kumar jadhav, C. Verma, J. Menghani, Effect of Grain refinement, Modifier and Stirring on properties of A356, Materials Today: Proceedings 4(2, Part A) (2017) 734-739.

[35] X. Wu, H. Zhang, F. Zhang, Z. Ma, L. Jia, B. Yang, T. Tao, H. Zhang, Effect of cooling rate and Co content on the formation of Fe-rich intermetallics in hypoeutectic Al7Si0.3Mg alloy with 0.5%Fe, Materials Characterization 139 (2018) 116-124.

[36] A.K. Prasada Rao, K. Das, B.S. Murty, M. Chakraborty, Microstructural features of as-cast A356 alloy inoculated with Sr, Sb modifiers and Al–Ti–C grain refiner simultaneously, Materials Letters 62(2) (2008) 273-275.

[37] Y.-C. Tsai, C.-Y. Chou, S.-L. Lee, C.-K. Lin, J.-C. Lin, S.W. Lim, Effect of trace La addition on the microstructures and mechanical properties of A356 (Al–7Si–0.35Mg) aluminum alloys, Journal of Alloys and Compounds 487(1) (2009) 157-162.

[38] T. Wang, Y. Zheng, Z. Chen, Y. Zhao, H. Kang, Effects of Sr on the microstructure and mechanical properties of in situ TiB2 reinforced A356 composite, Materials & Design 64 (2014) 185-193.

[39] F. Mao, G. Yan, Z. Xuan, Z. Cao, T. Wang, Effect of Eu addition on the microstructures and mechanical properties of A356 aluminum alloys, Journal of Alloys and Compounds 650 (2015) 896-906.

[40] Q. Li, T. Xia, Y. Lan, W. Zhao, L. Fan, P. Li, Effect of rare earth cerium addition on the microstructure and tensile properties of hypereutectic Al–20%Si alloy, Journal of Alloys and Compounds 562 (2013) 25-32.

[41] C. do Lee, Effect of T6 heat treatment on the defect susceptibility of fatigue properties to microporosity variations in a low-pressure die-cast A356 alloy, Materials Science and Engineering: A 559 (2013) 496-505.

[42] Copper Alloys - Early Applications and Current Performance - Enhancing Processes, InTech.

[43] Y. Besel, M. Besel, U. Alfaro Mercado, T. Kakiuchi, T. Hirata, Y. Uematsu, Influence of local fatigue damage evolution on crack initiation behavior in a friction stir welded Al-Mg-Sc alloy, International Journal of Fatigue 99 (2017) 151-162.

[44] C. Genevois, A. Deschamps, A. Denquin, B. Doisneau-cottignies, Quantitative investigation of precipitation and mechanical behaviour for AA2024 friction stir welds, Acta Materialia 53(8)

(2005) 2447-2458.

[45] A.L. Etter, T. Baudin, N. Fredj, R. Penelle, Recrystallization mechanisms in 5251 H14 and 5251 O aluminum friction stir welds, Materials Science and Engineering: A 445-446 (2007) 94-99.

[46] D. Baffari, G. Buffa, D. Campanella, L. Fratini, F. Micari, Friction based Solid State Welding Techniques for Transportation Industry Applications, Procedia CIRP 18 (2014) 162-167.

[47] M. Tocci, A. Pola, G.M. La Vecchia, M. Modigell, Characterization of a New Aluminium Alloy for the Production of Wheels by Hybrid Aluminium Forging, Procedia Engineering 109 (2015) 303-311.

[48] W.-B. Lee, Y.-M. Yeon, S.-B. Jung, The joint properties of dissimilar formed Al alloys by friction stir welding according to the fixed location of materials, Scripta Materialia 49(5) (2003) 423-428.

[49] Z.W. Chen, S. Yazdanian, Friction Stir Lap Welding: material flow, joint structure and strength, Journal of Achievements in Materials and Manufacturing Engineering (2012).

[50] S. Yazdanian, Z.W. Chen, G. Littlefair, Effects of friction stir lap welding parameters on weld features on advancing side and fracture strength of AA6060-T5 welds, Journal of Materials Science 47(3) (2011) 1251-1261.

[51] V. Soundararajan, E. Yarrapareddy, R. Kovacevic, Investigation of the Friction Stir Lap Welding of Aluminum Alloys AA 5182 and AA 6022, Journal of Materials Engineering and Performance 16(4) (2007) 477-484.

[52] K.A. Matori, M. Tamjidy, F. Fadaeifard, F. Gharvi, H.T. Baherodin, S. Paslar, Optimization Parameters of Friction Stir Lap Welding of Aluminum Alloy AA6061-T6, Journal of Applied Sciences 15(3) (2015) 465-473.

[53] C.-Y. Lee, W.-B. Lee, J.-W. Kim, D.-H. Choi, Y.-M. Yeon, S.-B. Jung, Lap joint properties of FSWed dissimilar formed 5052 Al and 6061 Al alloys with different thickness, Full Set - Includes `Journal of Materials Science Letters' 43(9) 3296-3304.

[54] S. Yazdanian, Z.W. Chen, G. Littlefair, Effects of friction stir lap welding parameters on weld features on advancing side and fracture strength of AA6060-T5 welds, Journal of Materials Science 47(3) (2012) 1251-1261.

[55] Y. Guo, T. Jung, Y.L. Chiu, H. Li, S. Bray, P. Bowen, Microstructure and microhardness of

Ti6246 linear friction weld, Materials Science and Engineering: A 562 (2013) 17-24.

[56] J. Romero, M.M. Attallah, M. Preuss, M. Karadge, S.E. Bray, Effect of the forging pressure on the microstructure and residual stress development in Tiâ "6Alâ "4V linear friction welds, Acta Materialia 57(18) (2009) 5582-5592.

[57] I. Bhamji, A.C. Addison, P.L. Threadgill, M. Preuss, Appendix: Linear friction welding in aerospace engineering, in: M.C. Chaturvedi (Ed.), Welding and Joining of Aerospace Materials, Woodhead Publishing2012, pp. 384-415.

[58] P. Wanjara, M. Jahazi, Linear friction welding of Ti-6Al-4V: Processing, microstructure, and mechanical-property inter-relationships, Metallurgical and Materials Transactions A 36(8) (2005) 2149-2164.

[59] R.S. Mishra, Z.Y. Ma, Friction stir welding and processing, Materials Science and Engineering: R: Reports 50(1) (2005) 1-78.

[60] D. Lohwasser, Friction stir welding : from basics to applications / edited by Daniela Lohwasser and Zhan Chen, Cambridge, England
Boca Raton, Florida : Woodhead Publishing Limited : CRC Press2010.

[61] R. Nandan, T. DebRoy, H.K.D.H. Bhadeshia, Recent advances in friction-stir welding – Process, weldment structure and properties, Progress in Materials Science 53(6) (2008) 980-1023.

[62] P.M.G.P. Moreira, F.M.F. de Oliveira, P.M.S.T. de Castro, Fatigue behaviour of notched specimens of friction stir welded aluminium alloy 6063-T6, Journal of Materials Processing Technology 207(1) (2008) 283-292.

[63] P.M.G.P. Moreira, M.A.V. de Figueiredo, P.M.S.T. de Castro, Fatigue behaviour of FSW and MIG weldments for two aluminium alloys, Theoretical and Applied Fracture Mechanics 48(2) (2007) 169-177.

[64] P.M.G.P. Moreira, T. Santos, S.M.O. Tavares, V. Richter-Trummer, P. VilaÃ§a, P.M.S.T. de Castro, Mechanical and metallurgical characterization of friction stir welding joints of AA6061-T6 with AA6082-T6, Materials and Design 30(1) (2009) 180-187.

[65] Y. Sato, S. Park, H. Kokawa, Microstructural factors governing hardness in friction-stir welds of solid-solution-hardened Al alloys, Metallurgical and Materials Transactions A 32(12) 3033-3042.

[66] F. Rotundo, L. Ceschini, A. Morri, T.S. Jun, A.M. Korsunsky, Mechanical and microstructural

characterization of 2124Al/25vol.%SiCp joints obtained by linear friction welding (LFW), Composites Part A: Applied Science and Manufacturing 41(9) (2010) 1028-1037.

[67] M.N. Avettand-Fènoël, G. Racineux, L. Debeugny, R. Taillard, Microstructural characterization and mechanical performance of an AA2024 aluminium alloy — Pure copper joint obtained by linear friction welding, Materials & Design 98 (2016) 305-318.

[68] Z.-b. He, Y.-y. Peng, Z.-m. Yin, X.-f. Lei, Comparison of FSW and TIG welded joints in Al-Mg-Mn-Sc-Zr alloy plates, Transactions of Nonferrous Metals Society of China 21(8) (2011) 1685-1691.

[69] J. Zhang, X.S. Feng, J.S. Gao, H. Huang, Z.Q. Ma, L.J. Guo, Effects of welding parameters and post-heat treatment on mechanical properties of friction stir welded AA2195-T8 Al-Li alloy, Journal of Materials Science & Technology 34(1) (2018) 219-227.

[70] I. Radisavljevic, A. Zivkovic, N. Radovic, V. Grabulov, Influence of FSW parameters on formation quality and mechanical properties of Al 2024-T351 butt welded joints, Transactions of Nonferrous Metals Society of China 23(12) (2013) 3525-3539.

[71] G. D'Urso, C. Giardini, S. Lorenzi, M. Cabrini, T. Pastore, The influence of process parameters on mechanical properties and corrosion behaviour of friction stir welded aluminum joints, Procedia Engineering 207 (2017) 591-596.

[72] M.W. Mahoney, C.G. Rhodes, J.G. Flintoff, W.H. Bingel, R.A. Spurling, Properties of friction-stir-welded 7075 T651 aluminum, Metallurgical and Materials Transactions A 29(7) (1998) 1955-1964.

[73] P.M.G.P. Moreira, T. Santos, S.M.O. Tavares, V. Richter-Trummer, P. Vilaça, P.M.S.T. de Castro, Mechanical and metallurgical characterization of friction stir welding joints of AA6061-T6 with AA6082-T6, Materials & Design 30(1) (2009) 180-187.

[74] L. Cederqvist, A.P. Reynolds, Factors affecting the properties of friction stir welded aluminum lap joints, 2001.

[75] M. Papadopoulos, S. Tavares, M. Pacchione, S. Pantelakis, Mechanical behaviour of AA 2024 friction stir overlap welds, International Journal of Structural Integrity 4(1) 108-120.

[76] G.S. Daehn, 13 - Sustainable design and manufacture of lightweight vehicle structures, Elsevier Ltd.

[77] S. Lim, S. Kim, C.-G. Lee, S. Kim, Tensile behavior of friction-stir-welded A356-T6/Al 6061-

T651 bi-alloy plate, Metallurgical and Materials Transactions A 35(9) (2004) 2837-2843.

[78] M. Ghosh, K. Kumar, S.V. Kailas, A.K. Ray, Optimization of friction stir welding parameters for dissimilar aluminum alloys, Materials & Design 31(6) (2010) 3033-3037.

[79] T. Muhamad, M. Prapas, B. Abdul, C. Somchai, U. Nisida, Influence of friction stir welding parameters on metallurgical and mechanical properties of dissimilar joint between semi-solid metal 356-T6 and aluminum alloys 6061-T651, Songklanakarin Journal of Science and Technology (SJST) 34(4) 415-421.

[80] C. Meengam, M. Tehyo, P. Muangjunburee, J. Wannasin, Dissimilar Materials Joining between SSM 356-T6 and AA6061-T651 by Friction Stir Welding, Applied Mechanics and Materials 372 478.

[81] H.H. Koo, W.A. Baeslack, Structure, properties, and fracture of linear friction welded Al-Fe-V-Si alloy 8009, Materials Characterization 28(2) (1992) 157-164.

[82] L. Ceschini, A. Morri, F. Rotundo, A. Korsunsky, T. Jun, Linear Friction Welding (LFW) of metal matrix composites, Metall. Ital. (3) 23-30.

[83] F. Rotundo, Mechanical and microstructural characterization of 2124Al/25vol.%SiC joints obtained by linear friction welding (LFW), Composites: Part A, Applied Science & Manufacturing 41(9) 1028-1038.

[84] F. Rotundo, A. Marconi, A. Morri, A. Ceschini, Dissimilar linear friction welding between a SiC particle reinforced aluminium composite and a monolithic aluminium alloy: microstructural, tensile and fatigue properties, Materials Science and Engineering A: Structural Materials: Properties, Microstructures and Processing 559 852-860.

[85] I. Bhamji, R.J. Moat, M. Preuss, P.L. Threadgill, A.C. Addison, M.J. Peel, Linear friction welding of aluminium to copper, Science and Technology of Welding and Joining 17(4) (2013) 314-320.

[86] M. Wu, C. Wu, S. Gao, Effect of ultrasonic vibration on fatigue performance of AA 2024-T3 friction stir weld joints, Journal of Manufacturing Processes 29 (2017) 85-95.

[87] H. Das, D. Chakraborty, T. Kumar Pal, High-cycle fatigue behavior of friction stir butt welded 6061 aluminium alloy, Transactions of Nonferrous Metals Society of China 24(3) (2014) 648-656.

[88] M. Kadlec, R. Růžek, L. Nováková, Mechanical behaviour of AA 7475 friction stir welds with the kissing bond defect, International Journal of Fatigue 74 (2015) 7-19.

[89] C. Zhou, X. Yang, G. Luan, Fatigue properties of friction stir welds in Al 5083 alloy, Scripta Materialia 53(10) (2005) 1187-1191.

[90] B.S. Naik, D.L. Chen, X. Cao, P. Wanjara, Microstructure and Fatigue Properties of a Friction Stir Lap Welded Magnesium Alloy, Metallurgical and Materials Transactions A 44(8) (2013) 3732-3746.

[91] H. Lombard, D.G. Hattingh, A. Steuwer, M.N. James, Optimising FSW process parameters to minimise defects and maximise fatigue life in 5083-H321 aluminium alloy, Engineering Fracture Mechanics 75(3) (2008) 341-354.

[92] M.N. James, D.G. Hattingh, G.R. Bradley, Weld tool travel speed effects on fatigue life of friction stir welds in 5083 aluminium, International Journal of Fatigue 25(12) (2003) 1389-1398.

[93] T.L. Dickerson, J. Przydatek, Fatigue of friction stir welds in aluminium alloys that contain root flaws, International Journal of Fatigue 25(12) (2003) 1399-1409.

[94] T. Ghidini, T. Vugrin, C. Dalle Donne, Residual stresses, defects and non-destructive evaluation of FSW joints, Welding International 19(10) (2005) 783-790.

[95] C. Zhou, X. Yang, G. Luan, Effect of kissing bond on fatigue behavior of friction stir welds on Al 5083 alloy, Journal of Materials Science 41(10) (2006) 2771-2777.

[96] P. Cavaliere, G. Campanile, F. Panella, A. Squillace, Effect of welding parameters on mechanical and microstructural properties of AA6056 joints produced by Friction Stir Welding, Journal of Materials Processing Technology 180(1) (2006) 263-270.

[97] A.L. Lafly, C. Dalle Donne, G. Biallas, D. Alléhaux, F. Marie, Role of Residual Stresses on Fatigue Crack Propagation of FSW 6056-T78 Aluminium Joints under Various Technologies, Materials Science Forum 519-521 (2006) 1089-1094.

[98] S. Kim, C.G. Lee, S.-J. Kim, Fatigue crack propagation behavior of friction stir welded 5083-H32 and 6061-T651 aluminum alloys, Materials Science and Engineering: A 478(1) (2008) 56-64.

[99] M. Ericsson, R. Sandström, Influence of welding speed on the fatigue of friction stir welds, and comparison with MIG and TIG, International Journal of Fatigue 25(12) (2003) 1379-1387.

[100] Y. Huang, L. Wan, X. Meng, Y. Xie, Z. Lv, L. Zhou, Probe shape design for eliminating the defects of friction stir lap welded dissimilar materials, Journal of Manufacturing Processes 35 (2018) 420-427.

[101] G.M.D. Cantin, S.A. David, W.M. Thomas, E. Lara-Curzio, S.S. Babu, Friction Skew-stir

welding of lap joints in 5083-O aluminium, Science and Technology of Welding and Joining 10(3) 268-280.

[102] D. Fersini, A. Pirondi, Analysis and modelling of fatigue failure of friction stir welded aluminum alloy single-lap joints, Engineering Fracture Mechanics 75(3) (2008) 790-803.

[103] W.J. Arbegast, A flow-partitioned deformation zone model for defect formation during friction stir welding, Scripta Materialia 58(5) (2008) 372-376.

[104] R. Zettler, T. Vugrin, M. Schmücker, 9 - Effects and defects of friction stir welds, in: D. Lohwasser, Z. Chen (Eds.), Friction Stir Welding, Woodhead Publishing2010, pp. 245-276.

[105] M. Pourali, A. Abdollah-zadeh, T. Saeid, F. Kargar, Influence of welding parameters on intermetallic compounds formation in dissimilar steel/aluminum friction stir welds, Journal of Alloys and Compounds 715 (2017) 1-8.

[106] Y.S. Sato, H. Takauchi, S.H.C. Park, H. Kokawa, Characteristics of the kissing-bond in friction stir welded Al alloy 1050, Materials Science and Engineering: A 405(1-2) (2005) 333-338.

[107] N. Zhou, D. Song, W. Qi, X. Li, J. Zou, M.M. Attallah, Influence of the kissing bond on the mechanical properties and fracture behaviour of AA5083-H112 friction stir welds, Materials Science and Engineering: A 719 (2018) 12-20.

[108] P.A. Colegrove, H.R. Shercliff, CFD modelling of friction stir welding of thick plate 7449 aluminium alloy, Science and Technology of Welding and Joining 11(4) (2006) 429-441.

[109] P.L. Threadgill, A.J. Leonard, H.R. Shercliff, P.J. Withers, Friction stir welding of aluminium alloys, pp. 49-93.

[110] Y.S. Sato, M. Urata, H. Kokawa, Parameters controlling microstructure and hardness during friction-stir welding of precipitation-hardenable aluminum alloy 6063, Metallurgical and Materials Transactions A 33(3) (2002) 625-635.

[111] V. Balasubramanian, Relationship between base metal properties and friction stir welding process parameters, Materials Science and Engineering: A 480(1) (2008) 397-403.

[112] K. Kumar, S.V. Kailas, T.S. Srivatsan, Influence of Tool Geometry in Friction Stir Welding, Materials and Manufacturing Processes 23(2) (2008) 188-194.

[113] A. Bastier, M.H. Maitournam, K. Dang Van, F. Roger, Steady state thermomechanical modelling of friction stir welding, Science and Technology of Welding and Joining 11(3) (2006) 278-288.

[114] S. Wei, C. Hao, J. Chen, Study of friction stir welding of 01420 aluminum–lithium alloy, Materials Science and Engineering: A 452-453 (2007) 170-177.

[115] Y.-h. Zhao, S.-b. Lin, L. Wu, F.-x. Qu, The influence of pin geometry on bonding and mechanical properties in friction stir weld 2014 Al alloy, Materials Letters 59(23) (2005) 2948-2952.

[116] R. Crawford, G.E. Cook, A.M. Strauss, D.A. Hartman, M.A. Stremler, Experimental defect analysis and force prediction simulation of high weld pitch friction stir welding, Science and Technology of Welding and Joining 11(6) (2006) 657-665.

[117] P.N. Banjare, P. Sahlot, A. Arora, An assisted heating tool design for FSW of thermoplastics, Journal of Materials Processing Technology 239 (2017) 83-91.

[118] M. Guerra, C. Schmidt, J.C. McClure, L.E. Murr, A.C. Nunes, Flow patterns during friction stir welding, Materials Characterization 49(2) (2002) 95-101.

[119] N.Z. Khan, A.N. Siddiquee, Z.A. Khan, S.K. Shihab, Investigations on tunneling and kissing bond defects in FSW joints for dissimilar aluminum alloys, Journal of Alloys and Compounds 648 (2015) 360-367.

[120] X. Cao, M. Jahazi, Effect of tool rotational speed and probe length on lap joint quality of a friction stir welded magnesium alloy, Materials & Design 32(1) (2011) 1-11.

[121] R.L. Vijaya Kumar, M.R. Bhat, C.R.L. Murthy, Evaluation of kissing bond in composite adhesive lap joints using digital image correlation: Preliminary studies, International Journal of Adhesion and Adhesives 42 (2013) 60-68.

[122] Y.S. Sato, H. Takauchi, S.H.C. Park, H. Kokawa, Characteristics of the kissing-bond in friction stir welded Al alloy 1050, Materials Science and Engineering: A 405(1) (2005) 333-338.

[123] K.N. Krishnan, On the formation of onion rings in friction stir welds, Materials Science and Engineering: A 327(2) (2002) 246-251.

[124] T.-J. Yoon, C.-Y. Kang, Observations on metallurgical phenomena and formation of onion ring nugget during friction stir lap welding of dissimilar aluminum by a new 3D technique, Materials Letters 142 (2015) 253-257.

[125] S. Muthukumaran, S.K. Mukherjee, Multi-layered metal flow and formation of onion rings in friction stir welds, The International Journal of Advanced Manufacturing Technology 38(1-2) (2007) 68-73.

[126] C. Luo, X. Li, D. Song, N. Zhou, Y. Li, W. Qi, Microstructure evolution and mechanical properties of friction stir welded dissimilar joints of Mg–Zn–Gd and Mg–Al–Zn alloys, Materials Science and Engineering: A 664 (2016) 103-113.

[127] Y.S. Sato, F. Yamashita, Y. Sugiura, S.H.C. Park, H. Kokawa, FIB-assisted TEM study of an oxide array in the root of a friction stir welded aluminium alloy, Scripta Materialia 50(3) (2004) 365-369.

[128] M. Tabatabaeipour, J. Hettler, S. Delrue, K. Van Den Abeele, Non-destructive ultrasonic examination of root defects in friction stir welded butt-joints, NDT & E International 80 (2016) 23-34.

[129] H.B. Chen, J.F. Wang, G.D. Zhen, S.B. Chen, T. Lin, Effects of initial oxide on microstructural and mechanical properties of friction stir welded AA2219 alloy, Materials & Design 86 (2015) 49-54.

[130] H.-B. Chen, K. Yan, T. Lin, S.-B. Chen, C.-Y. Jiang, Y. Zhao, The investigation of typical welding defects for 5456 aluminum alloy friction stir welds, Materials Science and Engineering: A 433(1) (2006) 64-69.

[131] H. Jin, S. Saimoto, M. Ball, P.L. Threadgill, Characterisation of microstructure and texture in friction stir welded joints of 5754 and 5182 aluminium alloy sheets, Materials Science and Technology 17(12) (2001) 1605-1614.

[132] H. Okamura, K. Aota, M. Sakamoto, M. Ezumi, K. Ikeuchi, Behaviour of oxides during friction stir welding of aluminium alloy and their effect on its mechanical properties, Welding International 16(4) (2002) 266-275.

[133] D. Baffari, G. Buffa, D. Campanella, E. Lo Valvo, L. Fratini, Experimental and numerical investigation on a new FSW based metal to composite joining technique, Journal of Manufacturing Processes 34 (2018) 758-764.

[134] Y. Tao, Z. Zhang, D.R. Ni, D. Wang, B.L. Xiao, Z.Y. Ma, Influence of welding parameter on mechanical properties and fracture behavior of friction stir welded Al–Mg–Sc joints, Materials Science and Engineering: A 612 (2014) 236-245.

[135] C. Zhou, X. Yang, G. Luan, Effect of oxide array on the fatigue property of friction stir welds, Scripta Materialia 54(8) (2006) 1515-1520.

[136] G. Staniek, M. Schmucker, T. Vugrin, Oxides in friction-stir-welded aluminium alloys,

Welding and cutting 4(5) (2005) 271-276.

[137] H. Okamura, K. Aota, M. Ezumi, Friction stir welding of aluminum alloy and application to structure, Journal of Japan Institute of Light Metals 50(4) (2000) 166-172.

[138] A.P. Reynolds, Visualisation of material flow in autogenous friction stir welds, Science and Technology of Welding and Joining 5(2) (2000) 120-124.

[139] R. Zettler, Material deformation and joint formation in friction stir welding, (2010) 42-72.

[140] T. Le Jolu, T.F. Morgeneyer, A. Denquin, A.F. Gourgues-Lorenzon, Fatigue lifetime and tearing resistance of AA2198 Al–Cu–Li alloy friction stir welds: Effect of defects, International Journal of Fatigue 70 (2015) 463-472.

[141] Z. Zhang, B.L. Xiao, Z.Y. Ma, Effect of Segregation of Secondary Phase Particles and “S” Line on Tensile Fracture Behavior of Friction Stir-Welded 2024Al-T351 Joints, Metallurgical and Materials Transactions A 44(9) (2013) 4081-4097.

[142] S. Babu, G.D.J. Ram, P.V. Venkitakrishnan, G.M. Reddy, K.P. Rao, Microstructure and Mechanical Properties of Friction Stir Lap Welded Aluminum Alloy AA2014, Journal of Materials Science & Technology 28(5) (2012) 414-426.

[143] Q. Yang, X. Li, K. Chen, Y.J. Shi, Effect of tool geometry and process condition on static strength of a magnesium friction stir lap linear weld, Materials Science and Engineering: A 528(6) (2011) 2463-2478.

[144] X. He, F. Gu, A. Ball, A review of numerical analysis of friction stir welding, Progress in Materials Science 65(C) 1-66.

[145] A. Elrefaey, M. Takahashi, K. Ikeuchi, Preliminary Investigation of Friction Stir Welding Aluminium/Copper Lap Joints, Welding in the World 49(3) (2005) 93-101.

[146] A. Abdollah-Zadeh, T. Saeid, B. Sazgari, Microstructural and mechanical properties of friction stir welded aluminum/copper lap joints, Journal of Alloys and Compounds 460(1-2) (2008) 535-538.

[147] P. Wanjara, E. Dalgaard, G. Trigo, C. Mandache, G. Comeau, J.J. Jonas, Linear friction welding of Al–Cu: Part 1 – Process evaluation, Canadian Metallurgical Quarterly 50(4) (2013) 350-359.

[148] E. Dalgaard, P. Wanjara, G. Trigo, M. Jahazi, G. Comeau, J.J. Jonas, Linear friction welding of Al–Cu Part 2 – Interfacial characteristics, Canadian Metallurgical Quarterly 50(4) (2013) 360-

370.

[149] V. Firouzdor, S. Kou, Al-to-Cu Friction Stir Lap Welding, Metallurgical and Materials Transactions A 43(1) (2012) 303-315.

[150] V. Firouzdor, S. Kou, Al-to-Mg Friction Stir Welding: Effect of Material Position, Travel Speed, and Rotation Speed, Metallurgical and Materials Transactions 41a(11) 2914-2935.

[151] I. Bhamji, M. Preuss, R.J. Moat, P.L. Threadgill, A.C. Addison, Linear friction welding of aluminium to magnesium, Science and Technology of Welding and Joining 17(5) (2013) 368-374.

[152] A.A. McLean, G.L.F. Powell, I.H. Brown, V.M. Linton, Friction stir welding of magnesium alloy AZ31B to aluminium alloy 5083, Science and Technology of Welding and Joining 8(6) (2003) 462-464.

[153] Breedis, F. John, Fister, C. Julius, Copper alloys for suppressing growth of Cu-Al intermetallic compounds.

[154] A. Elrefaey, Preliminary Investigation of Friction Stir Welding Aluminum/Copper Lap Joint, IIW Pew-Assembly Meeting on FSW in Nagoya 2004 (2004).

3 Materials & Experimental Methods

3.1 Materials

In this study, three kinds of friction welding processes were used including FSW butt welding, friction stir lap welding (FSLW), and linear friction welding (LFW). For FSBW, the base material was 6mm AA5083-H112 rolled sheets; for FSLW, the base materials were 6mm AA6061-T6 rolled sheets and 6mm A356 squeeze casting sheets; for LFW, the base materials were AA5083-H112 sheets and C101 copper sheets with the dimension of 550×300×150 mm. The chemical compositions of all the welding materials are shown in Table 3. 1.

Table 3. 1 Chemical composition of aluminium alloys and copper for welding (wt %)

Material	Temper	Si	Fe	Cu	Mn	Mg	Zn	Cr	Ti	Others	Al
AA6061	T6	0.59	0.36	0.20	0.033	1.01	0.0084	0.18	0.022	≤0.15	Bal.
A356	Squeeze casting	7.02	0.13	0.0042	0.0043	0.34	0.016	0.0025	0.13	≤0.15	Bal.
AA5083	H112	0.4	0.1	0.1	0.6	4.0	0.2	0.15	0.1	≤0.15	Bal.
Cu	F	-	-	≥99.9	-	-	-	-	-	-	-

AA5083 6 mm thick sheets were supplied by Northeast Light Alloy Co., Ltd., (China) in the H112 temper (hot work / cold work, then slight work-hardening to meet the specific mechanical performance requirements). The AA5083-H112 alloy, which has a medium strength and good corrosion resistance and welding properties, has been widely used in many industrial fields including automobile, shipbuilding, rail vehicles, etc. AA6061 6 mm thick sheets were also supplied by Northeast Light Alloy Co., Ltd., (China) in the T6 condition (solution and artificial aging). A356 sheets were supplied by Guangzhou Jinbang Non-ferrous Alloy Metals Co. Ltd. (China) in the squeeze casting condition. Squeeze casting is a kind of casting method, by which the liquid metal poured into the mold cavity is formed, crystallized and solidified at high mechanical pressure. It is a process between casting and forging, which has advantages of both processes. Copper sheets were supplied by Jiangxi Copper Corporation (China) with a hot rolling condition. C101 copper has good electrical conductivity, heat conduction, corrosion resistance and processing performance, which can be welded and brazed.

3.2 Friction Welding Processes

3.2.1 Friction stir butt welding

The friction stir butt welds were prepared with an FSW-3LM-4012 FSW machine located at Guangdong Academy of Sciences (GDAS), Guangzhou, China (shown in Fig. 3. 1). The AA5083 sheets were cut to 100 mm × 200 mm (TD × RD), and the two sheets were fixed as the schematic diagram in Fig. 3. 2. Prior to welding, the surfaces of the plates especially the contact surfaces were ground to get rid of the surface oxide and cleaned using acetone to clear the oil contamination. As shown in Fig. 3. 3, the FSW were conducted using a H13 steel tool with a 15mm diameter shoulder and a 6 mm pin, which had a triangular conical right-hand thread. During the FSW process, the rotating tool (anticlockwise) with a 2.5° tilt plunged into the sheet and then travel along the RD of the plates. Three levels of tool rotation speed (800, 1000, 1200 rpm) as well as three feed rates (100, 200, and 300 mm/min) were chosen in this study, based on multiple trials to confirm that sound welds could be obtained. After welding, all the welds were air cooled to the room temperature for microstructure and property analyses.

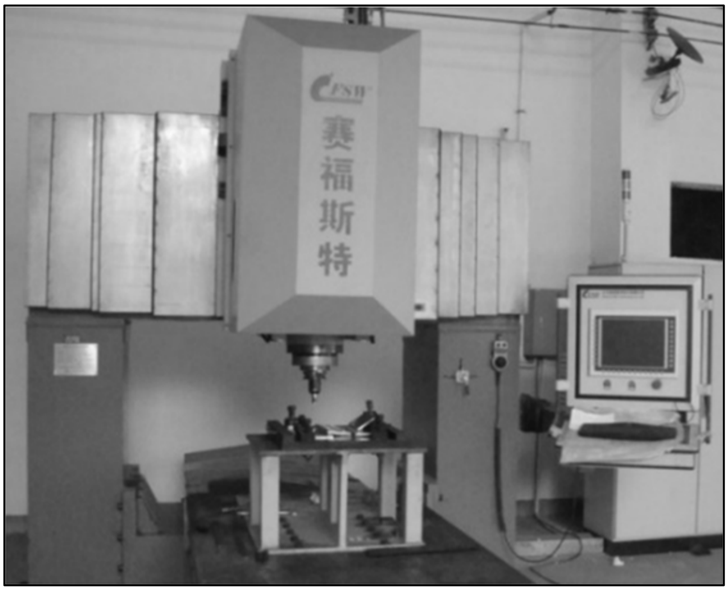

Fig. 3. 1 Photograph of the FSW machine at GDAS

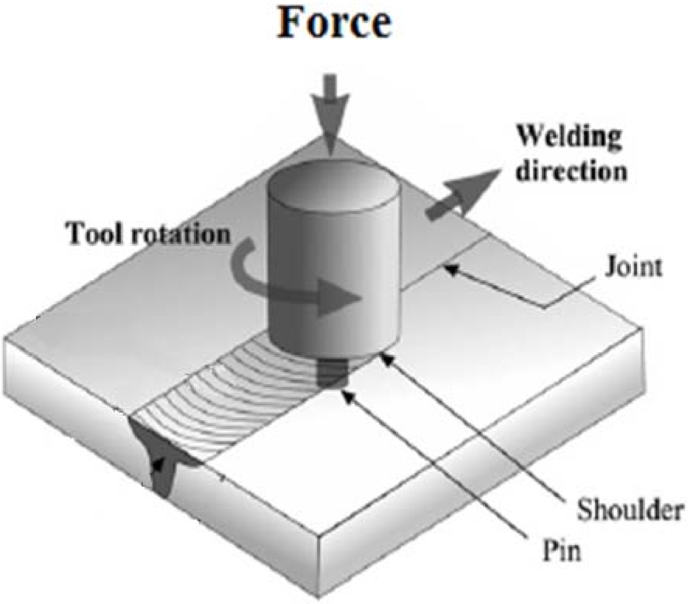

Fig. 3. 2 Schematic diagram of FSW butt welding process

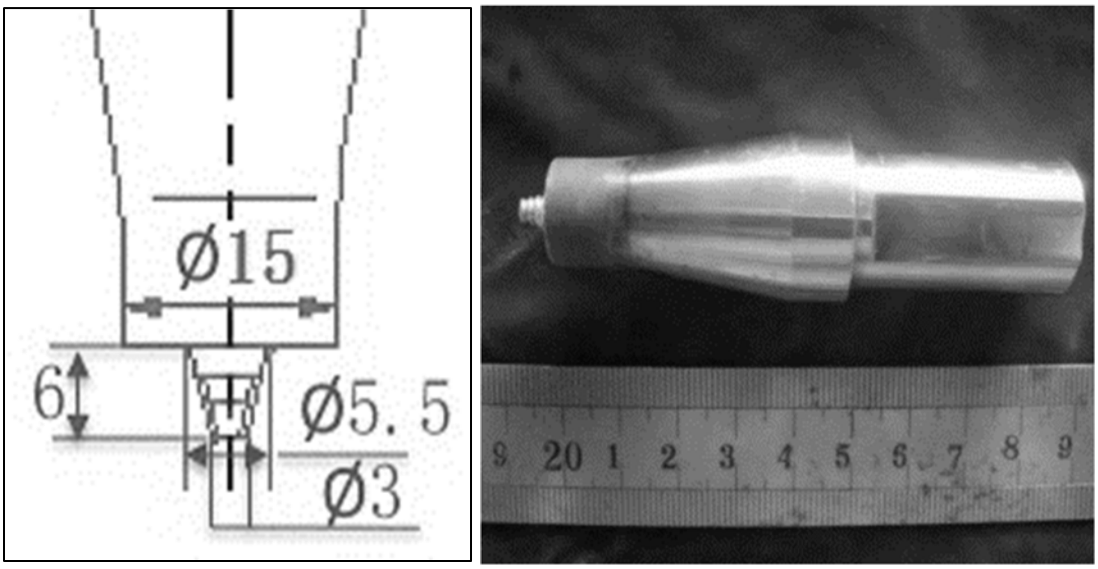

Fig. 3. 3 Sketch and photograph of the welding tool for FSW butt welding

3.2.2 Friction stir lap welding

Friction stir lap welding were produced using the same equipment as friction stir butt welding. Prior to welding, one AA6061-T6 sheet and one A356 sheet were fixed on the FSW machine in a lap mode shown in Fig. 3. 4 for welding (the AA6061 sheet was on the top). As shown in Fig. 3. 5, the lap welding tool was also made of H13 steel with triangular conical right-hand thread, but slightly different in specifications, which were 20 mm diameter shoulder and 10 mm pin. Three levels of tool rotation speed (800, 1000, and 1200 rpm) and one welding rate (100 mm/min) were chosen for lap welding, and natural cooling followed.

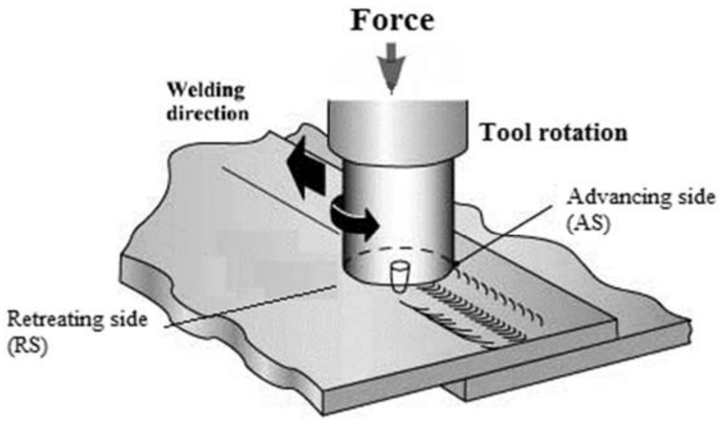

Fig. 3. 4 Schematic diagram of FSLW process

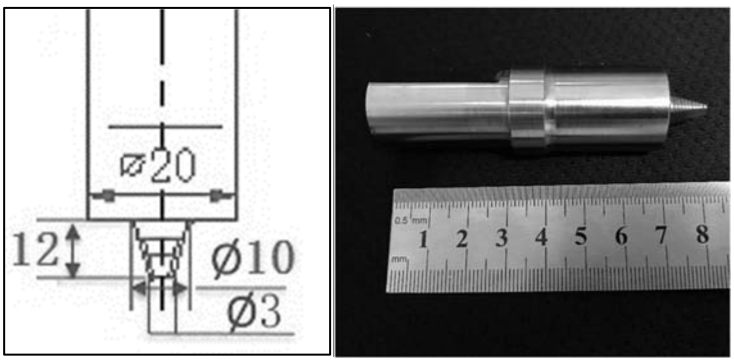

Fig. 3. 5 Sketch and photograph of the welding tool for FSLW

3.2.3 Linear friction welding

LFW experiments were carried out on the XMH-16 linear friction welding machine manufactured by Northwestern Polytechnical University, Xi'an, China (shown in Fig. 3. 6). Welding materials involved were AA5083-H112 aluminium to the same material as well as to dissimilar material Cu C101 which was 99.9% pure copper. Before welding, the friction surfaces of both samples were grinded with sandpaper and oil removed with acetone. Three different forging pressures (respectively 110, 80 and 60MPa) were chosen based on a large number of welding experiments. Other parameters were kept constant as welding time 5s, vibration frequency 35Hz, amplitude 2.5mm. When welding Al to Cu, the Cu weld side was vibrated while the Al side was kept stationary. The schematic diagram of linear friction welding is shown in Fig. 3. 7.

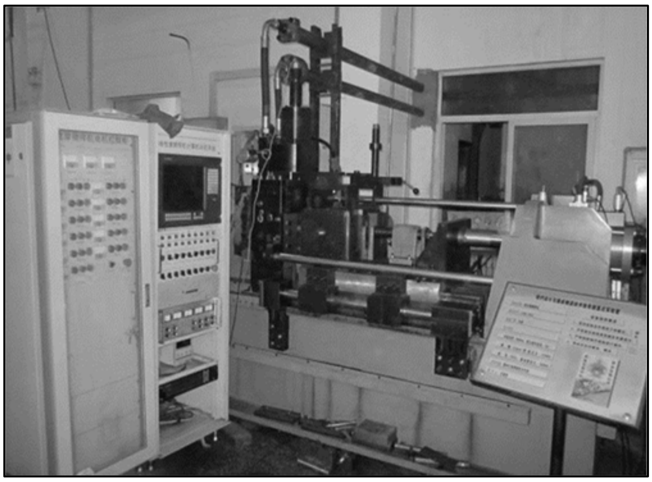

Fig. 3. 6 Photograph of the LFW machine at NWPU

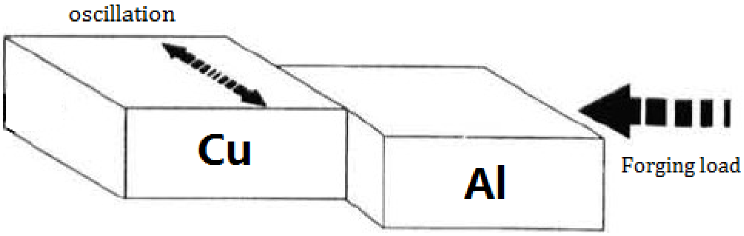

Fig. 3. 7 Schematic diagram of LFW process

3.3 Microstructure characterization

3.3.1 Optical microscopy (OM)

A ZEISS Axioskop 2 MAT mot optical microscope and a LEICA-DMI3000M optical microscope were used to examine the optical microstructures of the samples. Base metal and weldment specimens were cut using an EDM at a low speed to minimise deformation. Some of them which were no need for electronic polishing were mounted in self-curing resin. All the specimens for OM were ground to 2000 grade SiC paper, polished using 9, 6, 3 and 1μm diamond suspensions, to a final polishing stage using a magnesia suspension finish. Particle measurements of aluminium alloys were carried out on polished (without etching) specimens, and a commercial image analysis software ImageJ was used to analyse the particle fraction in the welds according to the colour difference between particles and matrix. Keller's reagent (3 ml nitric acid, 6 ml hydrochloric acid, 6 ml hydrofluoric acid and 150ml distilled water) was used to etch the aluminium samples to reveal the kissing bond structures in the welds, and ImageJ was also used to analyse the length of the kissing bond. An alkaline reagent, named Weck's reagent (4 g $KMnO_4$, 1 g NaOH and 100 ml distilled water) was used to show the grain structure of recrystallised aluminium alloys in the SZ, particularly effective for showing the grain structure of recrystallised AA6061. For revealing the grain structure of AA5083 friction stir welds, electrolytic-etching was conducted in fresh Barker's reagent (5 ml HBF_4 in 200 ml H_2O solution) with a stainless steel cathode for 2 minutes at 20 V. Besides, a solution of 5g $FeCl_3$, 10 ml HCl, 100 ml distilled H_2O was used to etch the copper samples to reveal the grain structure. The equivalent grain size was measured according to ASTM standard E112.

3.3.2 Scanning Electron Microscopy (SEM) and Energy Dispersive X-ray Spectroscopy (EDX)

The sample preparation for SEM is similar to OM. Polished specimens (without etching) were installed in a JEOL 6060 SEM equipped with an Oxford instruments Inca 300 energy dispersive X-ray spectroscopy (EDX) system to observe the morphology and to analyse the composition of the particles, precipitates, as well as the matrix. Specimens after etching could be suitable for kissing bond characterization using a JEOL 6060 SEM or a JEOL 7000 FEG SEM (see Fig. 3. 8 (a)). A JEOL JXA-8100 electron probe micro-analyser (EPMA) (at GDAS, China, shown in Fig. 3. 8 (b)) was used to analyse the tensile and fatigue fracture surfaces. All the SEM/EPMA microscopies were operated at 15 kV for spectroscopy, and 20 kV for imaging.

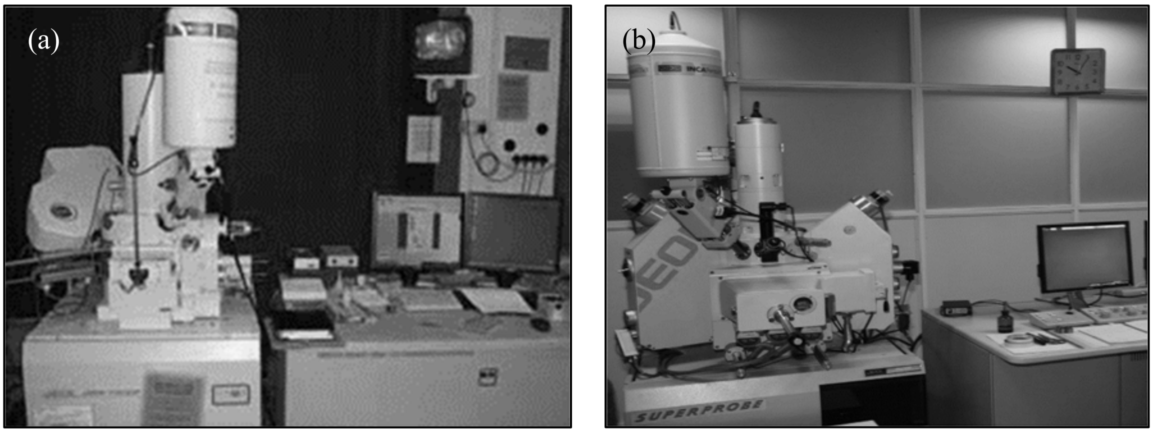

Fig. 3. 8 Photographs showing (a) JEOL 7000 FEG SEM at the University of Birmingham, UK; (b) JEOL JXA-8100 EPMA at GDAS, China

3.3.3 Transmission Electron Microscopy (TEM)

For TEM sample preparation, Φ3 mm discs were made by spark-eroding from 0.2mm thick slices which were collected from the welds or the base-metal. The discs were ground using 2000 grade SiC paper to the thickness of ~150μm, and then thinning in a twinjet electro-thinning system using

5% perchloric acid ethanol solution at -25 ˚C with a voltage of 20 V in order to form a thin area in the centre.

For kissing bond structure investigation in friction stir welds, the material of kissing bond region was cut out and thinned using a FEI Quanta 3D FEG SEM, equipped with a focused ion beam (FIB) system (see Fig. 3. 9 (a)) and directly examined under the TEM. FIB is an instrument which uses an electric lens to focus the ion beam for micro-cutting. The ion beam of the commercial FIB system is liquid metal ion source, and the metal material is gallium, which has low melting point, low vapor pressure and good oxidation resistance. The addition of electric field to the liquid metal ion source can cause the liquid gallium to form a fine tip, with a negative electric field to pull the tip of gallium, leading to a gallium ion beam. The beam was focusing on the surface of the specimen to achieve the purpose of cutting by physical collisions. The integration of SEM and FIB can be used to monitor the sample cutting during the process, so that a local slice of the sample can be observed. The procedure of the FIB sample collection is shown schematically in Fig. 3. 10, and the images of location and thinning for kissing bond samples using FIB are shown in Fig. 3. 11.

Bright-field imaging and diffraction were carried out on a JEOL 2100 TEM equipped with an Oxford EDS (see Fig. 3. 9 (b)) to investigate precipitates, dislocations, as well as kissing bond structures.

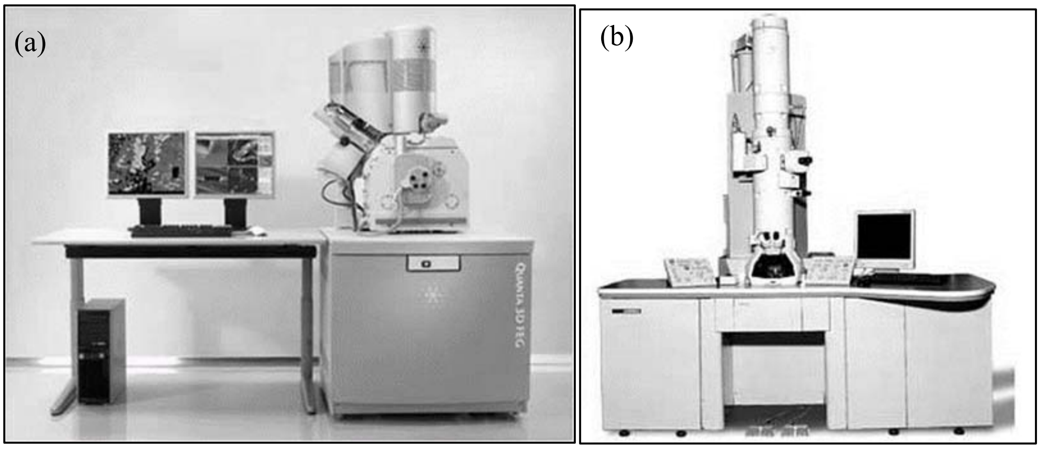

Fig. 3. 9 Pictures showing (a) FEI Quanta 3D FIB system; (b) JEOL 2100 TEM

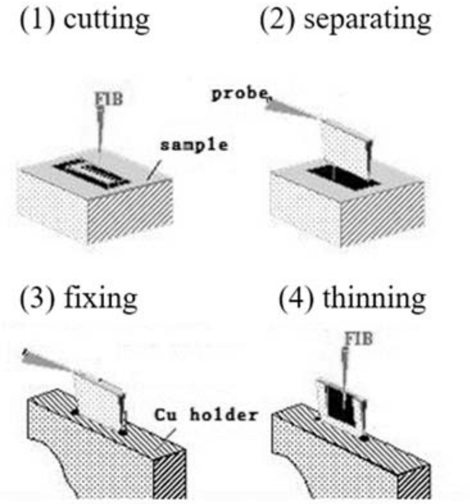

Fig. 3. 10 Schematic diagram illustrating the FIB sample collection procedure

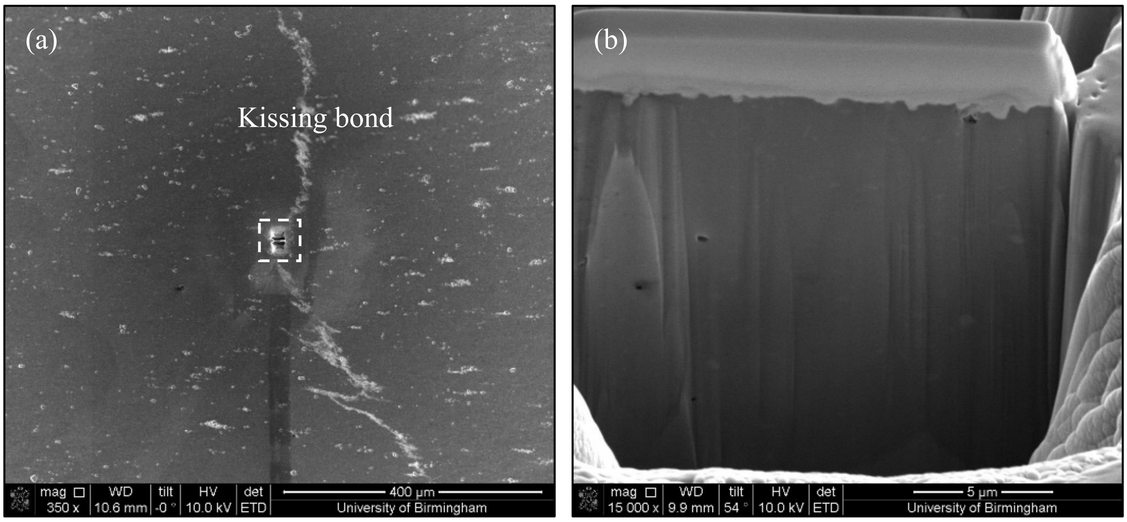

Fig. 3. 11 SEM images of FIB sample collection (a) location of the kissing bond, (b) magnification of dashed zone of (a)

3.3.4 Electron Backscattered Diffraction (EBSD)

EBSD was used in this study for the accurate characterization of the grain structures, especially the recrystallised microstructures in the SZ of FSW. A Nova nano FEG SEM equipped with an Oxford INCA crystal EBSD system was used in this study for EBSD image photography and data analysis. The specimens were ground and polished similar to OM samples, and then electro-polished in 5% perchloric acid ethanol solution at -20 ˚C for 1 minute at 20 V and 30 mA to remove the residual surface damage created during polishing. The EBSD was operated for data acquisition at a 70° tilt angle, a high voltage of 30 kV and a square grid of with a step size of 0.5μm. Finally, an HKL Channel 5 EBSD software was used for data analysis.

3.4 Differential Scanning Calorimetry (DSC)

In this study, a heat-flux DSC 404C Pegasus calorimeter was used for the thermal analysis of the samples. A specimen pan and a reference pan were equipped on the heat flux plate, where the temperature can be recorded in the process of isothermal and anisothermal cycles. To start the experiment, a sample was put into the specimen pan, while the reference pan could be left empty or with a reference specimen. When the experiment started, the isothermal heating or cooling was carried out under the same conditions and a temperature difference between the sample and the reference material could be produced when the phase transition took place. The power compensation amplifier automatically adjusted the current of the compensation heating wire to remain the same temperature for specimen and reference. This compensation heat is the thermal effect of the sample, which can be recorded as the data.

It was found that DSC can analyse the dislocation density of the deformed material by measuring the release of stored energy [1], instead of using TEM [2]. Small specimens (less than 40 mg) were cut from the weld transverse cross-section of the welds using an electrical wire cutting machine, and a fully annealed pure Al with the same weight as the specimen was taken as the reference. When the scan started, the temperature of the specimen and the reference increased to 420 ˚C at a heating rate of 20 ˚C /min and then naturally cooled down to the room temperature. After the first scan, the heating procedure was repeated as a second scan to determine the baseline. The change of the stored energy was determined according to the heat released or absorbed in the DSC peaks. The Proteus-NETZSCH software was used to analyse the DSC data.

3.5 X-ray Testing

3.5.1 X-ray diffraction (XRD)

XRD is a method to qualitatively analyse the phase composition of materials. Due to the regular arrangement of atoms or ions in the crystal, the radiation can be scattered, and the phase will be strengthened in the specific direction. A special X-ray diffraction phenomenon corresponding to the crystal structure is produced. In this study, the phase analysis of related materials was carried out by using SmartLab X-ray diffractometer, which was produced by RIGAKU. Cu target was used as anode, with 40kV working voltage and 20mA working current. The results of XRD were calibrated by a phase analysis software Jade and a graphics processing software Origin, respectively.

3.5.2 X-ray radiographic testing

Radiographic testing is commonly used on the industrial parts including welds, castings, composite materials, etc. for characterization of interior defects without destroying the components. In this study, X-ray radiographic non-destructive testing (NDT) was conducted for the FSW butt welds at Intertek NDT. X-ray was used to penetrate the tested weldments which were untreated after welding. The radiation was passed through the part and captured on radiographic film.

3.6 Mechanical properties

3.6.1 Hardness Measurements

Hardness is the most commonly used in testing the performance index in mechanical properties of metal materials, because of the speed and economy. In this study, contour mapping of the hardness measurements was conducted for both the welds as well as the base materials by an Indentec Vickers hardness tester.

For the base materials, samples were collected in the TD-ND plane, which was the same as the welds tested. For the welds, hardness traces at mid-thickness as well as the contour distributions of the whole transversal surface were tested. The oxidation layer on the surface of the sample was ground with fine metallographic sandpaper before testing, and the parallelism between the top and bottom of the specimen was ensured. In the testing process, a 5kg force load and a maintaining time of 10 s were applied on the samples. The distance between the testing spots was kept more than 5 times larger than the length of the indentation diagonal. After unloading, the indentation diagonals were measured, and consequently the Vickers Hardness Numbers (VHN) was calculated using the formula:

$$\text{VHN (Hv)} = 1.854\frac{P}{d^2} \tag{3.2}$$

where P is the load in kg, d is the average length of the indentation diagonals in mm (shown in Fig. 3. 12). Besides, the indentations were taken every other 1 mm in both horizontal and vertical direction on the weld faces for contour mapping.

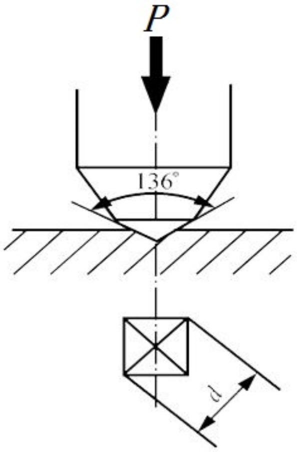

Fig. 3. 12 The schematic diagram of the Vickers hardness testing

3.6.2 Tensile Tests

Room temperature tensile test samples were obtained from the transverse directions of the base metal as well as the welds. The sample preparation method was following the standard BS EN 1002-1: 2001 for FSW butt welding and LFW, and ASTM D1002 for FSW lap welding. The specifications of the tensile test samples are shown in Fig. 3. 13-15. A DNS200 universal electronic tensile machine was used for the tensile tests, with a tensile speed of 2 mm/min. The 0.2% proof stress ($\sigma_{0.2}$) or yield strength (YS), ultimate tensile strength (UTS) and elongation were tested for each state of three parallel specimens.

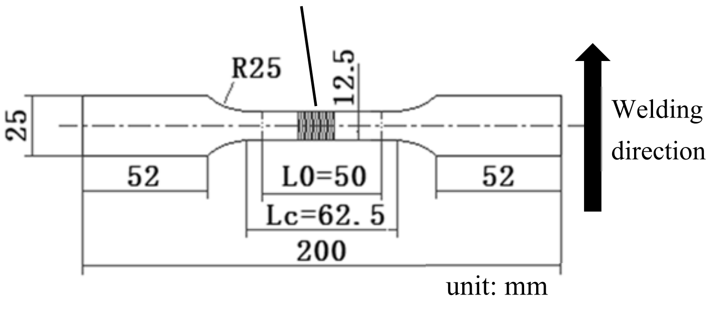

Fig. 3. 13 Tensile specimen dimensions for FSW butt welds

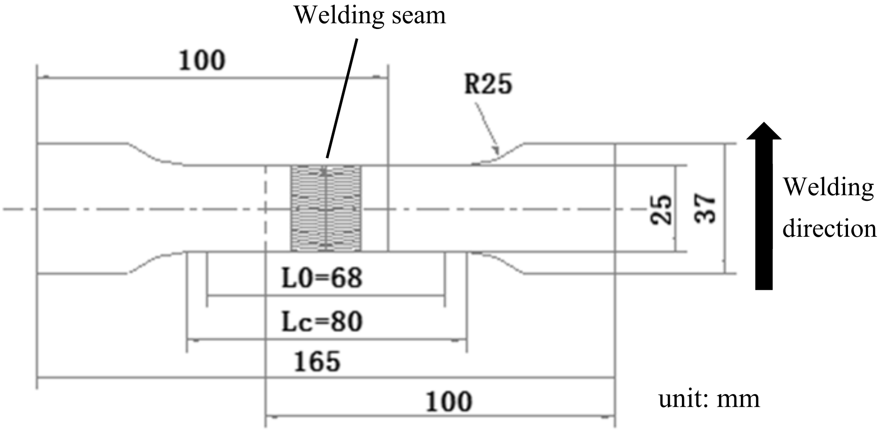

Fig. 3. 14 Tensile specimen dimensions for FSLW

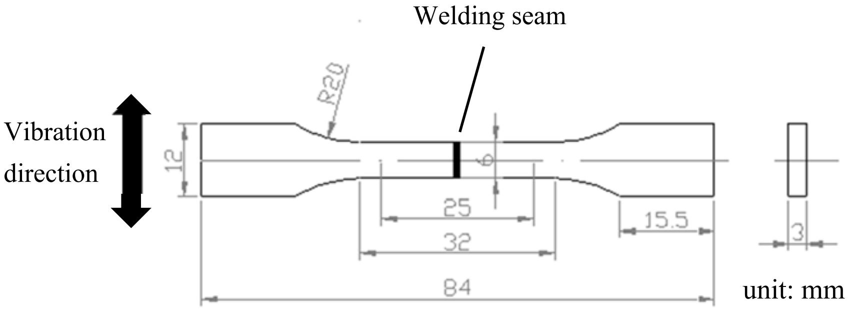

Fig. 3. 15 Tensile specimen dimensions for LFW

3.6.3 Fatigue tests

Tension-tension fatigue test were performed to investigate the fatigue fracture behaviour of the friction stir butt welds in this study. Samples were cut out according to the dimension shown in Fig. 3. 13, using EDM. Before testing, the sharp edges of samples were ground to prevent the surface stress concentration using 600 grade SiC paper. The surfaces were also ground to remove the surface striation formed during EDM machining. The fatigue test was performed on an Instron-8801 fatigue tester (see Fig. 3. 16) at a stress ratio R (R=σmin/σmax) of 0.1 and at frequencies of

30Hz.

Fracture fatigue samples were investigated using OM and digital camera for analysing the fatigue fracture type. Fracture surfaces were observed on SEM after ultrasonically cleaned in acetone, for analysing the fatigue behaviour as crack initiation, crack propagation etc.

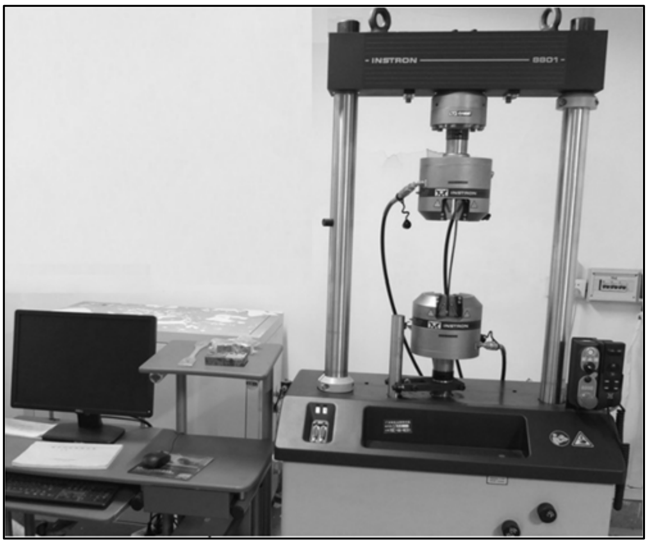

Fig. 3. 16 The photograph of the Instron-8801 fatigue tester

3.7 Heat Treatment

To further increase the mechanical properties of the welds, artificial aging at various temperatures was carried out for the welds which were cut vertical to the welding direction into specimens. Heat treatments were carried out in a laboratory oven, which had a temperature accuracy of ±5 ˚C. The heat treatment was carried out for the friction stir lap welds of AA6061-T6 and A356, to precipitate the strengthening phase (Mg_2Si for AA6061), followed by water (~25°C) cooling. After the heat treatment, hardness tests were carried out to simply reflect the effect.

3.8 References

[1] M. El-Tahawy, Y. Huang, T. Um, H. Choe, J.L. Lábár, T.G. Langdon, J. Gubicza, Stored energy in ultrafine-grained 316L stainless steel processed by high-pressure torsion, Journal of Materials Research and Technology 6(4) (2017) 339-347.

[2] M. Attallah, Microstructure property development in friction stir welds of aluminim based alloys, 2008.

4 Friction Stir Butt Weld of AA5083: Effect of Kissing Bond on Microstructure and Properties

4.1 Introduction

As reviewed in Chapter 2, AA5083, a kind of Al-Mg series alloy, has acceptable comprehensive properties including medium strength, high corrosion resistance, as well as high formability, etc. It has been widely used in many industrial fields as automobile, shipbuilding etc. [1, 2]. For high quality connection of AA5083 alloy, FSW has been successfully introduced in the industrial field, even before that, in the academic circles, the influence of the FSW parameters of AA5083 on the welding quality as well as a series of properties had been studied [3-8]. It was found that FSW joints had many advantages compared to fusion welds, in the field of mechanical properties, fatigue properties and corrosion resistance, et al. Besides, numerical simulations had been developed as well in optimising the FSW parameters in a simple way.

In FSW butt joints of aluminium alloys, “kissing bond” can be occasionally observed in the microstructure, showing a black zigzag curve, or C shape curve, etc., and it is supposed to generate originally form the oxide layer of the contact surface [9]. In the previous study, the kissing bond was identified as Al_2O_3 clusters which might affect the mechanical properties of the welds [10]. However, limited reports were found concerning the influence of kissing bond in FSW on the properties of the joints, particularly how to characterise or quantify the kissing bond in order to show the relation link to welding parameters and weld properties. In this chapter, the FSW butt configuration of AA5083 was systematically studied on the microstructure, mechanical properties and defects, with the special focus on the effect of FSW parameters including tool rotation speed and tool feed rate on the kissing bond morphology.

4.2 Friction stir butt weld of AA5083

4.2.1 Base material characterization

AA5083 is the main material investigated in this chapter. Microstructural characterisation was performed in the aim of investigating the microstructural-property relationship associated with FSW.

In this study, the AA5083 to be welded was in H112 heat treatment condition which was defined as slightly work-hardening after hot deformation. In the optical microstructure shown in Fig. 4.1, the grain morphology of the ST-RD plane was illustrated as elongated grains, along the RD, fine in thickness. Besides, the grains were uniform in shape and size especially in the through thickness direction, without any abnormal grain growth observed in the microstructure. It was also found that black particles with the size of several microns, which were reported as Al(Fe,Mn)Si phase and Mg_2Si phase[11], were uniformly dispersed in the matrix.

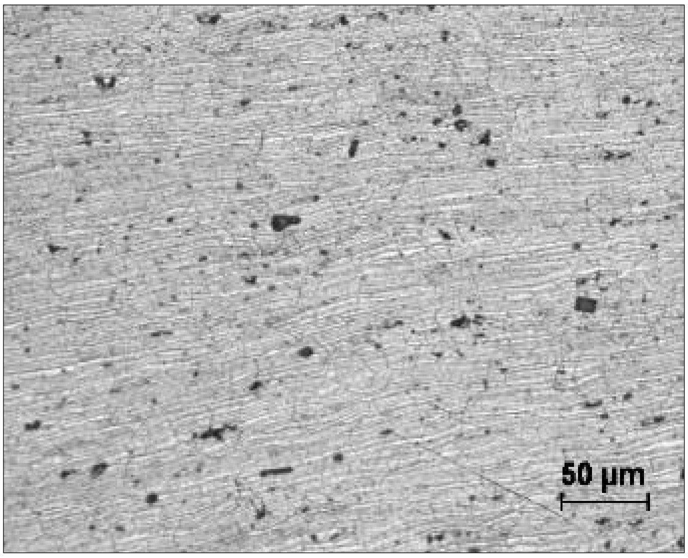

Fig. 4. 1 Optical microstructure of the AA5083-H112 base material.

In a higher magnification SEM image shown in Fig. 4. 2 (a), it was found that small white particles were dispersively distributed in the Al matrix. Observing the detail using TEM shown as Fig. 4. 2 (b), the particles were intragranular with the size varied from 0.1μm to 0.3μm. EDS result of the particle marked A (see Fig. 4. 3) showed that these particles contained Al, Mn, Cr and Cu elements. Combining with the XRD result shown in Fig. 4. 4, it was revealed that the phase with rod shape could be Al_6Mn, which is difficult to be observed by OM[12].

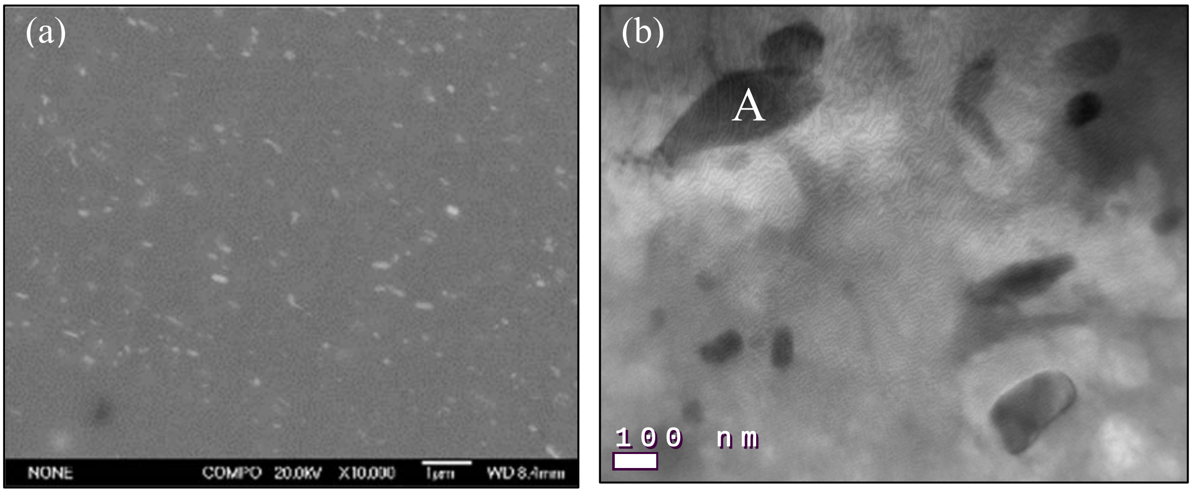

Fig. 4. 2 SEM (a) and TEM (b) image of the AA5083-H112 base material.

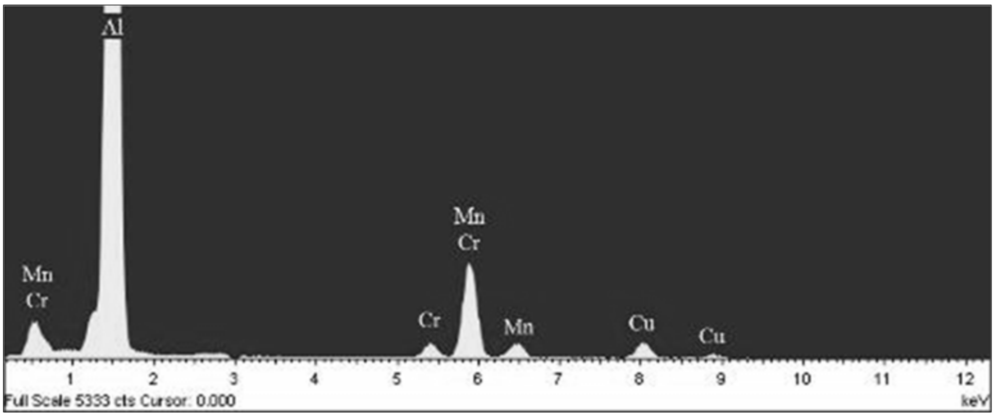

Fig. 4. 3 EDX spectra of particle A in Fig. 4. 2.

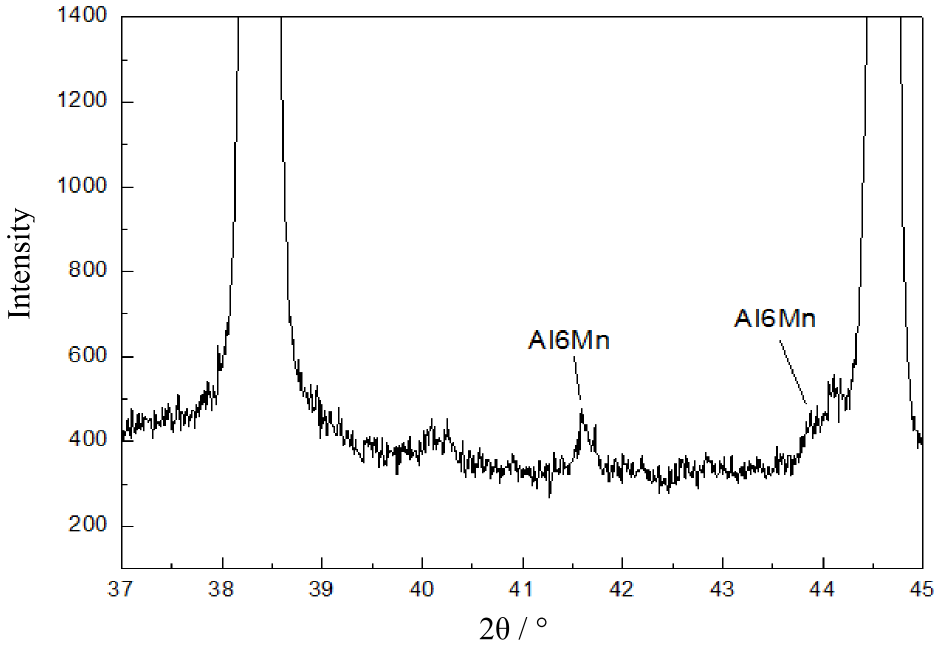

Fig. 4. 4 Partial enlarged image of the XRD spectrum for the experimental material.

Table 4. 1 shows the Vickers' hardness and tensile properties of the base material AA5083. It was found that the base material had a high elongation, moderate tensile strength and relatively low yield strength as well as hardness. Therefore, this aluminium plate had excellent processing properties and good ability of deformation, which can be properly used in the field of automobile manufacturing.

Table 4. 1 Hardness and tensile properties of the base material AA5083

Experimental material	Hardness / HV	UTS / MPa	YS / MPa	EL / %
AA5083	84.8	335	163	20

4.2.2 Microstructure of the FSW

The overall macrostructure of the AA5083 FSW weld seam is shown in Fig. 4. 5, including stir zone (SZ), thermo-mechanically affected zone (TMAZ), as well as heat-affected zone (HAZ). It is also shown that the TMAZ and SZ has a clear boundary towards the advancing side (AS), which can be easily distinguished according to the grayscale, while towards the retreating side (RS), the transition was not clear. The grayscale reflects the deformation extent in the FSW, revealing that the deformation is severer at AS than RS.

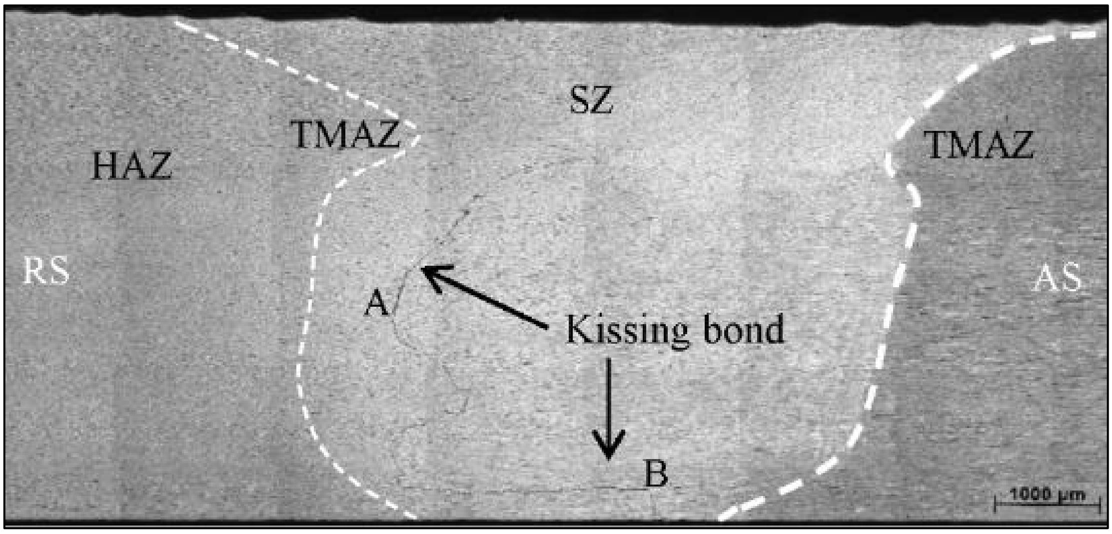

Fig. 4. 5 The weld zones macrostructure of the AA5083 FSW weld (ω=1000rpm, v=300mm/min).

Fig. 4. 6 shows the microstructure of SZ, TMAZ and HAZ, respectively. As shown in Fig. 4. 6 (a), SZ in FSW of AA5083 was composed of the recrystallization equiaxed grains, with the average grain size of approximately 5μm. Fig. 4. 6 (b) shows the microstructure of TMAZ to the AS, a hybrid microstructure including deformed original elongated grains and recrystallization fine grains. In the microstructure of the HAZ shown in Fig. 4. 6 (c), the original elongated grains started to disappear, indicating that the material experienced a recovery procedure during FSW.

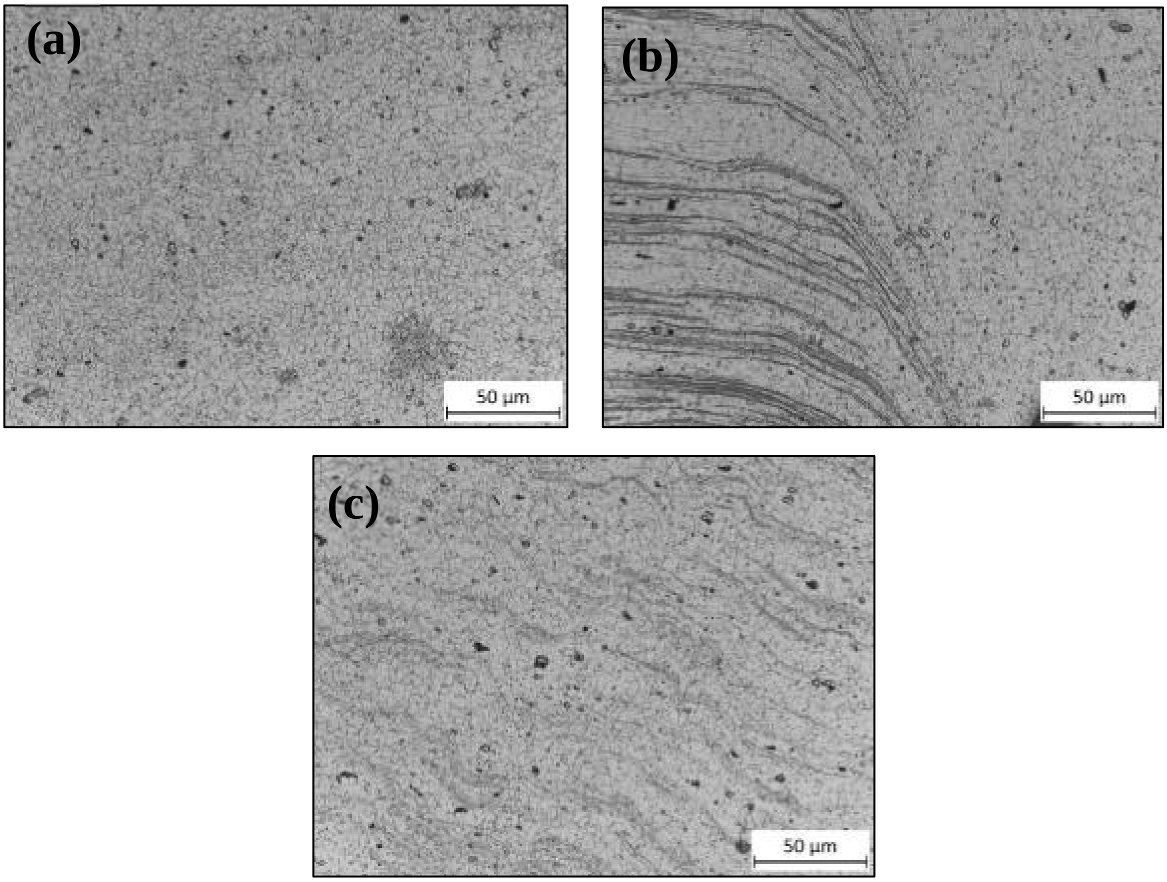

Fig. 4. 6 The optical microstructure of SZ (a), TMAZ at AS (b) and HAZ at RS (c) in Fig. 4. 5.

Besides, through testing the recrystallization grain size of the SZ in the FSW joints using different parameters, it was found that the recrystallization grain size was significantly influenced by welding parameters. Fig. 4. 7 shows the effect of the welding parameters on the average grain size in the SZ. The average grain size was ~4µm in the SZ of the weld obtained by 300mm/min, 800rpm, and nearly doubled to ~9µm at the welding parameters of 100mm/min, 1200rpm. It can be concluded that finer recrystallization grain size can be obtained when welding at a lower tool rotational rate and / or a higher welding speed in the FSW procedure. In metal materials, Zener-Hollomon parameter reveals the relationship of temperature, strain rate and grain size [13]. The formula related is:

$$Z = \dot{e} \cdot \exp\left(\frac{Q}{RT}\right) \tag{4.1}$$

where $\dot{e}$ is the strain rate, Q is the deformation activation energy, R is the gas constant and T is the temperature. It has been found that the decrease of Z could result in the increase of the average grain size (d), which followed the relation $d^{-1}=a+b\cdot ln(Z)$ where a and b were constants [13]. In this study, as the increase of the tool rotation speed, the $\dot{e}$ increased while T increased as well. As a result, the average grain size increased, meaning that the Z parameter decreased. Therefore, temperature was the main factor affecting dynamic recrystallization in the FSW joints.

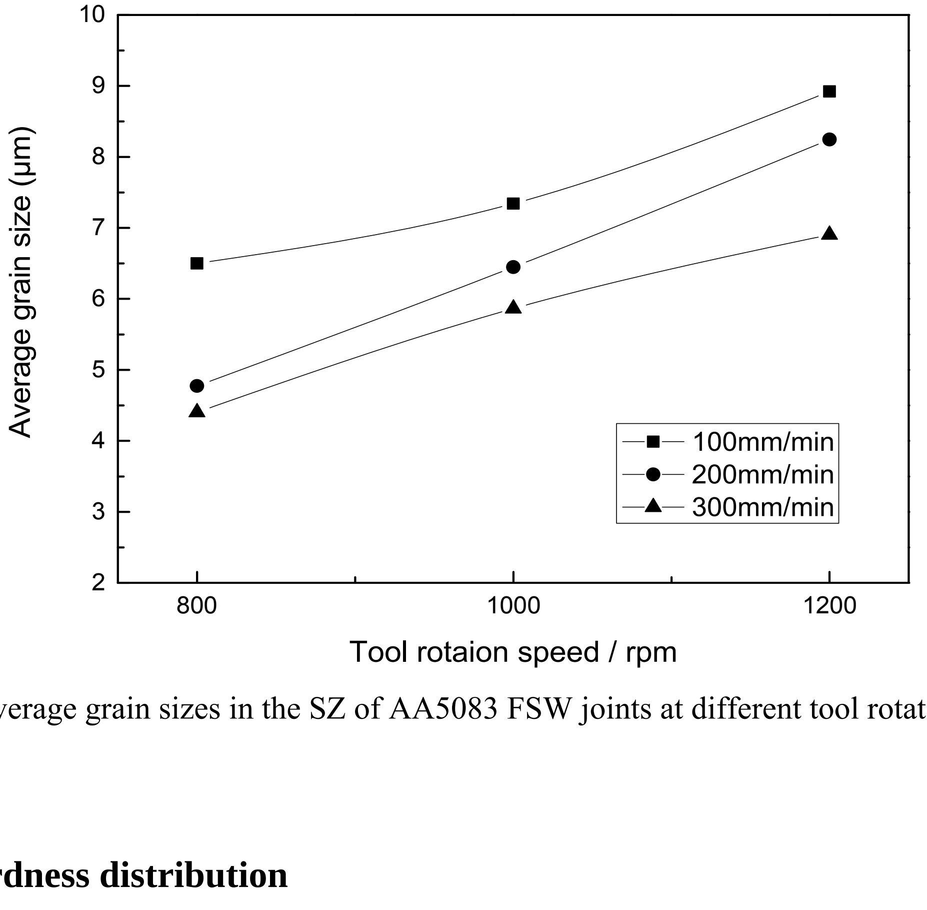

Fig. 4. 7 Average grain sizes in the SZ of AA5083 FSW joints at different tool rotation speeds.

4.2.3 Hardness distribution

Temperature can also affect the hardness distribution in the FSW joints. Fig. 4. 8 shows the Vickers' hardness distribution through the weld centre of the joints obtained at different parameters. It was found that the hardness profiles for all the welding conditions presented a “W” shape. The hardness of the HAZ in both AS and RS dropped significantly, while the hardness of SZ was similar or slightly lower to the base metal. Because the HAZ experienced only heat effect during FSW procedure, which lead to the hardness decrease. In the SZ, the materials experienced the synergistic effect of recrystallization softening and work hardening, which can keep the hardness close to the base metal. The TEM image of an FSW joint of AA5083 at SZ was shown in Fig. 4. 9, dislocation pile-up was found in the SZ of the welds, where it could contribute to the hardness. The dislocation density can be determined by measuring the release of stored energy using DSC, according to the formula [14]:

$$\rho = \frac{E}{\rho \alpha G b^2} \tag{4.2}$$

where ρ is dislocation density, E is released stored energy per unit volume, α is a dimensionless parameter related to dislocation interactions, G is the shear modulus, and b is the Burger’s vector, showing that the dislocation density is proportional to the released stored energy. Fig. 4. 10 shows the DSC traces and the stored energy in SZ centre of the FSW joints produced at different welding tool rotation speed. It was found that with the increasing tool rotation speed, the released stored energy decreased, which means that the dislocation density was lower, resulting in the loss of the hardness at the SN of the weld.

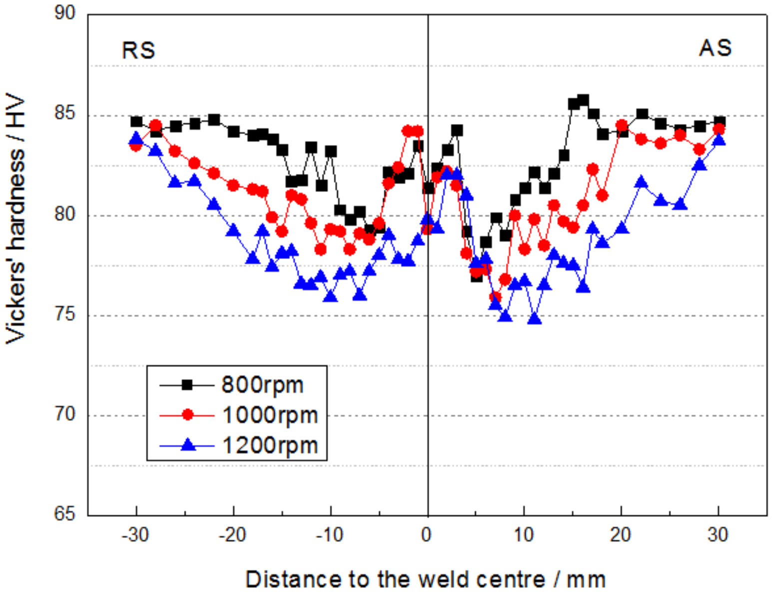

Fig. 4. 8 Vickers' hardness distribution through the weld centre of FSW AA5083 (tool feed rate 100mm/min).

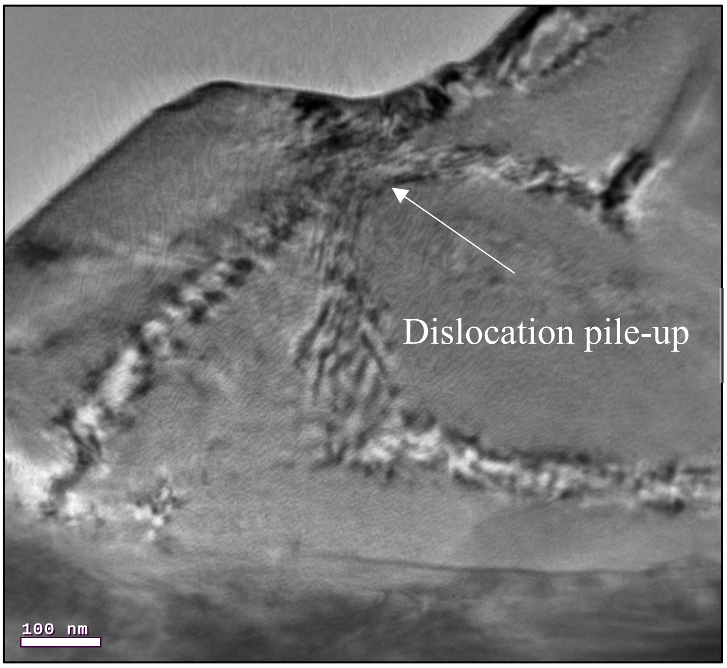

Fig. 4. 9 TEM image of an FSW joint of AA5083 at SZ (parameters: 100mm/min and 800rpm).

Therefore, for AA5083 FSW, the work hardening effect takes a significant role in the hardening of the welds, reflected in the dislocation density, however, precipitation effect could play a minor role in hardness contribution to the FSW joints, since it belongs to work-hardenable alloy.

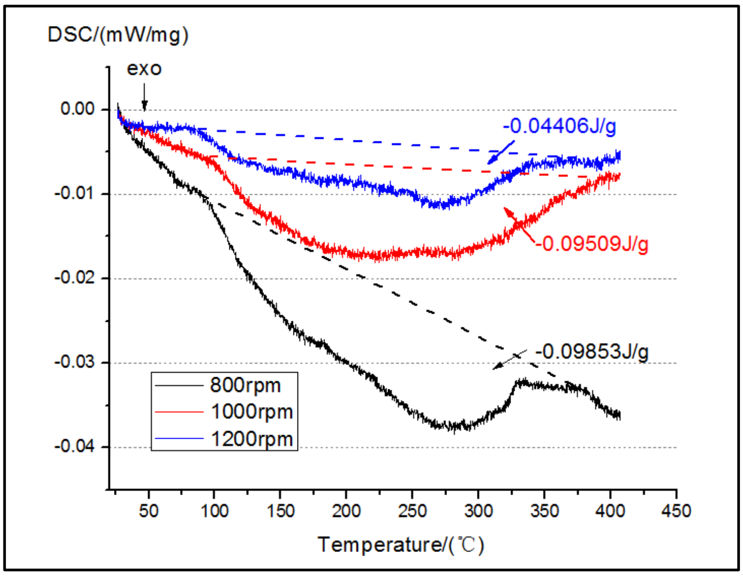

Fig. 4. 10 DSC traces for the SZ of the welds of various tool rotation speed and the amount of energy release.

Besides, as shown in Fig. 4. 8, with the increase of the tool rotation speed, the hardness of HAZ was lower, and the width of “low hardness zone”, corresponding to the width of HAZ significantly increased. It was also due to the higher tool rotation speed which can produce more heat, resulting in the broaden of the HAZ and decrease in hardness.

Fig. 4. 11 shows the hardness of the joints welded by various tool feed rates. It was found that with the increasing tool feed rate, the hardness in the SZ dropped significantly. When the tool feed rate increased, the stirring effect per unit time became less for the material in the SZ. For AA5083 which is a work-hardening alloy, the hardness in the SZ was dominated by the work-hardening effect of the material. Therefore, the hardness in the SZ decreased with the increasing tool feed rate. Besides, according to the results above, with the increasing welding feed rate, the

recrystallization grain size in the SZ was finer, thus the hardness in the SZ was lower. Therefore, the recrystallization softening also contributed to the hardness of the SZ when the tool feed rate was changing.

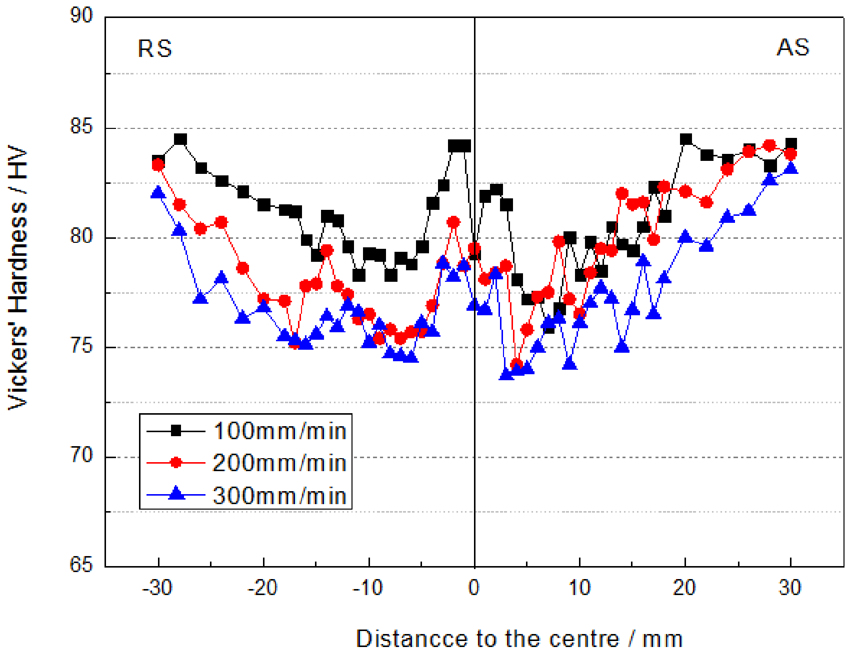

Fig. 4. 11 Vickers' hardness distribution through the weld centre of FSW AA5083 (tool rotation speed 1000rpm).

4.2.4 Non-destructive testing (NDT)

Non-destructive testing (NDT) was performed on the AA5083 FSW joints obtained at different tool feed rates using X-ray radiographic testing. The results showing X-ray inspection of the FSW joints is in Fig. 4. 12. It was found that no obvious defect was detected except for few small isolated gas pores at the finish step and surface features at the start step of the welding. Besides, under changing tool feed rate, no significant difference was observed in the X-ray results.

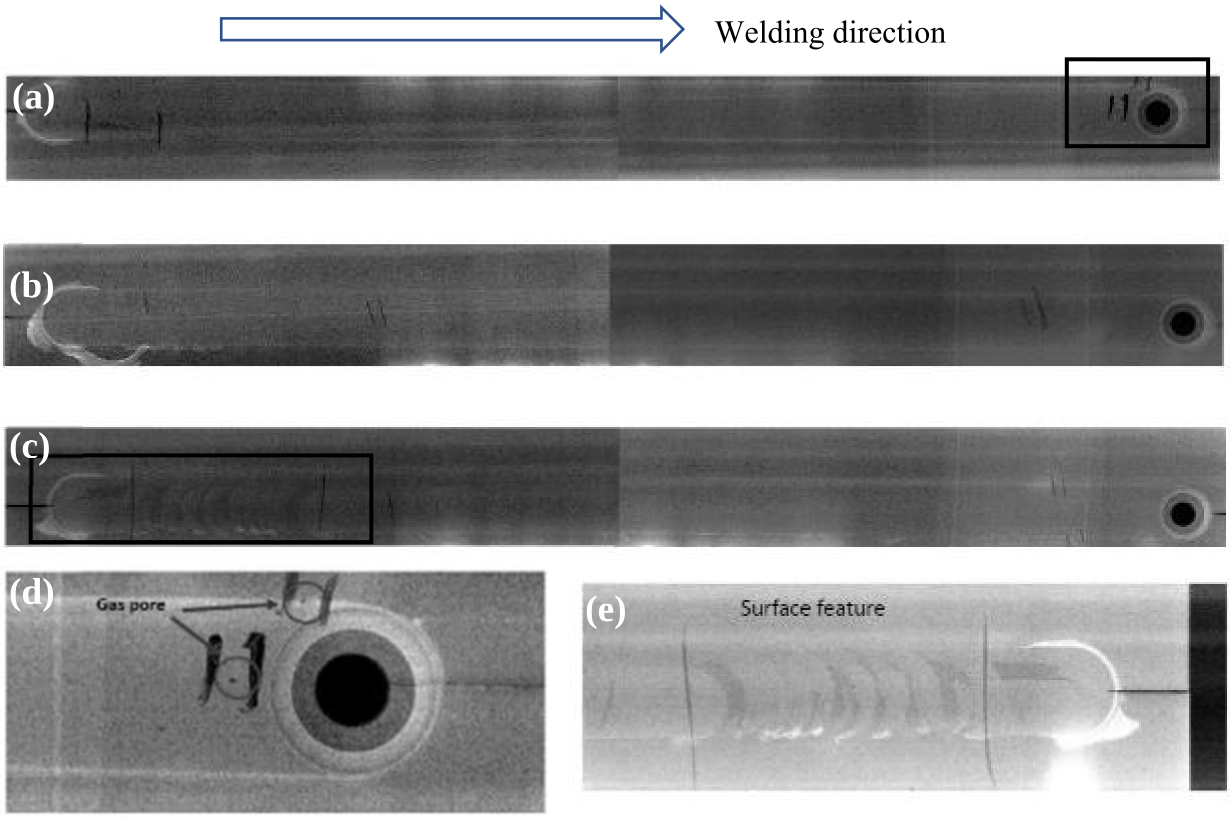

Fig. 4. 12 X-ray radiographs of AA5083 FSW joints.
(a) 100mm/min, 1000rpm; (b) 200mm/min, 1000rpm; (c) 300mm/min, 1000rpm; (d) High magnification picture of gas pores in (a); (e) High magnification picture of surface feature in (c)

4.3 Effect of kissing bond on microstructure and properties of FSW AA5083

4.3.1 Kissing bond characterization

It was noticed in Fig. 4. 5 that the kissing bond could be observed in the weld seam near the RS, showing a black curve which spreads from the centre thickness down to the bottom tip. It was revealed from the literature that kissing bond in the FSW butt welding generated due to the oxide layer of the contacting surface, stirred into the weld SZ during the process. The kissing bond usually shows various shapes as zigzag line, lazy S, or wavy pattern due to the welding parameters or tool design [15-17]. Tao et al. [18] defined the oxide curves as “lazy S” appeared at the mid-thickness of the welds and “kissing bond” appeared at the bottom and found micro-voids around the “kissing bond” apart from oxide particles. In this study, according to the above literature, Fig. 4. 5 A should be the “lazy S” and Fig. 4. 5 B should be the “kissing bond”. However, it was found that the “lazy S” and the “kissing bond” were continuous. Further SEM observations of A and B were shown in Fig. 4. 13 (a) and (b), respectively. In Fig. 4. 13 (a), it was found that apart from the oxide particles, exfoliation due to the etching can also be observed, and the similar morphology was shown in Fig. 4. 13 (b). Therefore, although the “lazy S” and “kissing bond” had different macroscale shapes probably due to stirring extents [19], they were both exfoliation of oxide particles in nature and continuous in most cases. As such, “kissing bond” will be used in this study to express all the forms of oxide curves in FSW.

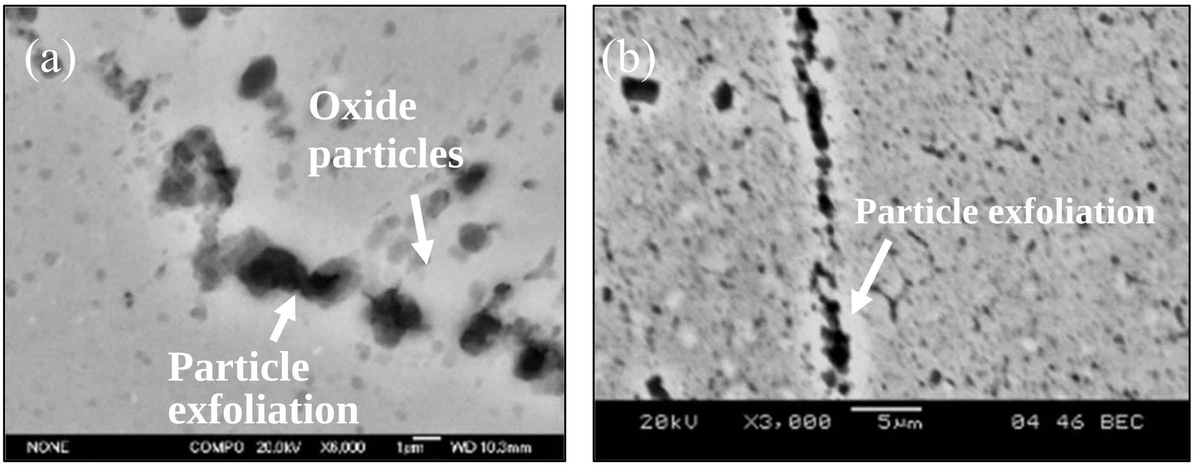

Fig. 4. 13 Backscattered SEM micrographs of (a) zone A and (b) zone B in Fig. 4. 5.

TEM of the material at the kissing bond was conducted, for the purpose of further clarifying the particles, and after all, the SEM can only show the particle exfoliation rather than composition confirmation. For accurately locating the position of kissing bond, FIB was used to extract the samples from the kissing bond area under SEM observation. Fig. 4. 14 (a) shows the TEM image of the material around the kissing bond. Local distributed bright particles were observed with an average size of ~100 nm. It was also found that most of the particles were intragranular, whereas, a few of them were distributed along the grain boundaries. Energy dispersive X-ray (EDX) results of the matrix and the particles are shown in Fig. 4. 14 (b) and (c). It was found that the matrix was composed of Al and Mg, as well as Cu and Pt which were probably introduced during the FIB process. Comparatively, the particles consisted of Al, Mg, as well as a large percentage of O, besides, an extremely higher content of Mg was also found to have. Therefore, it was confirmed that the bright particles were the mixture oxides of Al_2O_3 and MgO, which constituted the kissing bond in AA5083 FSW. It was also confirmed that the kissing bond generated because of the residual oxides on the contact interface prior to FSW, rather than occurring in-situ.

EBSD can clearly show the grain structure in the vicinity of the kissing bond, as Fig. 4. 14 (d). It was found that the oxides particles could not have significant impact on the grain orientation, however, it appeared to pin the grain boundaries, besides, to block the recrystallisation across the two sides. These effects of kissing bond could have an influence on the mechanical properties for the welds.

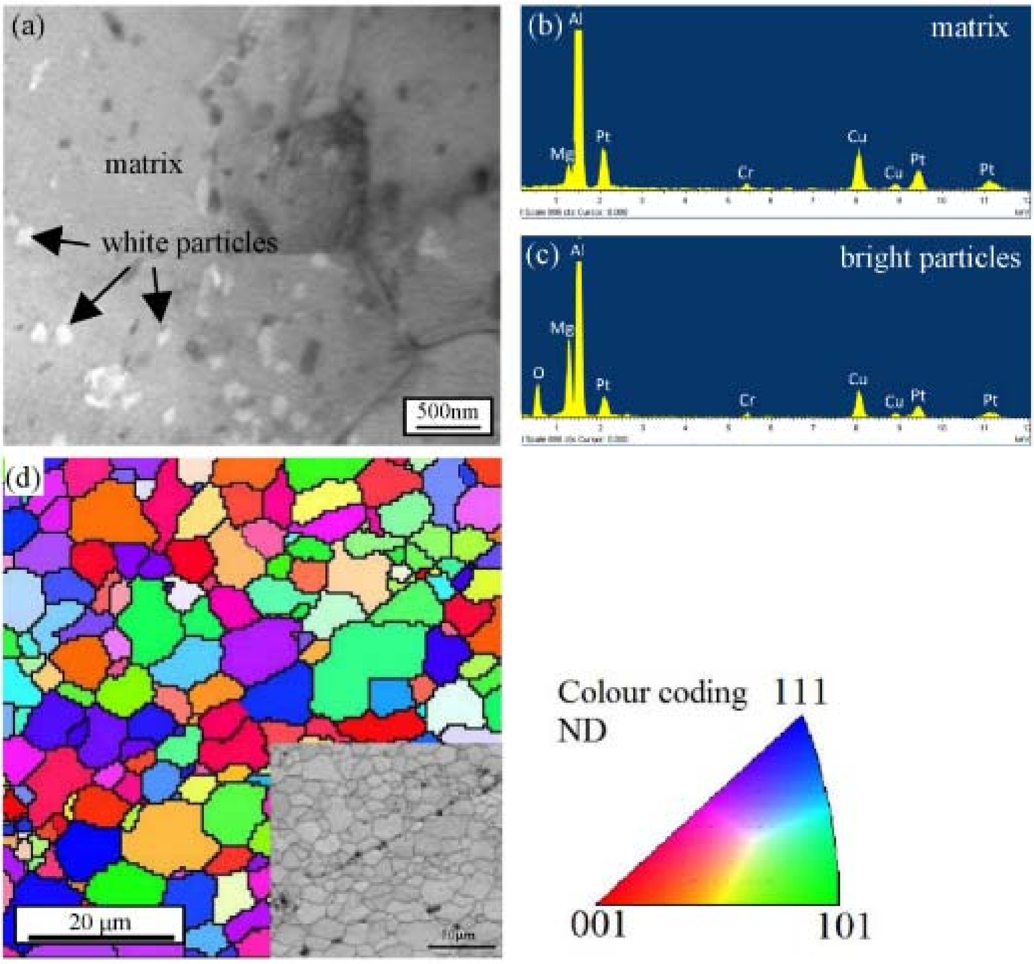

Fig. 4. 14 TEM and EBSD images of the kissing bond.
(a)-TEM image, (b)-EDX spectra of the matrix, (c)- EDX spectra of the particles, (d) EBSD map from the vicinity of the kissing bond.

4.3.2 Effect of FSW parameters on the kissing bond

Fig. 4. 15 shows the kissing bond morphologies in the welds prepared by various parameters. Among them, Fig. 4. 15 (a), (b) and (c) are the welds obtained at the same tool rotation speed of 800 rpm and various welding speeds of 100, 200 and 300 mm/min, whereas, Fig. 4. 15 (c), (d) and (e) are at the same welding speed of 300 mm/min and various tool rotation speeds of 800, 1000 and 1200 rpm. It was revealed that the welding speed could influence the waviness of the kissing bond, resulting in the change of the kissing bond profile from a smooth wave pattern to a complicated zigzag pattern, with the increasing welding speed (see Fig. 4. 15 (a), (b) and (c)). Moreover, the tool rotation speed could influence the kissing bond also in waviness, but mostly, in the range through welding thickness. When welded at 800 rpm, the kissing bond was detected as a zigzag curve from the top to the bottom throughout the weld thickness (see Fig. 4. 15 (c)). When welded at 1000 rpm, the kissing bond curve turned smoother but could only be detected from the upper centre to the bottom of the weld s (see Fig. 4. 15 (d)). Whereas at 1200 rpm, the kissing bond curve could be observed as a “C” shape, remaining in the centre of the weld thickness. (see Fig. 4. 15 (e)). Therefore, the welding parameter could obviously affect the morphology of the kissing bond in this study, in the waviness due to the various welding speed, as well as the region range in the weld thickness due to the different tool rotation speed.

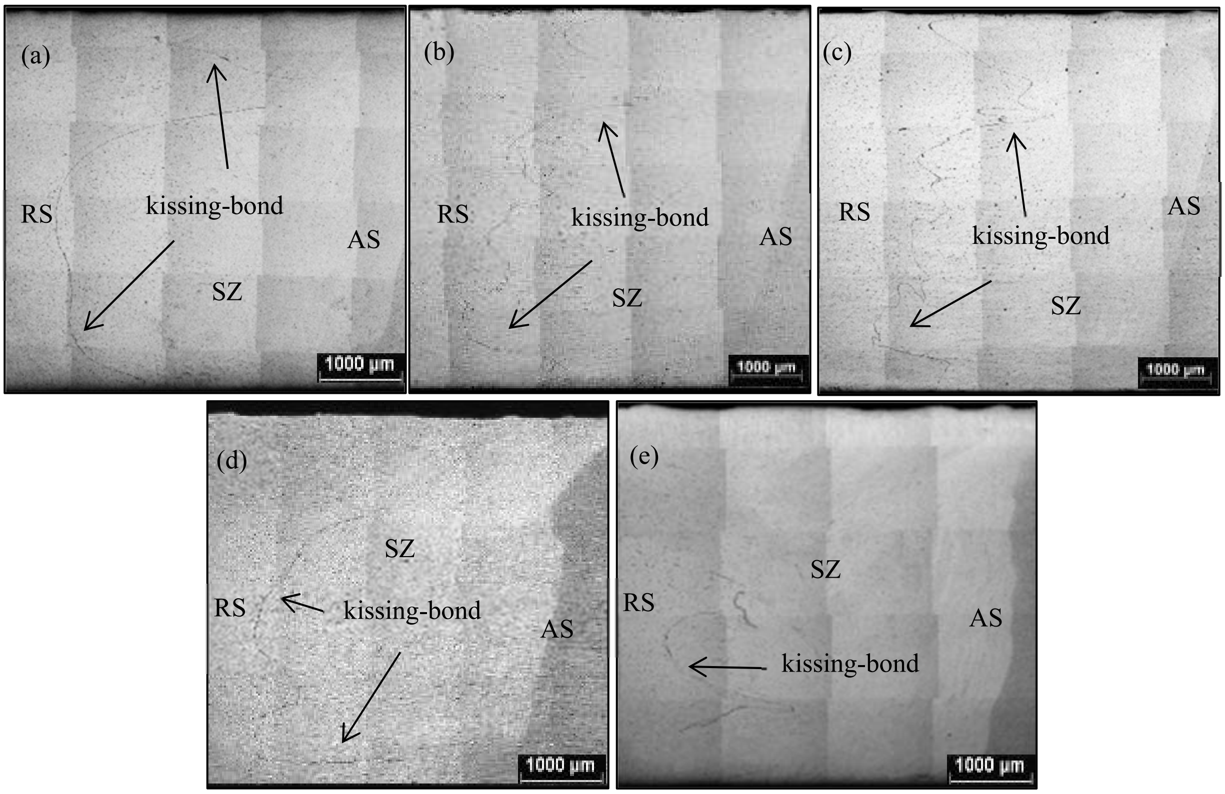

Fig. 4. 15 Macrostructure profiles of the AA5083 FSW welds at different welding parameters. (a)- ω=800rpm, v=100mm/min, (b)- ω=800rpm, v=200mm/min, (c)- ω=800rpm, v=300mm/min, (d)- ω=1000rpm, v=300mm/min, (e)- ω=1200rpm, v=300mm/min

In order to quantify the relationship between welding parameters (e.g. welding speed and tool rotation speed) and kissing bond, the total length of the kissing bond (L_o) in average was measured from at least three samples obtained in the mid position of a weld. The results of kissing bond length were put together with the welding speed and tool rotation speed, forming Fig. 4. 16. It was obviously found that the length of kissing bond increased with the increasing welding speed as well as decreasing tool rotation speed. In the FSW process, the oxide film of the contact interface is fragmented by the shear motion due to the rotation and feed of the welding tool. The increase of welding speed or the decrease of tool rotation speed which is equivalent to the less stirring effect per unit volume, can lead to the insufficient breakup to the oxide film, resulting in long kissing bond remaining.

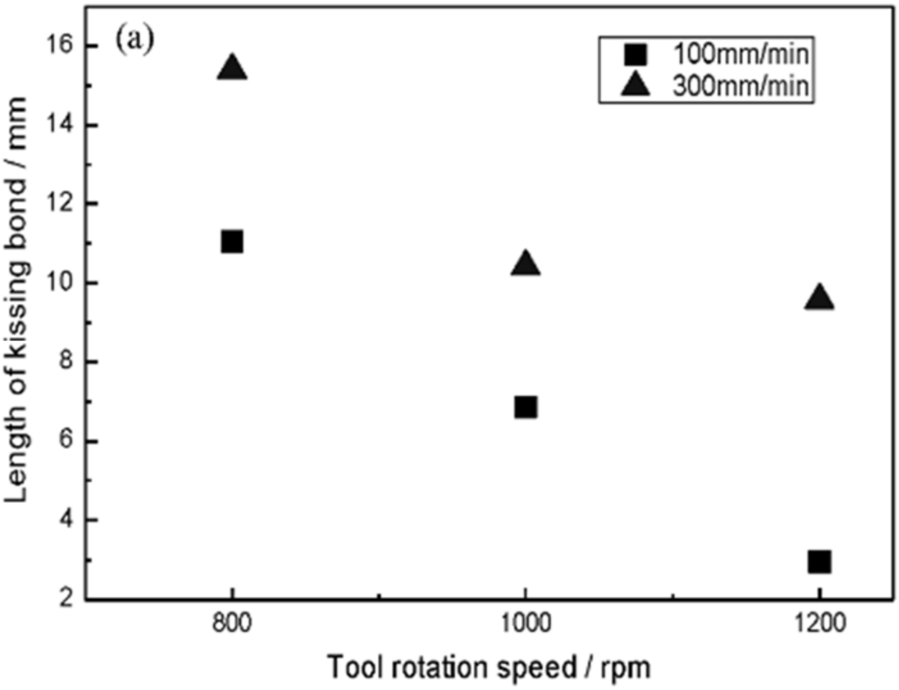

Fig. 4. 16 The effect of welding parameters on the length of kissing bond.

FSW is a multiple procedure of the high-speed tool rotation combined with the tool traverse, which are expressed using tool feed rate v and rotation speed ω, respectively. Therefore, friction heat which can make the welds to a maximum temperature, reportedly as high as 60% ~ 80% of the melting temperature [20], have been correlated to combinations of welding parameters ω and v through a “heat input parameter” which was proposed to be directly related to weld properties.

It was widely accepted that the increasing tool rotation speed or decreasing tool feed rate can raise the “heat input” level in the FSW process. A series of empirical equations have been established on heat indices as a function of input variables, such as pseudo heat index (square of rotational speed/travel speed) and advance per revolution, representing the heat input [21]. However, these equations could not reflect the resulting microstructure. Frigaard et al. [22] used the finite difference method to calculate the three-dimensional thermal fields in the FSW process, by assuming that the friction heat was produced at the tool shoulder. On this basis, a heat input equation corresponding with friction coefficient, pressure, rotational speed and radius of tool shoulder was proposed. In addition, the microstructural evolution and hardness distribution of the weld were calculated by using the results of the thermal model, in good agreement with the experimental data under certain conditions. However, this model has some limitations, which was not reliable for most welding parameters. Sato et al. [23] used calorimetry to measure the heat input for the FSW process of Al 5083. Through experimental measurements, the influence of heat input on the recrystallization grain size of the FSW SZ was also studied. It was clearly shown that a line relationship existed between the recrystallization grain size and heat input, as can be seen in Fig. 4. 17.

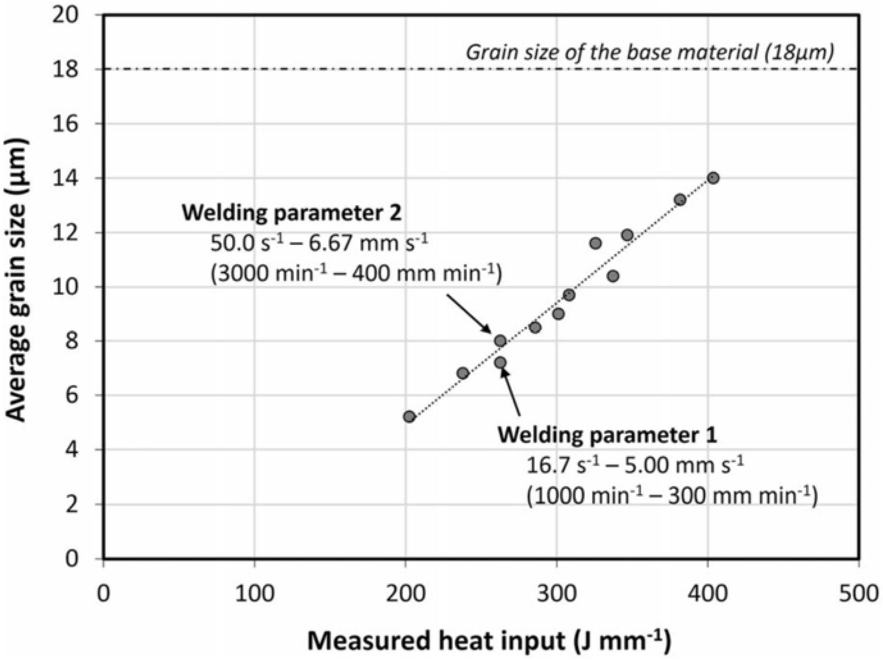

Fig. 4. 17 Effect of measured heat input on grain size of stir zone centre [23].

In this study, the effect of the heat input on the kissing bond of FSW AA5083 was examined through a semi-quantitative empirical function, which represents the heat input index (HI) as:

$$HI = \frac{\omega^2}{v \times 10^3} \tag{4.2}$$

where ω represents tool rotation speed (rpm) and v is welding speed (mm/min) [24]. Fig. 4. 18 shows the correlation of the heat input and the kissing bond length. It was found in the figure that the kissing bond length generally decreases with the increase of the HI during FSW process. It is well accepted that the FSW heat input increases with higher tool rotation speed or lower welding speed, which means, for the kissing bond that there are more time and chance to break up the oxide clusters, so that to restrict the forming of the kissing bond. Fig. 4. 18 shows the similar trends that the kissing bond length and heat input has a generally inversely proportional relationship.

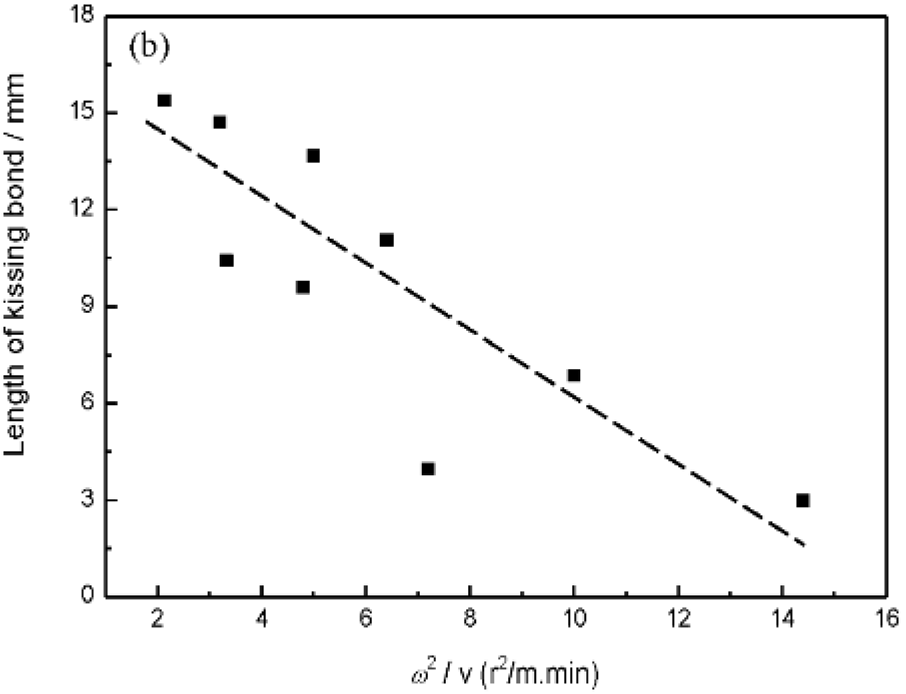

Fig. 4. 18 The effect of HI on the length of kissing bond.

4.3.3 Effect of the kissing bond on the tensile behaviour

Fig. 4. 19, Fig. 4. 20 and Fig. 4. 21 respectively illustrates the ultimate tensile stress (UTS), yield stress (YS) and elongation (EL) of the FSW joints, which have various length of kissing bond. It was revealed that with the increasing kissing bond length, the UTS and EL had a strong regulation. Except for an isolated point, they raised firstly and then dropped with increasing kissing bond length. However, it should be noticed that the YS could not be found any regulation with the kissing bond length, in other words, the heat input / welding parameters had little effect on the YS of the FSW joints.

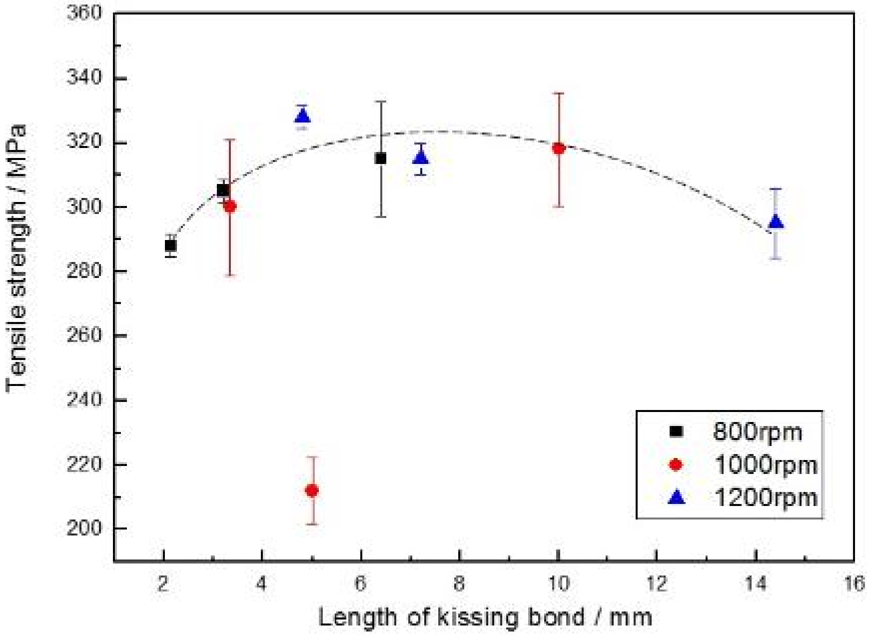

Fig. 4. 19 Ultimate Tensile Stress of FSW AA 5083 with different kissing bond length.

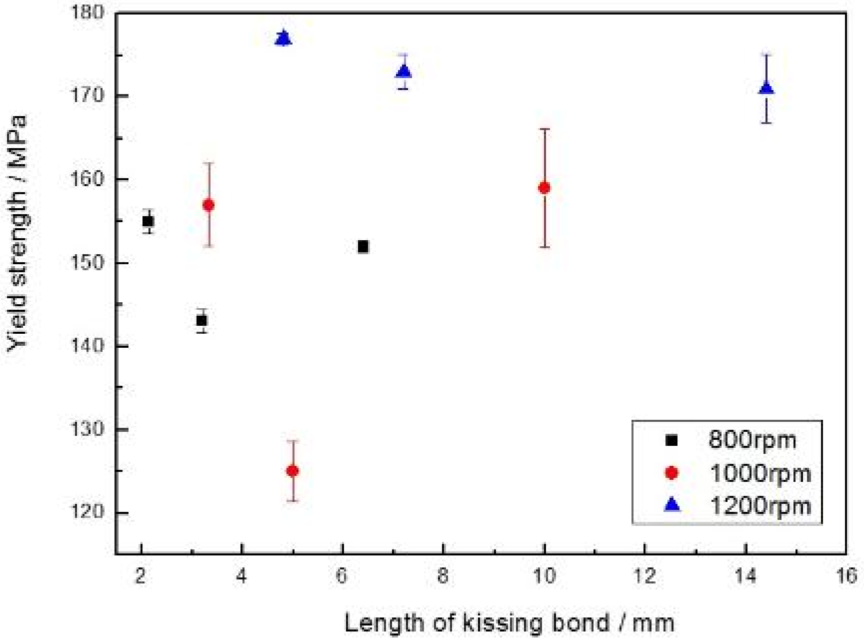

Fig. 4. 20 Yield Stress of FSW AA 5083 with different kissing bond length.

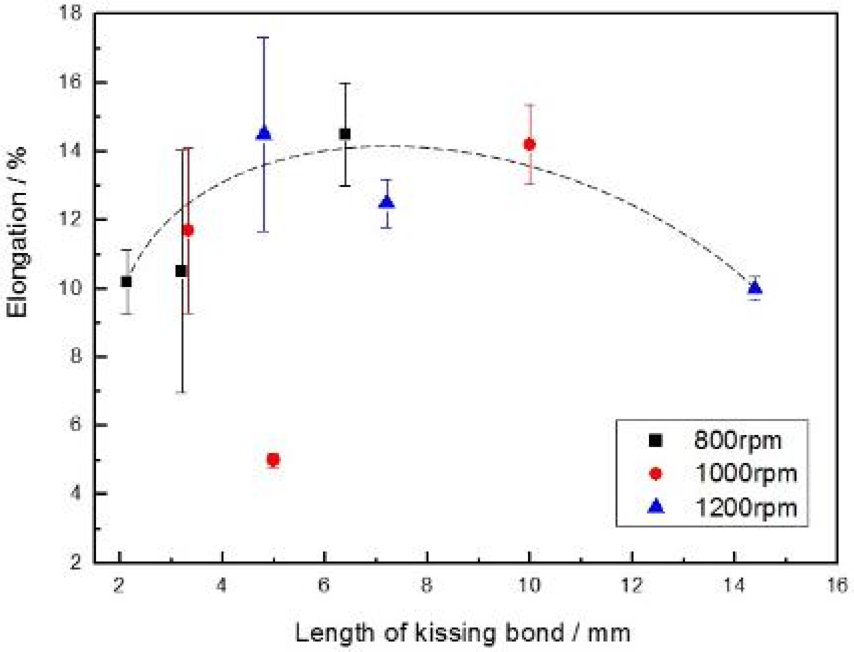

Fig. 4. 21 Elongation of FSW AA 5083 with different kissing bond length.

The Hall-Petch relation expresses the YS (σ) changing with the grain size (d) in a polycrystalline material which is shown below:

$$\sigma_{YS} = \sigma_0 + k_y d^{-1/2} \tag{4.3}$$

where, σ_{YS} represents the yield strength of the material, σ_0 is the frictional stress contribution, d represents the grain size, and k_y is the Hall-Petch slope. To find the effect factor, the YS of the welds was put with tool rotation speed, showing in Fig. 4. 22. It was generally shown that the YS increased with the increasing tool rotation speed except for a strange point. In this case, if the YS was only decided by the grain size, it should rather decrease with the increasing tool rotation speed to verify the hardness raise.

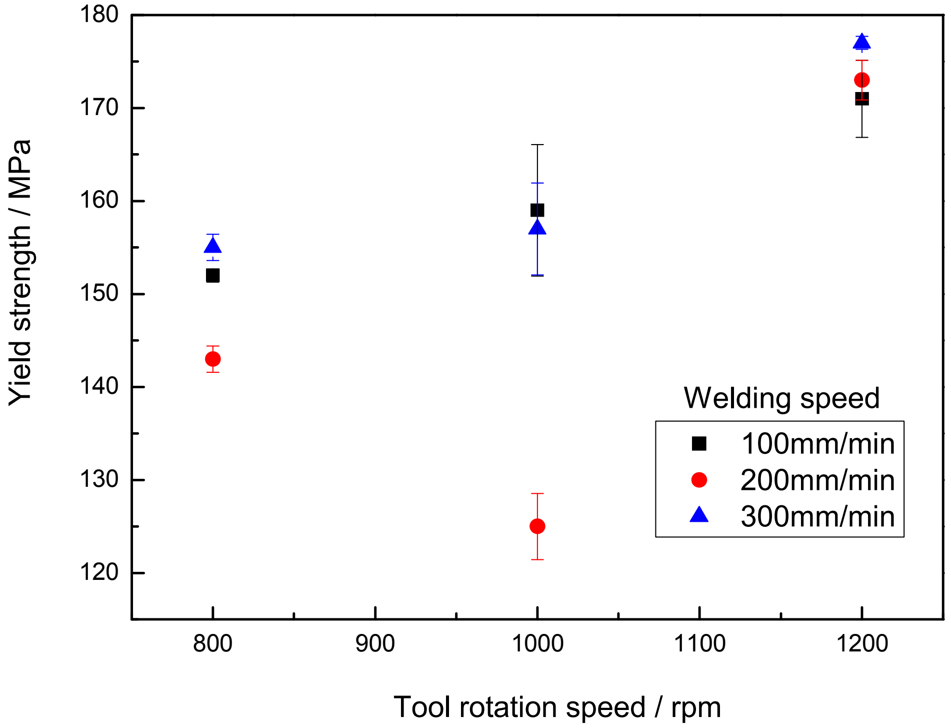

Fig. 4. 22 Yield strength of AA 5083 FSW joints with different tool rotation speeds.

However, the result on the grain size was opposite, as is previous shown in Fig. 4. 7. It was found that the recrystallization grains in the stir zone were coarser when welding at high tool rotation speed due to the generation of more heat which could lead to the grain growth. However, other strengthening mechanisms, for example, Orowan strengthening and dislocation strengthening, can make a contribution in the FSW joints for AA5xxx alloy [25, 26]. It was supposed that the efficient breakup of precipitates and the kissing bond oxides has resulted in the enhanced strength, despite the coarsening of the grain structure with the increase in rotation speed, which need further certification.

To further study the effect of kissing bond on the mechanical properties and fracture behaviour of the welds, macrostructure profiles of the tensile fracture for the welds with various kissing bond length were observed, and the traditional samples are shown in Fig. 4. 23. Three types of fracture were clearly found with the detailed descriptions as follows.

- Fracture type 1, in the condition of this experiment, was only found in the sample welding at the tool rotation speed of 1200rpm and the welding speed of 300mm/min (see Fig. 4. 23 (a)). Moreover, the fracture was in the SZ towards AS, with the fracture path showing a line throughout the thickness and approximately 45° to the stretch direction, indicating a shear fracture. Kissing bond could be clearly found in the SZ towards RS, as a C-shape in the middle of the sheet thickness, indicating that the kissing bond was not involved in the fracture procedure for this fracture type. In other words, the kissing bond had no effect on the tensile behaviour. The results of mechanical properties in this condition also prove this conclusion. The UTS, YS, and EL were 328 MPa, 178 MPa, and 14.5%, respectively, which were similar compared to the properties of the base material (328 MPa, 178 MPa, and 14.5%), even 15MPa higher in the yield strength due to the fine grains around the fracture. According to the fractography showing in Fig. 4. 24 (a) which was corresponding to Fig. 4. 23 (a), It was found that the fracture surface consisted of equiaxed dimples with various size and depth, indicating a ductile failure mode.

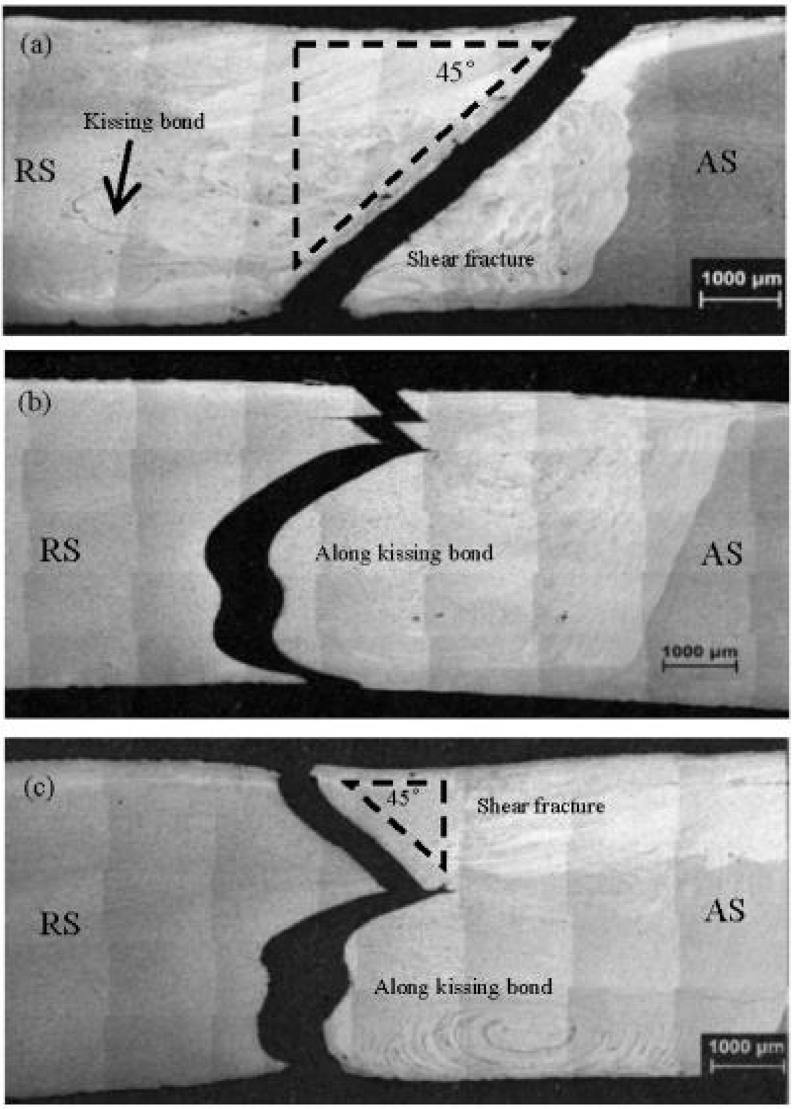

Fig. 4. 23 Macrostructure profiles of the fracture of AA5083-H112 FSW joints.
(a)- ω=1200rpm, v=300mm/min, (b)- ω=1000rpm, v=200mm/min, (c)- ω=1000rpm, v=100mm/min

- Fracture type 2, in the condition of this experiment, was only found in the sample welding at the tool rotation speed of 1000rpm and the welding speed of 200mm/min (see Fig. 4. 23 (b)).

The fracture was also found in the SZ, but initiation and propagation towards the RS, where the kissing bond usually located. Additionally, the fracture path was extremely the same as kissing bond, a zigzag from the top and a lazy S extended down. Therefore, it was revealed that the kissing bond had a significantly effect on the initiation and propagation of the crack in this type. Moreover, it was found that the mechanical properties including UTS, YS, and EL were 212 MPa, 125 MPa, and 5%, respectively, much lower than other welds. Compared to the fracture type 1, the difference was the shape of kissing bond, C shape in the middle of the weld for type 1 and zigzag and lazy S throughout the thickness for type 2. Thus, it can be concluded that the shape and location of kissing bond can have a significant influence on the properties and fracture behaviour of the welds.

- Fracture type 3, which could be detected in most cases, was a mixture for type 1 and type 2, thereby fracture path was the same as type 1 for half of the thickness and the same as type 2 for another half. It was shown in Fig. 4. 23 (c) that the fracture path was a 45° line from the top and a lazy-S along the kissing bond from the middle to the bottom. Fig. 4. 24 (b), (c), and (d) shows the fractography of fracture type 3. Fig. 4. 24 (b) shows the shear fracture part, showing dimples along the fine grain structure, similar to type 1. Fig. 4. 24 (c) shows the fractography corresponding to the fracture path along the kissing bond. It was found that no deep dimples could be detected in the fractography, but some discontinuous trench-like fracture areas were observed. Fig. 4. 24 (d) shows the trench-like zone at higher magnification, seeing that the trench included fine round particles. EDS results showed that the particles contained 8.7 % of O, 4.81 % of Mg and 86.49 % of Al in atom percentage, indicating that the particles were related to the kissing bond. Therefore, it can be concluded that the initiation of the fracture in type 3 was at the kissing bond tip in the middle of the weld thickness and propagation downward to the bottom along the kissing bond.

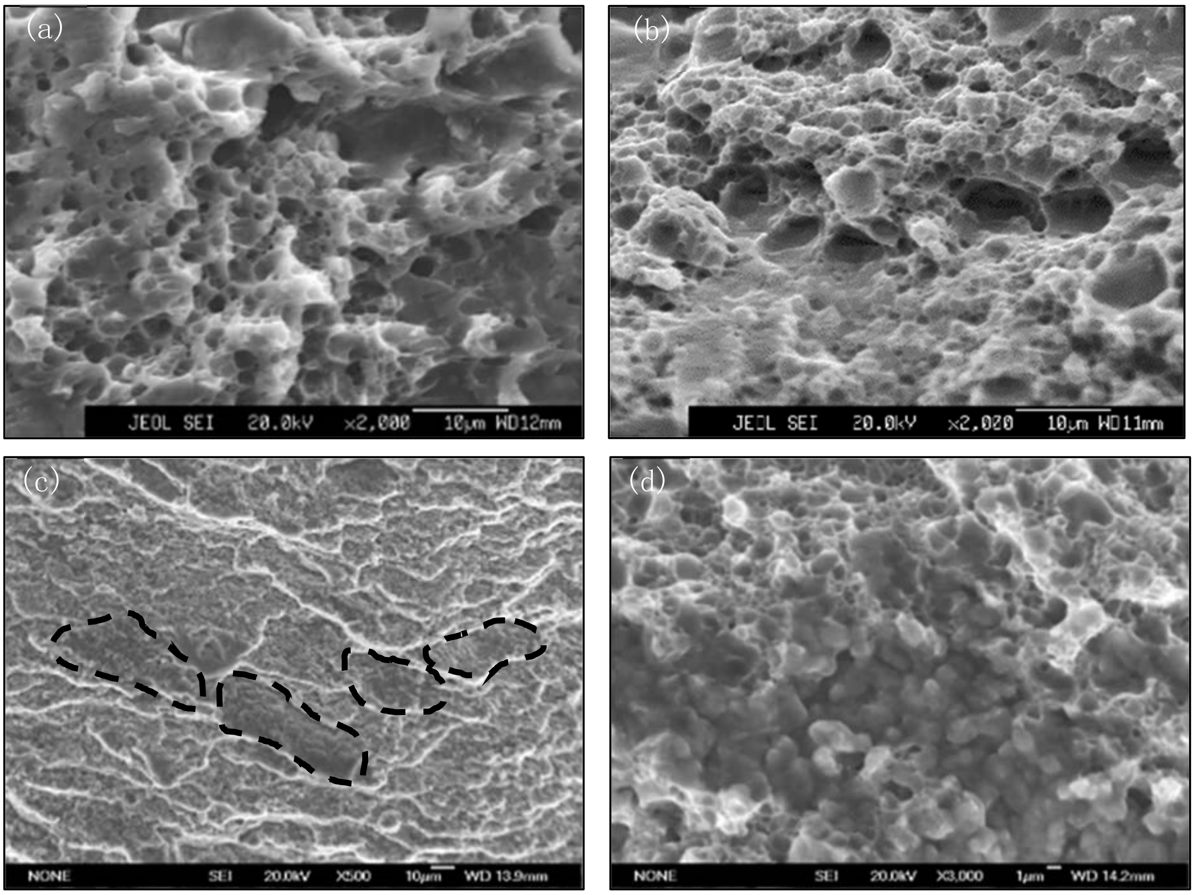

Fig. 4. 24 SEM micrographs for the fracture surfaces of AA5083-H112 FSW joints for (a) type 1, (b) type 3-shear fracture, (c) type 3-along the kissing bond, (d) high magnification of the dotted regions in (c).

4.3.4 Effect of the kissing bond on the fatigue behaviour

Fatigue fracture test was performed in the purpose of estimating the fatigue fracture behaviour of the FSW joints as well as how kissing bond could influence the fatigue fracture. Fig. 4. 25 reveals the effect of kissing bond length on the fatigue life of the welds. In this study, 130 MPa was used as the maximum circular stress, approximately 70% of the YS of the base material, for the purpose of assessing the effects of the kissing bond on the fatigue fracture behaviour. It was clearly shown that, with the increasing of the kissing bond length, the fatigue life was getting short from more than 10^6 times to less than 10^5 times, revealing that the kissing bond has a significant effect to decrease the fatigue property of the welds.

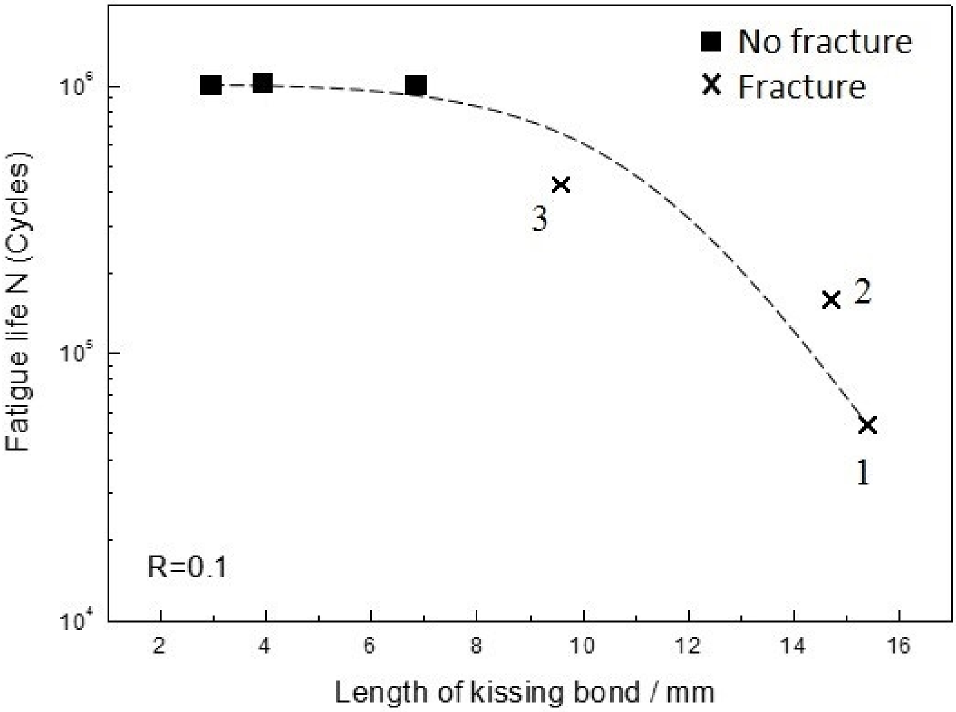

Fig. 4. 25 Fatigue test results for AA5083-H112 FSW joint with different kissing bond lengths.

Fig. 4. 26 (a), (b) and (c) display the fractography of the samples corresponding to point 1, 2 and 3 in Fig. 4. 25. For each sample, crack initiation, crack propagation and final fracture could be clearly distinguished but had various sizes compared to the three conditions. Generally, large area of crack initiation and crack propagation zones could reveal that the sample had shorter fatigue life. Especially, multiple initiations were found in Fig. 4. 26 (a) and (b), indicating that the fatigue life would be even short. Studies have shown that those multiple initiations were related to the

kissing bond tip from the welding bottom [27]. Furthermore, periodic striations were clearly shown in the crack propagation area in sample 1 and 2 (see Fig. 4. 26 (a) and (b)), from the multiple initiations to the final fracture zone. It was also found that the width of striations gradually decreased with the decreasing range of crack initiation and propagation zones, until invisible in the sample with the longest fatigue life. Similar striations were found by Zettler et al. [28] in AA6063-T6 FSW joints, where the striations formed because of the tool advance per revolution along the weld direction. However, it was a different kind of striations or bands, because these periodic striations were formed due to the fatigue crack propagation. To further clarify the microstructure, SEM fractography was conducted observing the detail of the striations shown in Fig. 4. 26 (d). It was found that the micro-scale striations, which have been considered as a feature of fatigue crack propagation, could be detected within the macro-scale striations, revealing that the crack growth could be in the vertical direction of the micro-scale fatigue striations [27].

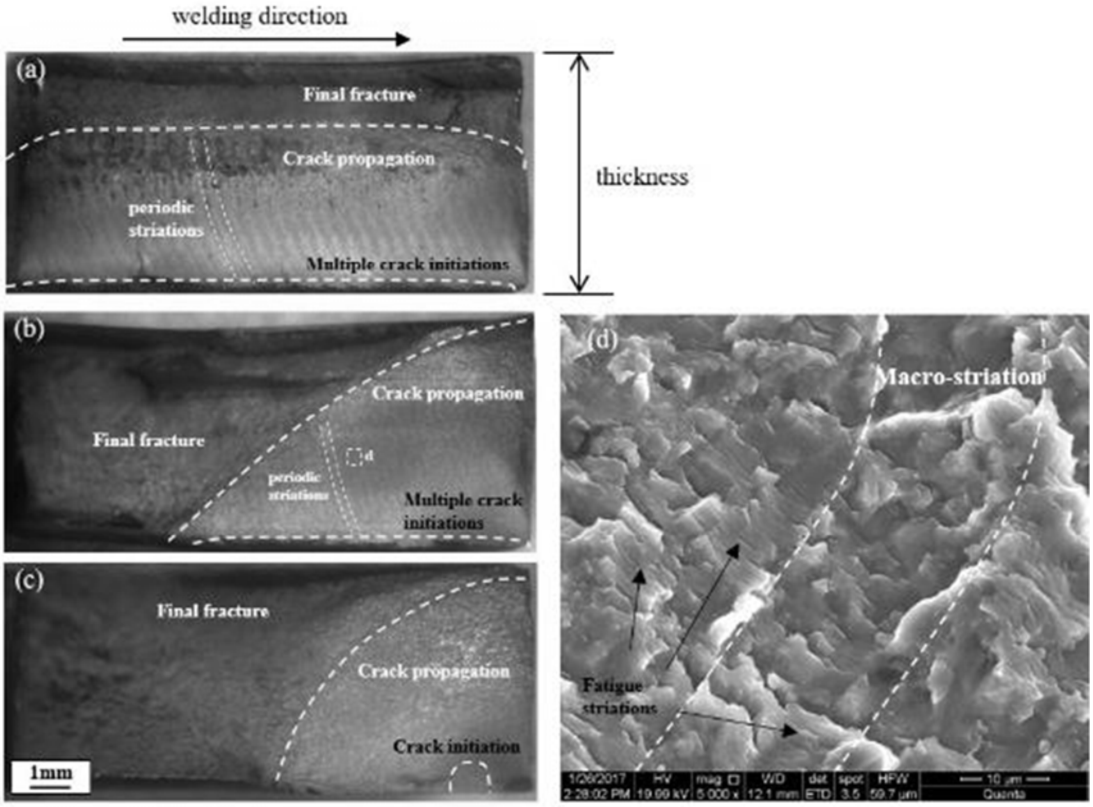

Fig. 4. 26 Macrograph of fractured surface of fatigue specimens corresponding to point 1-(a), 2-(b) and 3-(c) in Fig. 4. 25, and (d)-SEM of crack propagation zone in image (b).

The digital photos showing the fracture path of samples 1, 2 and 3 in Fig. 4. 25 were illustrated in Fig. 4. 27. For each sample, the upper and bottom photo represent the two sides of the fatigue specimen. It was found that, for various fatigue life samples, the fracture path had correspondingly different appearances. Fig. 4. 27 (a) shows the photos of specimen 1 in Fig. 4. 25, which was welded at the tool rotation speed of 800 rpm and the welding speed of 300 mm/min, and concequently had the lowest fatigue property. In this condition, the fracture path appeared similar at both sides, combining with the fractography in Fig. 4. 26 (a), a straight line at the multiple initiations from the bottom and a zigzag line near the final fracture area. It was indicated that the fracture initiated from the kissing bond bottom tip, to the top where the final fracture was along the kissing bond. Fig. 4. 27 (b) shows the photos of specimen 2, welded at 800 rpm and 200 mm/min, and better fatigue property. It was found that the fracture path was an approximative straight line at one side and a zigzag line at the other. Therefore, in this condition, the fatigue crack initiated at one side and afterwards developed and final fractured to the other side basically along the kissing bond, similar to tensile fracture. Fig. 4. 27 (c) shows the photos of specimen 3, welded at 1200 rpm and 300 mm/min, and had even better fatigue property. The fracture path is similar to specimen 2 except for the final fracture path, which appeared as a straight line 45° to the fatigue loading direction instead of a zigzag line. Comparing the three samples, it was concluded that the bottom tip of the kissing bond had a significant effect on the crack initiation, leading to the formation of multiple initiation microstructures at the bottom of the welds, which was harmful to the fatigue property. Moreover, if the final fracture path was generally along the kissing bond, the fatigue property would be lower than the welds in which the kissing bond was not involved, revealing that the kissing bond also had a significant effect on the final fracture, resulting in the decrease in fatigue property. Combined with the results which showed the relationship between welding parameters and the kissing bond, it was found that the weld prepared at higher tool rotation speed or lower welding speed which means higher stirring to break up the kissing bond oxides could have enhanced fatigue life.

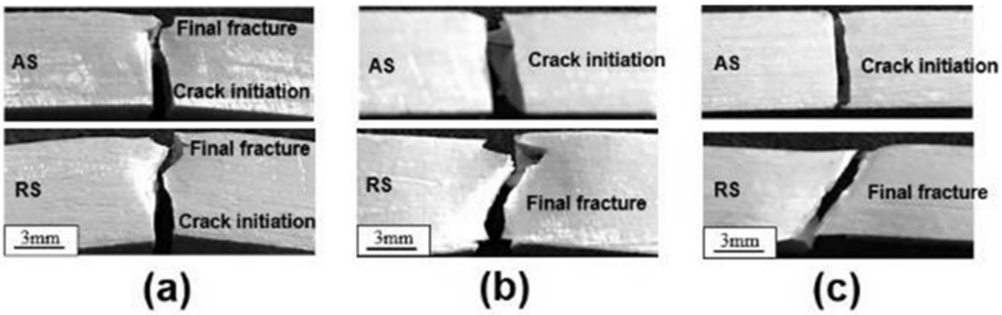

Fig. 4. 27 Fracture photos for fatigue specimens corresponding to point 1-(a), 2-(b) and 3-(c) in Fig. 4. 25.

4.4 Discussion

Fig. 4. 28 shows the fracture type and the corresponding UTS of the FSW AA5083. It could be found in the figure that if the fracture followed the type 1, it would have excellent UTS, which was close to the base material. However, fracture type 2 was related to the unqualified UTS. Most samples in this study could be classified as fracture type 3, which had medium UTS. It was also found that, when the heat input was between 5 and 10 r^2/m·min, the UTS was slightly lower than fracture type 1, which could reach above 90% of the base material. While, when the heat input was beyond this range, the UTS would be even lower. As mentioned above, the fracture type 3 was a combination of 1 and 2, when the type 2 was dominated in this condition, the UTS was consequently low. Therefore, it was concluded that the fracture type 2 could have a negative effect on the UTS of the weld. Besides, it could be noticed that, in one heat input condition approximately 5 r^2/m·min, two samples with different UTS were found, revealing that HI was not a reliable parameter determine the UTS which associated well with the kissing bond length in this study (Fig. 4. 18).

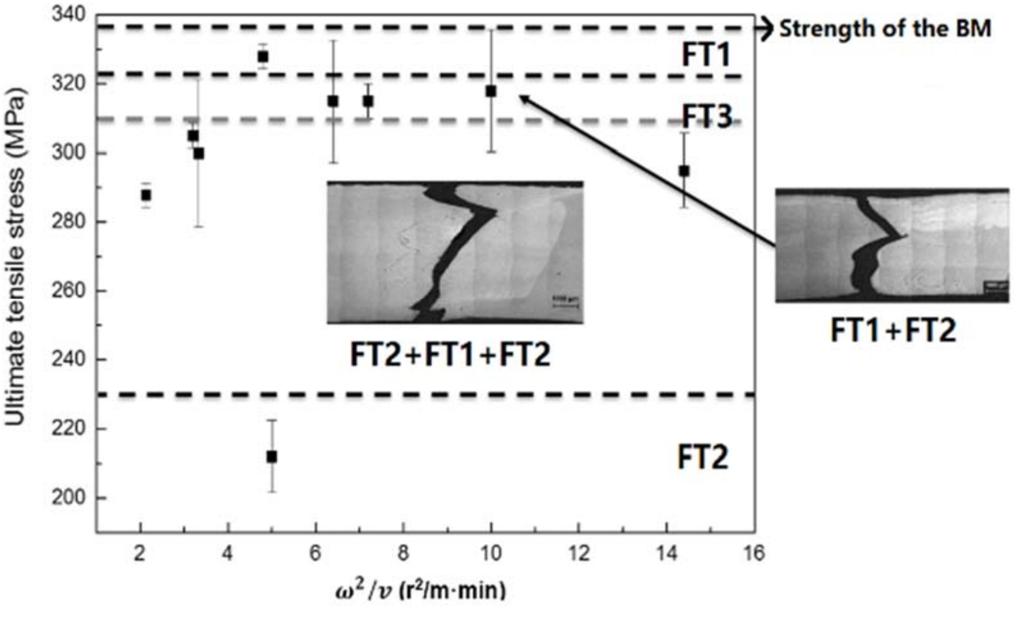

Fig. 4. 28 The relationship between fracture type (FT) and UTS of FSW AA5083.

Fatigue fracture had a similar regulation. The fracture path showing a straight line could related to the weld which had a longer fatigue life, whereas the path along the kissing bond had poor fatigue property. Therefore, the kissing bond length could impact on the range of crack initiation, and consequently the trends to fatigue failure.

Fig. 4. 29 (a) and (b) show the microstructures of the fractured welds following type 3 which was a hybrid fracture. It was obvious that the grains near shear fracture part (see Fig. 4. 29 (a)) were elongated, while grains near the kissing bond fracture part were (see Fig. 4. 29 (b)) equiaxed, indicating that the material in the vicinity of kissing bond did not experience deformation. Fig. 4. 29 (c) and (d) show the microstructures of the fractured welds following type 1 which was single shear fracture. It was found that grains were elongated in the vicinity of the fracture, while the grains were fine and equiaxed around the kissing bond where the sample could not crack during tensile test. Besides, similar results were obtained for the fatigue tests. As can be seen from these results, regardless of whether the sample was broken along the kissing bond, the vicinal grains could not deform because of the kissing bond particles. Besides, the TEM image (shown in Fig. 4. 14) illustrated that most oxide particles were located inside the grains. Hence, it was revealed that the kissing bond which was essentially oxide particles could block the intragranular slip of dislocations, which resulted in stress concentration and brittle fracture along the kissing bond during tensile process. Therefore, it could be assumed that, the kissing bond and the grains in the vicinity formed a kind of “defect” in the matrix. Thus, it could be explained why the YS increased exactly with the increase of the tool rotation speed rather than following the Hall-Petch relation in

the tensile tests. According to the results in Fig. 4. 15, when the tool rotation speed was higher, the kissing bond curve would become short in the thickness direction of the weld, as a result, less “defect” would be distributed in the thickness direction which was perpendicular to the stretching direction and a higher YS of the welds. Moreover, according to the tensile test results, the YS with the tool rotation speed 1200rpm was higher than the BM in average, while the YS was lower at the tool rotation speed 1000rpm and 800rpm. Therefore, the welds could be considered as homogeneous when welding at 1200rpm tool rotation speed, while at 800rpm and 1000rpm, “defect” take the significantly role in the fracture behaviour. Therefore, it was suggested that the kissing bond distributed in the thickness direction had a negative effect on the YS.

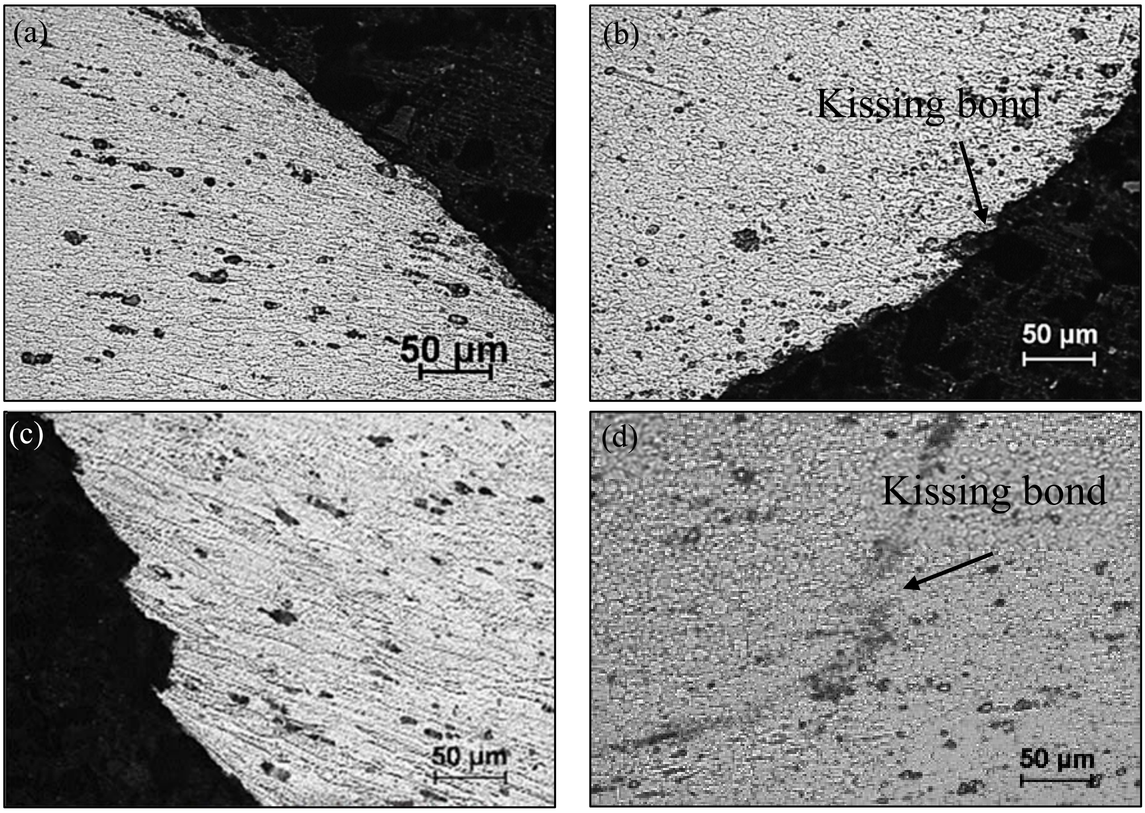

Fig. 4. 29 Microstructure of the fracture FSW AA5083 welds.
(a)- ω=1200rpm, v=300mm/min shear fracture part, (b)- ω=1200rpm, v=300mm/min kissing bond fracture part, (c)- ω=1200rpm, v=200mm/min fracture, (d)- ω=1200rpm, v=200mm/min kissing bond

4.5 Conclusions

In this chapter, AA5083 in H112 condition were FSW butt welded using various tool rotation speeds as well as tool feed rates. Firstly, the microstructure and mechanical properties of the base material were characterised. After welding, the microstructure, average grain size in the SZ, hardness distribution and macroscale defects were evaluated for the welds produced at various parameters. Among them, a special focus was taken on the kissing bond phenomenon, which can have a significant effect on the microstructure and properties of the FSW joints. For this purpose, the kissing bond was systematically characterized as well as its effects on tensile and fatigue properties. In addition, the tensile and fatigue fracture types were adequately discussed. The following conclusions can be drawn:

1. The AA5083 base material was composed of elongated grains along the (ST-RD) plane, fine in thickness, and Al(Mn,Fe)Si, Mg_2Si and Al_6Mn were observed in the Al matrix. The base material AA5083 had a high elongation (20%), moderate tensile strength (335MPa), relatively low yield strength (163MPa) and hardness (84.8HV), which was revealed that the aluminium plate had excellent processing properties and good ability of deformation.

2. The FSW AA5083 can be divided into several zones as BM, HAZ, TMAZ and SZ, which has different microstructure characteristic, respectively. Among them, the SZ experiences dynamic recrystallization during FSW process, and the recrystallization grain size decreases when welding at a lower heat input. The lowest hardness of the welds is at the HAZ, while in

the SZ, the hardness raises significantly to the level of the BM due to the work-hardening effect. The X-ray inspection results indicates that the FSW joints has no visible defects.

3. The kissing bond observation and characterization showed that the tool rotation speed determined the region range in the weld thickness and the welding speed determined the waviness. Besides, the kissing bond length had an approximate linear relation with the heat input. Property tests revealed that with the increasing length of kissing bond, the tensile UTS and EL increased first and then decreased, and the YS had no regulation but obviously increased with the increasing tool rotation speed. Fatigue property was also significantly affected by the kissing bond length. Fracture type analysis showed that it had strong relation with the tensile and fatigue property. The shear fracture was corresponding to high tensile and fatigue property, while fracture which was dominated by kissing bond could result in low properties.

4.6 References

[1] Y. Birol, S. Kasman, Effect of welding parameters on microstructure and mechanical properties of friction stir welded EN AW 5083 H111 plates, Materials Science and Technology 29(11) (2013) 1354-1362.

[2] S. Kimura, T. Wakisaka, I. Katou, T. Goto, H. Machida, Application of friction stir welding for all-terrain vehicle aluminum wheel, Journal of Japan Institute of Light Metals 57(11) (2007) 554-558.

[3] C.-H. Chien, W.-B. Lin, T. Chen, Optimal FSW process parameters for aluminum alloys AA5083, Journal of the Chinese Institute of Engineers 34(1) (2011) 99-105.

[4] D.-H. Choi, B.-W. Ahn, D.J. Quesnel, S.-B. Jung, Behavior of β phase (Al3Mg2) in AA 5083 during friction stir welding, Intermetallics 35 (2013) 120-127.

[5] T. Hirata, T. Oguri, H. Hagino, T. Tanaka, S.W. Chung, Y. Takigawa, K. Higashi, Influence of friction stir welding parameters on grain size and formability in 5083 aluminum alloy, Materials Science and Engineering: A 456(1-2) (2007) 344-349.

[6] M. Grujicic, G. Arakere, H.V. Yalavarthy, T. He, C.F. Yen, B.A. Cheeseman, Modeling of AA5083 Material-Microstructure Evolution During Butt Friction-Stir Welding, Journal of Materials Engineering and Performance 19(5) (2009) 672-684.

[7] C. Zhou, X. Yang, G. Luan, Effect of kissing bond on fatigue behavior of friction stir welds on Al 5083 alloy, Journal of Materials Science 41(10) (2006) 2771-2777.

[8] J. Seong, G. Frankel, N. Sridhar, Inhibition of Stress Corrosion Cracking of Sensitized AA5083, Corrosion (2015) 150825085022001.

[9] A.P. Reynolds, Visualisation of material flow in autogenous friction stir welds, Science and Technology of Welding and Joining 5(2) (2000) 120-124.

[10] Y.S. Sato, H. Takauchi, S.H.C. Park, H. Kokawa, Characteristics of the kissing-bond in friction stir welded Al alloy 1050, Materials Science and Engineering: A 405(1) (2005) 333-338.

[11] G. Yi, B. Sun, J.D. Poplawsky, Y. Zhu, M.L. Free, Investigation of pre-existing particles in Al 5083 alloys, Journal of Alloys and Compounds 740 (2018) 461-469.

[12] R. Goswami, G. Spanos, P.S. Pao, R.L. Holtz, Precipitation behavior of the ß phase in Al-5083, Materials Science and Engineering: A 527(4-5) (2010) 1089-1095.

[13] E.Cerria, E.Evangelista, A.Forcellese, H.J.McQueen, Comparative hot workability of 7012 and 7075 alloys after different pretreatments, Materials Science and Engineering: A 197 (1995) 181-198.

[14] M. Attallah, Microstructure property development in friction stir welds of aluminim based alloys, 2007.

[15] S. Di, X. Yang, G. Luan, B. Jian, Comparative study on fatigue properties between AA2024-T4 friction stir welds and base materials, Materials Science and Engineering: A 435-436 (2006) 389-395.

[16] H.-B. Chen, K. Yan, T. Lin, S.-B. Chen, C.-Y. Jiang, Y. Zhao, The investigation of typical welding defects for 5456 aluminum alloy friction stir welds, Materials Science and Engineering: A 433(1) (2006) 64-69.

[17] H. Okamura, K. Aota, M. Sakamoto, M. Ezumi, K. Ikeuchi, Behaviour of oxides during friction stir welding of aluminium alloy and their effect on its mechanical properties, Welding International 16(4) (2002) 266-275.

[18] Y. Tao, Z. Zhang, D.R. Ni, D. Wang, B.L. Xiao, Z.Y. Ma, Influence of welding parameter on mechanical properties and fracture behavior of friction stir welded Al–Mg–Sc joints, Materials Science and Engineering: A 612 (2014) 236-245.

[19] P.L. Threadgill, A.J. Leonard, H.R. Shercliff, P.J. Withers, Friction stir welding of aluminium alloys, International Materials Reviews 54(2) (2013) 49-93.

[20] R.S. Mishra, Z.Y. Ma, Friction stir welding and processing, Materials Science and Engineering: R: Reports 50(1) (2005) 1-78.

[21] N. Balasubramanian, B. Gattu, R.S. Mishra, Process forces during friction stir welding of aluminium alloys, Science and Technology of Welding and Joining 14(2) (2009) 141-145.

[22] Ø. Frigaard, Ø. Grong, O.T. Midling, A process model for friction stir welding of age hardening aluminum alloys, Metallurgical and Materials Transactions A 32(5) (2001) 1189-1200.

[23] Y.S. Sato, T. Onuma, K. Ikeda, H. Kokawa, Experimental verification of heat input during friction stir welding of Al alloy 5083, Science and Technology of Welding and Joining 21(4) (2016) 325-330.

[24] V. Dixit, R.S. Mishra, R.J. Lederich, R. Talwar, Effect of initial temper on mechanical properties of friction stir welded Al-2024 alloy, Science and Technology of Welding and Joining

12(4) (2007) 334-340.

[25] M.M. Attallah, M. Strangwood, C.L. Davis, Influence of the heating rate on the initiation of primary recrystallization in a deformed Al–Mg alloy, Scripta Materialia 63(4) (2010) 371-374.

[26] Y.S. Sato, S.H.C. Park, H. Kokawa, Microstructural factors governing hardness in friction-stir welds of solid-solution-hardened Al alloys, Metallurgical and Materials Transactions A 32(12) (2001) 3033-3042.

[27] M. Kadlec, R. Růžek, L. Nováková, Mechanical behaviour of AA 7475 friction stir welds with the kissing bond defect, International Journal of Fatigue 74 (2015) 7-19.

[28] R. Zettler, T. Vugrin, M. Schmücker, 9 - Effects and defects of friction stir welds, in: D. Lohwasser, Z. Chen (Eds.), Friction Stir Welding, Woodhead Publishing2010, pp. 245-276.

5 Friction Stir Lap Welding of Dissimilar AA6061/A356 Joints: Microstructural and Mechanical Properties Development

5.1 Introduction

The application of the FSW of aluminium alloys is rapidly growing, especially in automotive field. Recent studies focused on joining of dissimilar Al-alloys, which has been rather difficult to perform using fusion welding [1-3]. It has been proposed that connection of cast to wrought structures can probably be found many applications in particularly automotive wheels, as it can result in an efficient design while facilitating fabrication, by locating wrought materials at the highly or fatigue loaded regions to take advantage of their inherently superior bearing strength and damage tolerance [4]. Defect-free FSW joints have been obtained between wrought and casting Al alloys, and the microstructure evolution was thoroughly investigated as well in a number of studies. A study of FSW AA6061-T6 (a wrought heat treatable Al-alloy) and A356 (a casting Al-alloy) by Lee et al. [5] revealed that the mechanical properties of the welds were relatively low compared with both base materials. Lim et al. [4] attributed the low mechanical properties to the agglomeration of rod-shaped Si particles observed locally in the weld zone, which served as initiation sites for tensile fracture. Besides, it was found that the welding parameters significantly influenced the properties of dissimilar cast-wrought Al-alloys welds. A study on FSW AA6061 and A356 by Ghosh et al. [6] revealed that tool rotation and traversing speeds have a significant influence on the weld microstructure. Moreover, as the strength of AA6061 is much higher than A356, the mechanical properties of the stir zone were higher when AA6061 was at the retreating side.

The weld parts in lap configuration is also being widely used in the connection of aluminium alloy structures, particularly in automotive field [7-13]. In recent years, a series of studies have also been published on the FSLW of aluminium alloy. Making a good lap weld using FSW is more complicated than butt welding, determined by factors as welding parameters, tool design, weld setup, etc. Lee et al. [14] investigated AA6061 and AA5052 FSLW welds, focusing on the microstructural and mechanical properties development under different parameters. It was found that higher tool rotation speed and/or lower tool traverse speed (i.e. higher heat input) might result in severer material mixing and poorer mechanical properties in welded zones. However, available information on FSLW between wrought and cast Al-alloys is very limited.

In this chapter, FSLW of a wrought Al-alloy AA6061-T6 and a cast Al-alloy A356 was studied, mainly focusing on the microstructure evolution and hardness distribution in the as-welded and following post-weld heat treatment (PWHT), in order to develop an optimised process of FSLW between wrought and cast Al-alloys. This chapter also focuses on characterising the alterations in microstructure and properties and the evolutions of size, shape and distribution of second-phase particles due to FSLW process.

5.2 Microstructural development of FSLW AA6061-A356

5.2.1 Base metal characterization

AA6061 wrought aluminium alloy and A356 casting aluminium alloy are the main material investigated in this chapter. Microstructural characterisation was also performed in the aim of investigating the microstructural-property relationship associated with FSLW.

In this study, the AA6061 to be welded was in T6 heat treatment condition which was defined as peak aging after solution treatment. In the optical microstructures shown in Fig. 5. 1 (a), the grain structure on the ST-RD plane was also composed of elongated grains, elongated along the RD, compared with the ultrafine grans of AA5083-H112 in thickness, the average width of the grains in AA6061-T6 was ~30μm, and inhomogeneous obviously in terms of size or shape. Black particles were also found in the Al matrix, with the larger number than that in AA5083-H112.

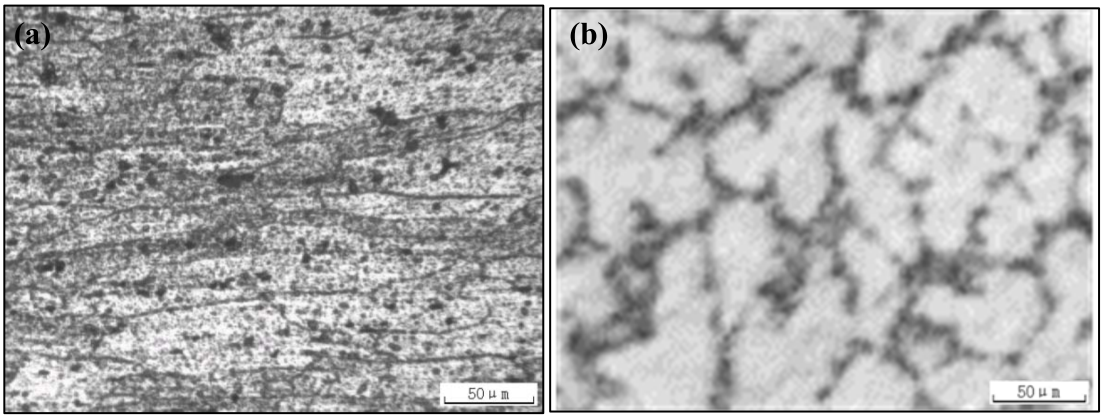

Fig. 5. 1 Optical microstructure of the AA6061-T6 (a) and as-cast A356 (b) base material.

The microstructure of the A356 in the as-cast condition is shown in Fig. 5. 1 (b). It was found that the as-cast A356 alloy was composed of dendrite grains, which was the traditional microstructure of a casting Al alloy, with the average grain size of ~100μm. Besides, the eutectic phase was distributed on the grain boundaries.

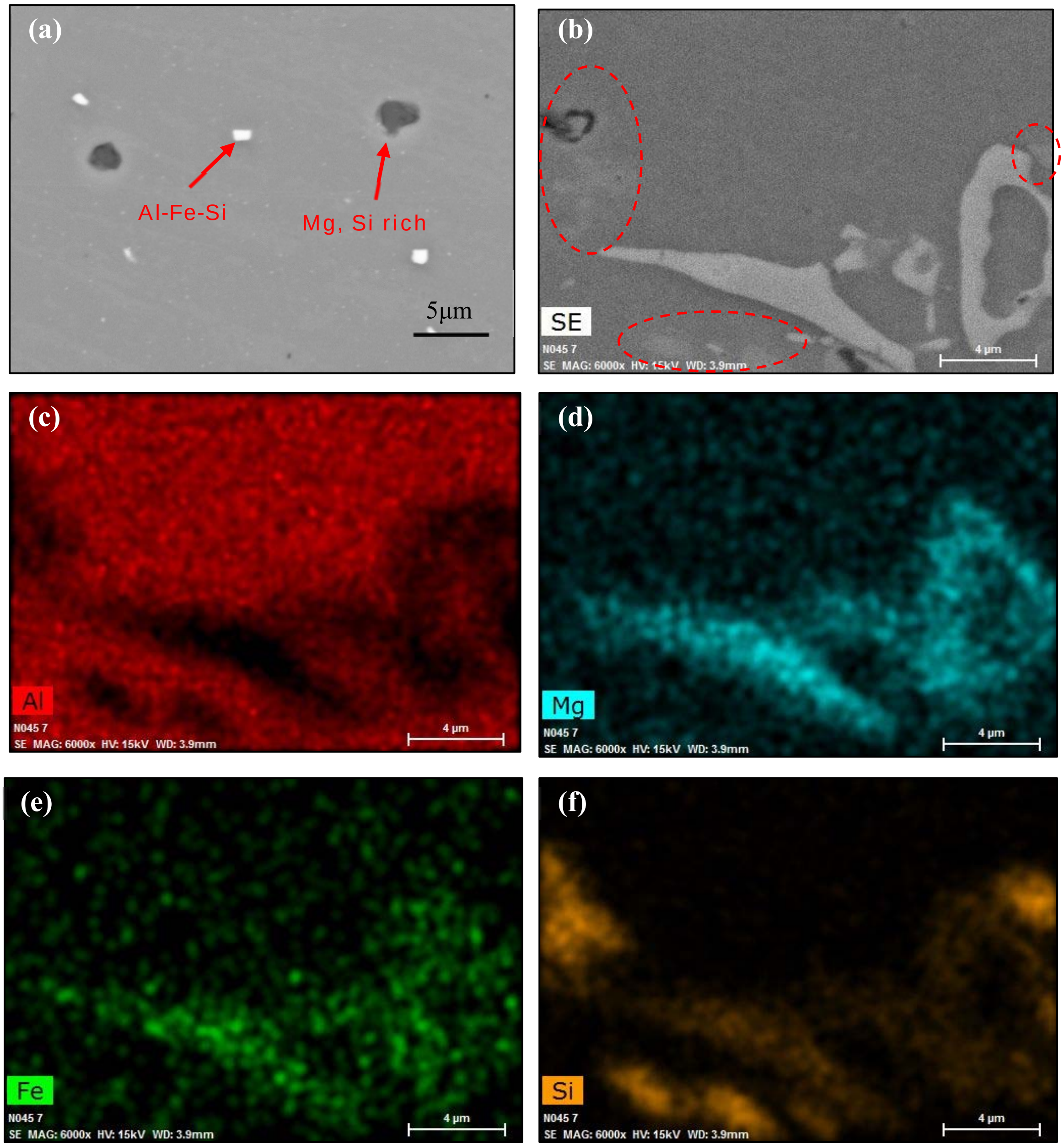

Fig. 5. 2 SEM images showing intermetallic particles in AA6061-T6 (a) and as-cast A356 (b) base material, (c) - (f) showing the mapping of the elements Al, Mg, Fe and Si in image (b).

Fig. 5. 2 shows the SEM images of the base materials AA6061 in (a) and A356 in (b), illustrating

the particle morphologies. Two types of constituent particles were found in the microstructure of the AA6061. According to the EDX results, the dark-coloured and white particles were identified as Mg, Si-rich, and Al-Fe-Si, respectively. In the microstructure of A356 shown in Fig. 5. 2 (b) and element mapping in (c), (d), (e) and (f), it was found that the script-shaped secondary phase was observed containing Mg, Fe and Si. Besides, eutectic Si was found showing very light grey colour which was difficulty to distinguish in the SEM image Fig. 5. 2 (b), however, element mapping shown as Fig. 5. 2 (c), (d), (e) and (f) clearly proved the existence of the eutectic Si.

5.2.2 Microstructural development of the FSLW joint

5.2.2.a Grain structure development

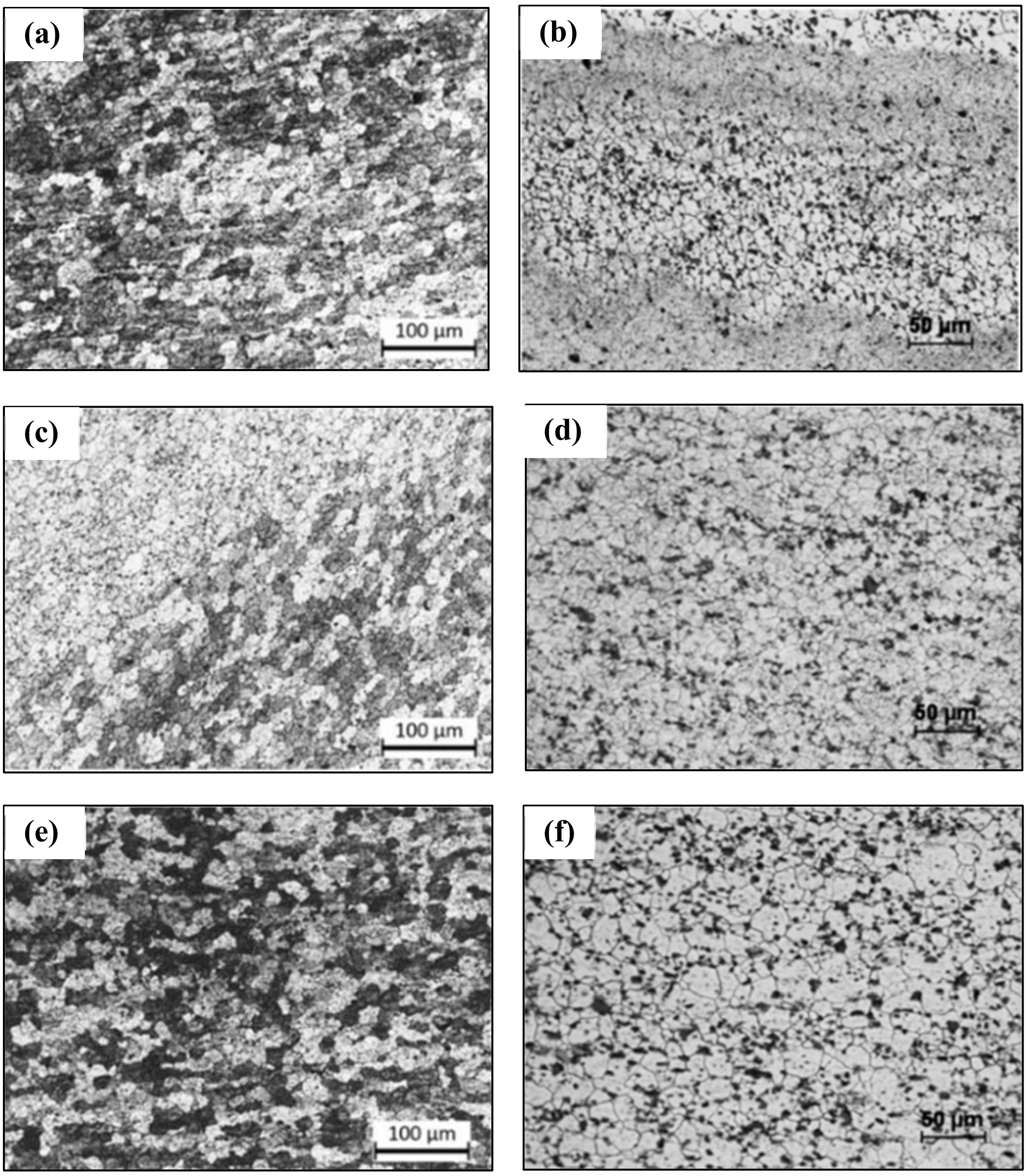

Fig. 5. 3 The micrographs of the AA6061-T6 /A356 FSLW joint.
(a) AA6061 SZ, (b) A356 SZ, (c) AA6061 TMAZ AS,
(d) A356 TMAZ AS, (e) AA6061 TMAZ RS, (f) A356 TMAZ RS

The detailed microstructures of the FSLW for AA6061 and A356 were shown in Fig. 5. 3. Similar to friction stir butt welding, the lap weld can be divided into the stir zone (SZ), thermo-mechanically affected zone (TMAZ), heat-affected zone (HAZ), as well as the base material (BM) according to the service condition of the involved material. It was found in Fig. 5. 3 that dynamic recrystallisation (DRX) occurred in the SZ of both AA6061 and A356 during the welding procedure. To further investigate the DRX in the friction stir lap welds, Fig. 5. 4 illustrates the recrystallized grain size distribution within the lap welding stir zone, and the corresponding microstructures are shown in Fig. 5. 3. In the AA6061 section, fine equiaxed grains were present in the SZ, while the elongated grains could be observed in the BM, which are typical of wrought (rolled) sheets. The BM grain structure was predominantly pancake-shaped extending >100μm along the rolling direction (RD), whereas the average grain size within the SZ ranged from 8μm to 15μm depending on the location. It was also found that the grain size towards advancing side (AS) was generally smaller than towards retreating side (RS), in addition, the grain size distribution varied significantly along the depth of the build. In the upper regions, the grains were relatively uniform in size ranging from 12μm to approximately 9.5μm at 1 mm level below the surface, whereas at 5 mm level, the grain size varied from 15μm to 8μm.

To correlate the grain size with the thermomechanical deformation conditions, Zener-Hollomon parameter, which encompasses the deformation related parameters, is commonly used (see equation 4.1). During FSLW, it appears that the material on AS experienced a severer plastic deformation and lower temperature compared with the RS, so the strain rate at AS was higher than RS, and the parameter Z was consequently higher at AS. Hence, the grains would be finer at AS, consistent with the experimental results (see Fig. 5. 3).

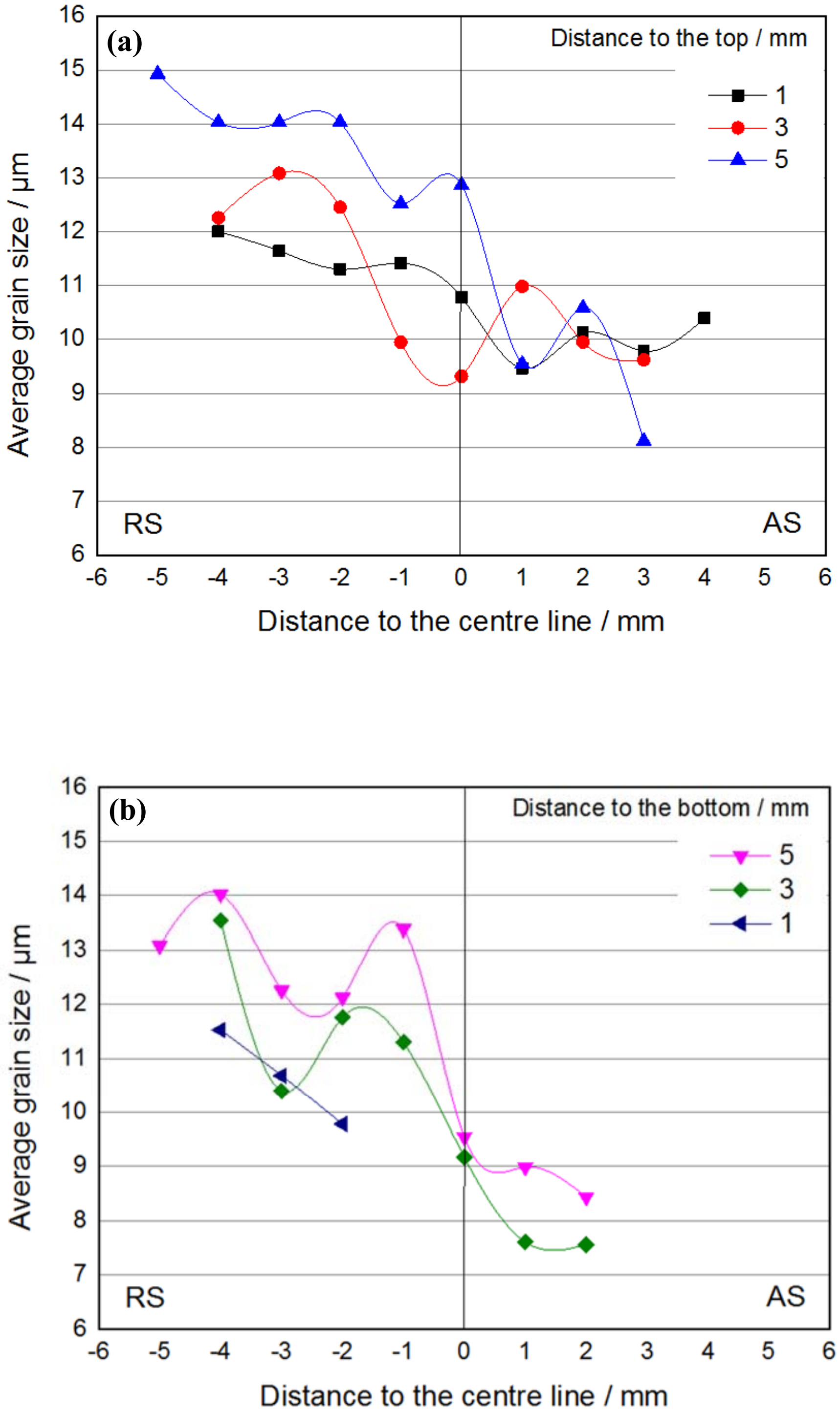

Fig. 5. 4 Average grain size in the SZ of AA6061 and A356 FSW lap welds.
(a) AA6061 SZ, (b) A356 SZ

Moreover, in the A356 part, significant grain refinement occurred in the SZ as well as the TMAZ, and similar to 6061 part, the grain size was slightly finer in AS. It was also found that the average grain size was smaller with the increasing sheet depth, as shown in Fig. 5. 3 and Fig. 5. 4, and in some conditions, onion ring was detected in the microstructure at the centre bottom, where the grain size was too fine to be quantified.

5.2.2.b Microstructural features

In Chapter 4, it was found that kissing bond can influence the mechanical properties of the FSW butt joints to some extent. In FSLW, the bonding structure is different from the butt weld, because the interface plane of the two materials is vertical to the interface which butt welding forms. Besides, it was found in Chapter 4 that the kissing bond forms due to the oxide films on the sheet surface, especially the sides at the joint line in a butt configuration. Thus, kissing bond tends to be severer in FSLW because of the oxide surface of the contact interface where there is a larger contact area than butt welding.

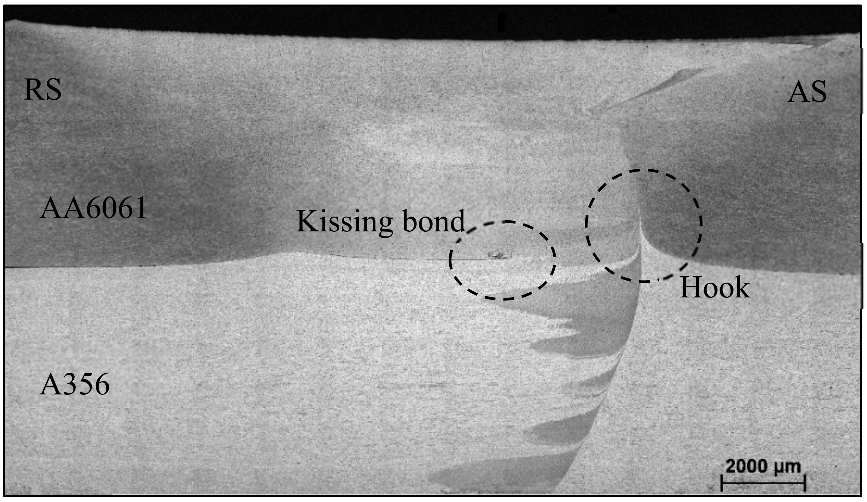

Fig. 5. 5 The macrostructure profile of the AA6061 A356 FSLW joint.

Fig. 5. 5 shows the macrostructure profile of the AA6061 A356 FSLW joint. It was found that

kissing bond existed at the boundary of the two materials in the welds centre. Different from the butt welds, the kissing bond in the lap weld was distributed non-continuously with the substance of the oxide particle cluster.

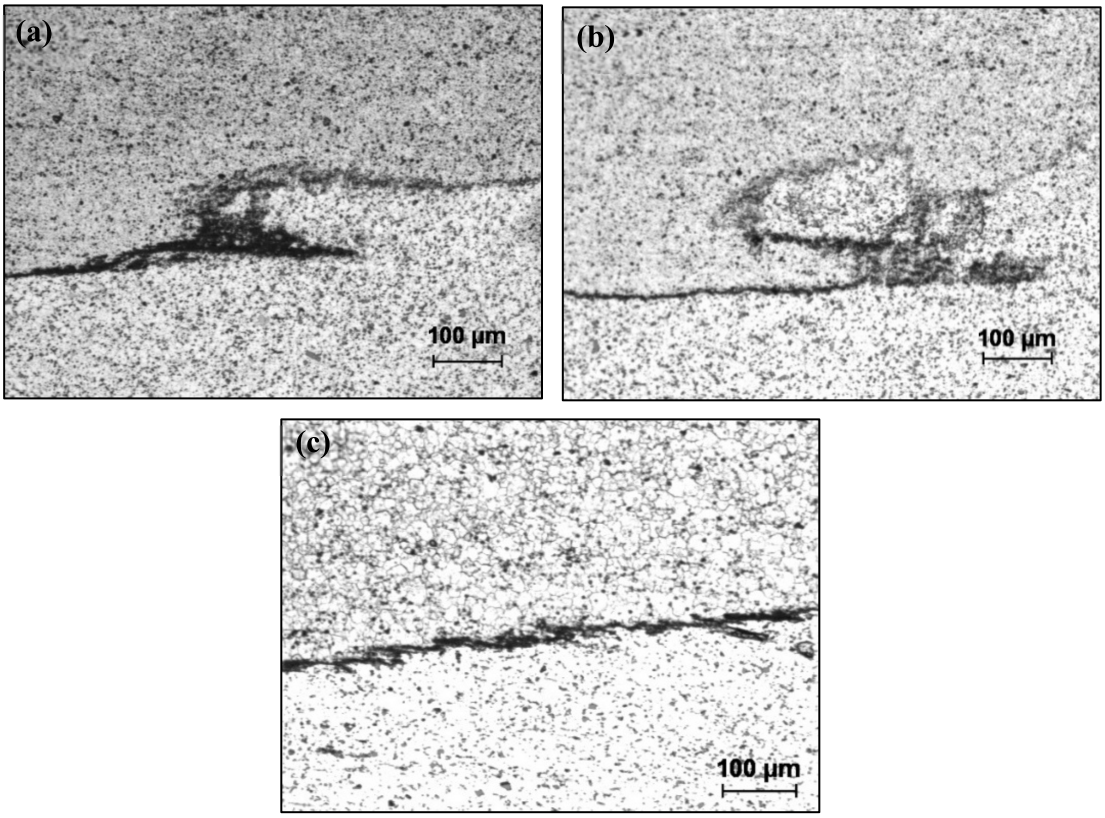

Fig. 5. 6 Kissing bond interfaces between the top and bottom sheets at a welding speed of 100 mm/min ((a) ω = 800rpm, (b) ω = 1000rpm, (c) ω = 1200rpm)

Fig. 5. 6 shows the detailed morphology of the kissing bond in the welds which were obtained by different tool rotation speed. It was found that the kissing bond existed in all the welds prepared at various rotation speeds of 800, 1000 and 1200 rpm, and a constant welding speed of 100 mm/min. As shown in Fig. 5. 6 (a), (b), and (c), with the increasing tool rotation speed, the severity of the kissing bonds was reduced. During FSLW, the oxide film was broken by the moving/rotating effect of the welding tool. Therefore, the formation of kissing bond was significantly influenced by the

stirring extent, which can be inversely correlated to the tool feed speed/rotational speed ratio (advanced per revolution). This ratio was inversely related to the heat input in FSW/FSLW. More severe kissing bonds were likely to be formed at lower heat input, corresponding to less stirring effect, consequently generating the kissing bond in the form of continuous zigzag line.

Moreover, it was also found in Fig. 5. 5 that a hook-shaped structure was observed in the weld seam towards AS. Many attentions have been paid to the hook structure in FSW especially lap welds or spot welds [15-17]. In FSLW, crack initiation was likely to occur from the tip of the hood and then along the hook curve during the shear tensile procedure [18].

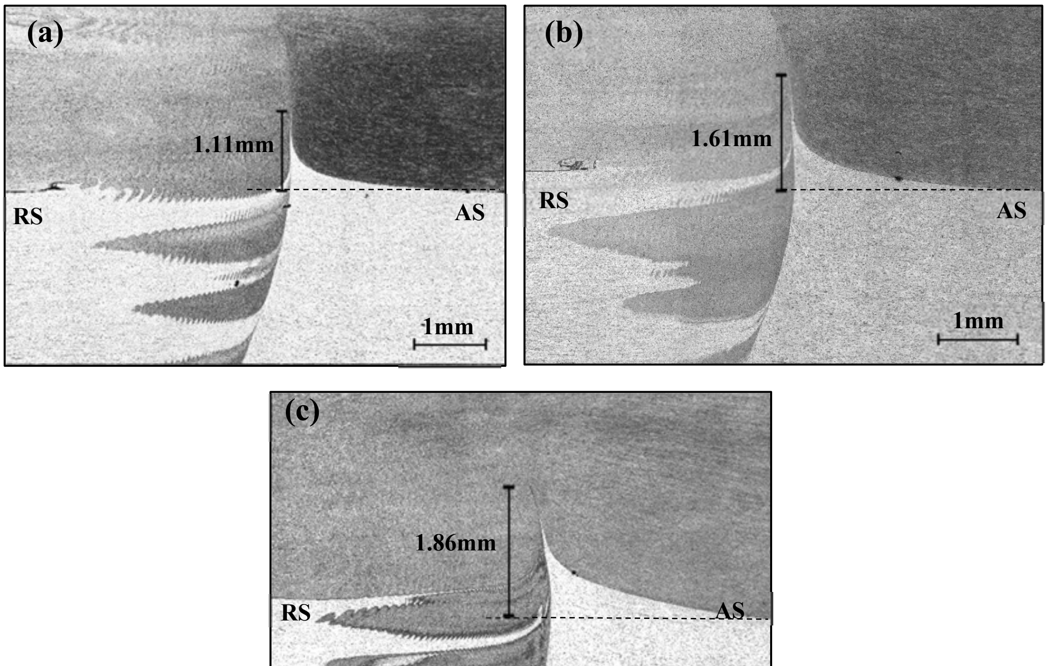

Fig. 5. 7 Hook structure in the FSLW of AA6061 and A356.
(a) ω = 800rpm, (b) ω = 1000rpm, (c) ω = 1200rpm

Fig. 5. 7 shows the hook structure in the FSLW joints obtained by different tool rotation speed. It

was found that with the increasing tool rotation speed, the shape of hook did not significantly change, just the hook tip directed slightly towards the RS. Besides, to further characterize the hook, the height of the hook for each sample was measured from the interface line to the hook tip (shown as Fig. 5. 7). With the increase of the tool rotation speed, the height of the hooking increased correspondingly, revealing that the stirring movement was severer due to the increasing tool rotation speed. Moreover, another evidence proving the severer motion was that more AA6061 material flowed to the A356 matrix during the FSLW procedure (the dark material is showing AA6061 in Fig. 5. 7).

5.2.2.c Particle distribution

Fig. 5. 8 shows the FSLW microstructures in the SZ and BM. It was found in Fig. 5. 8 (a) that two different kinds of intermetallic particles which were light grey faceted and black round particles were detected in the AA6061 base material. According to the previous work on the intermetallics of AA6061-T6, they were Al-Fe-Si particles and Mg, Si-rich particles, respectively. Fig. 5. 8 (b) shows the particle morphology of AA6061 part of FSLW SZ. Comparing the microstructure of the BM and SZ, the Al-Fe-Si phase experienced stirring-assisted fragmentation during FSLW, whereas the Mg, Si-rich particles did not significantly change.

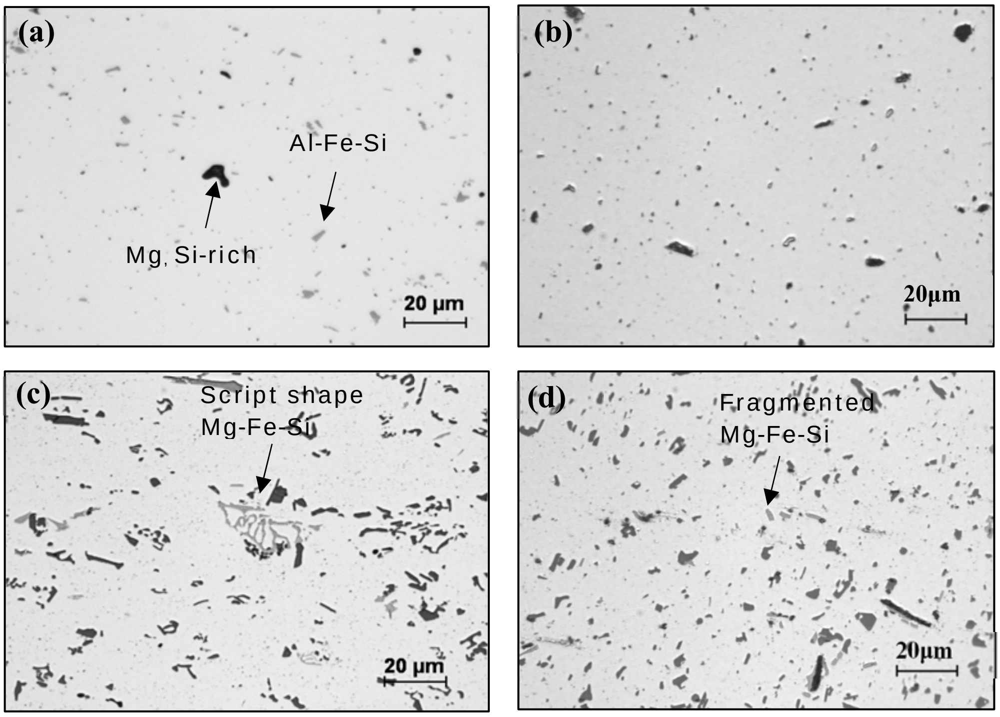

Fig. 5. 8 Microstructure for FSW lap welding of AA6061-T6 and as-cast A356 aluminium alloys. (a) AA6061 BM, (b) AA6061 SZ, (c) A356 BM, (d) A356 SZ

In A356 (Fig. 5. 8 (c)), the majority of the individual faceted/elongated particles were found to be Si-rich phase, whereas the Mg-Fe-Si phase showed script morphology. Both types were frequently detected in the BM and HAZ. However, the FSLW procedure resulted in a severe fragmentation of the Mg-Fe-Si phase in the SZ and a more random redistribution of Mg-Fe-Si phase, while the Si-rich particles did not significantly change in the A356 SZ, shown in Fig. 5. 8 (d).

Image analysis was used to map the distribution of the intermetallic particles in the weld. As shown from Fig. 5. 9 to Fig. 5. 12, the area fraction of the various second-phases in the welds were illustrated, respectively. In Fig. 5. 9 and Fig. 5. 10 which show the particle distribution in FSLW AA6061, it was found that after the FSW process, the total amount of the particles, either Al-Fe-

Si phase or Mg, Si-rich phase, did not significantly change in AA6061, although the decrease in the particle size could be observed by OM in the SZ (see Fig. 5. 8). Therefore, for the AA6061, the stirring could mainly bring crushing effect on the second-phase in the SZ. However, as shown in Fig. 5. 11 and Fig. 5. 12, the amount of the second-phase in SZ especially on AS of A356 part exhibited an obvious decrease, which could be due to the particles being fragmented beyond the optical microscope resolution, and/or their dissolution due to the thermal effects associated with stirring and thermomechanical deformation during FSLW. The dissolution of the second-phase including Mg-Fe-Si phase and Si-rich phase, as well as their refinement by stirring, combined with the fine grains within the weld could probably increase the strength of the SZ of A356 through solid solution strengthening or Orowan strengthening. As such, it can be predicted that the hardness would have an increase in the A356 SZ, and therefore the weakest part of the joint is likely to be the HAZ where crack initiation located in the process of shear loading of the lap welds, which will be discussed in the next section.

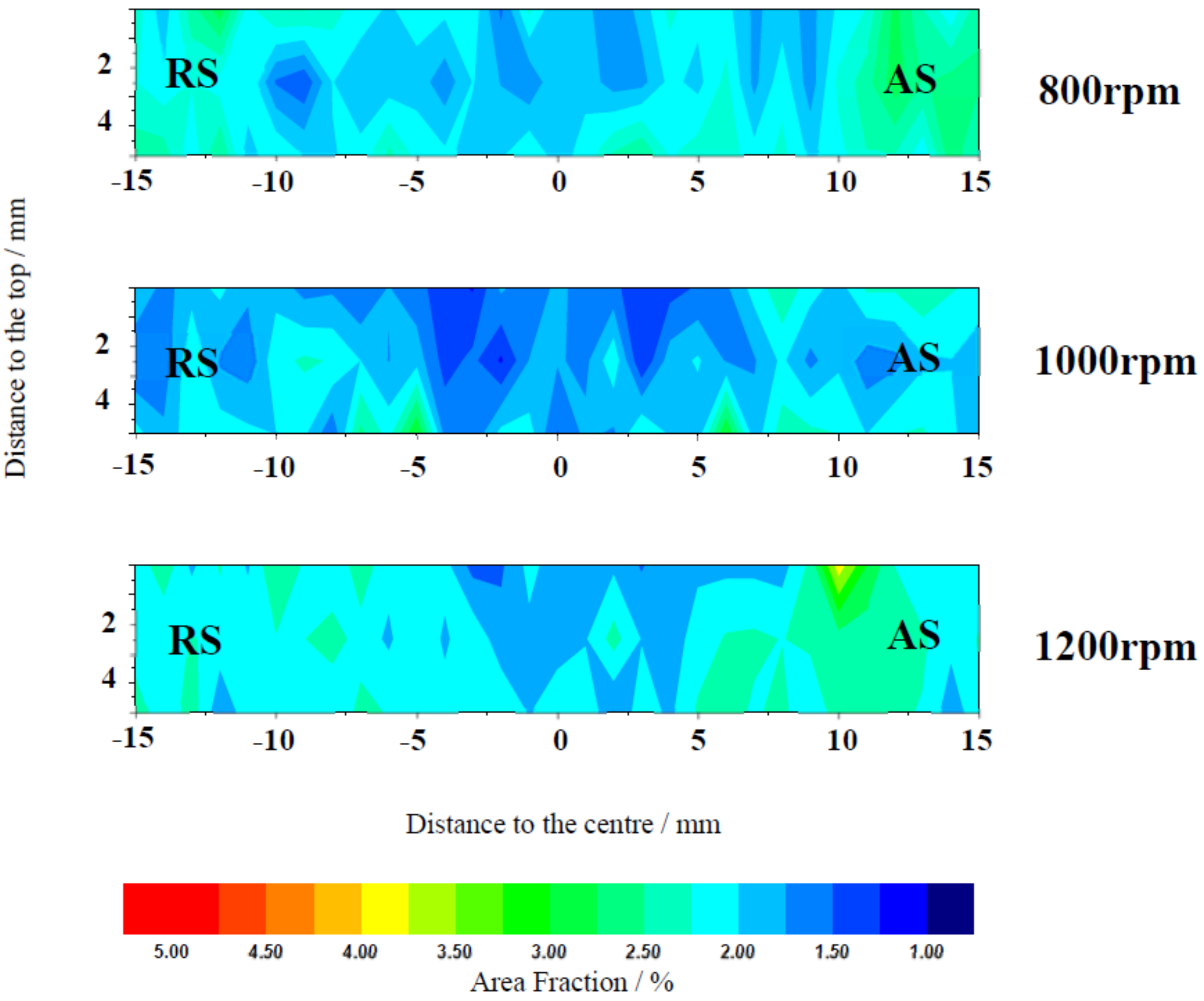

Fig. 5. 9 Area fraction distribution for the Al-Fe-Si phase in the AA6061 part of the FSLW weld obtained at different tool rotation speed.

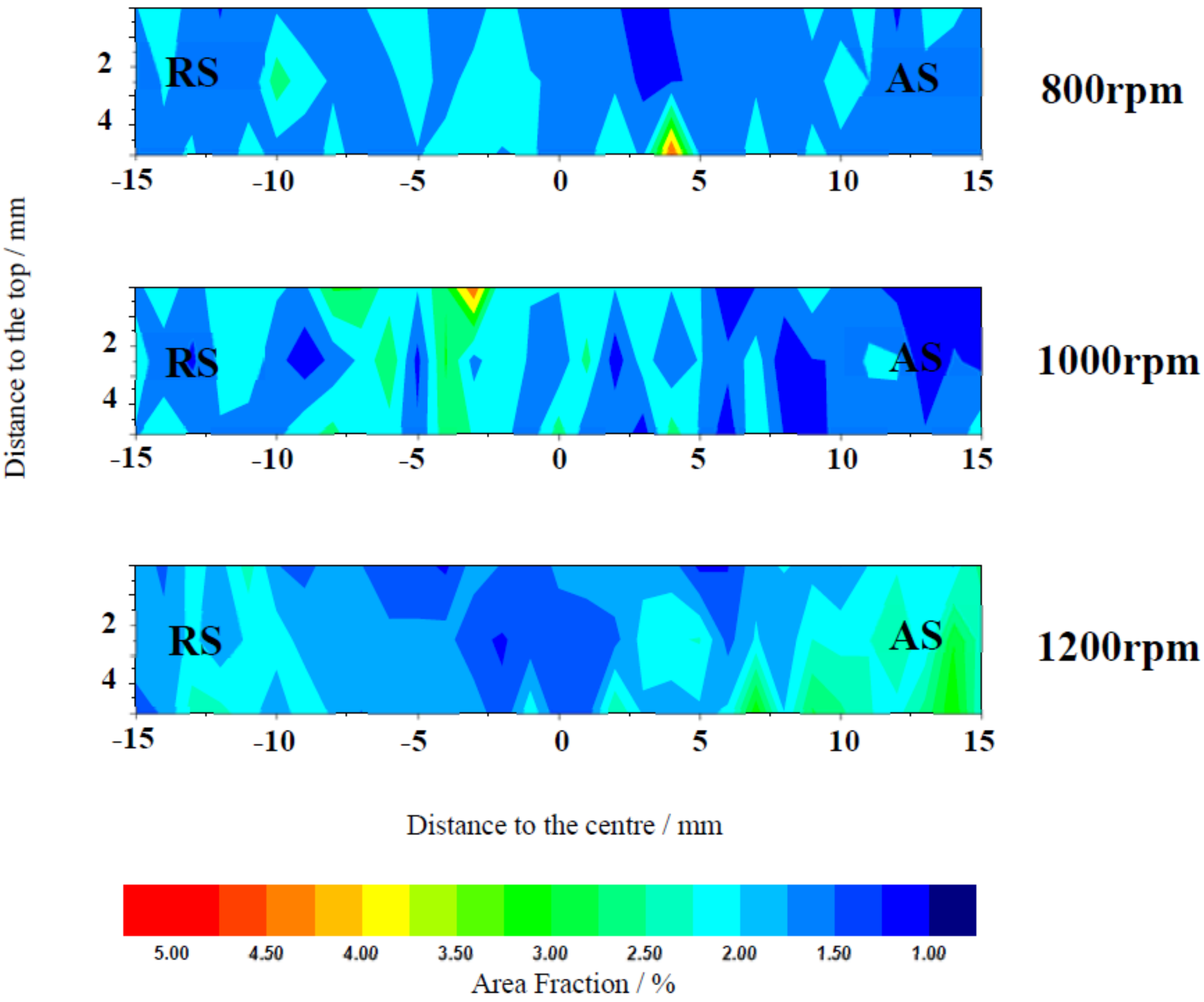

Fig. 5. 10 Area fraction distribution for the Mg, Si-rich phase in the AA6061 part of the FSLW weld obtained at different tool rotation speed.

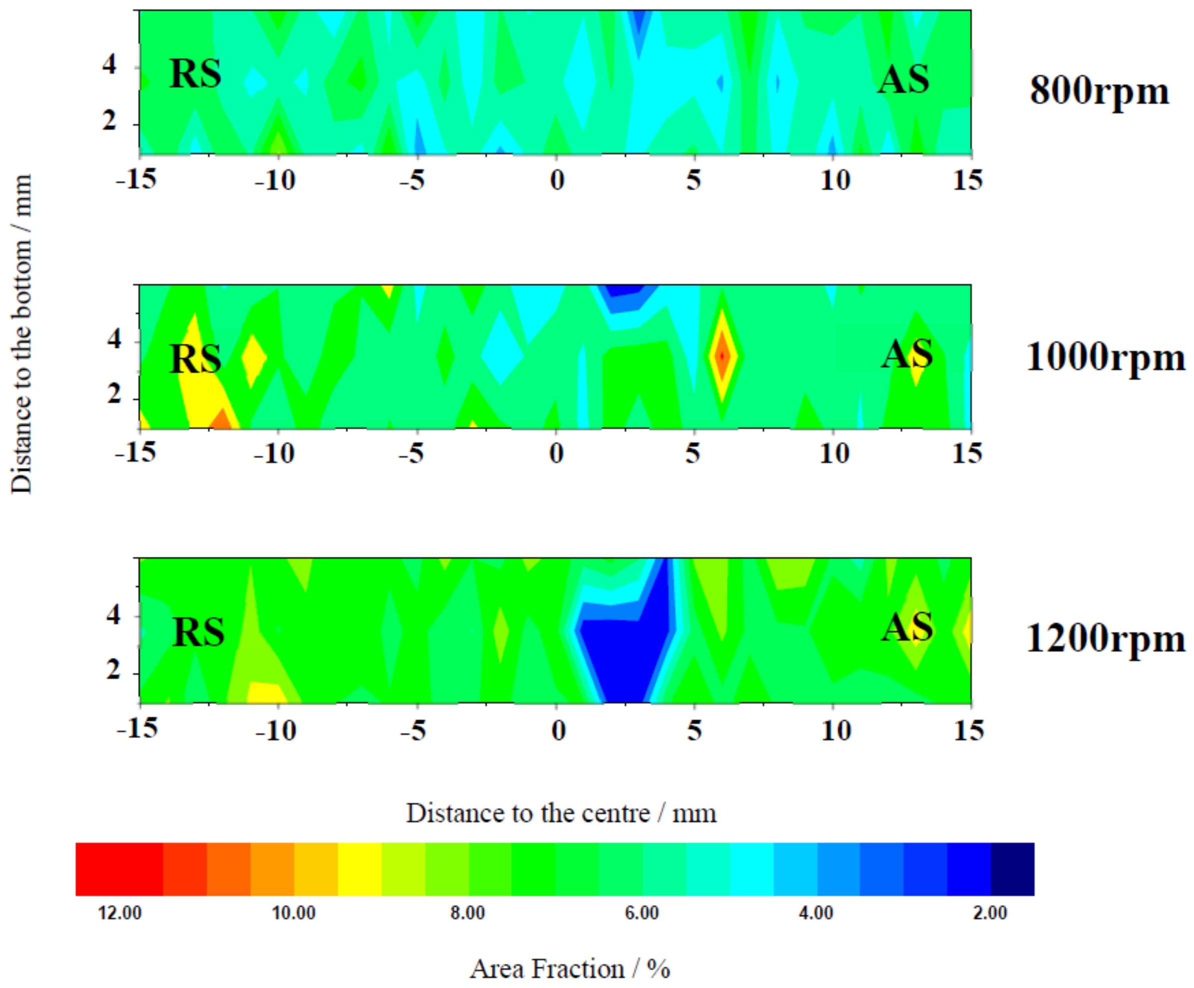

Fig. 5. 11 Area fraction distribution for the Si-rich phase in the A356 part of the FSLW weld obtained at different tool rotation speed.

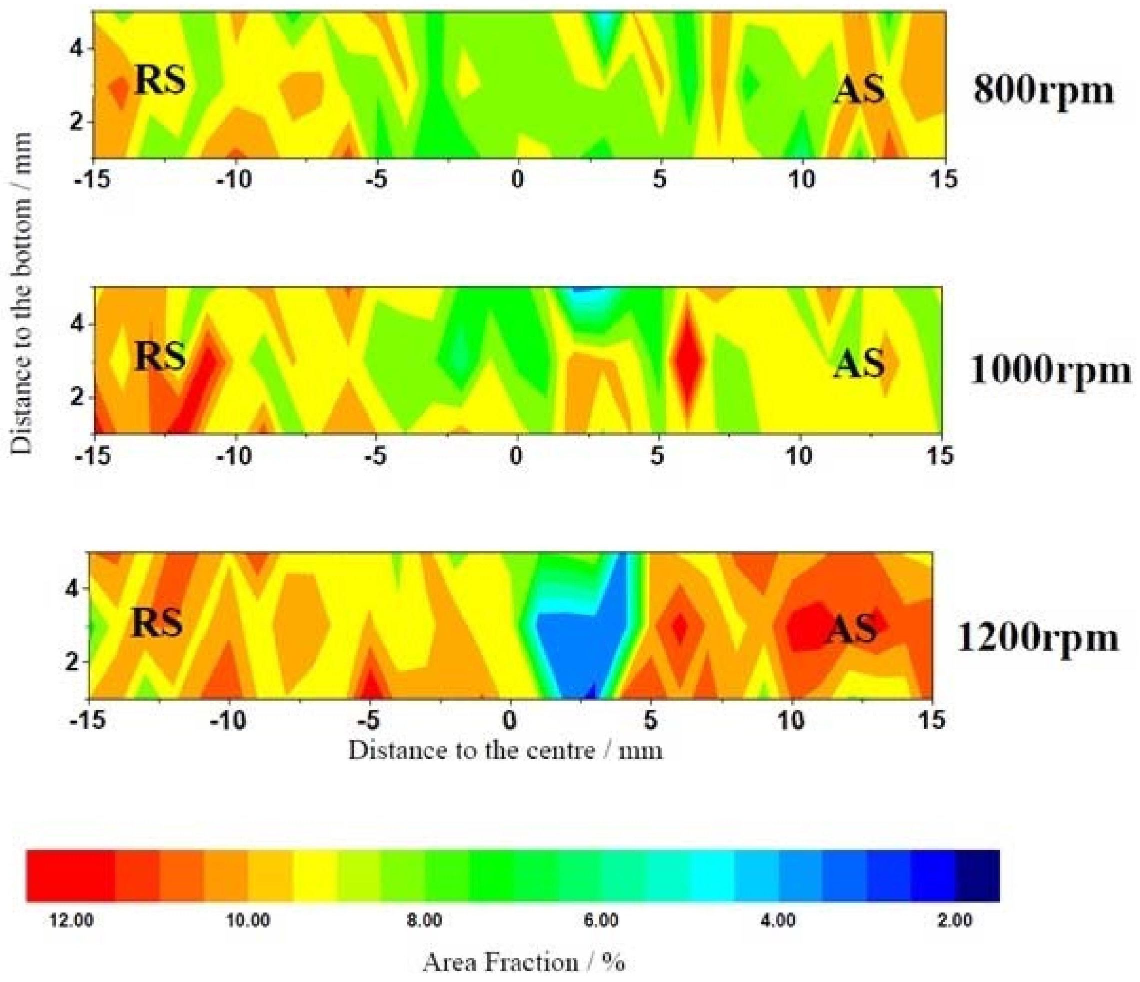

Fig. 5. 12 Area fraction distribution for the Mg-Fe-Si phase in the A356 part of the FSLW weld obtained at different tool rotation speed.

5.3 Mechanical properties of FSLW AA6061-A356

5.3.1 As-welded hardness distribution

Fig. 5. 13 shows the hardness distribution in different trends for both AA6061 alloy and A356 alloy sections. In AA6061 side, the highest hardness (96 HV) appeared in BM, and towards the centre, decreased to ~52HV in the HAZ and TMAZ, and finally rose up to ~70 HV in the SZ. In A356 side, the hardness was much lower than AA6061 as ~41HV in BM and HAZ, increasing to ~50 HV in the bottom of the sheet to ~60 HV in the upper part of the SZ, as expected previously due to the stirring and dissolution effects. It was also found in Fig. 5. 13, for all the samples, the symmetry axis of the hardness was slightly deviated towards the AS, because of the severer deformation in the AS than RS in the welding procedure.

With the increasing tool rotation speed, it was found in Fig. 5. 13 that the high hardness area in A356 SZ was getting larger especially towards the AS, which was because of the increasing dissolution strengthening effect in the A356 SZ towards AS, as well as the severer stirring effect resulting in the entrainment of the AA6061 material downward to the A356 matrix. Besides, it was also found in Fig. 5. 13 that, with the increasing tool rotation speed, wider was found in the zone where the hardness decreased at AA6061 side, revealing that the HAZ becomes wider because of the higher heat input during FSLW. However, at A356 side, no hardness decreasing zone was found according to the hardness contour, showing that the temperature in the A356 HAZ had little effect on the hardness.

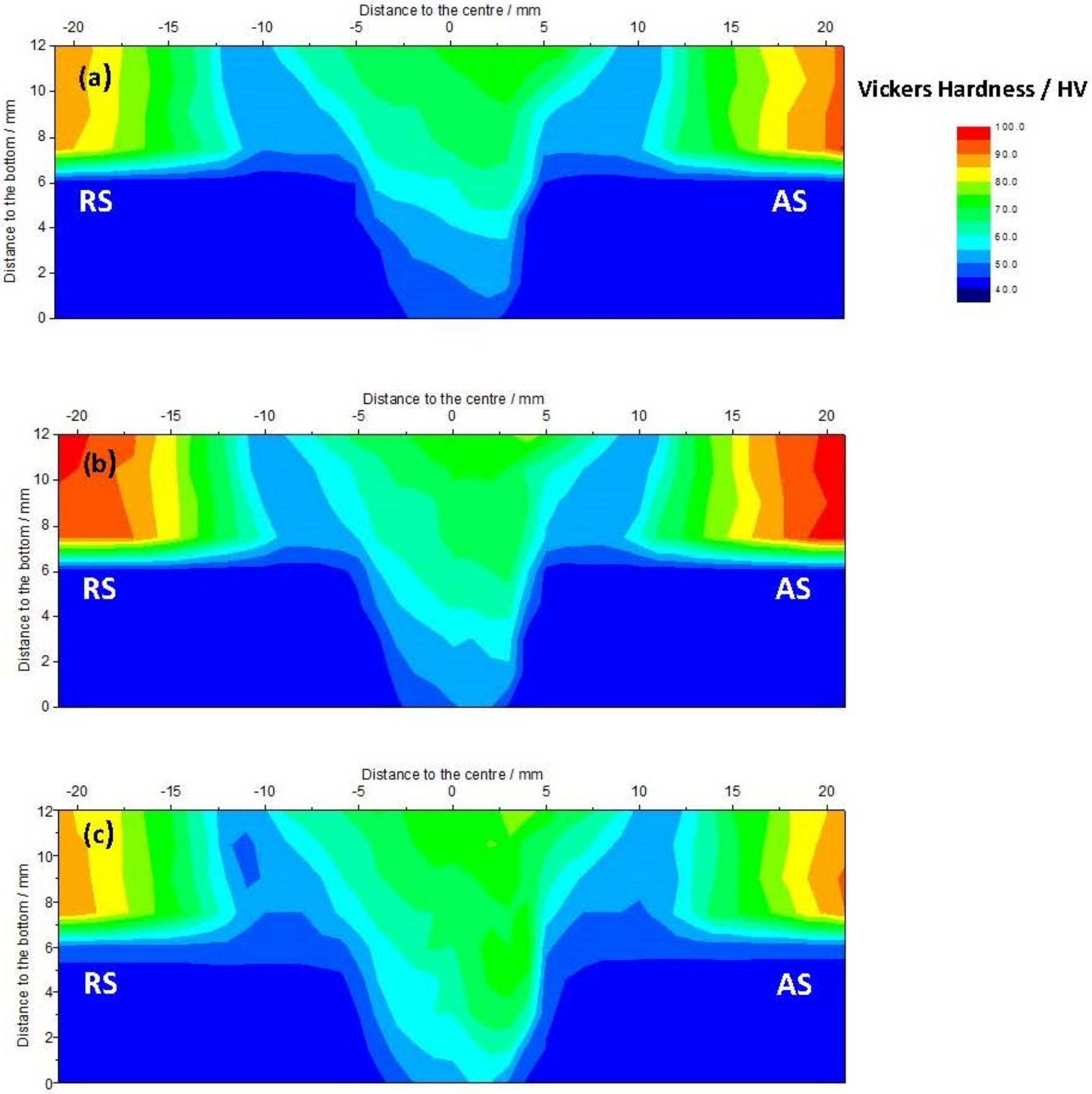

Fig. 5. 13 Vickers hardness contours of the FSLW joints obtained at different tool rotation speeds ((a) ω = 800rpm, (b) ω= 1000rpm, (c) ω = 1200rpm)

5.3.2 As-welded shear strength

Fig. 5. 14 shows the shear test results for the FSLW joints. It was found that the ultimate shear force decreased with the increasing tool rotation speed, which corresponding to higher heat input in the FSW procedure. Consequently, the material in HAZ of the weld could be softened due to

more heat input, making the HAZ to be the weakest part of the weld. The hardness contours (see Fig. 5. 13) also revealed that the HAZ was larger with the increase of the tool rotation speed. Therefore, the strength of the welds dropped with the increase of the tool rotation speed. However, sound joints could be obtained using proper welding parameters, or e.g. if a too slow tool rotation speed was used, the heat input becomes insufficient to achieve sound bonding resulting in a channel or wormhole defect.

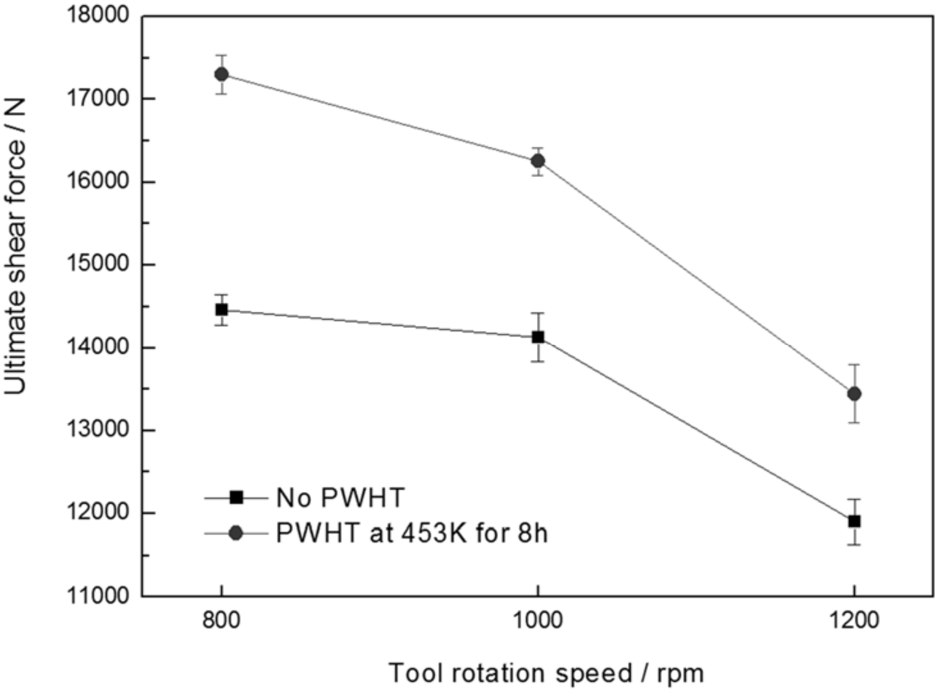

Fig. 5. 14 Results of lap-shear test (*v* = 100 mm/min)

Relevant studies have shown that the kissing bond in the FSW is likely to harm the mechanical properties because it is partially-bonded in that area to some extent [19, 20]. It can reduce the mechanical strength because of the different properties between the oxides and the matrix around, which is likely to cause stress concentration and crack initiation during deformation. However, it was also reported that the kissing bond may not be the key factor that significantly reduces the mechanical properties[21]. For FSW lap welding, it was reported that hook defect can play an important role affecting the mechanical properties[18, 22, 23]. In AZ31B-H24 Mg FSLW joints, the existence of hook-like kissing bond defects significantly affected the properties because of the sharp tips[24]. As shown in Fig. 5. 14, at a constant feed speed, the ultimate shear force decreases with the increase in the rotation speed. As shown in Fig. 5. 7, the higher rotating speed can decrease the ultimate tensile force of the sample, because of the increase in size and range of the hook defect in the weld, although the severity of the kissing bond reduced. Besides, higher tool rotation speed increases the heat input, which leads to grain coarsening and softening in the HAZ, making the joints weaker. As the strength of A356 BM is much lower than that of AA6061 BM, stress concentration and crack initiation are prone to occur at the hook tip, where the A356 forms as a sharp tip, rather than the kissing bond.

5.4 Post welding heat treatment (PWHT)

According to the results in section 5.3, A356 has lower hardness and strength than AA6061. Moreover, it was found that FSLW procedure can bring dissolution effect on the weld especially for A356. Therefore, aging treatment (T5) was conducted in the aim of increasing the hardness and strength of A356 so as to enhance the overall performance of the weld. According to the reports on the T5 heat treatment A356[25, 26], three levels of the temperatures (433K, 453K and 473K) for 8 hours were chosen for T5 treatment on the weld which had the highest tensile shear strength in this study (v=100mm/min, ω=800rpm).

The microhardness profiles of the PWHT AA6061-A356 FSLW welds are shown in Fig. 5. 15 (a) and (b). The hardness traces were performed at mid-weld thickness in both alloy sheets. After the PWHT, the hardness in the AA6061 section of the weld increased significantly in the WN, TMAZ and slightly in the HAZ towards the AS, while staying constant towards the RS, regardless of the PWHT temperatures. Comparing the different PWHT temperatures, the highest hardness in the weld was achieved in the WN and TMAZ (AS) at 453K. For A356, the hardness in the WN increased significantly, whereas the hardness remained unaffected in the TMAZ or HAZ. As shown in Fig. 8, the maximum tensile shear force increased following the ageing treatment at the optimised temperature 453K, where the ultimate shear force of the welds increased by more than 10% in all the welding conditions.

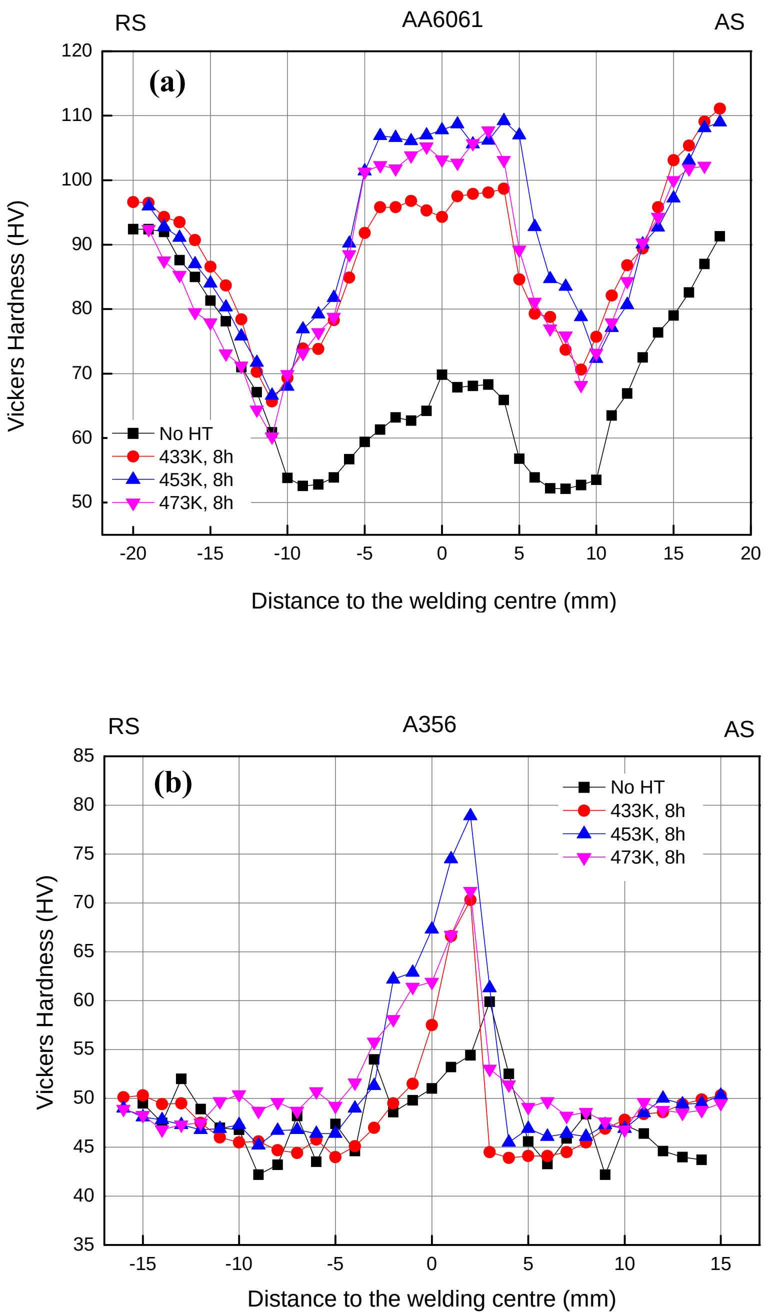

Fig. 5. 15 Microhardness profiles of the PWHT weld (welding condition, *v*=100mm/min, *ω*=800rpm). (a) AA6061, (b)A356

In AA6061, Mg_2Si is the main strengthening phase[27]. During FSLW procedure, the Mg_2Si in T6-condition AA6061 is expected to partly dissolve at the temperature in the WN which was reported as ~753K[28]. Following PWHT, the Mg_2Si phase would precipitate again and increase the hardness and tensile shear properties (see Fig. 5. 14). Furthermore, as discussed previously, the stirring effect towards the AS is more than RS, leading to more stirring-assisted Mg_2Si dissolution, which upon heat treatment results in the hardness increase in the AS rather than the RS. In A356, stirring and forging effect of the FSLW could bring the AA6061 material downwards towards the A356 WN (as evident through the etch contrast in Fig. 5. 7). As a result, after the PWHT, the hardness in the WN of A356 would increase due to the additional precipitation strengthening effect from the AA6061 material that is forged into the A356 section. It can also be seen that the peak hardness in the A356 welds is not exactly at the centre of the welds, but shifted from the centreline by ~2 mm towards the AS, which shows again that the stirring effect is more pronounced in the AS than the RS.

5.5 Conclusions

This chapter demonstrated the feasibility of FSLW of AA6061-T6 to as-cast A356 sheets. FSLW was successfully performed using a tool rotating speed range from 800rpm to 1200 rpm. After welding, the microstructure, average grain size in the SZ, second-phase distribution and microscale defects including kissing bond and hook were evaluated for the welds. Besides, the hardness and shear properties and their correlation with the welding parameters were studied before and after PWHT. The following conclusions could be drawn:

1. The welds showed inhomogeneous grain size distribution, and the recrystallised grains in the stir zone were slightly finer towards the AS than RS. This supports the view that the stirring effect is severer in the AS than RS, which could increase the strain rate resulting in grain refinement.

2. Kissing bond and hook were detected in the microstructure of the welds. Kissing bond, formed due to the presence of fine fragmented oxide particles, decreased with the increasing tool rotation speed. It was found that the kissing bond did not significantly affect the shear behaviour of the joints. Hook defect, found in the vicinity of the weld interface towards AS, increased in height and range with the increasing tool rotation speed. It was found that the hook defect had a significantly influence on the shear behaviour of the joints.

3. Intermetallic particles in the WN especially A356 side experienced stirring-assisted dissolution, whose severity increased with the increase in the tool rotation speed. After PWHT, the hardness in the WN increased significantly due to the re-formation of precipitates.

4. Shear test showed that the ultimate shear force could be higher for the weld which was prepared at a less heat-input welding parameters. In addition, the PWHT led to an improvement in the mechanical strength of the welds by more than 10% for all the welding conditions.

5.6 References

[1] P. Cavaliere, E. Cerri, A. Squillace, Mechanical response of 2024-7075 aluminium alloys joined by Friction Stir Welding, Journal of Materials Science 40(14) (2005) 3669-3676.

[2] M. Koilraj, V. Sundareswaran, S. Vijayan, S.R. Koteswara Rao, Friction stir welding of dissimilar aluminum alloys AA2219 to AA5083 – Optimization of process parameters using Taguchi technique, Materials & Design 42 (2012) 1-7.

[3] I. Dinaharan, K. Kalaiselvan, S.J. Vijay, P. Raja, Effect of material location and tool rotational speed on microstructure and tensile strength of dissimilar friction stir welded aluminum alloys, Archives of Civil and Mechanical Engineering 12(4) (2012) 446-454.

[4] S. Lim, S. Kim, C. Lee, S. Kim, Tensile behavior of friction-stir-welded A356-T6Al 6061-T651 bi-alloy plate, Metallurgical and Materials Transactions A 35A (2004) 2837-2843.

[5] W.-B. Lee, Y.-M. Yeon, S.-B. Jung, The joint properties of dissimilar formed Al alloys by friction stir welding according to the fixed location of materials, Scripta Materialia 49(5) (2003) 423-428.

[6] M. Ghosh, K. Kumar, S.V. Kailas, A.K. Ray, Optimization of friction stir welding parameters for dissimilar aluminum alloys, Materials & Design 31(6) (2010) 3033-3037.

[7] S. Yazdanian, Z.W. Chen, G. Littlefair, Effects of friction stir lap welding parameters on weld features on advancing side and fracture strength of AA6060-T5 welds, Journal of Materials Science 47(3) (2011) 1251-1261.

[8] V. Soundararajan, E. Yarrapareddy, R. Kovacevic, Investigation of the Friction Stir Lap Welding of Aluminum Alloys AA 5182 and AA 6022, Journal of Materials Engineering and Performance 16(4) (2007) 477-484.

[9] T. Saeid, A. Abdollah-zadeh, B. Sazgari, Weldability and mechanical properties of dissimilar aluminum–copper lap joints made by friction stir welding, Journal of Alloys and Compounds 490(1) (2010) 652-655.

[10] M.K. Kulekci, I. Sevim, U. Esme, Fracture Toughness of Friction Stir-Welded Lap Joints of Aluminum Alloys, Journal of Materials Engineering and Performance 21(7) (2011) 1260-1265.

[11] I. Galvão, D. Verdera, D. Gesto, A. Loureiro, D.M. Rodrigues, Influence of aluminium alloy type on dissimilar friction stir lap welding of aluminium to copper, Journal of Materials Processing

Technology 213(11) (2013) 1920-1928.

[12] M. Ericsson, L. Jin, R. Sandstrom, Fatigue properties of friction stir overlap welds, International Journal of Fatigue 29(1) (2007) 57-68.

[13] G. Buffa, G. Campanile, L. Fratini, A. Prisco, Friction stir welding of lap joints: Influence of process parameters on the metallurgical and mechanical properties, Materials Science and Engineering: A 519(1-2) (2009) 19-26.

[14] C.-Y. Lee, W.-B. Lee, J.-W. Kim, D.-H. Choi, Y.-M. Yeon, S.-B. Jung, Lap joint properties of FSWed dissimilar formed 5052 Al and 6061 Al alloys with different thickness, Journal of Materials Science 43(9) (2008) 3296-3304.

[15] K.K. Ravi, R.G. Narayanan, P.K. Rana, Friction Stir Spot Welding of Al6082-T6/HDPE/Al6082-T6/HDPE/Al6082-T6 sandwich sheets: hook formation and lap shear test performance, Journal of Materials Research and Technology (2018).

[16] Q. Zheng, X. Feng, Y. Shen, G. Huang, P. Zhao, Effect of plunge depth on microstructure and mechanical properties of FSW lap joint between aluminum alloy and nickel-base alloy, Journal of Alloys and Compounds 695 (2017) 952-961.

[17] J.Y. Cao, M. Wang, L. Kong, L.J. Guo, Hook formation and mechanical properties of friction spot welding in alloy 6061-T6, Journal of Materials Processing Technology 230 (2016) 254-262.

[18] Y. Song, X. Yang, L. Cui, X. Hou, Z. Shen, Y. Xu, Defect features and mechanical properties of friction stir lap welded dissimilar AA2024–AA7075 aluminum alloy sheets, Materials & Design 55 (2014) 9-18.

[19] H. Okamura, K. Aota, M. Sakamoto, M. Ezumi, K. Ikeuchi, Behaviour of oxides during friction stir welding of aluminium alloy and their effect on its mechanical properties, Welding International 16(4) (2002) 266-275.

[20] M. Kadlec, R. Růžek, L. Nováková, Mechanical behaviour of AA 7475 friction stir welds with the kissing bond defect, International Journal of Fatigue 74 (2015) 7-19.

[21] B.S. Naik, D.L. Chen, X. Cao, P. Wanjara, Microstructure and Fatigue Properties of a Friction Stir Lap Welded Magnesium Alloy, Metallurgical and Materials Transactions A 44(8) (2013) 3732-3746.

[22] L. Dubourg, A. Merati, M. Jahazi, Process optimisation and mechanical properties of friction stir lap welds of 7075-T6 stringers on 2024-T3 skin, Materials & Design 31(7) (2010) 3324-3330.

[23] H. Chen, L. Fu, P. Liang, F. Liu, Defect features, texture and mechanical properties of friction stir welded lap joints of 2A97 Al-Li alloy thin sheets, Materials Characterization 125 (2017) 160-173.

[24] X. Cao, M. Jahazi, Effect of tool rotational speed and probe length on lap joint quality of a friction stir welded magnesium alloy, Materials & Design 32(1) (2011) 1-11.

[25] L. BoChao, P. YoungKoo, D. HongSheng, Effects of rheocasting and heat treatment on microstructure and mechanical properties of A356 alloy, Materials Science and Engineering: A 528(3) (2011) 986-995.

[26] S.W. Youn, C.G. Kang, Characterization of age-hardening behavior of eutectic region in squeeze-cast A356-T5 alloy using nanoindenter and atomic force microscope, Materials Science and Engineering: A 425(1) (2006) 28-35.

[27] A.H. Naronikar, H.N.A. Jamadagni, A. Simha, B. Saikiran, Optimizing the Heat Treatment Parameters of Al-6061 Required for Better Formability, Materials Today: Proceedings 5(11, Part 3) (2018) 24240-24247.

[28] P.-c. Zhao, Y.-f. Shen, G.-q. Huang, Q.-x. Zheng, Numerical simulation of friction stir butt-welding of 6061 aluminum alloy, Transactions of Nonferrous Metals Society of China 28(6) (2018) 1216-1225.

6 Linear Friction Welding of Al-Al and Al-Cu: Influence of defects on Microstructure and Properties

6.1 Introduction

Linear friction welding technology has attracted more and more attention because of its high welding efficiency, joint quality and wide application range [1-7]. Especially in the field of aircraft engine manufacturing, linear friction welding technology has become the key technology in solving the design and manufacture for the integrated blade of advanced aero-engines [8-11]. In recent years, with the continuous development of linear friction welding, welding materials are gradually extended from titanium to aluminium alloy, nickel superalloy, steel, copper as well as LFW of dissimilar metals [12-17].

Aluminium alloy has been widely used in the fields of machinery manufacturing, transportation and aviation industry for its high specific strength. However, there are few literatures on the LFW technology for aluminium alloy. One of the reasons is that aluminium alloy was considered difficulty in LFW because it has higher thermal conductivity than titanium so that more vibration frequency and greater forging force are needed to obtain sufficient heat for sound joints. However, due to much lower thermoplastic state temperature than titanium alloy, successful LFW for aluminium and aluminium alloy have been reported, and it has a broad application prospect in the industry [12, 14, 18, 19]. However, among these literatures, the influence of technological parameters on the microstructure and properties of linear friction welded joints of aluminium alloys and the formation mechanism of welded joints have been rarely reported.

Al-Cu LFW joints are used as the conductive material in automotive application due to the excellent electrical conductivities of Al and Cu. As mentioned in Chapter 2, the quality of the Al-Cu joints depends on the weld microstructure formed, especially the presence of intermetallic phases, due to their detrimental influence on the mechanical properties. According to the binary Al-Cu phase diagram [20] shown in Fig. 6. 1, five types of thermodynamically stable intermetallic phases may exist, which are: $CuAl_2$ (θ), CuAl (η), Cu_4Al_3 (ζ), Cu_3Al_2 (δ), and Cu_9Al_4 (γ). As summarised in Chapter 2, all the phases above have been found in the Al-Cu friction welds including FSW and LFW, and as the review of the literature has shown, the generation of Al-Cu intermetallic compounds is detrimental to the joint mechanical properties. As a result, effective control of the formation and growth of intermetallic compounds is essential to achieve an acceptable performance. However, a series of problems remain unresolved such as which affect the most to the mechanical properties among these Al-Cu intermetallic phases, and how the intermetallic particles change with the different composition of Al base material, etc.

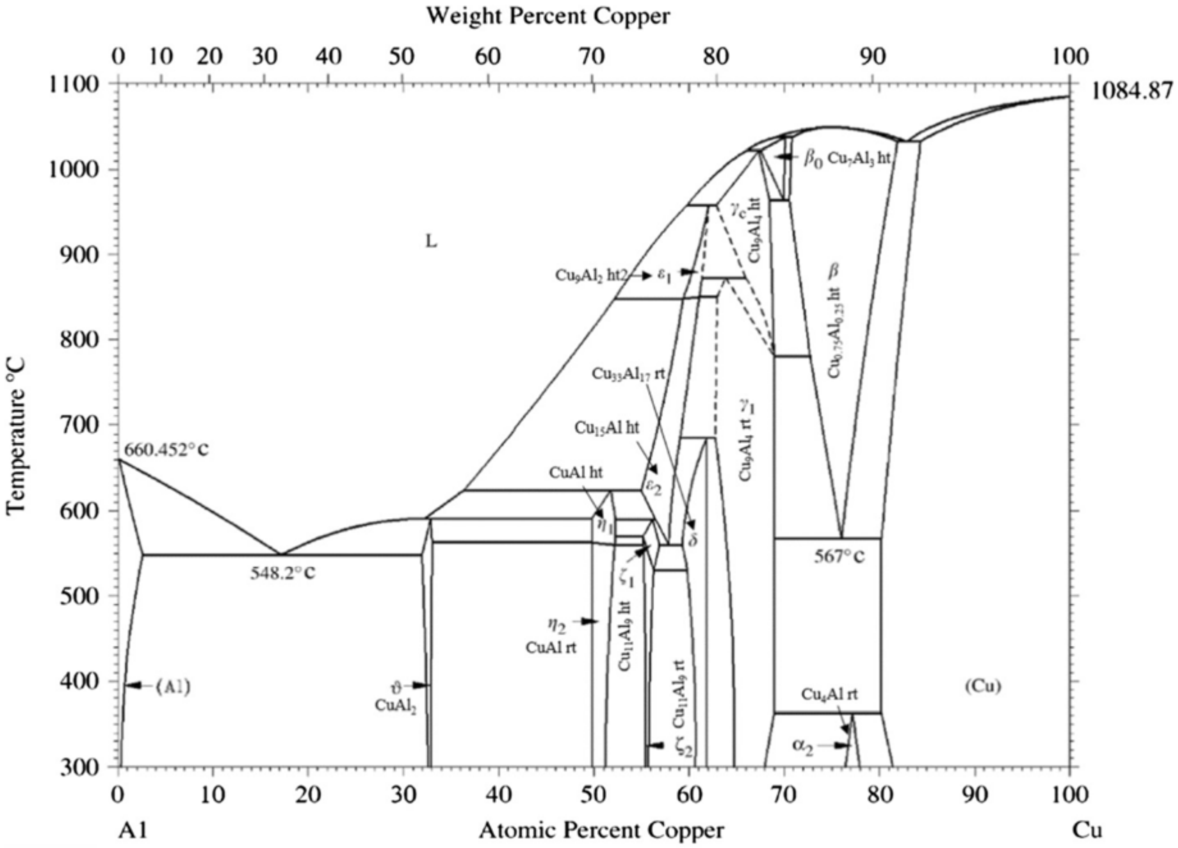

Fig. 6. 1 Binary phase diagram of Al-Cu system. [20]

In this chapter, LFW of AA5083 aluminium alloy is investigated to reveal the evolution of the microstructure and properties of the material during the LFW process, focusing on the defect and its effect on the microstructure and mechanical properties with the changing forging pressures. Dissimilar welding of AA5083 aluminium alloy and C101 Cu is also performed, assessing the influence of LFW parameters, especially the forging pressure on the microstructure and mechanical properties of joints. For special attention, intermetallics in the Al-Cu welds are also assessed on the type, size, and distribution, with the different welding forging pressures, as well as the influenced on the mechanical properties.

6.2 Linear friction welding of AA5083

6.2.1 Macrostructure and material flow

Fig. 6. 2 shows the macroscopic appearance of an AA5083-H112 linear friction welded joints. 1, 2 and 3 represent the samples which were welded at the forging pressures of 60MPa, 80MPa and 110MPa, respectively. It is shown that good welding joints can be obtained under different welding forging pressures. As can be seen from the diagram, the flash produced by the linear friction welding occurs only on one side along the direction of vibration for each workpiece, while along the vertical direction of vibration, flash occurs on both sides. This is because the linear friction welding device was set at a start position that was staggered by an amplitude distance, and only vibration to the position where two samples are coaxial. As shown in Fig. 6. 3, when applying forging force, the upper left corner of workpiece B pushed the material of the right side of workpiece A, so that the flash formed at the upper right corner of workpiece A. In the same way, flash also formed at the bottom left corner of workpiece B. Because the vibration stopped when the two workpieces placed to a straight line, the material in the upper left corner of workpiece B itself was not subject to the thrust of workpiece A. Therefore, flash occurs only at one side.

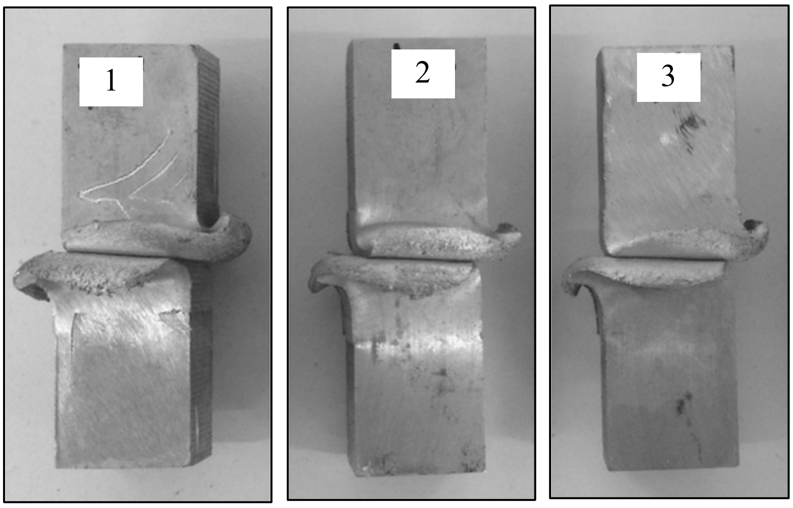

Fig. 6. 2 Macroscopic morphologies of the linear friction welds.

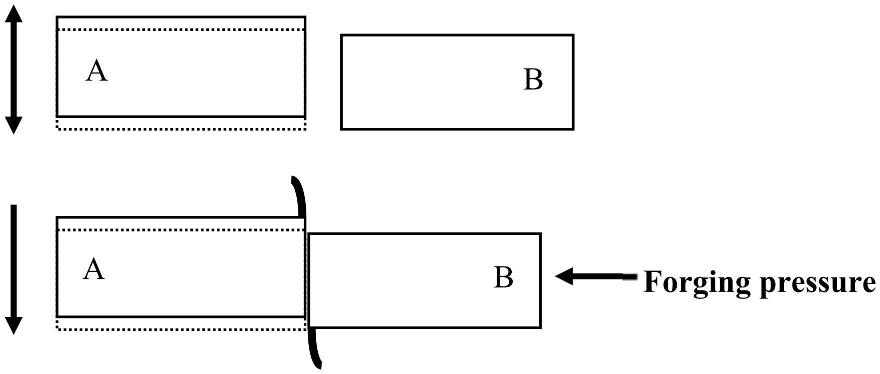

Fig. 6. 3 The schematic diagram of linear friction welding in this study.

6.2.2 Microstructure and defect characterization

Fig. 6. 4 is the overall microstructure of the linear friction welding joint of the experimental alloy in the vicinity of the flash edge. It was shown that the linear friction weld joint was metallurgical bonded in structure. No macroscopic lamellar transition zone has been found in the joint, and no macroscopic defects, cracks or other cracks have been found except for few isolated pores. Organizational characteristics of melting and solidification can not be observed in the

microstructure, revealing that the temperature did not reach the melting point of aluminium during LFW procedure. Besides, the microstructure of the flash the parent material was continuous, which means that the temperature of the material near the welding interface rose to thermoplastic state due to the friction heat, the material flowed out between the interface by forging force, and thus formed the flash. As mentioned above, melting does not happen during the LFW process of aluminium alloy. Actually, this process should be classified to the hot forging process. In the LFW process, friction provides heat for the process. When the workpiece material reaches a local thermoplastic state, appropriate pressure and friction of local materials could form a metallurgical combination, so as to realize the connection.

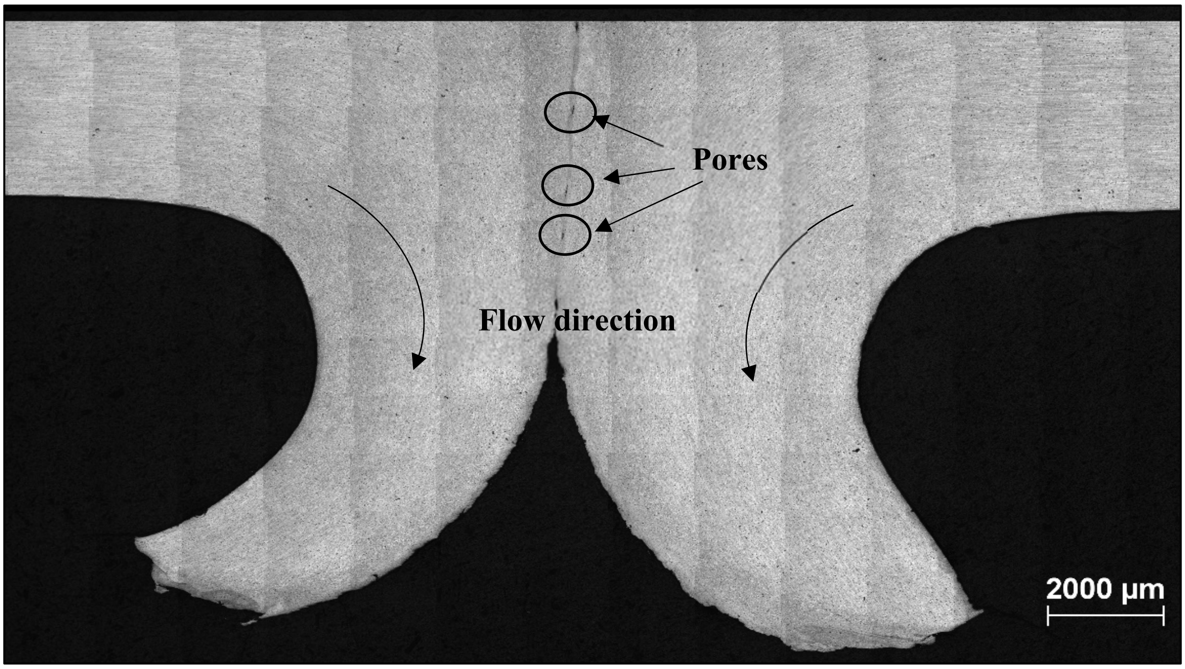

Fig. 6. 4 The overall microstructure of the AA5083 linear friction welds.

Fig. 6. 5 shows the enlarged microstructure of the LFW joint of the experimental alloy. According to the pictures, the welding joints can be divided into base metal zone, heat affected zone and weld zone according to the various microstructures. Among them, Fig. 6. 5 (a) is the microstructure of

parent material, (b) is the heat affected zone, (c) and (d) is the microstructure near the weld zone. It was found that the microstructure of base metal was a typical rolling morphology, while in the heat affected zone, the grains coarsened due to the friction heat. In the weld nugget zone shown in Fig. 6. 5 (c), it was found that a fine grain zone existed in the vicinity of the interface with the width of approximately 150-200μm, revealing that local dynamic recrystallization occurred during the process of LFW at the welding interface. Moreover, it was found in Fig. 6. 4 and Fig. 6. 5 (c) that isolated lack of connection defects were distributed long the welding interface. In Fig. 6. 5 (d) which is showing SEM morphology of the weld interface, it was found that the lack of connection defect was fusiform with the length of 100μm and width of 20μm. Except from that, the matrix around the defect was uniform, revealing that the defects were uncontinuously distributed. Besides, no significant second-phase particles or layers was observed. Fig. 6. 6 shows the microstructure of the LFW joints under two different forging pressures, it can be seen that with the forging force increased from 60MPa (as shown in Fig. 6. 6 (a)) to 110MPa (as shown in Fig. 6. 6 (b) below), the size of the defect was significantly reduced at the weld interface, indicating that larger pressure can make the weld more compact.

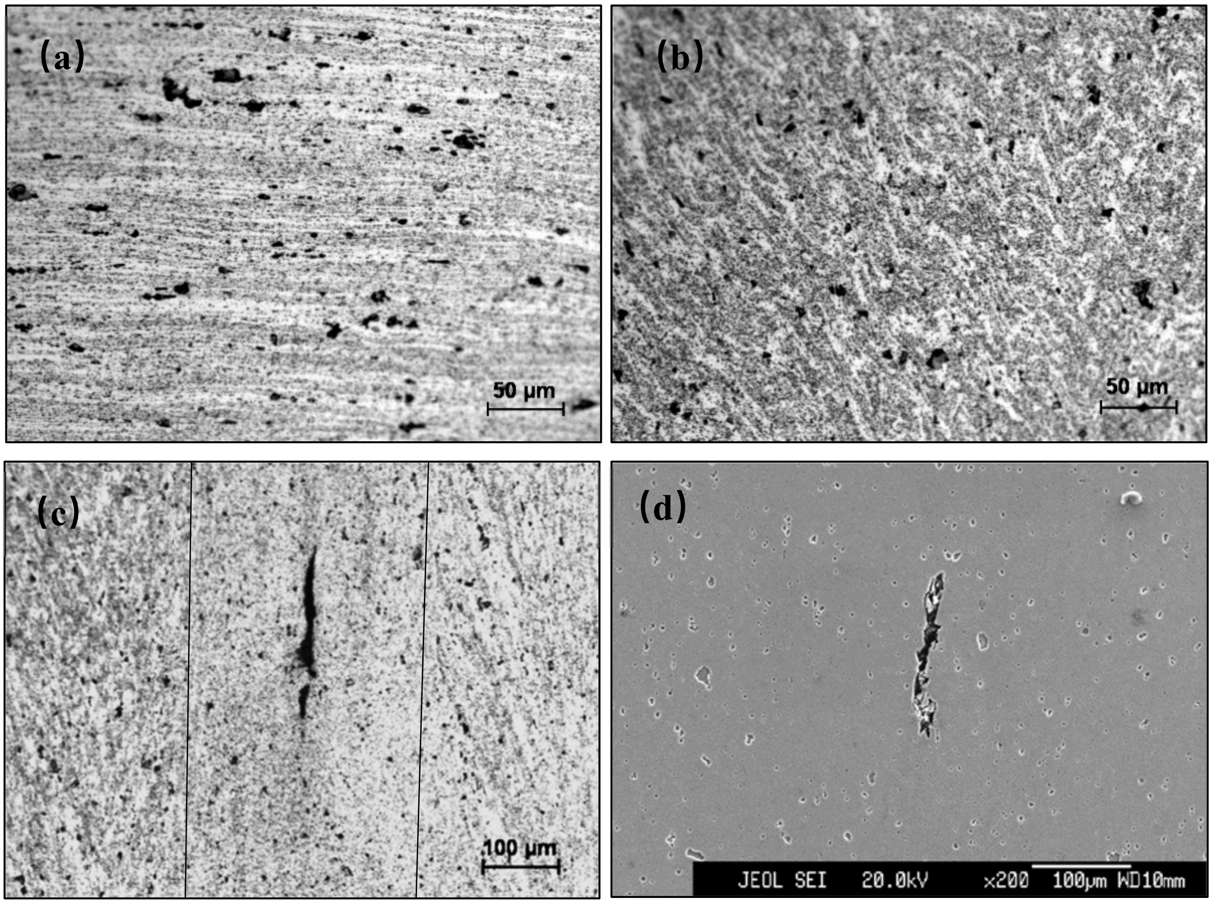

Fig. 6. 5 Microstructures of an AA5083 linear friction weld.
(a) base metal, (b) heat affected zone, (c) OM of the weld zone, (d) SEM of the weld zone

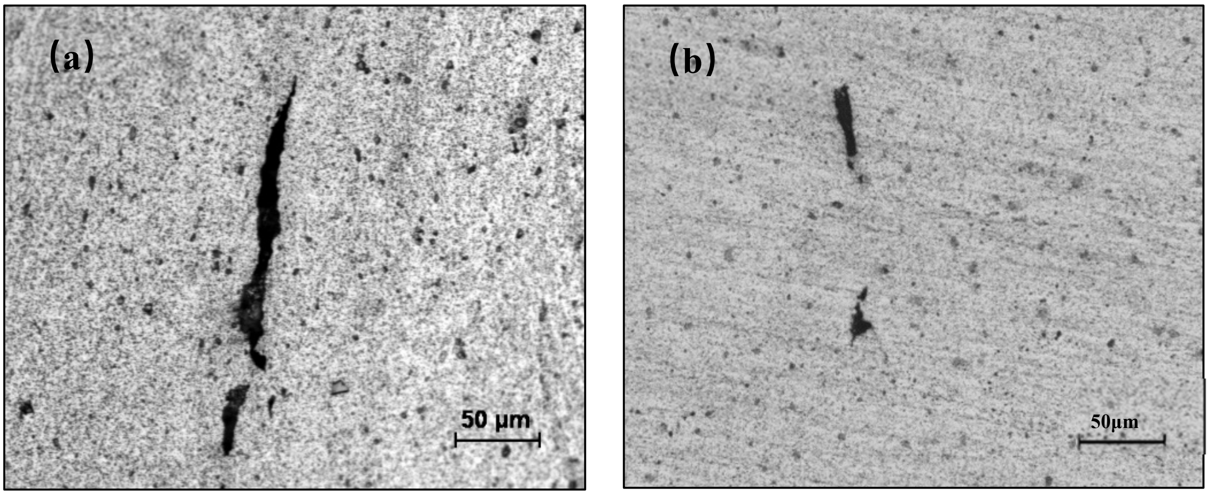

Fig. 6. 6 Microstructures of the linear friction welds obtained at different forging pressures.
(a) 60MPa and (b) 110MPa

6.2.3 Hardness distribution and mechanical properties

Fig. 6. 7 shows the hardness distribution diagram of the joint. It can be seen from the diagram that the dynamic recrystallization occurred in the weld area due to the friction heat and material deformation during LFW, resulting in fine crystalline microstructure, so that the hardness in the vicinity of the interface reached its peak value. However, the hardness of the welds decreases sharply at HAZ, indicating that the HAZ was affected by the friction heat and the grain coarsening, so that the hardness of the heat affected zone is lower. In addition, when the forging force is increased from 60MPa to 110MPa, the hardness of the HAZ decreased, which indicates that the heat input increased during the LFW with the increasing forging pressures.

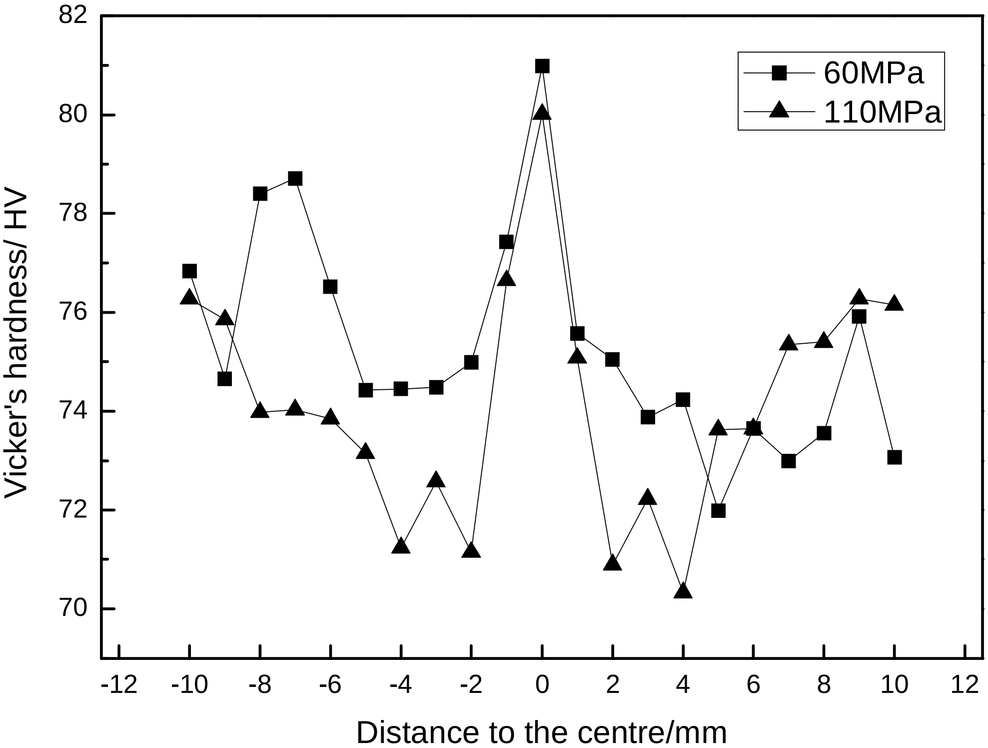

Fig. 6. 7 The micro-hardness distribution of AA5083 linear friction welds.

The mechanical properties of AA5083 linear friction welding of aluminum alloy under different forging conditions are shown in Table 6. 1. It was found that the LFW joints had relatively high mechanical properties. Compared to the base material which has a tensile strength of 335MPa, yield strength 165MPa, and elongation of 20%, the highest tensile strength of the LFW welds was 310MPa, which was 92.5% of the base metal. It was noticed that the yield strength of the LFW welds was higher, up to 142%, than that of the base material, due to the recrystallized fine grains at the weld interface. The elongation was slightly lower than that of base metal, and the maximum elongation was 88% of base metal, can also reach 17.6%, showing that the LFW joints had good quality.

Table 6. 1 The mechanical properties of linear friction welded AA5083-H112 joints

Sample No.	Forging pressure/ MPa	UTS/ MPa	YS/ MPa	EL/ %
1	60	303	223	13.25
2	80	305	227	14.35
3	110	310	235	17.6
Base metal		335	165	20

In addition, the mechanical properties of the LFW joints (including tensile strength, yield strength) raised slightly with the increase of forging force, while the elongation increased significantly at the forging force of 110MPa, from 13.25% to 17.6%.

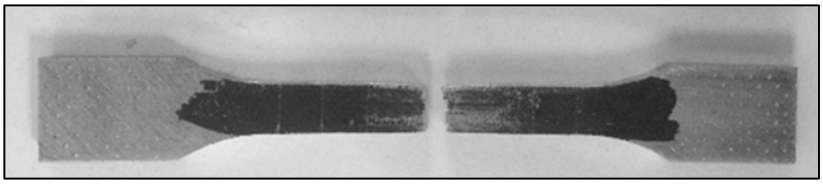

Fig. 6. 8 The macroscopic morphology of a weld after tensile fracture.

It was noticed that the fracture occurred at the weld interface for all the LFW forging pressures in this study, as shown in Fig. 6. 8, which is a typical macroscopic fracture image of the tensile fracture of the LFW joint. Besides, it was found that a certain amount of plastic deformation occurred near the joint before the fracture. Fig. 6. 9 shows the SEM of the tensile fracture surface of the LFW joint. Fig. 6. 9 (a) is a low magnification image of the fracture structure. Fig. 6. 9 (b) is a local enlargement of Fig. 6. 9 (a). It was found from Fig. 6. 9 that the fracture could be classified as mixed fracture, because in low magnification image, a large number of dimples can be observed, as well as a small amount of cleavage planes. From the higher magnification structure of the dimples, it can be seen that the grain size near the welding interface was relatively small, which revealed that the dynamic recrystallization occurred during the LFW process. The fine recrystallized grain at the fracture was the reason why the yield strength of the welded joint was much higher than that of the base materials according to the Hall-Petch relation.

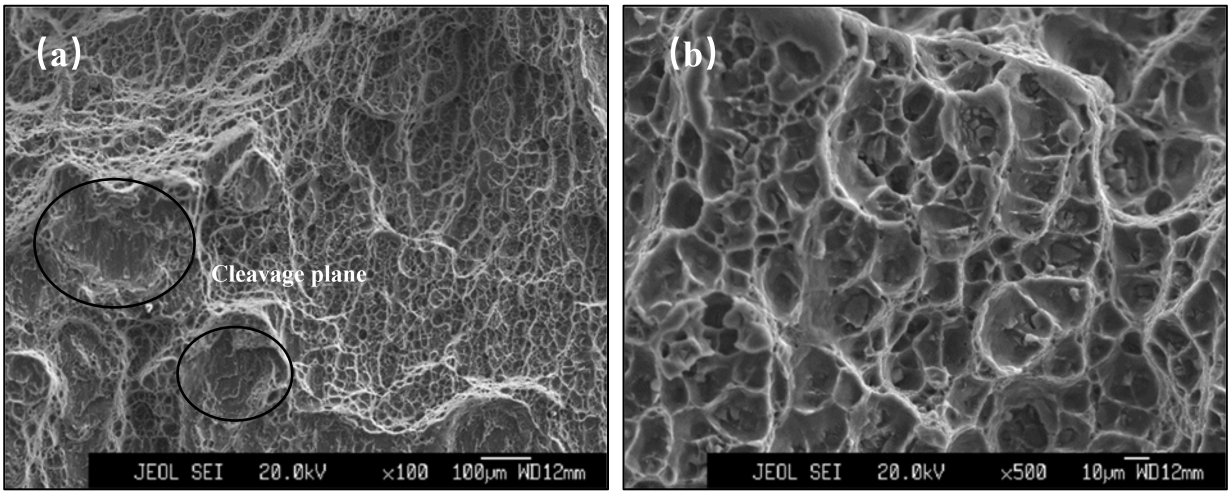

Fig. 6. 9 Fracture morphologies of tensile specimens of the AA5083 linear friction weld.
(a) lower magnification and (b) higher magnification

6.3 Linear friction welding of AA5083 and Cu C101

6.3.1 Macrostructure and material flow

Fig. 6. 10 shows the effect of the forging pressure on the weld macrostructure and flash morphology. It was found that the flash came from the aluminium side, with only a limited deformation (flattening) near the joint interface from the copper side instead of flash. As the frictional heating during LFW is fairly localised to the region close to the joint interface, it is clear that the temperature was sufficient to plastically deform the aluminium side (e.g. ~500˚C), while the copper side was still solid. It can be also seen that the flash in the aluminium side shows as a curled "hook" shape, which curls internally with the increase in the forging pressure, besides, the change in height due to forging was 14 mm 10.4 mm, and 8.5 mm, respectively. This is because the higher forging pressure supplies more heat input during LFW, so the metal softens resulting in more forging.

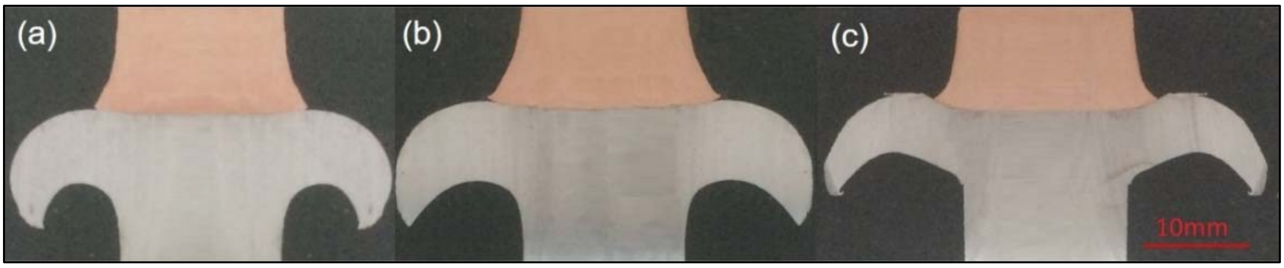

Fig. 6. 10 Flash formation at the Al weld side (bottom) of LFW joints welded under different forging pressures. (a) 110MPa, (b) 80MPa, and (c) 60MPa

6.3.2 Microstructure evolution

Fig. 6. 11 shows the microstructures of the base materials (a, b) as well as the LFW joint (c) which was achieved at the forging pressure of 80 MPa. Elongated grains were found along the rolling

direction in the microstructure of AA5083 (see Fig. 6. 11 (a)), whereas, equiaxed grains with annealed twins were found in the microstructure of Cu base material, ~110μm in grain size (see Fig. 6. 11 (b)). Fig. 6. 11 (c) shows the microstructure of the Al-Cu LFW focusing on the interface. It was found that recrystallization occurred for the Al alloy close to the interface, resulting in significant change in microstructure compared to the base material. Moreover, a transition zone could be detected towards the Cu side, where grain boundary could not be shown, suggesting that recrystallization occurred in this region. Further away, elongated grains were found in the Cu side, revealing the deformation for Cu grains due to the oscillation.

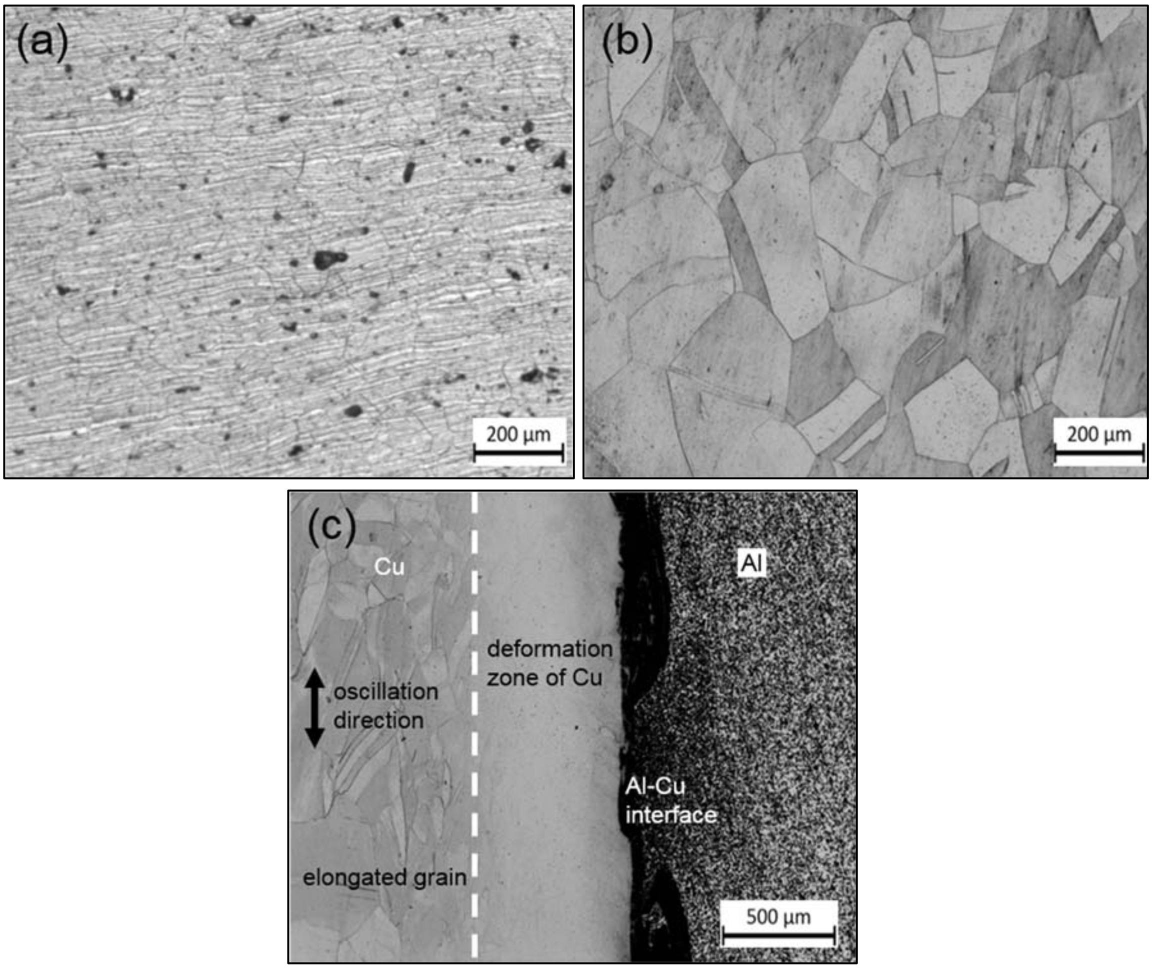

Fig. 6. 11 Microstructure of the Al-Cu LFW joint.
(a) Al base metal, (b) Cu base metal, (c) Al-Cu interface showing the weld regions

To further investigate the detailed evolution in the microstructure, SEM backscattered images were obtained for all the welds focusing on the vicinity of the weld interface, as shown in Fig. 6. 12. As was seen in the images, macroscale defects including cracks, pores, etc. could not be found in any weld. However, intermetallic particles were found along the weld interface, showing as dispersive particles in the Al side and layered structures on the edge of the Cu side. Moreover, some Cu particles maybe accompanied with intermetallics were found in the Al matrix, and generally more were found with the decreasing forging pressures in the LFW process.

Table 6. 2 shows the EDS results of the intermetallic particles existed in the Al matrix marked in Fig. 6. 12 (a). It was found that A was Cu particles which were entrained into the Al base during LFW process. A large number of tiny particles (marked B) which existed close to the Al-Cu interface but could not observed in the Al base material, had the main composition of Al, Mg and Cu, revealing that these small particles were generated during LFW process. The relatively larger particles (marked C) were containing Al, Fe, Mn and Si, which were primary phase of the Al base material. The black particles D were shown as oxides.

It should be noted that the intermetallics at the weld interface could be obviously detected showing continuous layered structure when the forging pressure was high (Fig. 6. 12 (a), (b), (d) and (e)), but was difficult to be observed in low forging pressure samples. On the contrary, in the low forging pressure samples, e.g., at 60 MPa, a large number of Cu-rich fragments could be seen in the Al matrix close to the weld interface, and generally decreased in amount when using higher forging pressure. Therefore, it could be concluded that the forging pressure in the LFW process had a significant effect on the mechanical mixing of Al-Cu and generation of Al-Cu intermetallics which had a reciprocal relationship.

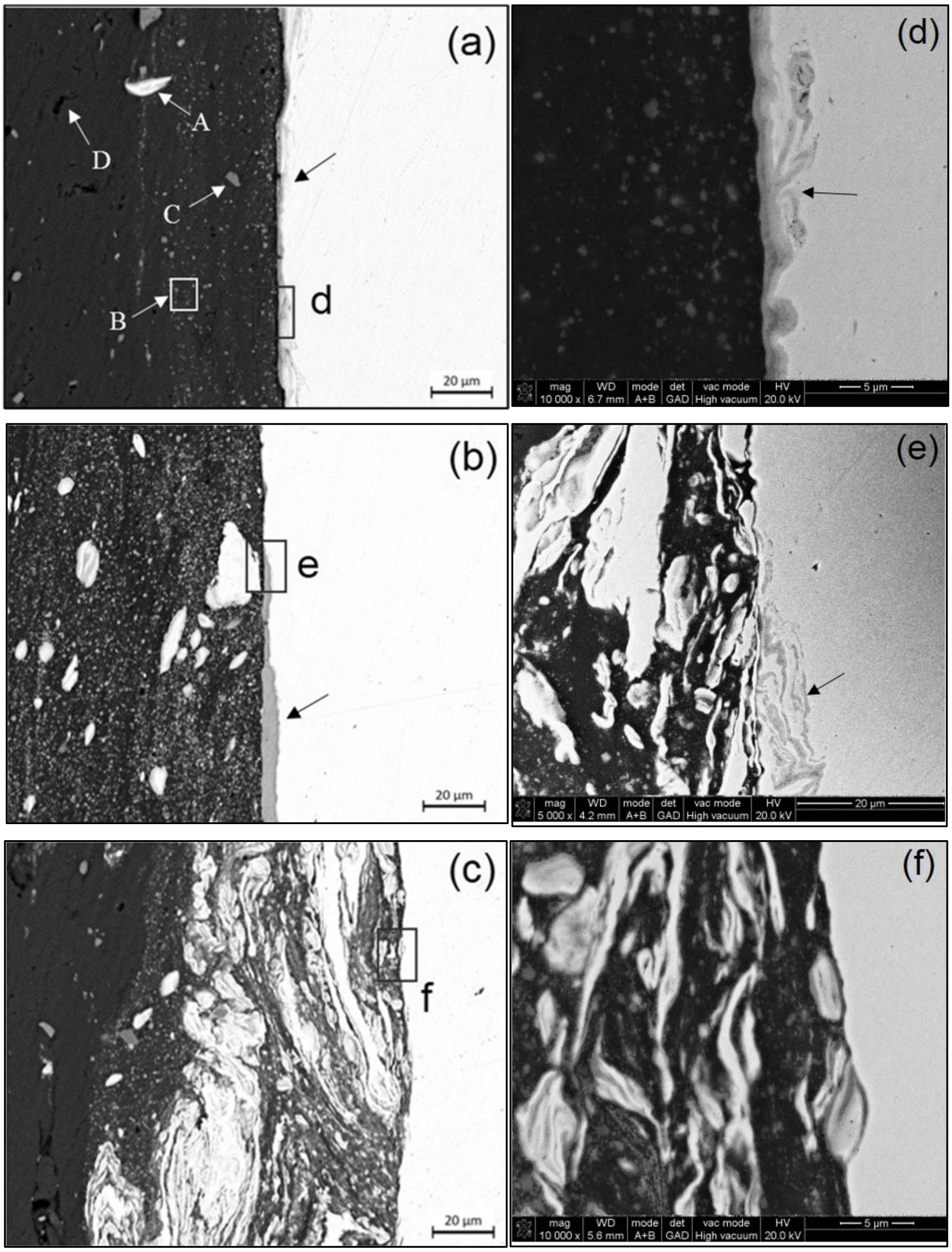

Fig. 6. 12 SEM backscattered electron micrographs of the joint, showing the Al side (bottom/left) and Cu side (top/right), welded using different forging pressures: (a,d) 110 MPa, (b,e) 80 MPa, and (c,f) 60 MPa.

Table 6. 2 EDS results of the intermetallic particles in Fig. 6. 12 (a).

Point	Composition (at. %)							
	Al	Si	Mn	Fe	Mg	Cu	O	Total
A	-	-	-	-	-	100%	-	100%
B	78.83%	-	-	-	10.43%	10.74%	-	100%
C	77.10%	5.16%	6.77%	10.97%	-	-	-	100%
D	29.94%	18.56%	-	-	19.25%	-	32.25%	100%

Fig. 6. 13 shows a higher magnification SEM micrograph at the Al-Cu interface. It was clearly shown that intermetallics also existed on the Cu fragments entrained into the Al matrix. Moreover, the intermetallics were showing two different types in morphology, which were particles (marked as 1 in Fig. 6. 13) and layered structures (marked as 2 in Fig. 6. 13). The element composition of these intermetallics were identified by EDX. It was found that the Al:Cu in atomic percentage for the particles was 66.5:33.5, suggesting CuAl$_2$ phase, whereas for layered phase was 27.8:72.2, suggesting Cu$_9$Al$_4$ phase.

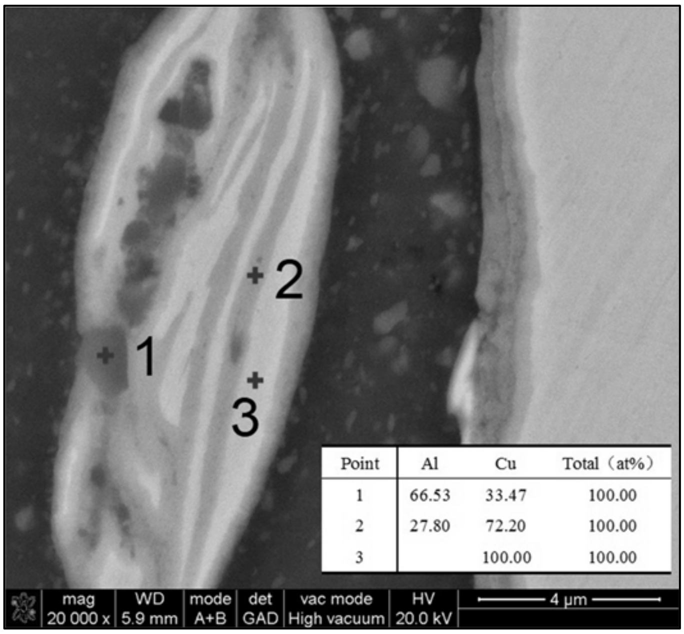

Point	Al	Cu	Total（at%）
1	66.53	33.47	100.00
2	27.80	72.20	100.00
3		100.00	100.00

Fig. 6. 13 EDX analyses of the particle intermetallic phase in the vicinity of the joint interface.

Besides, an intermetallic layer was found between Al and Cu matrix in Fig. 6. 13, and identified in Fig. 6. 14. Fig. 6. 14 (a) is the EDX line scan, showing that the layered intermetallic phase is composed of Al, Cu, as well as Mg, because of the Mg content in the Al base alloy AA5083. Therefore, the layered intermetallic phase was suggested to be an Al-Mg-Cu ternary phase. Further EPMA was conducted for the tensile fracture sample and the results were shown in Fig. 6. 14 (b). It was found that the Al:Cu:Mg in atomic percentage for the layered intermetallic phase (marked as point 1) was 19.8:54.1:26.1, suggesting Al_2CuMg phase.

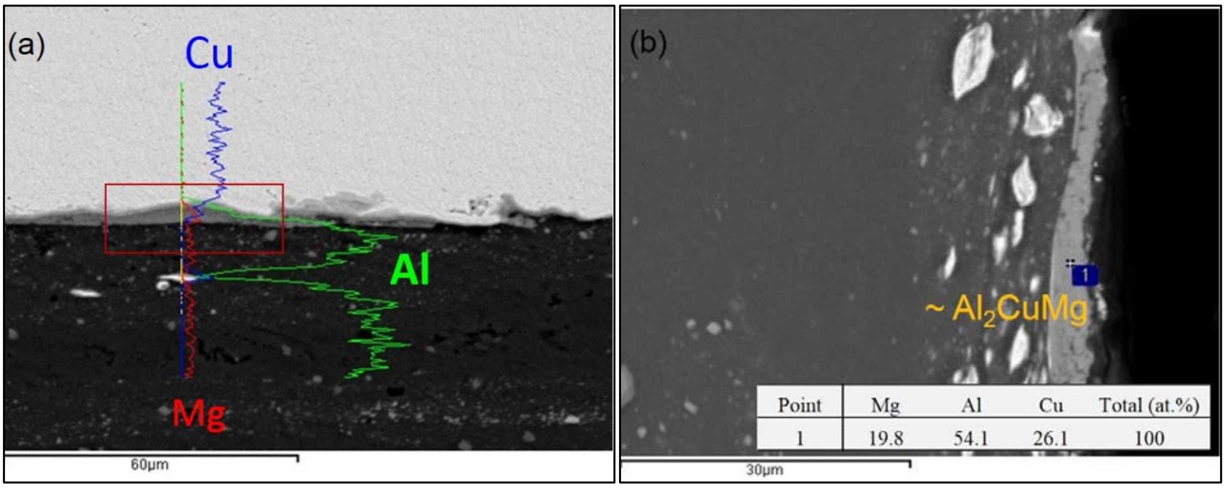

Point	Mg	Al	Cu	Total (at.%)
1	19.8	54.1	26.1	100

Fig. 6. 14 EPMA and EDX analyses of the layered intermetallic phase in the vicinity of the joint interface. (a) the weld (b) a fractured tensile sample

6.3.3 Hardness distribution

Fig. 6. 15 shows hardness traces through the joint line for the experimental welding conditions. Generally, the hardness increased significantly when close to the welding interface where the hardness was to the peak value. Moreover, it was found no obvious hardness drop in the HAZ. It was noticed that the peak hardness varied with the different forging pressures. In the 80 MPa

sample, the peak hardness could reach 137 HV, while in the 110 MPa and 60 MPa samples, the peak hardness was respectively 87 HV and 107 HV. It could be explained according to the microstructure observation for different samples. In the hardness profiles, it was found that the base material of Al and Cu were similar in hardness, so the hardness peak was produced due to the intermetallics, especially dispersed particles. In the 110 MPa weld, a small quantity of the particles was found around the interface (Fig. 6. 12 (a)), resulting in a lower peak hardness, while in 80 MPa weld, a larger quantity of the particles was shown (Fig. 6. 12 (b)), resulting in a higher peak hardness. Specially, for the 60 MPa weld, Cu fragments were observed around the weld interface (Fig. 6. 12 (c)), resulting in a slight decrease compared to 80 MPa sample.

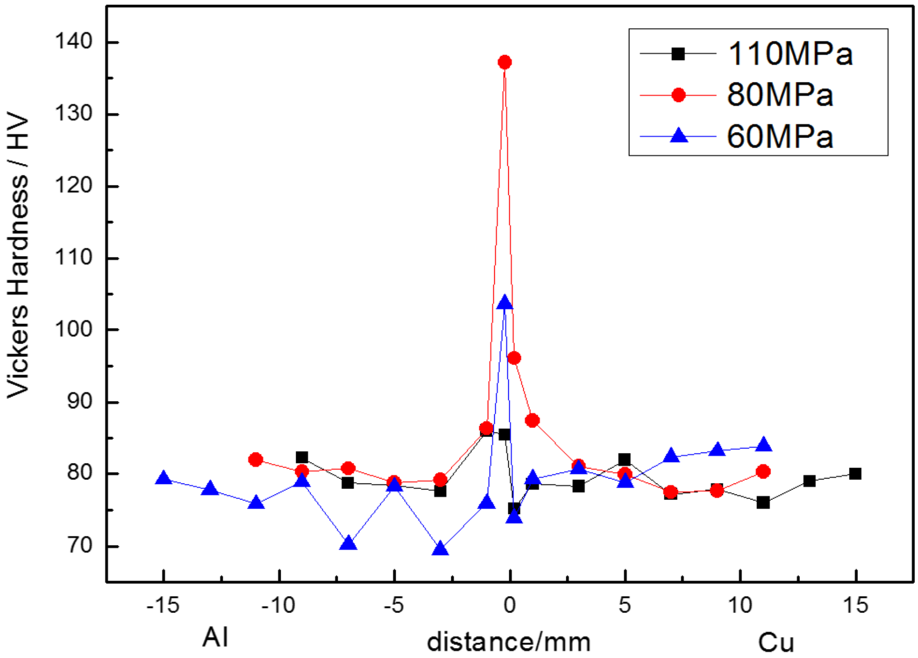

Fig. 6. 15 Vickers hardness distribution in the Al-Cu LFWs welded at different forging pressures.

6.3.4 Tensile properties

Fig. 6. 16 shows the tensile test results performed for the welds prepared at various forging

pressures. It was found that, with the increasing forging pressure, the tensile property decreased significantly from ~160MPa to less than 50 MPa which was not qualified for application. It was noticed that the yield strength and elongation data could not be obtained in this experiment because the fracture happened in the elastic stage. Furthermore, for all the samples, failure occurred at the Al-Cu weld interface, exactly along the layered intermetallic phase (see Fig. 6. 14 (b)), suggesting that the layered intermetallic phase should be avoided through controlling the welding parameters especially the forging pressure.

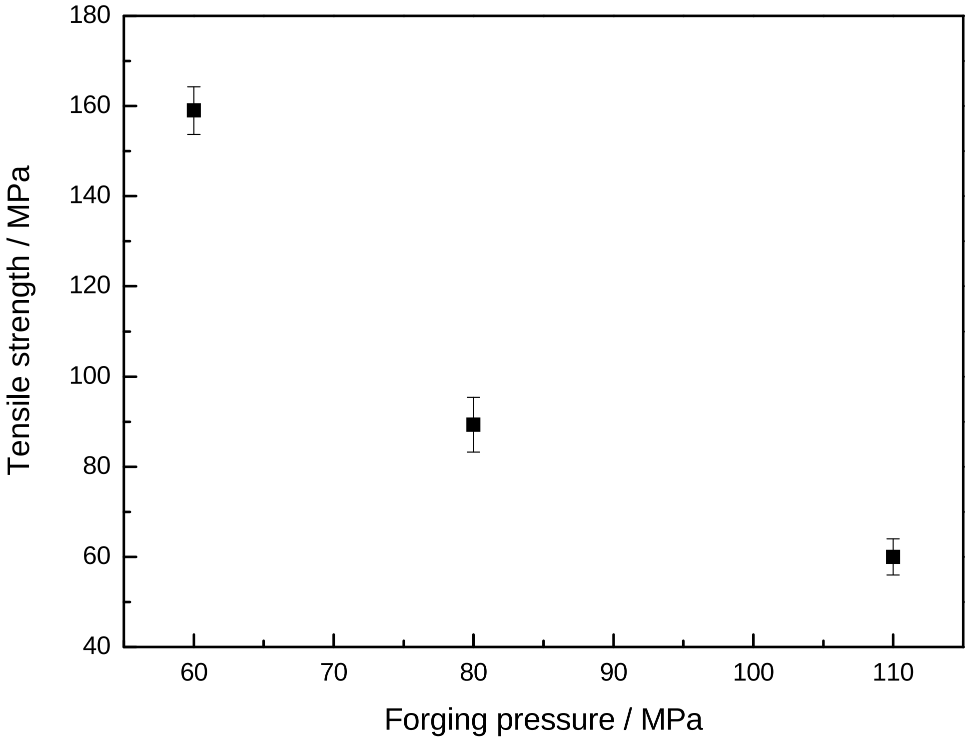

Fig. 6. 16 Tensile strength of the Al-Cu LFW joints at different forging pressures.

The fracture surfaces taken from the Cu side of the broken samples are shown in Fig. 6. 17. It was found that the morphology varied due to different forging pressures. For the 110 MPa sample, grey areas (arrowed in Fig. 6. 17 (a)) corresponding to the layer structure intermetallics in Fig. 6. 12 (a) and (d) were widely distributed, suggesting that the sample fractured mainly due to the layered intermetallics. For the 80 MPa sample, less layered phases were found in the fracture, but a big quantity of fine intermetallic particles were detected in the Al matrix (Fig. 6. 17 (b)), instead of layered intermetallics. It was revealed that the sample fractured due to the intermetallic layers combined with fine particles. For the 60 MPa sample, it was found that intermetallic layers as well as fine particles reduced significantly, so that the tensile strength had a marked improvement to the highest of all the samples.

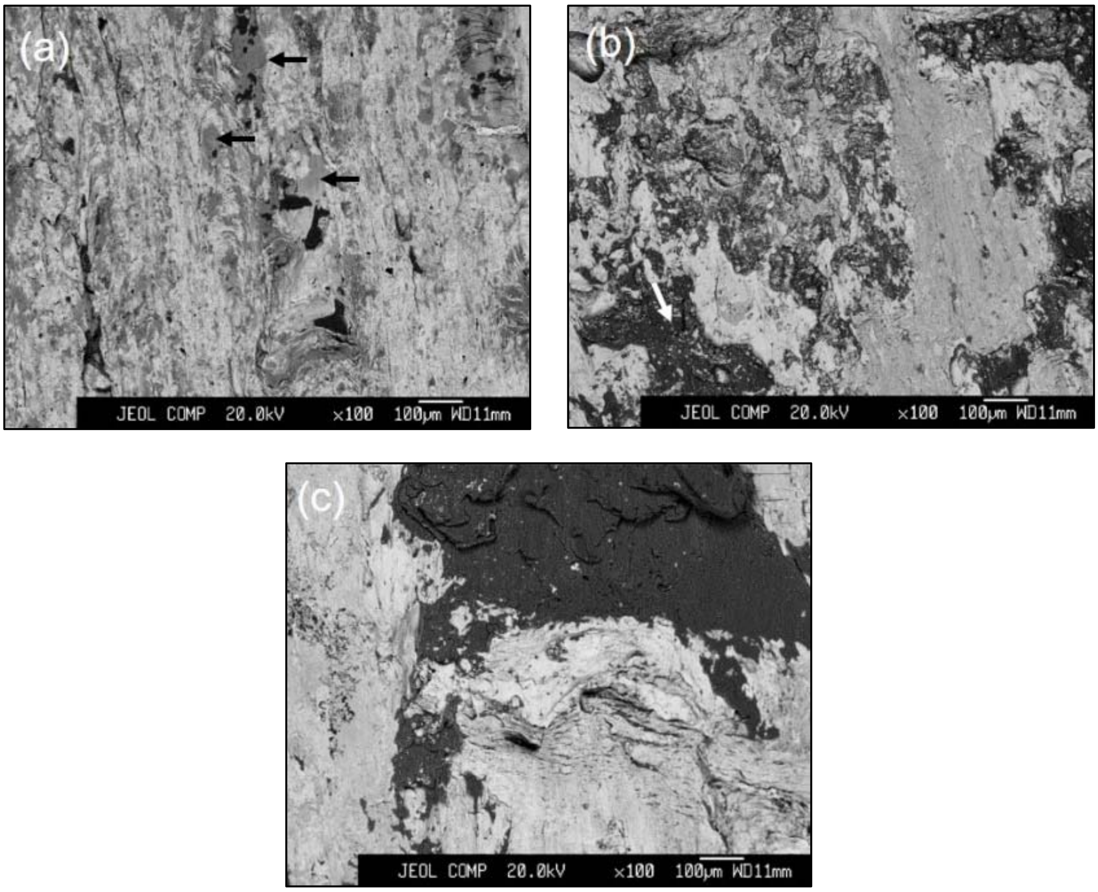

Fig. 6. 17 Backscattered electron micrographs of fracture surface of the welds observed from the copper part under different forging pressures: (a) 110 MPa, (b) 80 MPa, and (c) 60 MPa. In Fig. 8 (a), the gray zone shows the layered intermetallics (arrowed). In Fig. 8 (b) the arrows point at the intermetallic particles in the Al-rich region.

6.3.5 Discussion

From the experiment results above, it could be concluded that the intermetallic phase around the Al-Cu interface had a significant effect on the mechanical properties, especially the intermetallic layers (estimated as Al_2CuMg phase) existing between Al and Cu matrix. Besides, the fine particles could also influence the tensile property to some extent. According to the literature, intermetallics were commonly found in LFW Al to Cu. Wanjara et al. [21] found $CuAl_2$ particles in the LFW AA6063 to pure copper. Xue et al. [22] detected layered $CuAl_2$ phase in FSW Al to Cu, which was found to have a negative influence on the mechanical properties. In this study, 4% of Mg in weight was contained in AA5083, affecting the composition of the intermetallic phase.

Similar to FSW, the heat in LFW process is also generated through mainly friction heating by two materials as well as the deformation heat during forging process. Vairis et al. [2] expressed the heat input during the LFW process using the equation:

$$\text{LFW Heat input} = \mu P_f \alpha 2\pi f \frac{1}{\sqrt{2}} \tag{6.1}$$

where, μ is the friction coefficient, P_f is the forging pressure, α is the oscillation amplitude, and f is the frequency of the oscillation. It was found that the heat input increased with the increasing forging pressure as well as the frequency and amplitude of the oscillation during the LFW process. In this study, the frequency and amplitude of the oscillation were kept constant, so the heat input was only decided by the forging pressure. Since the forging pressure was added basically at the end of the oscillation, the LFW procedure could be considered as the friction and the subsequent forging. According to the microstructure observation in this study, the friction could promote the entrainment of Cu particles to the Al matrix, and at the same time produce a considerable amount of heat to plasticize the materials. Notably that this process is the same for all the samples, no matter how much the forging pressure is, resulting that the microstructure should be the same, which should be a large amount of Cu particles were entrained to the Al matrix. However, as the forging pressure was applied, the heat input increased, so that the temperature at the Al-Cu interface had a further raise, which trends to the generation of Al-Cu-(Mg) intermetallics in the vicinity. With the increasing forging pressure, the heat input continued to rise until sufficient temperature was reached to form Al_2CuMg phase, thus resulting in lower properties. Accordingly, the Cu particles entrained to the Al matrix were less as was seen in the microstructure.

6.4 Conclusions

In this chapter, AA5083 LFW welds and AA5083-Cu C101 welds were obtained using different forging pressures, to assess the impact of the forging pressure, as well as the defects on the mechanical properties and microstructural development. The following conclusions can be drawn:

1. The linear friction welded joint of AA5083 aluminum alloy has been successfully prepared without macro defects under the experimental conditions. The mechanical properties of the LFW joints increased with the decrease of the forging force. When the forging force was 110MPa, the tensile strength and elongation of the weld were up to 310MPa and 17.6%, which were 92.5% and 88% of parent materials, respectively. It was noticed that the yield strength of the joint was obviously higher (up to 142%) than that of base metal due to the dynamic recrystallization in the weld zone. Moreover, there were discontinuous lack of connection defects on the welding interface, where crack source formed on the in the stretching process. With the increase of the forging force, which led to the increase of the heat input, the size of the defect was significantly decreased, resulting in the increase of the mechanical properties.

2. Sound dissimilar AA5083 Cu C101 LFW joints could be produced. Different with the LFW of AA5083 to itself, the mechanical properties decreased significantly with the increasing forging pressures. No lack of connection defect was observed for all the samples, instead, the intermetallic phases with various morphology were detected in the vicinity of the weld interface, which influenced the mechanical properties of the welds. With the increasing forging pressure, more heat was generated during the LFW process, resulting in the formation

of Al_2CuMg layer structure intermetallic phase, which was found to have a negative effect on the mechanical properties. Besides, fine intermetallic particles were found in samples produced using lower forging pressure, also affecting the mechanical properties. With the reducing forging pressure, more Cu-rich particles were distributed into the Al matrix, resulting in a relatively higher mechanical properties for the welds.

6.5 References

[1] A. Vairis, M. Frost, On the extrusion stage of linear friction welding of Ti 6Al 4V, Materials Science and Engineering: A 271(1) (1999) 477-484.

[2] A. Vairis, M. Frost, High frequency linear friction welding of a titanium alloy, Wear 217(1) (1998) 117-131.

[3] E. Dalgaard, P. Wanjara, J. Gholipour, X. Cao, J.J. Jonas, Linear friction welding of a near-β titanium alloy, Acta Materialia 60(2) (2012) 770-780.

[4] Y. Guo, T. Jung, Y.L. Chiu, H. Li, S. Bray, P. Bowen, Microstructure and microhardness of Ti6246 linear friction weld, Materials Science and Engineering: A 562 (2013) 17-24.

[5] Y. Ji, Z. Chai, D. Zhao, S. Wu, Linear friction welding of Ti–5Al–2Sn–2Zr–4Mo–4Cr alloy with dissimilar microstructure, Journal of Materials Processing Technology 214(4) (2014) 979-987.

[6] C.-c. Zhang, T.-c. Zhang, Y.-j. Ji, J.-h. Huang, Effects of heat treatment on microstructure and microhardness of linear friction welded dissimilar Ti alloys, Transactions of Nonferrous Metals Society of China 23(12) (2013) 3540-3544.

[7] C. Song, T. Lin, P. He, Z. Jiao, J. Tao, Y. Ji, Molecular dynamics simulation of linear friction welding between dissimilar Ti-based alloys, Computational Materials Science 83 (2014) 35-38.

[8] J. Romero, M.M. Attallah, M. Preuss, M. Karadge, S.E. Bray, Effect of the forging pressure on the microstructure and residual stress development in Ti-6Al-4V linear friction welds, Acta Materialia 57(18) (2009) 5582-5592.

[9] M. Karadge, M. Preuss, C. Lovell, P.J. Withers, S. Bray, Texture development in Ti–6Al–4V linear friction welds, Materials Science and Engineering: A 459(1) (2007) 182-191.

[10] T.J. Ma, W.Y. Li, S.Y. Yang, Impact toughness and fracture analysis of linear friction welded Ti–6Al–4V alloy joints, Materials & Design 30(6) (2009) 2128-2132.

[11] T. Ma, T. Chen, W.-Y. Li, S. Wang, S. Yang, Formation mechanism of linear friction welded Ti–6Al–4V alloy joint based on microstructure observation, Materials Characterization 62(1) (2011) 130-135.

[12] G. Buffa, M. Cammalleri, D. Campanella, L. Fratini, Shear coefficient determination in linear friction welding of aluminum alloys, Materials & Design 82 (2015) 238-246.

[13] X. Yang, W. Li, J. Ma, S. Hu, Y. He, L. Li, B. Xiao, Thermo-physical simulation of the compression testing for constitutive modeling of GH4169 superalloy during linear friction welding, Journal of Alloys and Compounds 656 (2016) 395-407.

[14] G. Buffa, D. Campanella, S. Pellegrino, L. Fratini, Weld quality prediction in linear friction welding of AA6082-T6 through an integrated numerical tool, Journal of Materials Processing Technology 231 (2016) 389-396.

[15] A. Astarita, F. Scherillo, M. Curioni, P. Aprea, F. Impero, A. Squillace, X. Zhou, Study of the Linear Friction Welding Process of Dissimilar Ti-6Al-4V–Stainless Steel Joints, Materials and Manufacturing Processes 31(16) (2016) 2115-2122.

[16] M.N. Avettand-Fènoël, G. Racineux, L. Debeugny, R. Taillard, Microstructural characterization and mechanical performance of an AA2024 aluminium alloy — Pure copper joint obtained by linear friction welding, Materials & Design 98 (2016) 305-318.

[17] M. Karadge, M. Preuss, P.J. Withers, S. Bray, Importance of crystal orientation in linear friction joining of single crystal to polycrystalline nickel-based superalloys, Materials Science and Engineering: A 491(1) (2008) 446-453.

[18] L. Fratini, G. Buffa, M. Cammalleri, D. Campanella, On the linear friction welding process of aluminum alloys: Experimental insights through process monitoring, CIRP Annals 62(1) (2013) 295-298.

[19] X. Song, M. Xie, F. Hofmann, T.S. Jun, T. Connolley, C. Reinhard, R.C. Atwood, L. Connor, M. Drakopoulos, S. Harding, A.M. Korsunsky, Residual stresses in Linear Friction Welding of aluminium alloys, Materials & Design 50 (2013) 360-369.

[20] C. Xia, Y. Li, U.A. Puchkov, S.A. Gerasimov, J. Wang, Microstructure and phase constitution near the interface of Cu/Al vacuum brazing using Al–Si filler metal, Vacuum 82(8) (2008) 799-804.

[21] P. Wanjara, E. Dalgaard, G. Trigo, C. Mandache, G. Comeau, J.J. Jonas, Linear friction welding of Al–Cu: Part 1 – Process evaluation, Canadian Metallurgical Quarterly 50(4) (2011) 350-359.

[22] P. Xue, D.R. Ni, D. Wang, B.L. Xiao, Z.Y. Ma, Effect of friction stir welding parameters on the microstructure and mechanical properties of the dissimilar Al–Cu joints, Materials Science and Engineering: A 528(13-14) (2011) 4683-4689.

7 Conclusions and Future Work

7.1 Summary and conclusions

7.1.1 Friction stir butt welding of AA5083

The present work has prepared a series of sound welds by FSW butt welding for AA5083-H112 using different welding parameters combinations. The microstructure morphologies, grain size distribution in the SZ, hardness distribution throughout the welds were evaluated. Moreover, a special focus was taken on the kissing bond defect, which can have a significant effect on the microstructure and properties of the FSW joints. A combination of several experiment techniques including OM, SEM, EBSD, TEM, DSC, NDT, microhardness tester, tensile tester, and fatigue tester were used to study the kissing bond in the FSW joints as well as its influence on the microstructure evolution, tensile/fatigue properties, and failure behaviour of the welds. The following conclusions can be drawn:

- For base material characterization, the AA5083-H112 was composed of elongated grains along the (ST-RD) plane, fine in thickness, and Al(Mn,Fe)Si, Mg_2Si and Al_6Mn were observed in the Al matrix. The base material AA5083 had a high elongation (20%), moderate tensile strength (335MPa), relatively low yield strength (163MPa) and hardness (84.8HV), which was revealed that the aluminium plate had excellent processing properties and good ability of deformation.

- The FSW AA5083 can be divided into several zones as BM, HAZ, TMAZ and SZ, which has different microstructure characteristic, respectively. Among them, the SZ experiences dynamic recrystallization during FSW process, and the recrystallization grain size decreases when welding at a lower heat input.
- The lowest hardness of the welds is at the HAZ, while in the SZ, the hardness raises significantly to the level of the BM due to the work-hardening effect.
- The X-ray inspection results indicates that the FSW joints has no visible defects.
- The length of the kissing bond was found to have a reasonably linear relation with heat input (HI), which depends on the tool rotation speed and feed rate.
- With the increase in the length of the kissing bond, the tensile UTS and EL increased first and then decreased, while the YS had no obvious trend with the kissing bond length.
- The fatigue life of the welds was longer with the shorter kissing bond.
- The tensile UTS and fatigue life of the welds were strongly correlated with the fracture types. The shear fracture resulted in higher tensile UTS and longer fatigue life, while poor strength and fatigue properties were associated with the welds showing a fracture path along the kissing bond.

7.1.2 Friction stir lap welding of AA6061 and A356

The present work has demonstrated the feasibility of FSLW of a wrought aluminium alloy (AA6061-T6) to a casting aluminium (as-cast A356) sheets. The microstructure evolution, second-phase distribution and microscale defects including kissing bond and hook were evaluated using OM, SEM, hardness tester, tensile tester. To further improve the mechanical properties suitable for automotive application, PWHT were conducted with a comparation of the hardness and shear properties, and a discussion with their relationship with different process parameters. The following conclusions could be drawn:

- The welds showed inhomogeneous grain size distribution, notably with the dynamically recrystallised grain being finer towards the AS, compared with the RS. This supports the view that the stirring effect is severer in the AS than RS, which could increase the strain rate resulting in grain refinement.
- Kissing bond, formed due to the presence of oxide particle clusters, were detected in the microstructure of the welds, showing less with the increasing tool rotation speed. It was found that the kissing bond did not significantly affect the shear behaviour of the joints.
- Hook defect, found in the vicinity of the weld interface towards AS, increased in height and range with the increasing tool rotation speed. It was found that the hook defect had a significantly influence on the shear behaviour of the joints.
- Intermetallic particles in the WN especially A356 side experienced stirring-assisted dissolution, whose severity increased with the increase in the tool rotation speed. After PWHT, the hardness in the WN increased significantly due to the re-formation of precipitates.

- Shear testing showed that the ultimate shear force of the welded joints was higher when less heat-input was used during the welding process. Besides, the PWHT resulted in an improvement in the mechanical strength of the welds by more than 10% for all the welding conditions.

7.1.3 Linear friction welding of AA5083 and dissimilar AA5083 to Cu C101

The present work has investigated the LFW of AA5083 welds and dissimilar AA5083-Cu C101 welds using different forging pressures, to assess the impact of the defects, as well as the forging pressure on the mechanical properties and microstructural development. The following conclusions can be drawn:

- The linear friction welded joint of AA5083 aluminium alloy has been successfully prepared without macro defects under the experimental conditions. The mechanical properties of the LFW joints increased with the increase of the forging force. When the forging force was 110MPa, the tensile strength of the weld was up to 88% of parent material. It was noticed that the yield strength of the joint was obviously higher (up to 142%) than that of base metal due to the dynamic recrystallization in the weld zone.
- Discontinuous lack of connection defects were detected on the welding interface, where crack source formed on the in the stretching process. With the increase of the forging force, which led to the increase of the heat input, the size of the defect was significantly decreased, resulting in the increase of the mechanical properties.

- Sound dissimilar AA5083 Cu C101 LFW joints could be produced. Different with the LFW of AA5083 to itself, the mechanical properties decreased significantly with the increasing forging pressures.
- The LFW process can lead to the formation of intermetallic phases with various morphology, which influenced the mechanical properties. With the increasing forging pressure, more heat was generated during the LFW process, resulting in the formation of Al_2CuMg layer structure intermetallic phase, which was found to have a negative effect on the mechanical properties. Besides, fine intermetallic particles were found in samples produced using lower forging pressure, also affecting the mechanical properties. With the reducing forging pressure, more Cu-rich particles were distributed into the Al matrix, resulting in a relatively higher mechanical properties for the welds.

7.2 Future work

The present work has been focused on the relationship between the microstructure and mechanical properties in friction welding joints, which covered FSW butt welding, FSW lap welding as well as LFW, especially on the characterization of various defects in these friction welds and their influence regulations on the mechanical properties. Future work is still required to establish a simple model on the welding parameters and welding heat input, which consciously reflect the heat and temperature contribution in the welds, and further quantify the influence of the defects on the weld microstructure and mechanical properties, as well as to produce simple and quick numerical models to predict the production of the defects in the friction welds. This would concentrate on the following aspects:

- To establish a numerical model for the heat input of the friction welding procedure, under the influence of the welding parameters, tool structure design, and friction conditions, which can consciously predict the temperature distribution in the welds to control the production of strengthening phase as well as the harmful intermetallics.
- To study the influence of the starting heat treatment condition especially phase composition on the weld mechanical properties based on the heat input model, which is beneficial to further optimize the mechanical properties of the products.
- To establish a simple and quick numerical model to predict the production of the defects in the friction welds, based on the study of the material flow during the welding procedures, to simulate the defects including microscopic defects such as tunnel and lack of fusion and macroscopic defects such as the kissing bond within friction welding process.

Appendix

The peer-reviewed papers that were published (or submitted) to date as a result of this project were listed as follows:

[1] Nan Zhou, Dongfu Song, Wenjun Qi, Xiaohui Li, Ji Zou, Moataz M. Attallah. Influence of the kissing bond on the mechanical properties and fracture behaviour of AA5083-H112 friction stir welds[J]. Materials Science and Engineering A, 2018, 719: 12-20. (Corresponding to the content of Chapter 4)

[2] Nan Zhou, Dongfu Song, Wenjun Qi, Chunlei Qiu, Moataz M. Attallah. Microstructure and mechanical properties evolution in dissimilar AA6061-T6/A356 friction stir lap-welded joints[C]. 11th International Symposium on Friction Stir Welding, Cambridge, UK, 2016. (Corresponding to the content of Chapter 5)

[3] Nan Zhou, Chunlei Gan, Dongfu Song, Wenjun Qi, Moataz. M Attallah. Influence of forging pressure on microstructural and mechanical properties development in linear friction welded Al-Cu dissimilar joint[J]. Soldagem & Inspeção, 2019, 24: e2401 (Corresponding to the content of Chapter 6)